NASA CR-191203

NASA-E-8143

NASA

National Aeronautics and
Space Administration

Energy Efficient Engine

Low Pressure Turbine
Cooled Test Vehicle
Performance Report

by

W.J. Bruckner, D.G. Cherry, J. Pedersen

General Electric Company
Aircraft Engine Business Group
Cincinnati, Ohio 45215

Prepared for
National Aeronautics and Space Administration

[redacted]

NASA Lewis Research Center
Contract NAS3-23384

1. Report No.	2. Government Accession No.	3. Recipient's Catalog No.
NASA CR-168290		

4. Title and Subtitle	5. Report Date
NASA/GE Energy Efficient Engine Low Pressure Turbine Scaled Test Vehicle Performance Report	July 1983
	6. Performing Organization Code
7. Author(s)	8. Performing Organization Report No.
BRIDGEMAN, M.J.; CHERRY, D.G.; and PEDERSEN, J.	R83AEB143
	10. Work Unit No.
9. Performing Organization Name and Address	
General Electric Company Aircraft Engine Business Group Evendale, Ohio 45215	11. Contract or Grant No. NAS3-20643
	13. Type of Report and Period Covered Topical 1979-1982
12. Sponsoring Agency Name and Address NASA-LEWIS Research Center 21000 Brookpark Road Cleveland, Ohio 44135	14. Sponsoring Agency Code

15. Supplementary Notes

NASA Project Manager: C.C. Ciepluch G.E. Project Manager: R.W. Bucy
NASA Project Engineer: R. Dengler

16. Abstract

The low pressure turbine for the NASA/General Electric Energy Efficient Engine is a highly loaded five-stage design featuring high outer wall slope, controlled vortex aerodynamics, low stage flow coefficient, and reduced clearances.

An assessment of the performance of the LPT has been made based on a series of scaled air-turbine tests divided into two phases: Block I and Block II. The transition duct and the first two stages of the turbine were evaluated during the Block I phase from March through August 1979. The full five-stage scale model, representing the final integrated core/low spool (ICLS) design and incorporating redesigns of stages 1 and 2 based on Block I data analysis, was tested as Block II in June through September 1981.

Results from the scaled air-turbine tests, reviewed herein, indicate that the five-stage turbine designed for the ICLS application will attain an efficiency level of 91.5% at the Mach 0.8/10.67-km (35,000-ft), max-climb design point. This is relative to program goals of 91.1% for the ICLS and 91.7% for the flight propulsion system (FPS).

17. Key Words (Suggested by Author(s))	18. Distribution Statement
Turbine Performance, Fan Turbine, High Stage Loading, Close-Coupled, Controlled Vortex	[redacted]

19. Security Classif. (of this report)	20. Security Classif. (of this page)	21. No. of Pages	22. Price*
Unclassified	Unclassified		

[redacted]

TABLE OF CONTENTS

TABLE OF CONTENTS (Concluded)

LIST OF ILLUSTRATIONS

LIST OF ILLUSTRATIONS (Continued)

LIST OF ILLUSTRATIONS (Continued)

LIST OF ILLUSTRATIONS (Continued)

LIST OF ILLUSTRATIONS (Continued)

LIST OF ILLUSTRATIONS (Continued)

Figures

LIST OF ILLUSTRATIONS (Continued)

LIST OF ILLUSTRATIONS (Concluded)

LIST OF TABLES

SYMBOLS AND ABBREVIATIONS

ACC	Active Clearance Control
AR	Aspect Ratio, h/d_o or h/AW
AW	Airfoil Axial Width, cm (in.)
BTU	British Thermal Unit
C_o or Co	Isentropic Stage Velocity, cm/sec (ft/sec) - defined in Appendix D.
Cm	Centimeter
CF6	General Electric Commercial Turbofan Engine
D	Diameter, cm (in.), or Scale Factor (Table VI)
d_o	Airfoil Throat Dimension, cm (in.)
DOC	Direct Operating Cost
E^3	Energy Efficient Engine
F	Separation Parameter
ft	Feet
F-idle	Flight Idle Operating Point
FPS	Flight Propulsion System - The fully developed configuration of the E^3 which would be suitable for installation on an airframe.
g	Gravitational Constant 32.2 (lb_m ft/lb_f sec^2), or Gram
H	Hub
h	Airfoil Height, cm (in.)
HLFT	Highly Loaded Fan Turbine
HPT	High Pressure Turbine
in	Inches
ICLS	Integrated Core/Low Spool - the Turbofan Configuration of the E^3
J	Joule, Mechanical Equivalent of Heat, 778.2 (ft-lb_f)/BTU
K	Kelvin
Kg	Kilogram

l	Characteristic Length
lb_f	Pound Force
lb_m	Pound Mass
LE	Leading Edge
LPT	Low Pressure Turbine
M	Mach Number
m	Meter
MXCL	Maximum Climb Operating Point
MXCR	Maximum Cruise Operating Point
N	Turbine Speed, rpm
NM	Newton Meter
n	Number of Airfoils per Blade Row
P	Pressure, Pa (psi), or Pitch
Pa	Pascal
PL	Denotes Instrumentation Plane (e.g., PL42)
q	Dynamic Head ($lb_f/in.^2$)
R	Rotor or Rankine
R1	Stage 1 Rotor
R2	Stage 2 Rotor
R3	Stage 3 Rotor
R4	Stage 4 Rotor
R5	Stage 5 Rotor
Rad	Radian
RN	Reynolds Number - defined in Appendix E
S	Stator
S1	Stage 1 Stator

S2	Stage 2 Stator
S3	Stage 3 Stator
S4	Stage 4 Stator
S5	Stage 5 Stator
Sec	Second
SFC	Specific Fuel Consumption, kg/N hr (lb_m/lb_f hr)
T	Total Temperature, K(°R), °C(°F), or Tip
t	Airfoil Tangential Spacing, cm (in.)
TE	Trailing Edge
TKOF	Take Off Operating Point
Tq	Torque, NM (ft-lb_f)
u or U	Rotor Tangential Velocity at the Mean Radius, m/sec (ft/sec)
V	Absolute Velocity, m/sec (ft/sec)
W	Flow, kg/sec (lb_m/sec)
α	Absolute Flow Angle, Degrees from Axial
β	Relative Flow Angle, Degrees from Axial
Γ	Turbine Exhaust Swirl, Degrees
Δ	Differential or Incremental Value (Prefix)
Δh	Energy Extraction, J/g (Btu/lb_m)
η	Turbine Efficiency
ψ	Turbine Loading, $gJ\Delta h/2u^2$
ψ_z	Zweifel Loading Coefficient
$\bar{\omega}$	Average Inlet Loss Coefficient, defined in Section 4.5.1

Subscripts

0	Turbine Inlet
1	Nozzle Exit
2	Turbine or Blade Row Exit
39	Rig Front Frame Strut Plane
42	Rig Inlet Traverse Plane
49	Cycle Designation for LPT Inlet Plane
50	Rig Exhaust Traverse Plane
S5	Rig Exhaust Rake Plane, also Exhaust P_s Plane, all Builds
p	Pitchline (Mean radius), or Peak
R	Relative
S	Static, or Stator
T	Total
TS	Total-to-Static
TT	Total-to-Total
z	Denotes Axial Component or Zwiefel

1.0 SUMMARY

The low pressure turbine for the NASA/General Electric Energy Efficient Engine is a highly loaded five-stage design featuring high outer wall slope, controlled vortex aerodynamics, low stage flow coefficient, and reduced clearances.

An assessment of the performance of the LPT has been made based on a series of scaled air-turbine tests divided into two phases: Block I and Block II. The transition duct and the first two stages of the turbine were evaluated during the Block I phase from March through August 1979. The full five-stage scale model, representing the final integrated core/low spool (ICLS) design and incorporating redesigns of stages 1 and 2 based on Block I data analysis, was tested as Block II in June through September 1981.

Results from the scaled air-turbine tests, summarized in this report, indicate that the five-stage turbine designed for the ICLS application will attain an efficiency level of 91.5% at the Mach 0.8/10.67-km (35,000-ft), max-climb design point. This is relative to program goals of 91.1% for the ICLS and 91.7% for the flight propulsion system (FPS).

2.0 INTRODUCTION

The NASA/GE Energy Efficient Engine (E^3) Component Development and Integration Program was initiated on January 2, 1978. The program has as its objective the development of technology which will improve the energy efficiency of propulsion systems for subsonic commercial aircraft of the late 1980's or early 1990's.

Four major technical tasks were established for the E^3 program at it's inception. Task 1 addressed the design and evaluation of the E^3 flight propulsion system (EPS). The Task 1 results established the requirement for the experimental test hardware, which included the components, core, and integrated core/low spool. Task 2 consisted of the design, fabrication and testing of the components and included supporting technology efforts. These supporting technology efforts were performed where required to provide verification of advanced concepts included in the propulsion system design. Task 3 involved the design, fabrication, and test evaluation of a core engine, consisting of the compressor, combustor, and high pressure turbine. Integration of the core with the low-spool components and test evaluation of the integrated core/low-spool (ICLS) comprise Task 4 which is currently scheduled for completion in the first quarter of 1983.

The low pressure turbine for the Task 4 ICLS evaluation is a five-stage machine which is coupled to the high pressure turbine via a short (3-inch) transition duct. The close-coupling of the turbines results in reduced diameters for the forward stages of the LPT and, consequently, in a reduction in rotor tangential velocity, u. In addition, the relatively high cycle bypass ratio of the E^3 engine (BPR=7) is manifested by increased fan power requirement coupled with reduced core flow resulting in higher specific energy requirement, Δh, for the fan turbine. The high bypass ratio in conjunction with the close-coupled turbine system result in a significant increase in LPT aerodynamic loading, $\Delta h/2u^2$, relative to fan turbines in current production high bypass engines such as the General Electric CF6.

Further, this increase in loading is to be accomplished without sacrifice to the efficiency level now being demonstrated by the CF6 fan turbines.

The technology available to GE which most nearly attains this performance goal is that which has been demonstrated in the IR&D funded Highly Loaded Fan Turbine (HLFT) Program. This technology was applied to the E^3 LPT aerodynamic design as part of Task 2.

Additional technology features incorporated into the LPT design include an active clearance control (ACC) system to reduce blade tip and interstage seal radial clearances and the use of 360° stator casings to improve roundness control.

Included in the Task 2 supporting technology effort was a detailed evaluation of the LPT aerodynamic design using a 0.67 size scale model test vehicle. Design, fabrication, and test of this scaled rig was divided into two phases: Block I and Block II.

The transition duct and first two stages of the turbine were evaluated during the Block I phase from March thru August 1979. The configurations tested as part of the Block I evaluation were:

- Stage 1 nozzle annular cascade
- Stage 1
- Stage 1 with Stage 2 nozzle annular cascade
- Two-stage group.

The full five-stage scale model, representing the final ICLS design and incorporating redesign features to address problem areas evident from Block I data analysis, was tested during the Block II phase from June thru September, 1981. The configurations tested as part of the Block II evaluation were:

- Stage 1 nozzle annular cascade (redesigned)
- Two-stage group (redesigned)
- Five-stage group (Final ICLS configuration).

This report presents detailed results from the Block I and Block II rig test series.

3.0 AERODYNAMIC DESIGN

3.1 DESIGN REQUIREMENTS

Historically in prototype engines, turbomachinery component efficiencies fall short of design goals by significant amounts. The consequent cycle rebalance causes components to operate off-design, further reducing efficiency. In an attempt to obviate this trend, the ICLS cycle was devised with appropriate derates on component efficiencies. Depending on the accuracy of the efficiency derates, turbomachinery components designed to requirements of the resultant cycle will avoid off-design penalties.

Table I presents LPT cycle data for the Block II ICLS max-climb aerodynamic design point and, for comparison, data for the FPS maximum climb, maximum cruise, and sea level takeoff points. Note the relatively small differences between climb and cruise for the FPS. Note further that the ICLS has been designed to a flow function approximately 4% higher at climb than the FPS. This reflects the derated component efficiencies and estimated instrumentation losses in the ICLS. It should be noted that a minor change in cycle definition occurred between Block I and Block II causing a slight difference in rig design points for the two blocks of testing. This will be documented in Section 4.3.1.

Efficiency goals at Mach 0.8/10.67 km (35,000 ft) maximum climb are 0.911 (or 91.1%) for the ICLS and 0.917 (91.7%) for the FPS.

3.2 NUMBER OF STAGES

The selection of a five-stage configuration for the E3 LPT was based in part on results obtained during the IR&D-funding Highly Loaded Fan Turbine (HLFT) technology development program and also on system studies aimed at minimizing direct operating cost (DOC). These system studies evaluated the impact of turbine loading, weight, and cost on DOC and indicated a relative optimum at a loading level attainable in five stages. Further, significant performance gains at this loading level have been demonstrated in the HLFT program, indicating that the ICLS goal could be met with a five-stage turbine.

3.3 BLOCK I AERODYNAMIC DESIGN.

Maximum tip diameters for the HPT and LPT were set by mechanical and configuration control requirements at 76.2 cm (30 in.) and 118.1 cm (46.5 in.), respectively. In addition, the LPT flowpath outer-wall slope was limited to 25 degrees through Stage 3, transitioning to cylindrical at the Stage 5 exit. The wall slope limit was set by aero as the maximum consistent with good performance.

Table I. Critical LPT Operating Point Data.

Parameter	Units	ICLS	FPS		
		Maximum Climb	Maximum Climb	Maximum Cruise	Sea Level Takeoff +27° F
Inlet Temperature, T	K	1099.8	1083.2	1054.6	1128.7
	° R	1979.7	1949.8	1898.2	2031.6
Energy $\Delta h/T$	J/kg/K	318.1	326.5	322.3	306.3
	Btu/lbm/° R	0.07597	0.07798	0.07697	0.07315
Speed $N/\sqrt{T}$	rad/s$\sqrt{K}$	11.07	11.26	11.08	10.61
	rpm/$\sqrt{°\ R}$	78.82	80.14	78.86	75.53
Corrected Flow, $W\sqrt{T}/P$	g$\sqrt{K}$/s.Pa	4.098	3.936	3.947	3.967
	lbm$\sqrt{°\ R}$/s.psi	83.57	80.27	80.33	80.90
Loading, $\Delta h/2u^2$	---	1.292	1.283	1.308	1.355
Efficiency, η	---	0.911	0.917	0.916	0.921

The initial (Block I) five-stage flowpath was defined through an iterative technique whereby a candidate outer-wall contour was selected (within the limitations on wall slope and exit diameter) and the inner wall contour and stage energy distribution were iterated concurrently to yield acceptable levels of loading ($gJ\Delta h/2u^2$) and flow coefficient (Vz/u) for each stage. The best of the candidate flowpaths was selected based on a stage-by-stage efficiency estimate which accounted for the effects of loading, flow coefficient, tip slope, aspect ratio, and clearance.

Figure 1 shows the engine configuration of the Block I flowpath.

Detailed vector diagram calculations were executed for the first four bladerows of the Block I flowpath using a method that solves the full three-dimensional, radial equilibrium equation for circumferentially averaged flow. The procedure accounts for streamline slope and curvature, effect of radial blade force component due to airfoil sweep and dihedral, airfoil blockage, and radial gradients of flow properties, including bladerow loss gradients. Tables II and III present, respectively, vector diagram and bladerow parameters for Stages 1 and 2 of the Block I design.

Airfoil cascade analysis was accomplished by a streamtube curvature method which calculates along a stream surface determined from the through-flow analysis, accounting for variations in streamtube thickness. Airfoil contours and velocity distributions for the Block I bladerows are shown in Figures 2 thru 5 for streamsurface sections at 10%, 50%, and 90% from the inner wall. The peak Mach number (M_p) is indicated on each Mach number distribution.

Block I test results are presented in detail in Section 4.5.1 of this report; however, those aspects of the results which have directly impacted the Block II design will now be summarized briefly.

Total-to-total efficiency (defined in Appendix F) for the Block I two-stage group was below the pretest prediction. The following items were identified as possible contributors to the deficiency.

1. A region of secondary flow over the outer 40% of span of the Stage 1 vane was detected during the Configuration 1 test. This loss core, caused by the combination of a weakened inlet boundary layer (from the diffusing outer wall of the transition duct) and the high vane tip slope, caused excess loss, relative to design intent, near the stator tip.

2. Similar secondary flow effects were noted over the outer 20% span of the Stage 2 vane during the stage-and-a-half test.

3. Both rotating tests revealed unexpectedly poor performance in the region of the rotor hubs. In addition to the severe dropoff at the hub, performance in the outer half of the annulus is depressed due, in part, to the vane tip losses.

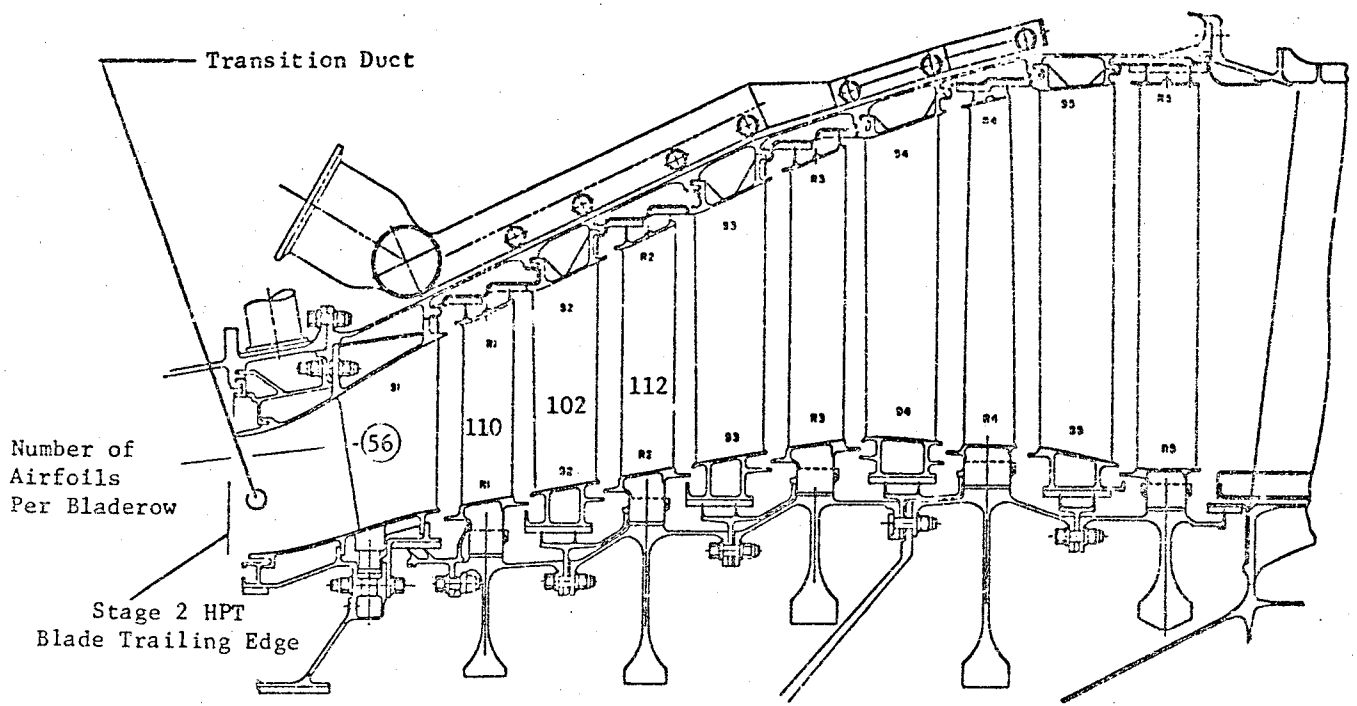

Figure 1. Block I LPT Flowpath

Table II. Block I Vector Diagram Summary.

	Stage 1			Stage 2		
Energy Extraction, Δh J/g (BTU/lbm)	72.81 (31.3)			80.48 (34.6)		
Pressure Ratio, P_{T_0}/P_{T_2}	1.30			1.36		
Aero Loading, $gJ\Delta h/2U^2$	1.69			1.61		
Flow Coefficient, V_z/U	1.16			1.02		
	Hub	Pitch	Tip	Hub	Pitch	Tip
Reaction	0.210	0.350	0.393	0.279	0.365	0.437
Stator Exit Angle, α_1 (degrees)	54.8	61.7	61.4	58.1	65.7	61.6
Stator Exit Mach Number, M_1	0.640	0.625	0.513	0.626	0.641	0.552
Rotor Relative Inlet Angle, β_1 (degrees)	46.6	47.9	37.0	45.5	51.6	35.0
Rotor Relative Inlet Mach Number, M_{R_1}	0.437	0.416	0.305	0.438	0.409	0.324
Rotor Relative Exit Angle, β_2 (degrees)	57.6	63.1	60.4	58.8	65.3	62.6
Rotor Relative Exit Mach Number, M_{R_2}	0.541	0.615	0.543	0.577	0.639	0.593
Stage Exit Swirl, Γ, (degrees)	40.9	47.5	35.7	42.3	49.0	37.9
Stage Exit Axial Mach Number, M_{Z_2}	0.292	0.283	0.280	0.300	0.272	0.284

Table III. Block I Blading Average Solidity and Aspect Ratio Tabulations.

Blade Row	S1	R1	S2	R2
AW/t	1.24	1.32	1.47	1.30
ψ_z	.776	1.047	.875	1.005
TE BLOCKAGE cm (in.)	.0838(.033)	.1676(.066)	.1575(.062)	.1676(.066)
AR, h/d_o	4.57	10.53	11.20	13.29
AR, h/AW	1.87	3.75	3.39	4.50

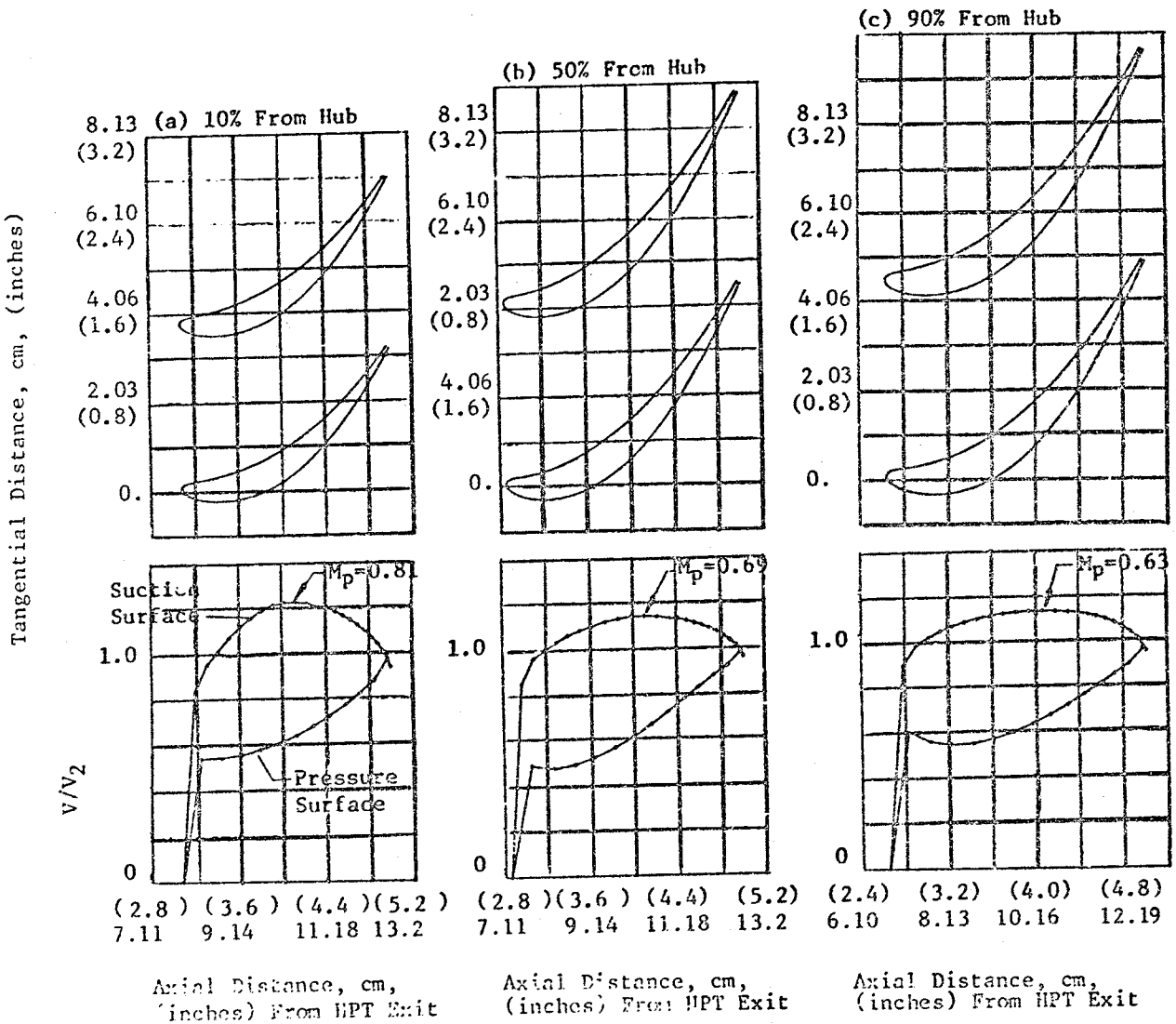

Figure 2. Block I Stage 1 Vane Shapes and Stream Surface Velocity Distributions

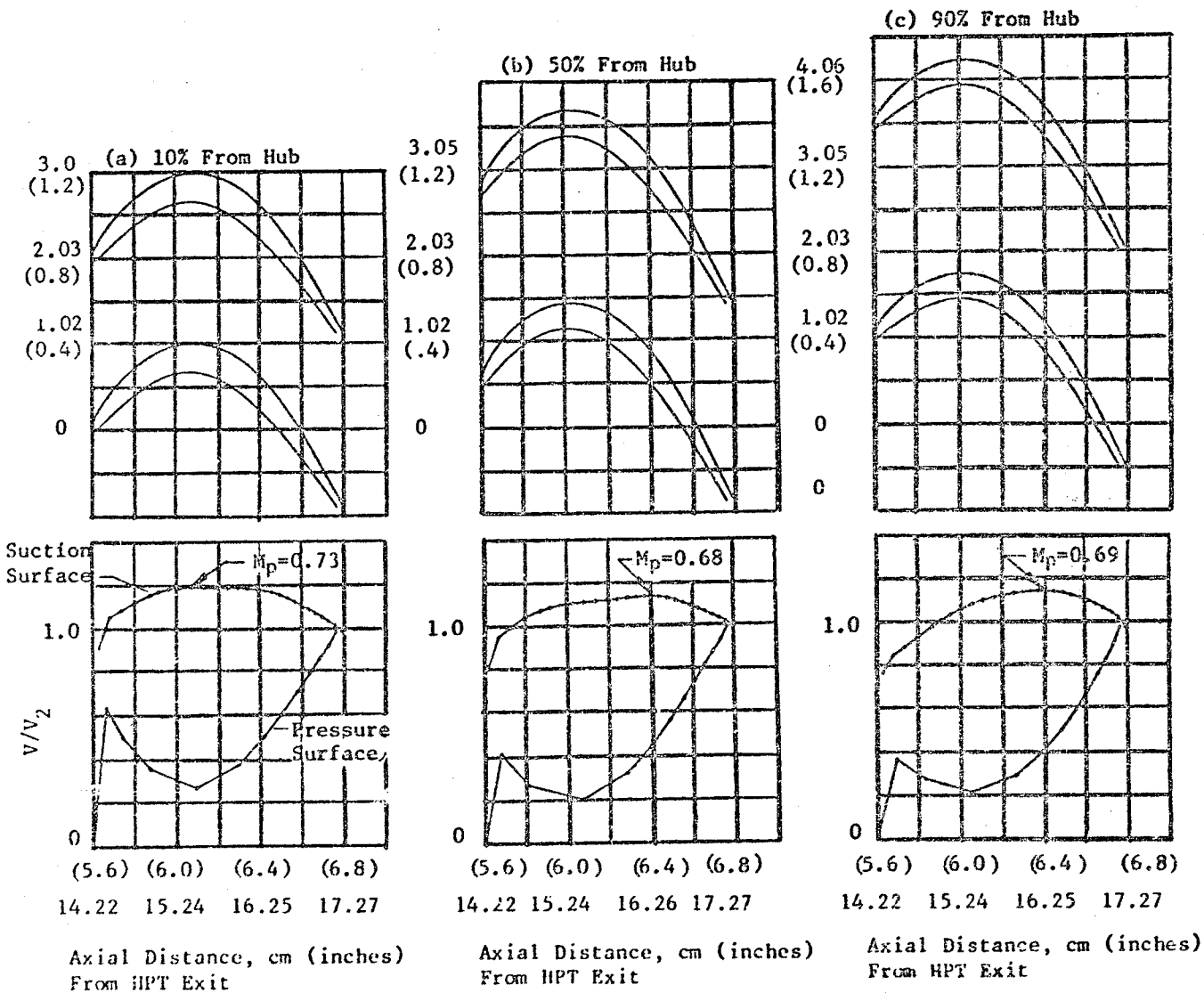

Figure 3. Block I Stage 1 Blade Shapes and Stream Surface Velocity Distribution

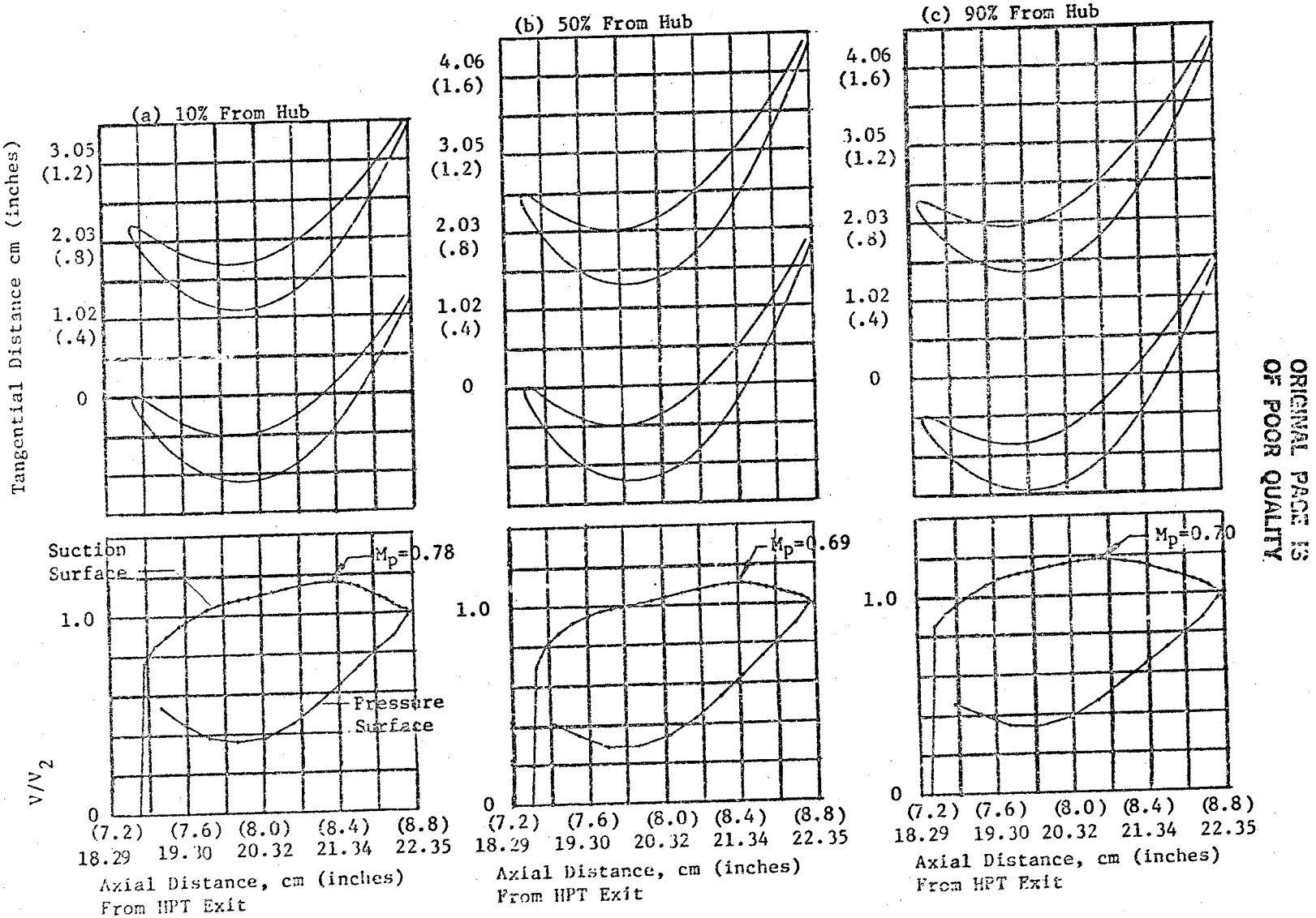

Figure 4. Block I Stage 2 Vane Shapes and Stream Surface Velocity Distributions.

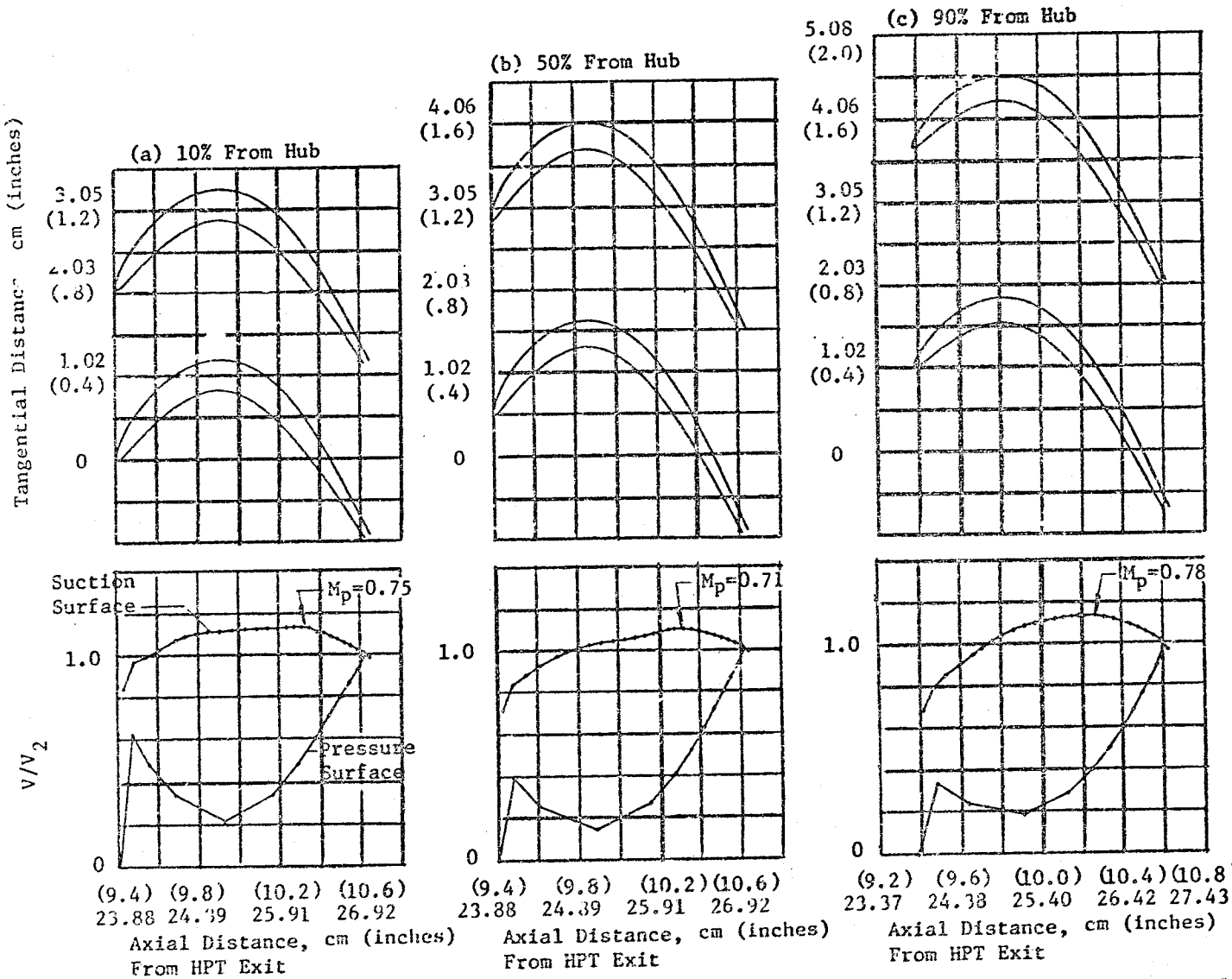

Figure 5. Block I Stage 2 Blade Shapes and Stream Surface Velocity Distributions.

A stage-by-stage performance stackup for the ICLS turbine, using the trend and the level of the stage efficiency versus loading characteristic established by the Block I test series, indicated a status efficiency of 90.4% versus the ICLS goal of 91.1%, a 0.7% deficiency.

3.4 BLOCK II AERODYNAMIC DESIGN

Based on extensive post-test data matching and analysis of the Block I results, the following were identified as crucial items to be addressed during the Block II redesign:

- Stage 1 vane solidity is low, especially at the hub.
- Stage 1 vane aspect ratio is low, especially near the tip.
- The solidities of rotor blade hubs are low, and there is excessive pressure-side diffusion near the leading edges.
- A substantial performance penalty is incurred by the increase in outer wall slope to 25°. This is especially true in the vicinity of low aspect ratio vane tips.
- Inner and outer-wall overlap geometry needs improvement, as evidenced by poor performance near the walls. This refers specifically to the amount (or lack) of axial overlap between the stator bands and the rotor platforms/tip-shroud extensions.

In order to address the issue of outer-wall slope and its influence on performance, several alternate flowpaths were developed and analyzed by those methods previously described. One ground rule that was enforced during this alternate-flowpath study was that the overall length and exhaust tip diameter remain unchanged. Results of the study indicated that configurations which reduce wall slope via an increase in loading or through-flow velocity show a net loss relative to the base Block I flowpath. Consequently, the Block II (final aero) flowpath has remained essentially unchanged from the Block I status. However, the following modifications were incorporated to address the specific problems identified during Block I testing:

- A higher aspect ratio, higher solidity version of the Stage 1 vane has been added, along with a modified transition duct, to accommodate the new vane design. Figure 6 shows a comparison of the Block I duct/vane with that of Block II. Note that the solidity was increased by raising the airfoil count from 56 to 72 which also increased the airfoil throat aspect ratio (height/throat). The chordal aspect ratio was increased by reducing the axial chord at the outer wall.

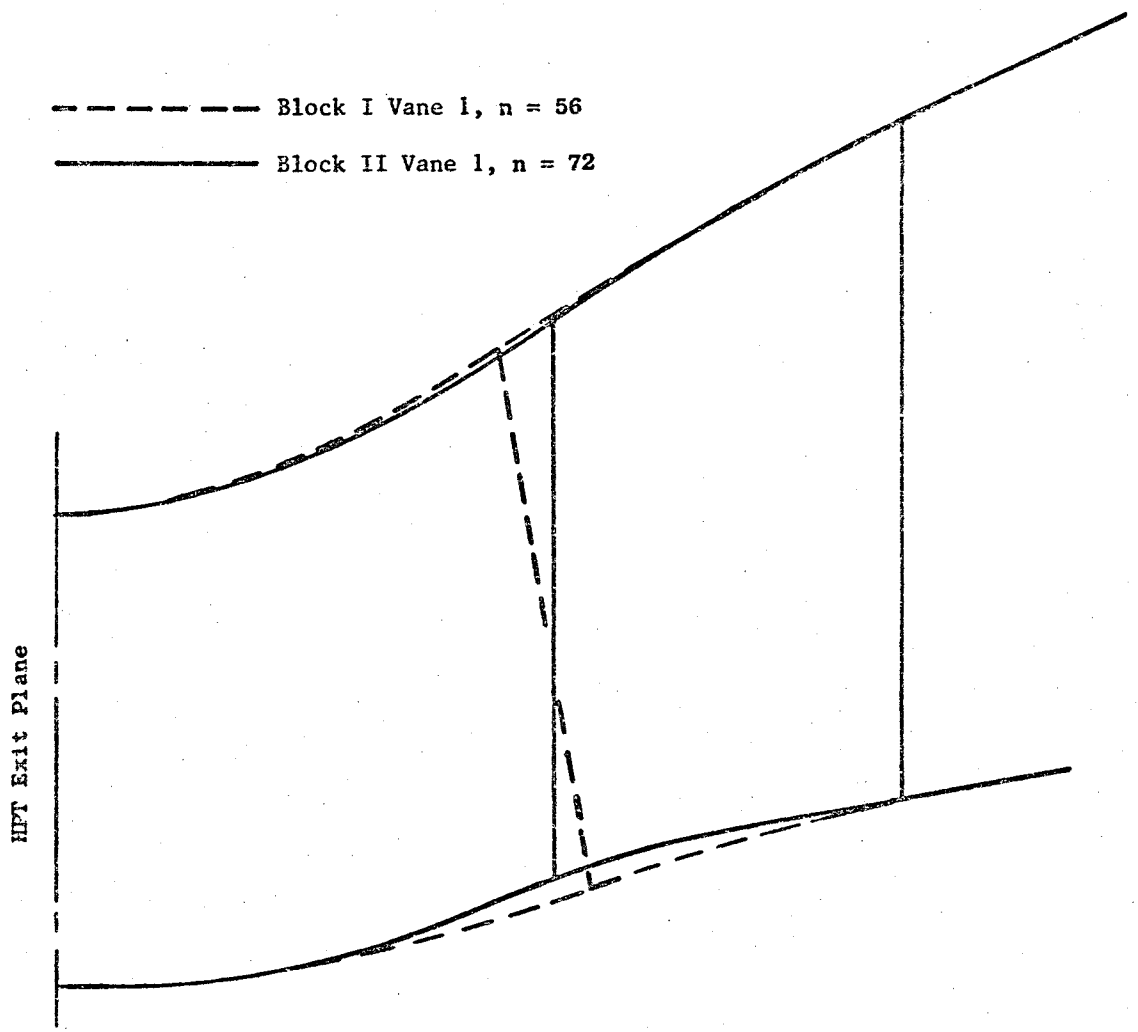

Figure 6. Block II Stage 1 Stator and Transition Duct Compared with Block I.

- An effort to improve flowpath overlaps resulted in the Block II five-stage flowpath shown in Figure 7. A comparison of typical inner-wall overlap geometry for Block II with that of Block I (Inset, Figure 7) shows that the rotor platforms have been extended to lap under the stator inner bands. It is believed that the poor performance of the Block I stages near the walls is partly attributable to the overlap geometry.

- In an effort to increase blade hub solidity locally without a significant weight increase, rotor hub axial widths were retained at the Block I levels while the numbers of blades for each rotor were increased to yield the desired solidity at the hub, and the axial widths from the pitch line to the tip were reduced to maintain solidities at Block I levels.

Figure 8 presents the results, including inner- and outer-wall Mach number distributions, from an axisymmetric analysis of the final transition duct. Note that two additional lines have been added on the outer wall in the vicinity of the vane leading edge to show stagnation and midchannel streamline Mach numbers as they approach the leading edge. Also included is a plot of a "separation parameter". This is an indicator of the sensitivity of a turbulent boundary layer (on the outer wall in this case) to separation in the presence of an adverse pressure gradient.

The gas path vector diagram analysis was accomplished using the same calculation procedure as that described for Block I. Calculations were made with radial gradients of blading losses to simulate end-loss effects. The calculation model for the Block II LPT showing meridional streamlines and intrabladerow calculation stations is shown on Figure 9. Table IV presents final Block II vector diagram data. These data served as input for the airfoil design.

Airfoil aerodynamic design was initiated using vector diagram data from the vector diagram analysis, Table IV, and preliminry solidities determined during design studies. A tabulation of Block II blading aerodynamic geometry is presented in Table V.

Final airfoil shapes and velocity distributions are shown in Figures 10 through 19 for stream surface sections at 10%, 50%, and 90% from the inner wall. The data are represented by plots of local surface velocity normalized by downstream exit velocity. The peak Mach number (M_p) is indicated on each velocity distribution.

Comparison of the velocity distributions at 10% for the Stage 1 and 2 blades (Figures 11 and 13) with those of their Block I counterparts (Figures 3 and 5) will show how the pressure surface diffusion near the leading edge has been reduced in the Block II designs.

The aerodynamic, heat transfer, and mechanical design details of the ICLS LPT are presented in detail in Reference 1. Also included in that reference are full scale streamsurface coordinates for all Block II bladerows.

Block II test results are presented in Section 4.5.2 of this report.

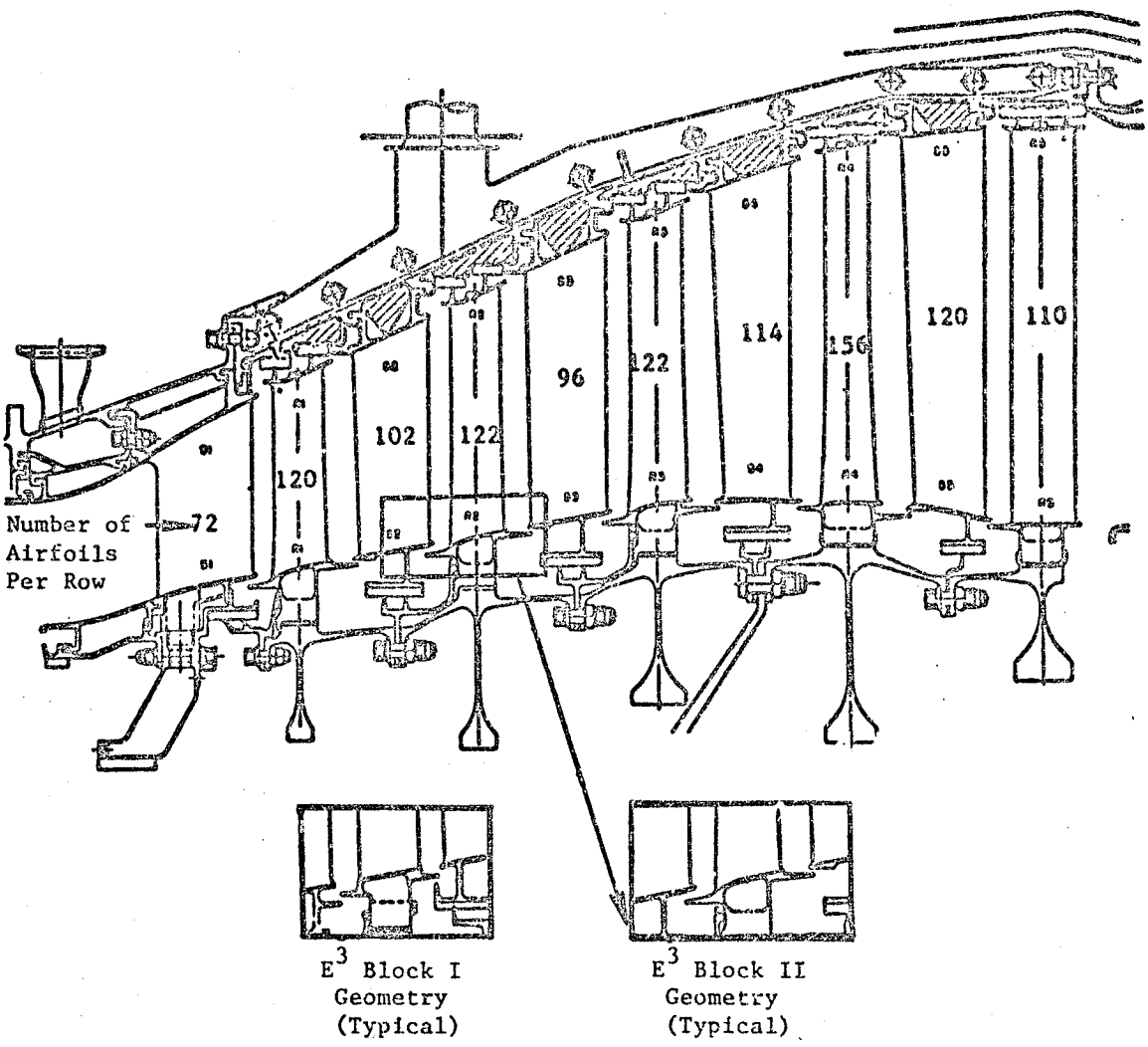

Figure 7. LP Turbine Flowpath Final for Block II and ICLS.

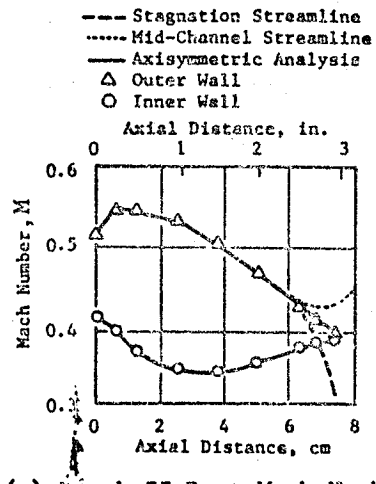

(a) Block II Duct Mach Number

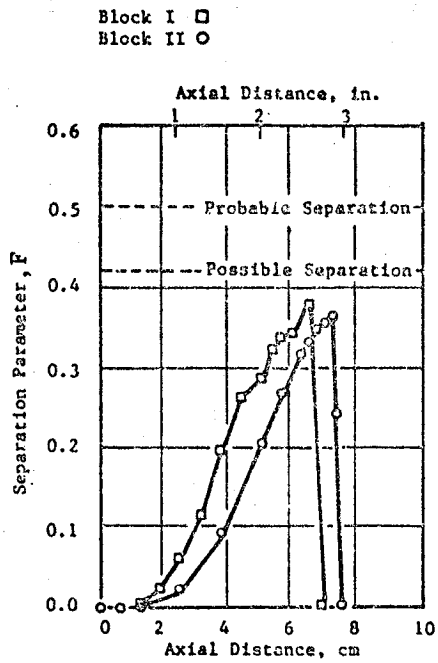

(b) Outer Wall Separation Parameter Comparison

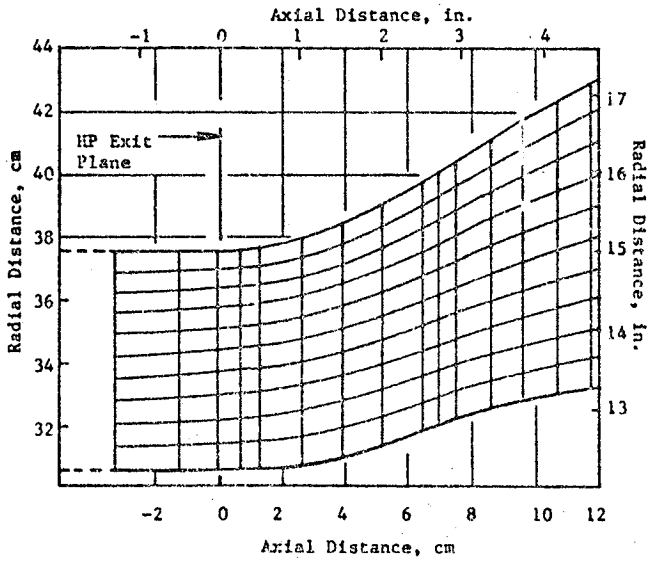

(c) Block II Flowpath Streamlines

Figure 8. Axisymmetric Flow Analysis of Stage 1 Vane Including Outer Wall Separation Sensitivities.

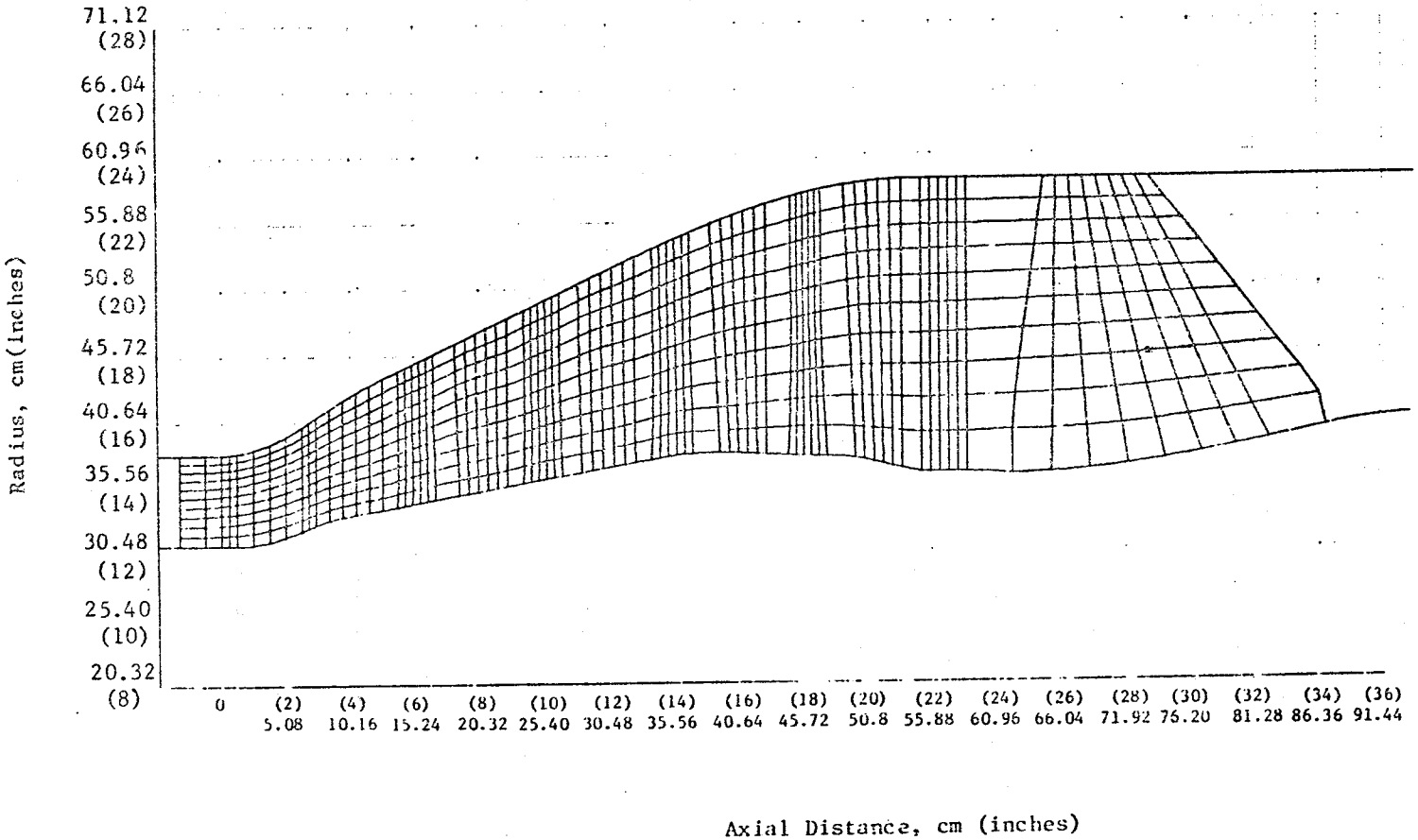

Figure 9. E^3 ICLS (Block II) LP Turbine Axisymmetric Calculation Model

Table IV. Final LPT Vector Diagram Summary (Block II and ICLS).

	Stage 1			Stage 2			Stage 3			Stage 4			Stage 5		
Energy Extraction, Δh J/g (BTU/lb$_m$)	73.04 (31.4)			79.09 (34.0)			82.11 (35.3)			70.25 (30.2)			49.31 (21.2)		
Pressure Ratio, P_T/P_T	1.30			1.35			1.40			1.36			1.26		
Aero Loading, $\Delta h/2u^2$	1.71			1.58			1.43			1.13			0.80		
Flow Coefficient, V_x/u	1.25			1.08			1.04			0.98			1.07		
	H	P	T	H	P	T	H	P	T	H	P	T	H	P	T
Reaction	0.256	0.305	0.390	0.280	0.351	0.422	0.312	0.372	0.440	0.255	0.385	0.481	0.205	0.330	0.478
Stator Exit Angle, α_1 (degree)	53.7	61.0	50.0	55.8	64.1	62.9	56.3	64.8	63.7	56.2	62.3	59.7	55.4	56.0	48.5
Stator Exit Mach Number, M_1	0.660	0.633	0.550	0.669	0.625	0.553	0.711	0.641	0.538	0.686	0.593	0.490	0.575	0.531	0.452
Rotor Relative Inlet Angle, β_1 (degree)	43.0	47.9	35.7	44.5	49.3	37.0	44.7	47.8	31.1	44.3	40.0	10.0	40.5	24.2	-8.0
Rotor Relative Inlet Mach Number, M_{R_1}	0.485	0.430	0.368	0.475	0.407	0.330	0.508	0 397	0.290	0.474	0.344	0.253	0.365	0.323	0.305
Rotor Relative Exit Angle, β_2 (degrees)	55.6	61.3	60.0	55.8	63.8	62.8	55.7	63.6	62.7	55.4	60.5	58.2	48.5	50.0	48.4
Rotor Relative Exit Mach Number, M_{R_1}	0.600	0.601	0.572	0.619	0.623	0.585	0.670	0.646	0.564	0.619	0.600	0.544	0.464	0.503	0.542
Stage Exit Swirl, degrees	41.2	47.6	37.0	40.0	49.1	36.8	39.7	47.7	31.0	36.5	37.0	16.5	20.0	12.5	3.0
Stage Exit Axial Mach Number	0.335	0.261	0.303	0.349	0.255	0.283	0.400	0.261	0.257	0.364	0.280	0.291	0.302	0.319	0.385

Table V. Final LPT Blading Average Solidity and Aspect Ratio Tabulations.

Blade Row	S1	R1	S2	R2	S3	R3	S4	R4	S5	R5
AW/t	1.55	1.33	1.44	1.26	1.47	1.24	1.46	1.23	1.48	1.30
ψ_z	0.606	1.094	0.924	1.069	0.884	1.065	0.966	1.079	0.984	1.023
TE Blockage	0.043	0.070	0.058	0.070	0.055	0.065	0.054	0.072	0.045	0.041
AR, h/do	5.96	11.04	10.51	13.93	12.13	15.61	14.51	20.82	13.87	12.80
AR, h/AW	1.92	4.02	3.27	5.02	3.64	5.74	4.77	8.62	5.41	6.36

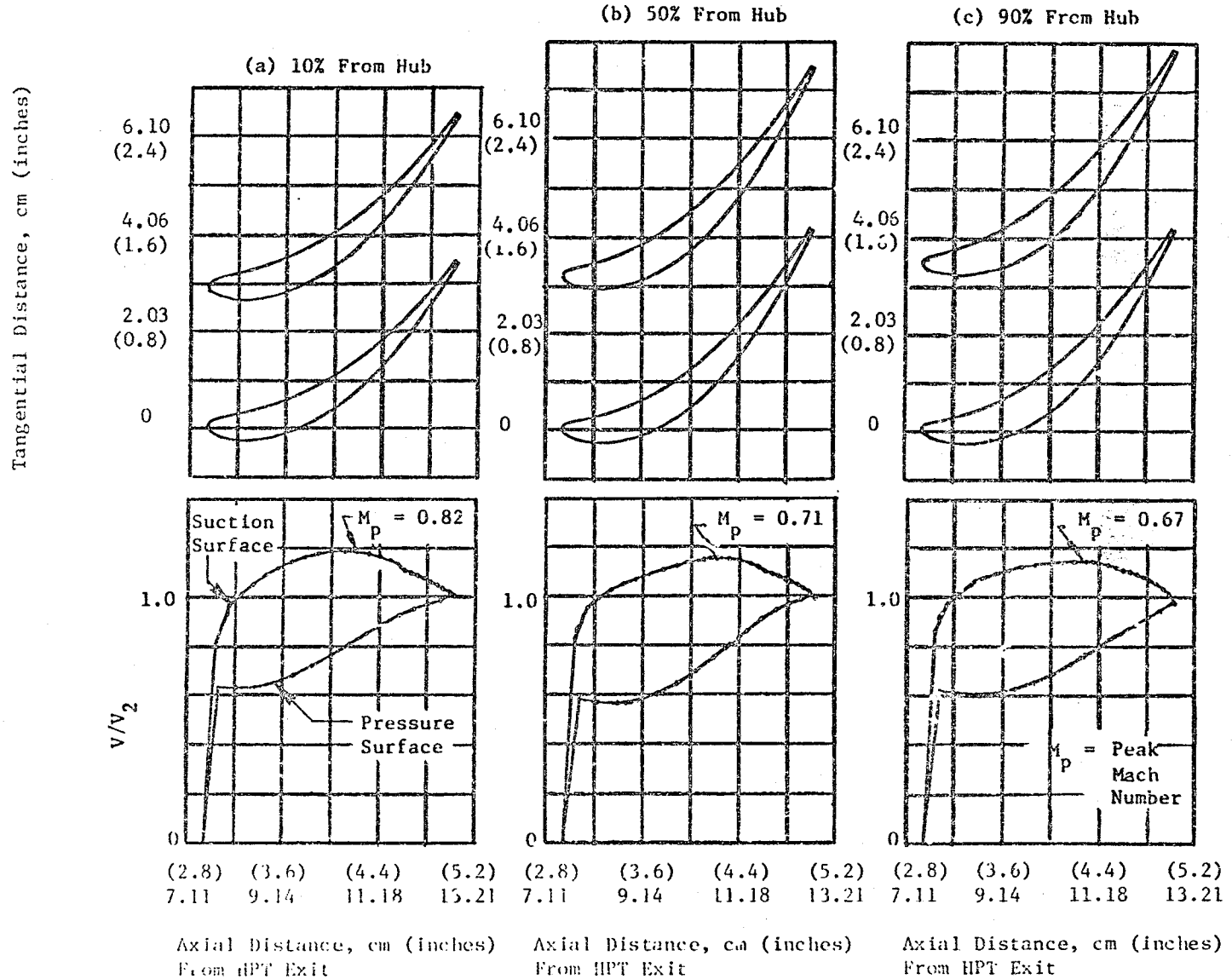

Figure 10. Block II Stage 1 Vane Shapes and Stream Surface Velocity Distributions

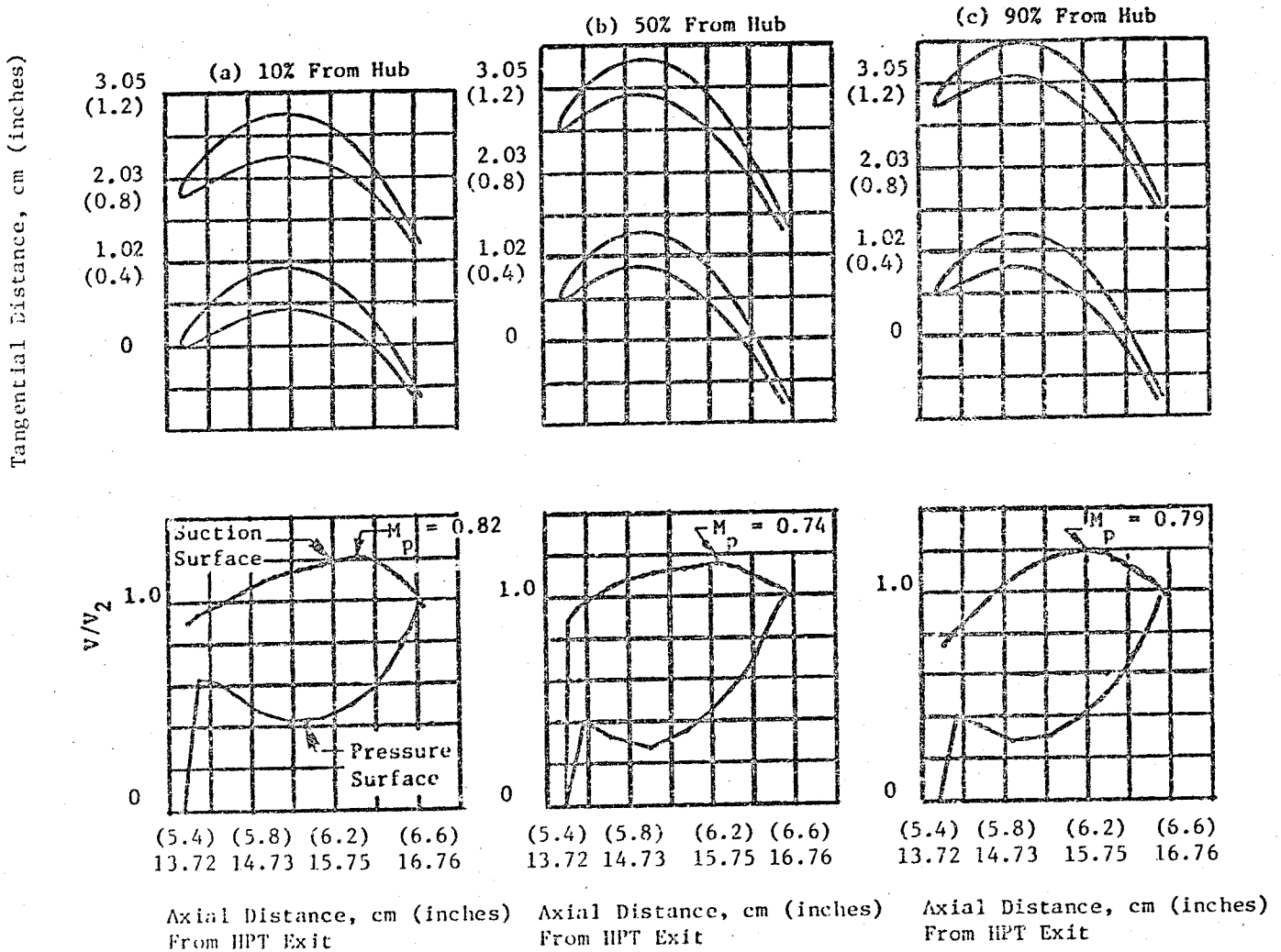

Figure 11. Block II Stage 1 Blade Shapes and Stream Surface Velocity Distributions

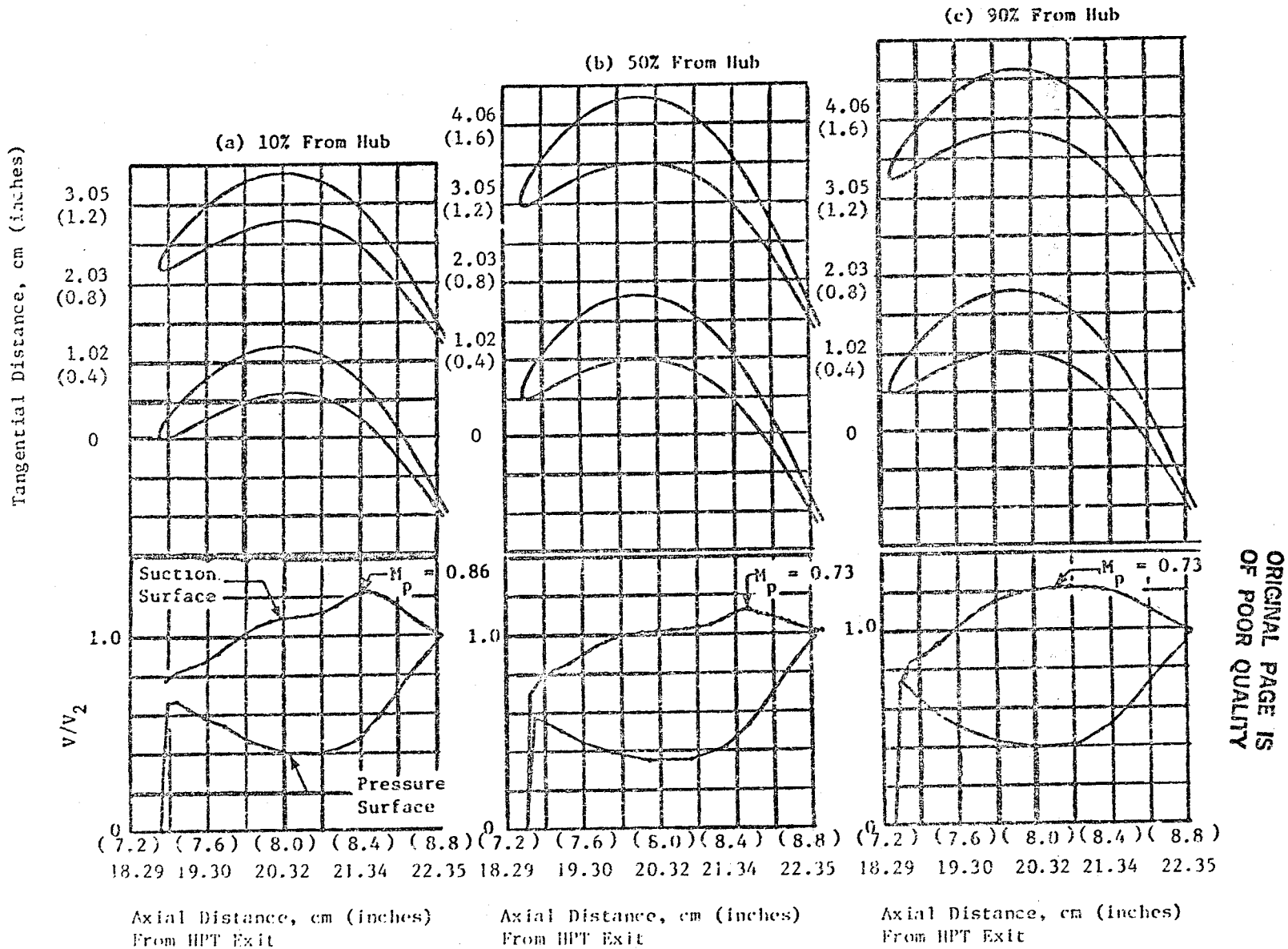

ORIGINAL PAGE IS OF POOR QUALITY

Figure 12. Block II Stage 2 Vane Shapes and Stream Surface Velocity Distributions

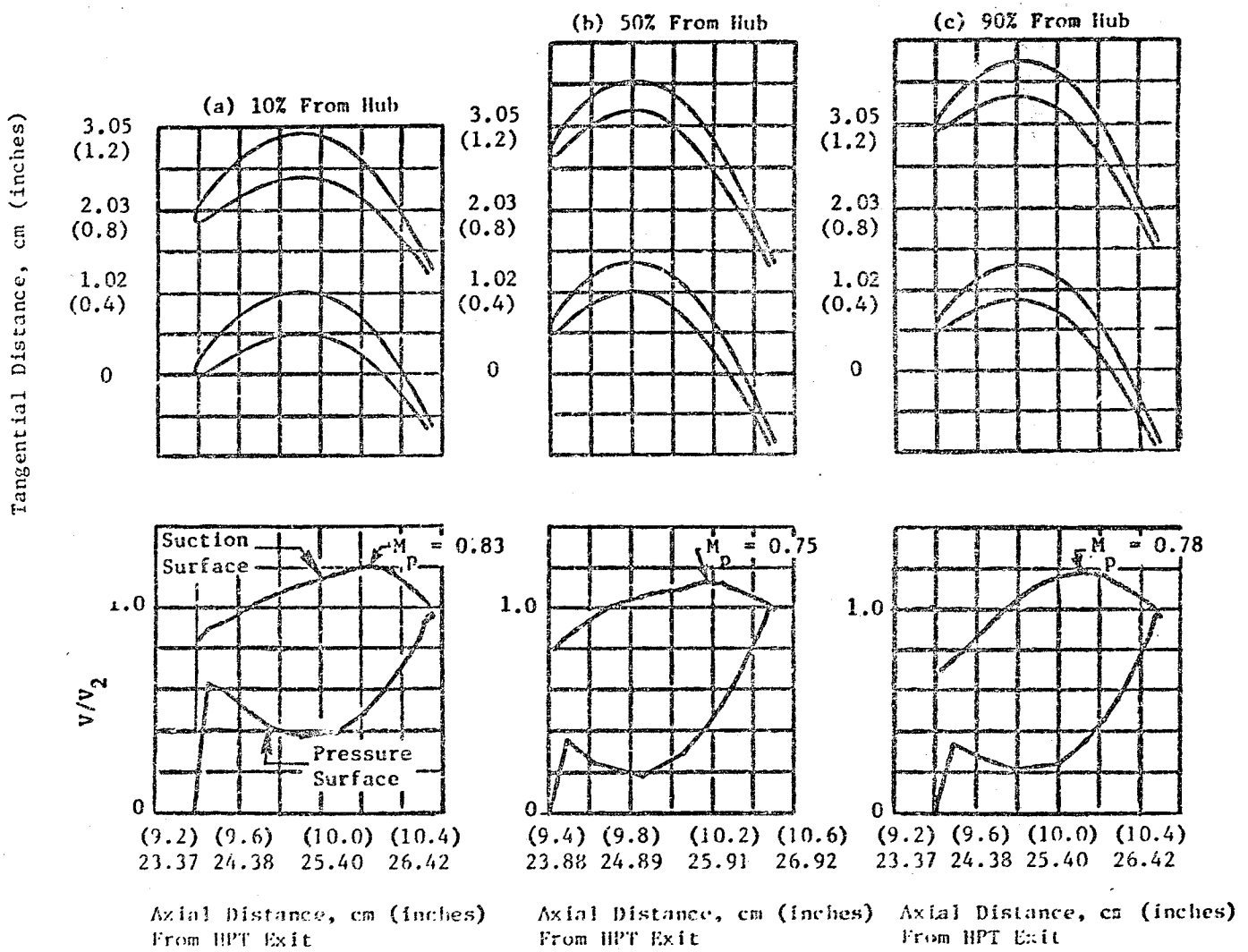

Figure 13. Block II Stage 2 Blade Shapes and Stream Surface Velocity Distributions

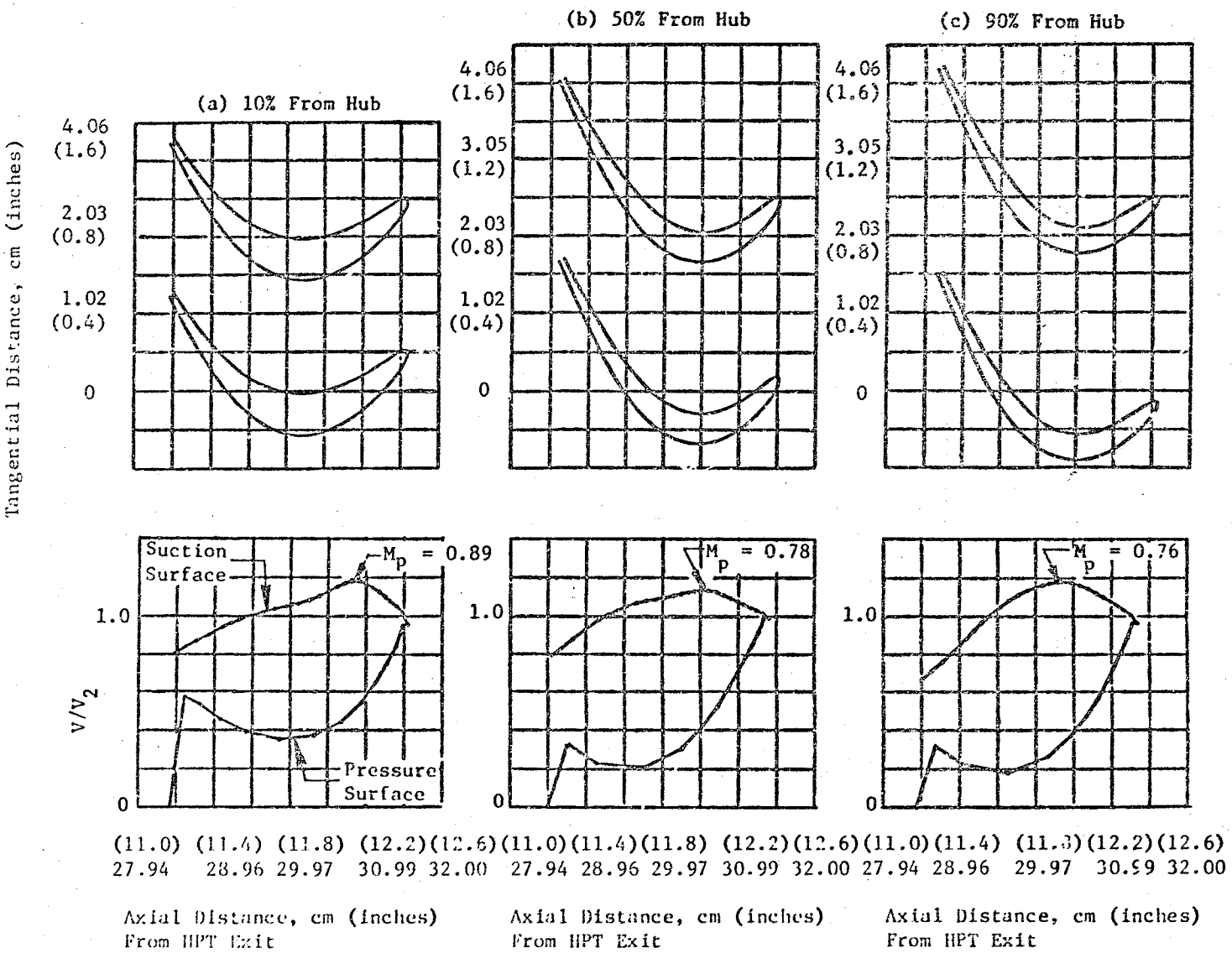

Figure 14. Block II Stage 3 Vane Shapes and Stream Surface Velocity Distributions

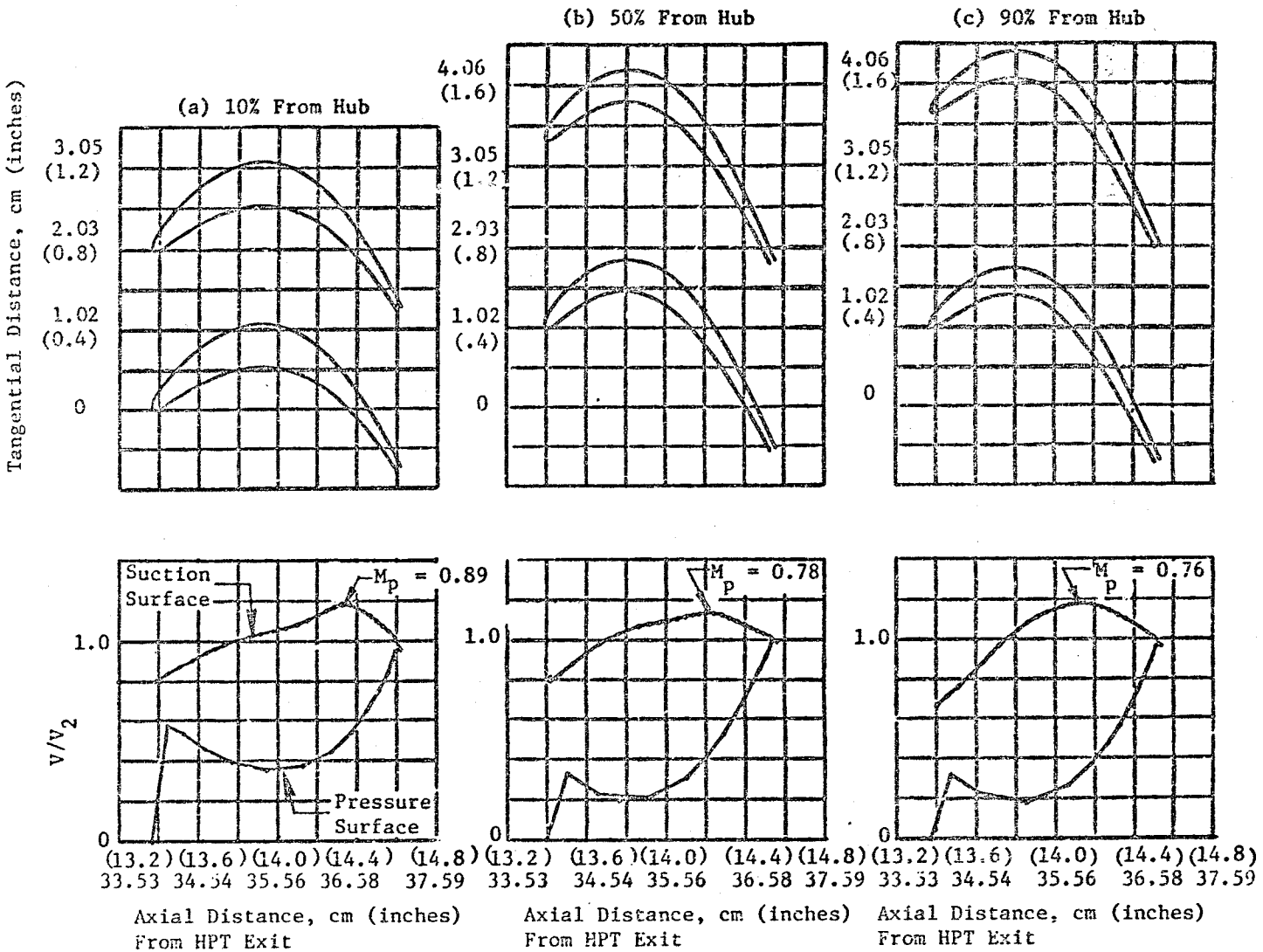

Figure 15. Block II Stage 3 Blade Shapes and Stream Surface Surface Velocity Distributions.

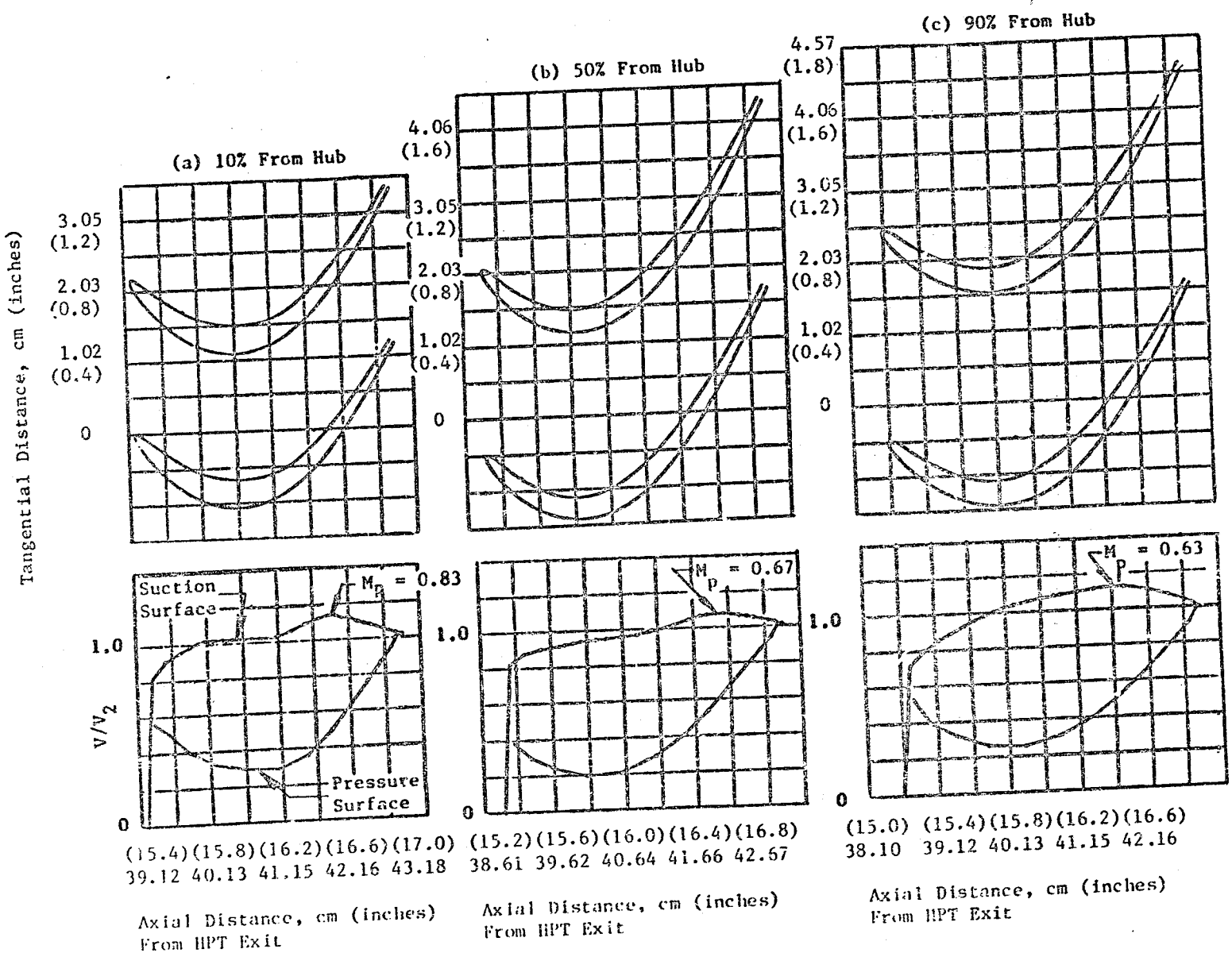

Figure 16. Block II Stage 4 Vane Shapes and Stream Surface Velocity Distributions

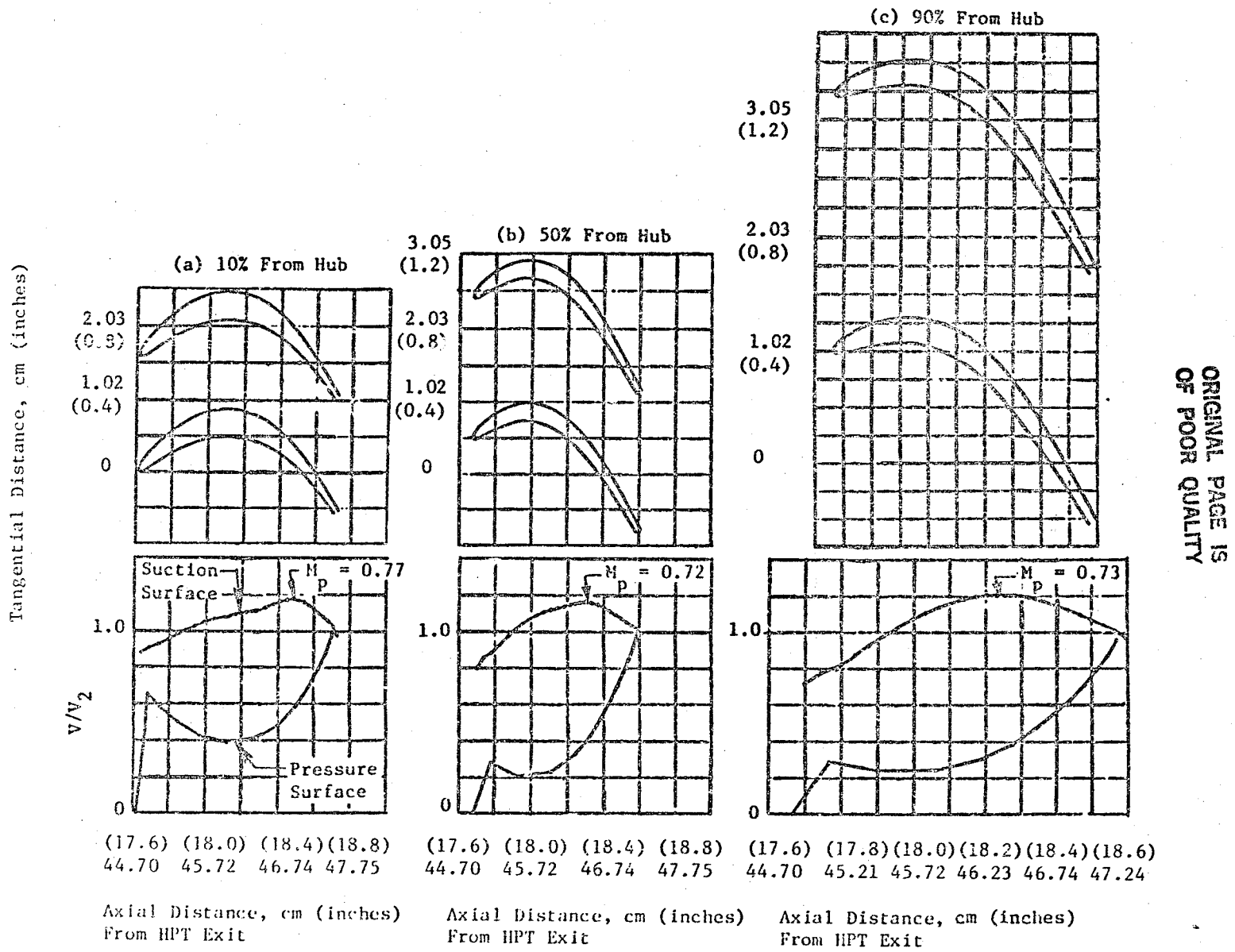

ORIGINAL PAGE IS OF POOR QUALITY

Figure 17. Block II Stage 4 Blade Shapes and Stream Surface Velocity Distrib...

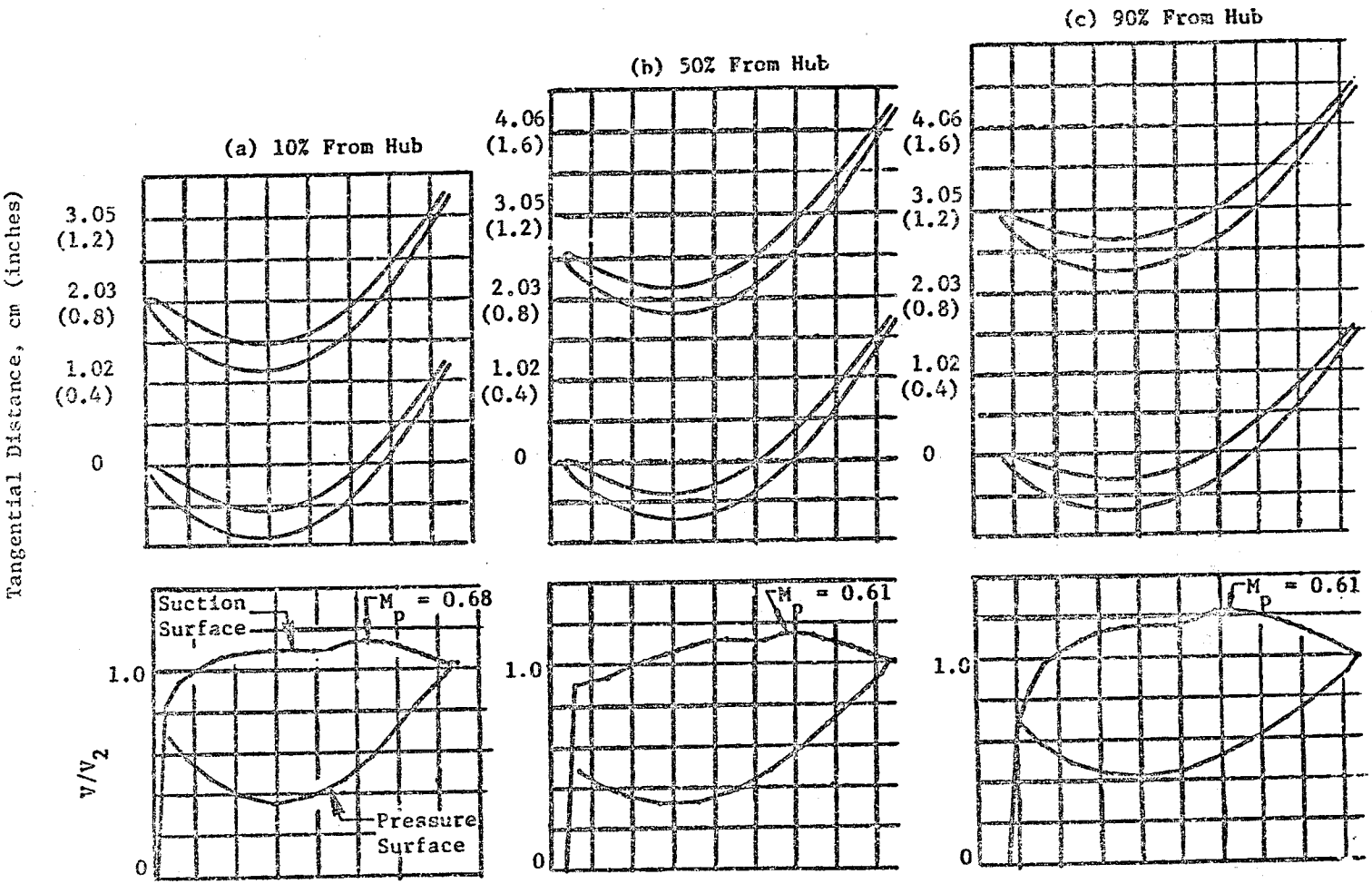

Figure 18. Block II Stage 5 Vane Shapes and Stream Surface Velocity Distributions

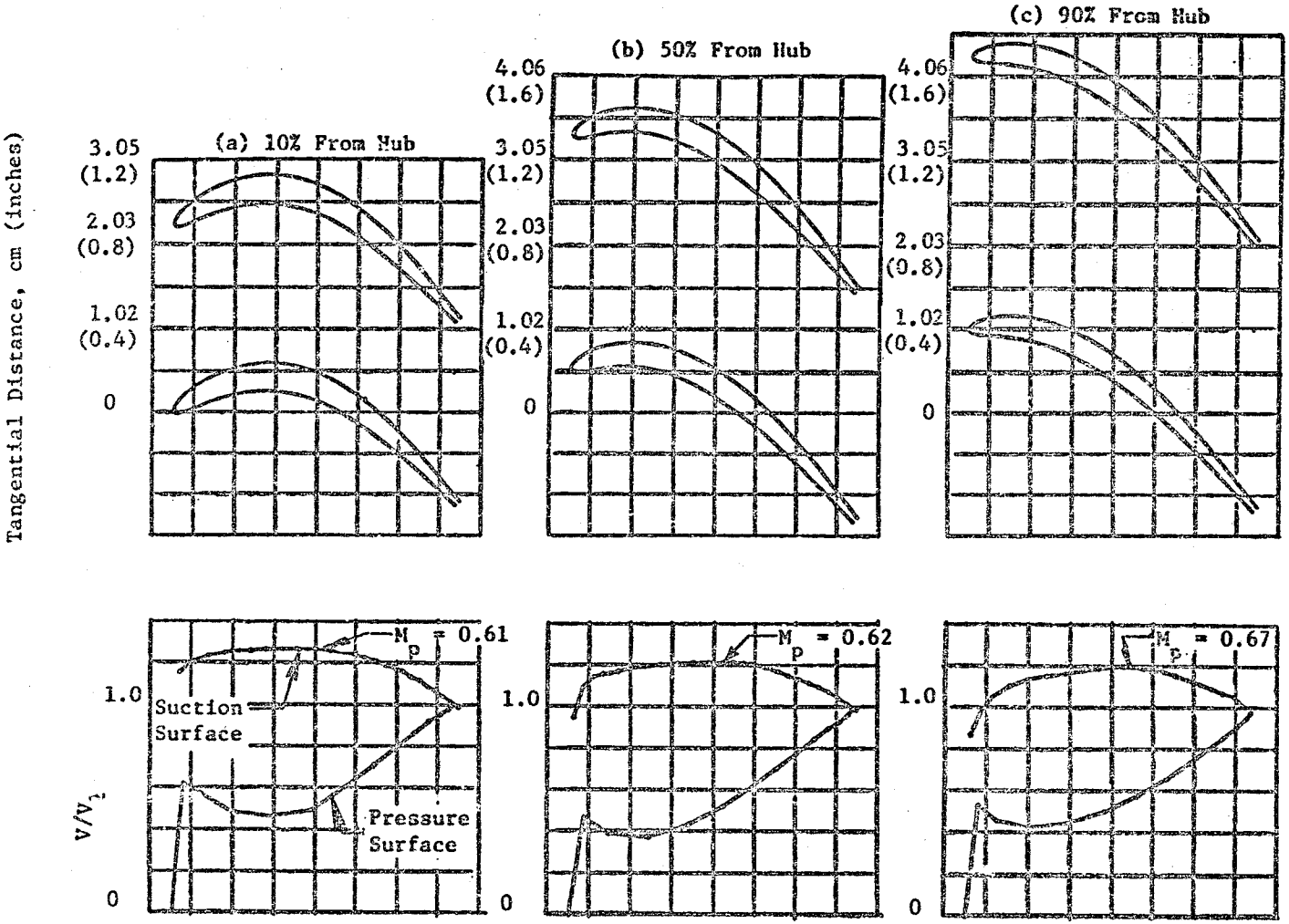

Figure 19. Block II Stage 5 Blade Shapes and Stream Surface Velocity Distributions

4.0 AERODYNAMIC EVALUATION

The basic objective of the air-turbine test program was to utilize the air-turbine facility, not simply to measure turbine efficiency, but to conduct an experimental program aimed at locating and reducing losses so that the required performance would ultimately be attained. In light of this objective, a building block approach was deemed most appropriate.

Since the HP to LP turbine transition duct and the first two stages of the low pressure turbine presented the most severe aerodynamic challenge, Block I testing was dedicated exclusively to the evaluation of those items.

Results of the Block I testing were factored into redesigns of the first two stages and were also reflected in the design of stages 3, 4, and 5. These designs, representing the final ICLS aero configuration, were then tested as Block II.

4.1 TEST VEHICLE

4.1.1 Vehicle Design

All rig flowpath and blading hardware was fabricated in stainless steel as a 0.67 scale of the engine configurations.

Scaling was required since neither test facility airflow capacity nor the existing rig frames were adequate for full-size testing. All flowpath diameters, airfoil shapes, axial gaps, and flowpath overlap geometry (i.e. axial and radial spacing between stator bands and rotor platforms or tip shrouds) were faithfully scaled from the engine turbine designs documented in Section 3.0.

All stage tests ran at a nominal 0.0254 cm (0.01 in.) radial clearance at design speed, thus preserving the relative clearance in the ICLS with active clearance control air on (estimated running clearance 0.0381 cm (0.015 in.)).

4.1.2 Configurations Tested

Block I

Evaluation of the transition duct and first two stages of the Block I LPT aero design was accomplished by consecutive testing of the following configurations:

Configuration	Description
1	Stage 1 Nozzle Annular Cascade
2	Stage 1 Rig
3	Stage 1 Rig with Stage 2 Nozzle Annular Cascade
4	Two-Stage Rig

Rig cross sections for the Block I configurations are shown in Figures 20 through 22. Pertinent dimensions for the flowpaths are presented in Appendix A.

Note that the transition duct is an integral part of the Stage 1 nozzle assembly and, consequently, all quoted performances include the duct pressure loss.

Block II

As discussed in Section 3.3, Block II consisted of redesigns of all four Block I bladerows, including the Stage 1 nozzle and transition duct (Figure 6), and new designs for Stages 3, 4, and 5. In order to evaluate the performance improvements relative to Block I and to establish the performance baseline for the five-stage (ICLS) turbine, the following configurations were tested as part of the Block II evaluation:

Configuration	Description
1a	Stage 1 Nozzle Annular Cascade (redesigned)
4a	Two-Stage Rig (redesigned)
5	Five-Stage Rig (final ICLS configuration)

Rig cross sections for Block II configurations 4a and 5 are shown in Figures 23 and 24.

The rig flowpath for Configuration 1a was identical to that for Configuration 1, Figure 20, except for the differences in transition duct and nozzle band contour and in airfoil count noted in Figure 6. Pertinent dimensions for the flowpaths are presented in Appendix A.

Photographs of the Block II hardware are presented in Appendix C.

4.1.3. Vehicle Instrumentation

Total pressure, total temperature, static pressure, and flow angle measurements were provided for the test vehicle (rig) as described in this section.

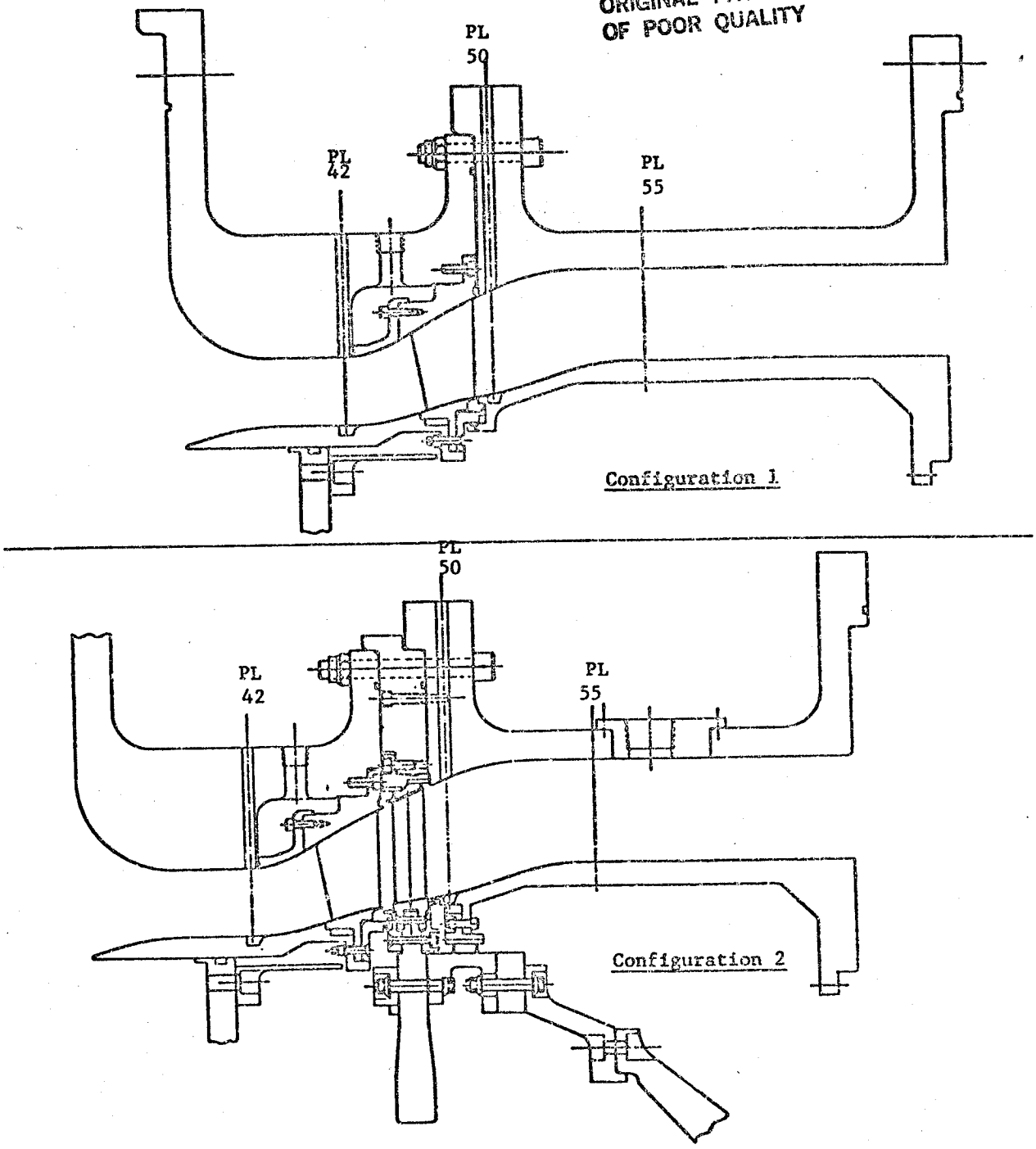

Figure 20. Block I Rig Assemblies - Configurations 1 and 2.

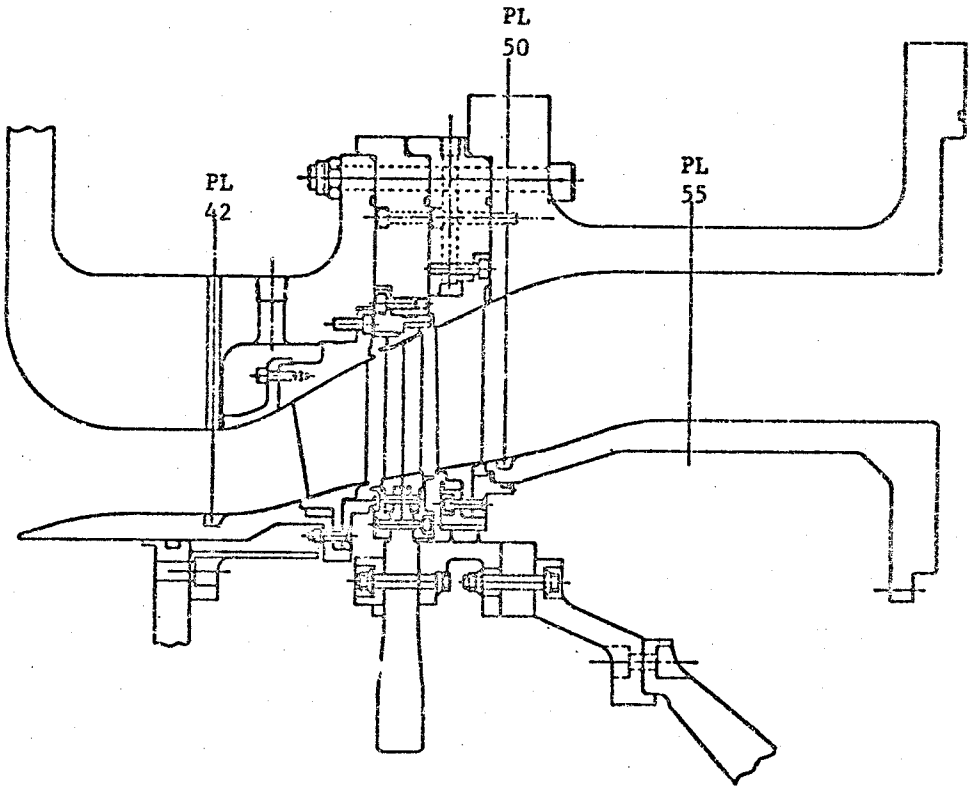

Figure 21. Block I Rig Assembly - Configuration 3.

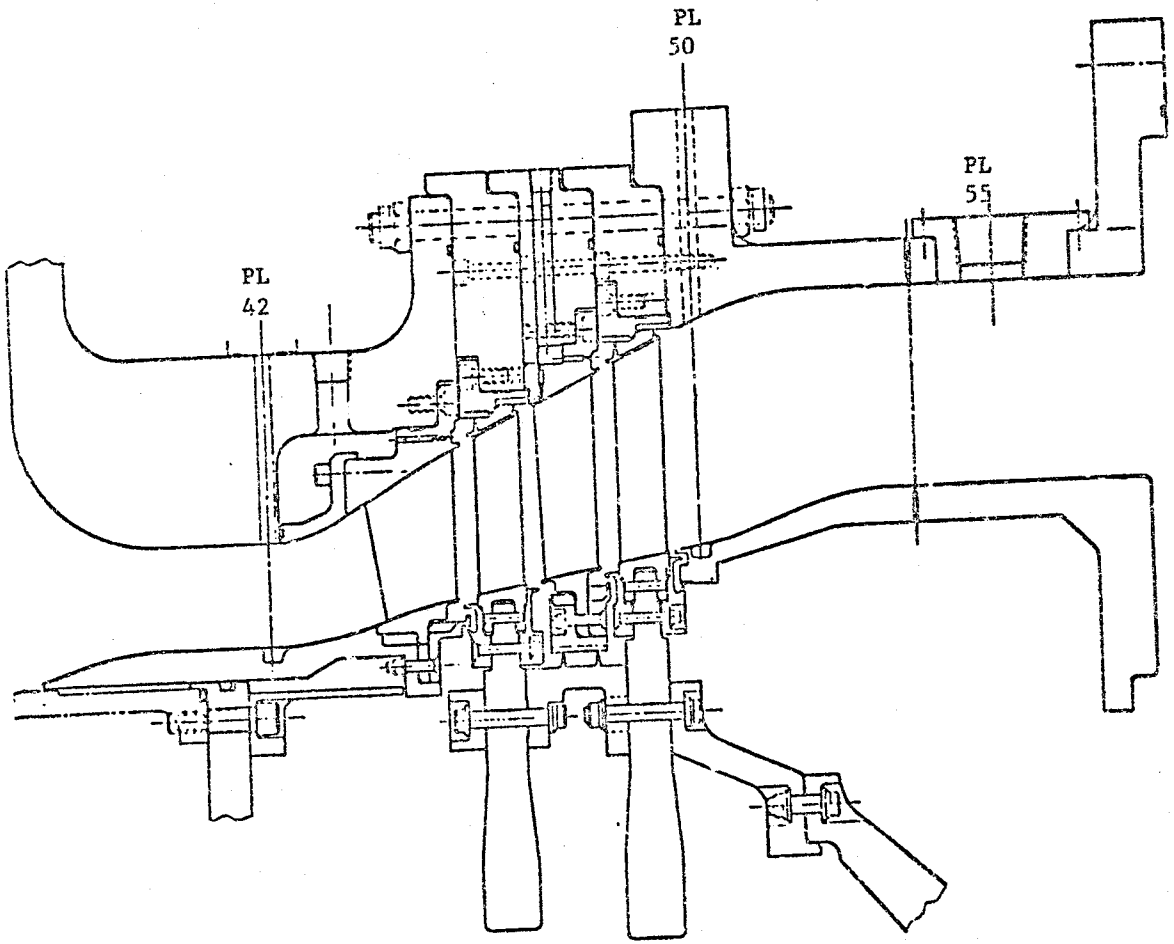

Figure 22. Block I Rig Assembly - Configuration 4.

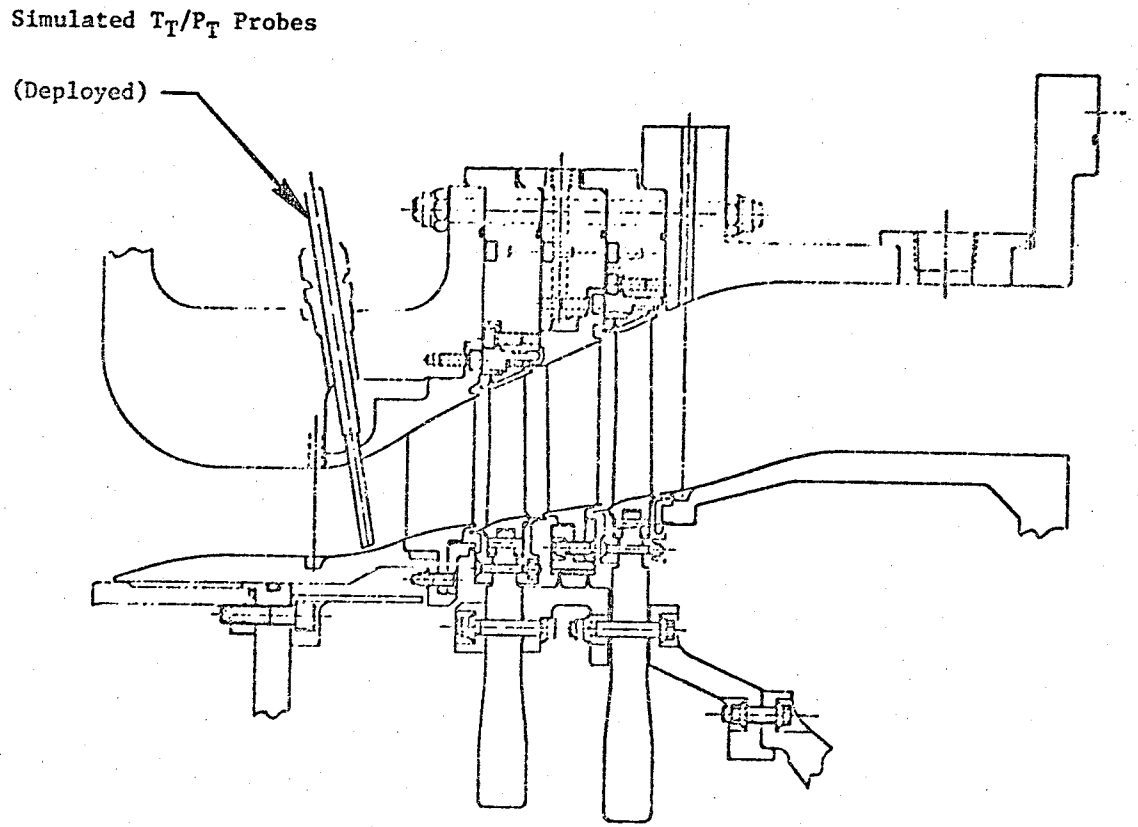

Figure 23. Block II Rig Assembly - Configuration 4a.

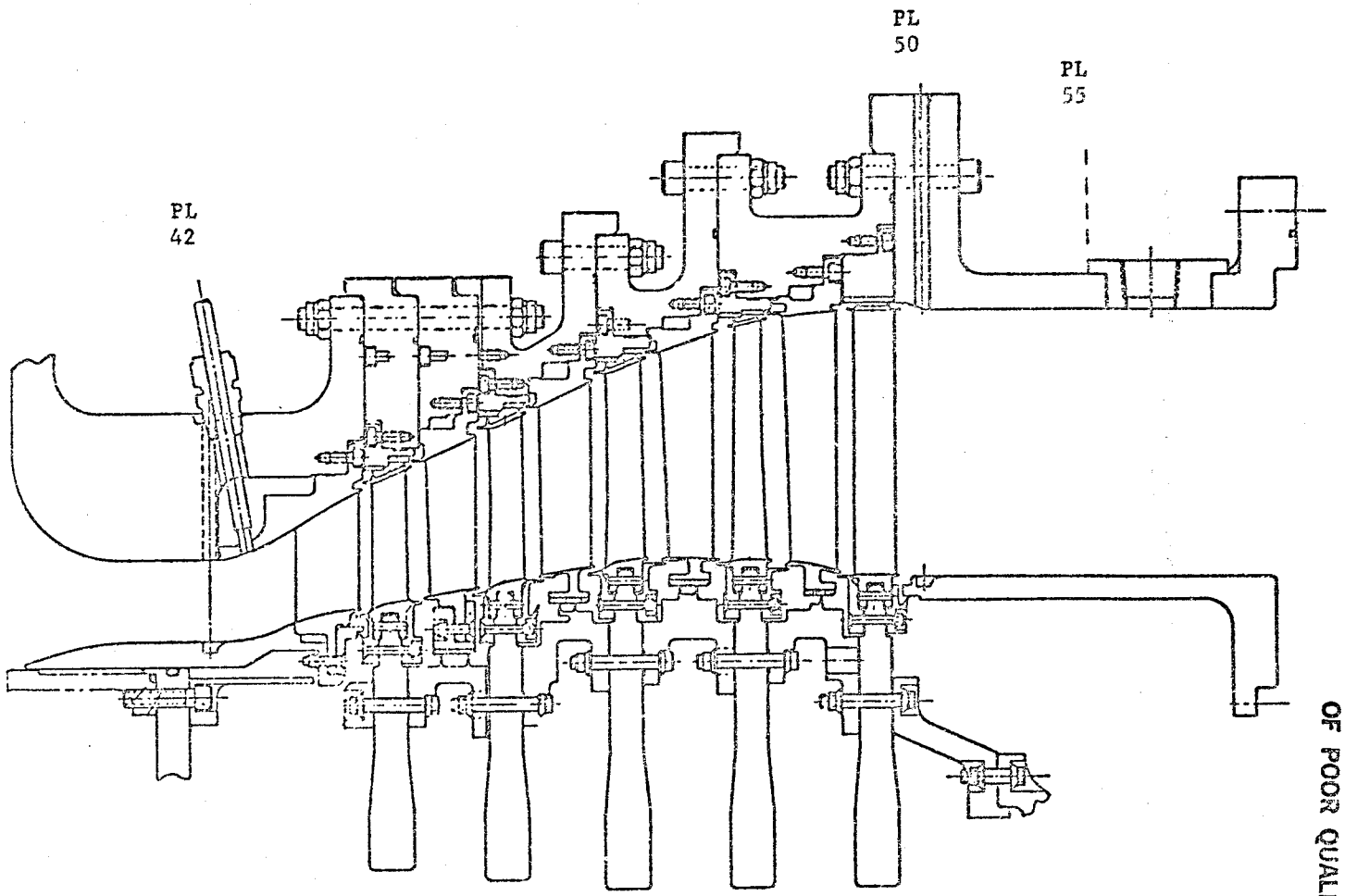

Figure 24. Block II Rig Assembly-Configuration 5.

Figures 25 thru 28 provide details of the instrumentation layouts for all four Block I configurations. Figure 29 is the instrumentation layout for the Block II five-stage vehicle. Instrumentation for Block II configurations 1a (annular cascade) and 4a (two-stage group) were the same as their Block I counterparts, except as noted in this section.

Note that each piece of instrumentation is assigned a three digit channel number to facilitate hookup. Rig instrumentation callout, referenced when applicable to the instrumentation drawings, follows. A tabulation of rig instrumentation is contained in Tables VI through X.

Plane 39 - Inlet Strut Frame

Temperature and pressure instrumentation were mounted on the leading edge of each of the ten inlet frame struts which were spaced 36° apart circumferentially and located approximately 38.1 cm (15. in.) upstream of the first stage stator. Temperature was measured with 25 chromel alumel thermocouples mounted in high recovery stagnation tubes affixed to five of the struts (72° apart). The thermocouples were grouped five to a strut and located radially at the area center of five equal annular areas. The temperatures at this station were used for turbine inlet temperatures. Total pressure was measured by 25 Kiel type probes located on five alternate struts, also 72° apart, and located in an identical manner as the thermocouples. These pressures were measured independently by means of the scanner-transducer system and then arithmetically averaged in the data reduction program. They were also pneumatically averaged, using a specially designed averaging block, measuring an average output on a single pressure transducer.

Plane 42 - Duct Inlet Plane

Radial and circumferential surveys of total pressure, total temperature and flow angle were taken with a traversing combination probe to verify uniform flow conditions at the transition duct inlet plane. The probe circumferential travel surveyed the wake from at least one of the inlet struts. The traverse mechanism was removed after the configuration 1 test, and the slot was plugged.

Five static pressure taps, equally spaced circumferentially, monitored flow uniformity on both the inner and outer walls.

Intra-Duct

Two static pressure taps, equally spaced circumferentially, were located at each of five equi-distant axial stations on both the inner and outer walls of the transition duct to monitor wall Mach number distribution in this diffusing passage.

Plane 48 - Stage 1 Nozzle Inlet Plane

One boundary layer rake was installed on each wall at the duct exit/nozzle inlet plane to monitor the total pressure profile through the wall boundary

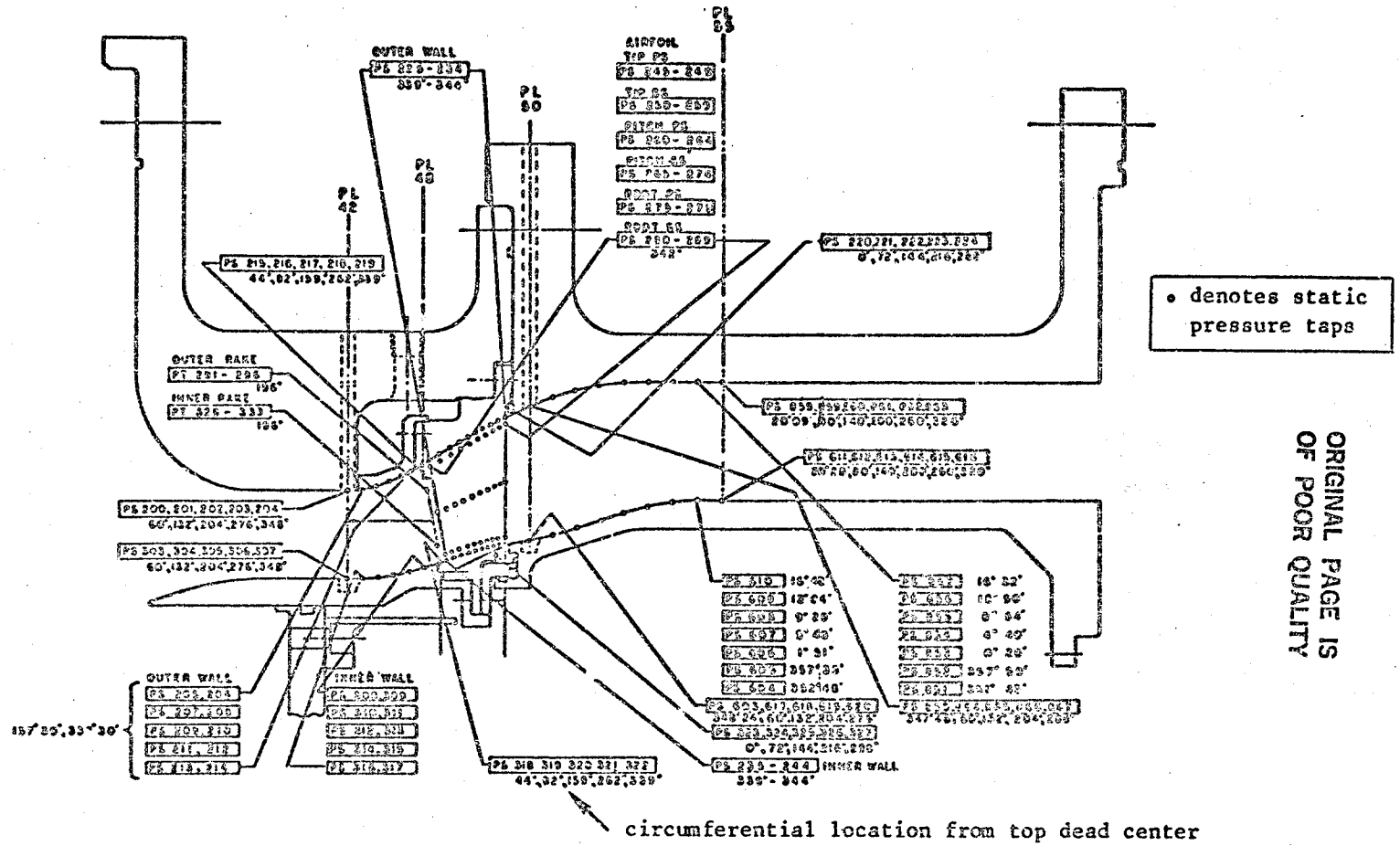

Figure 25. Block I Configuration 1 Instrumentation

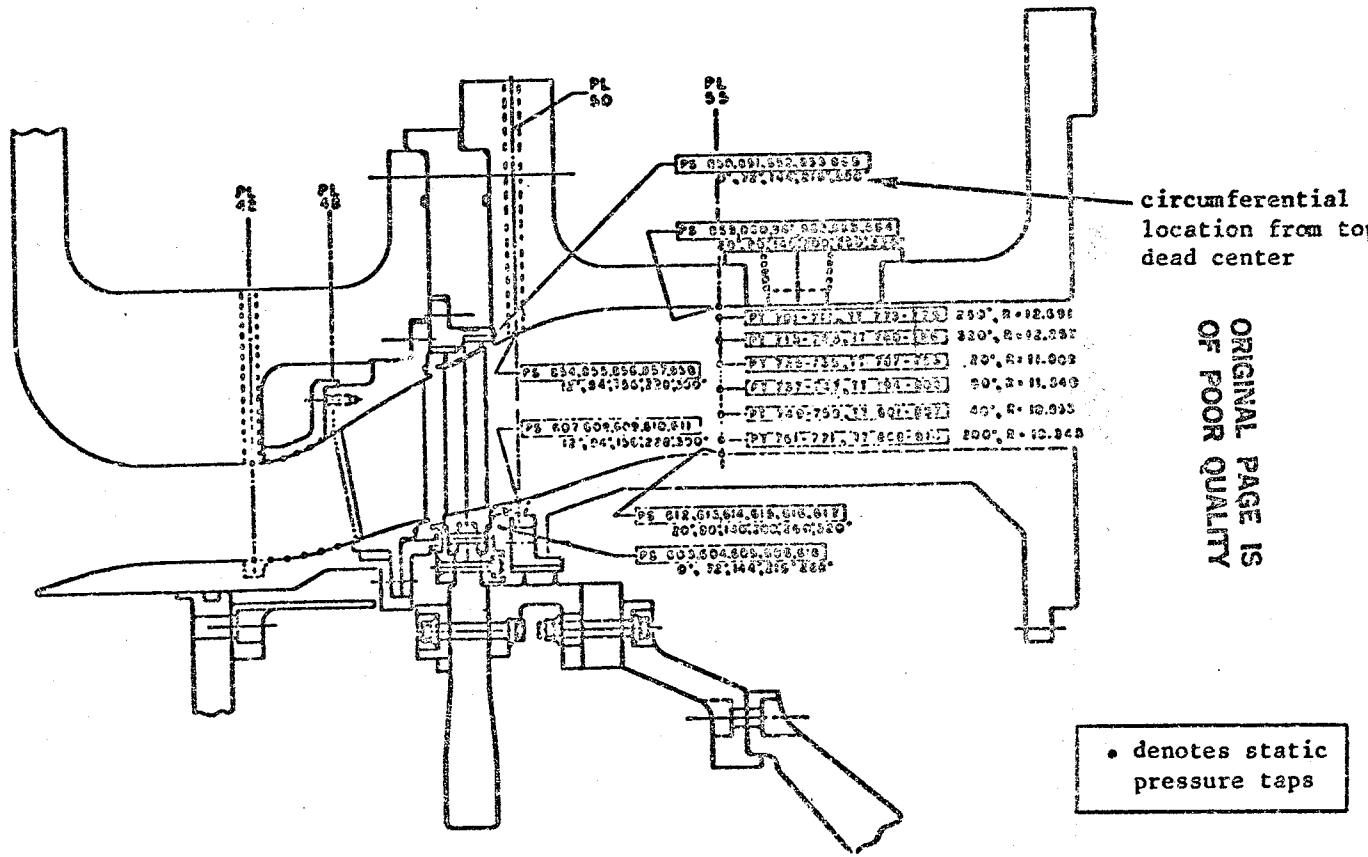

Figure 26. Block I Configuration 2 Instrumentation.

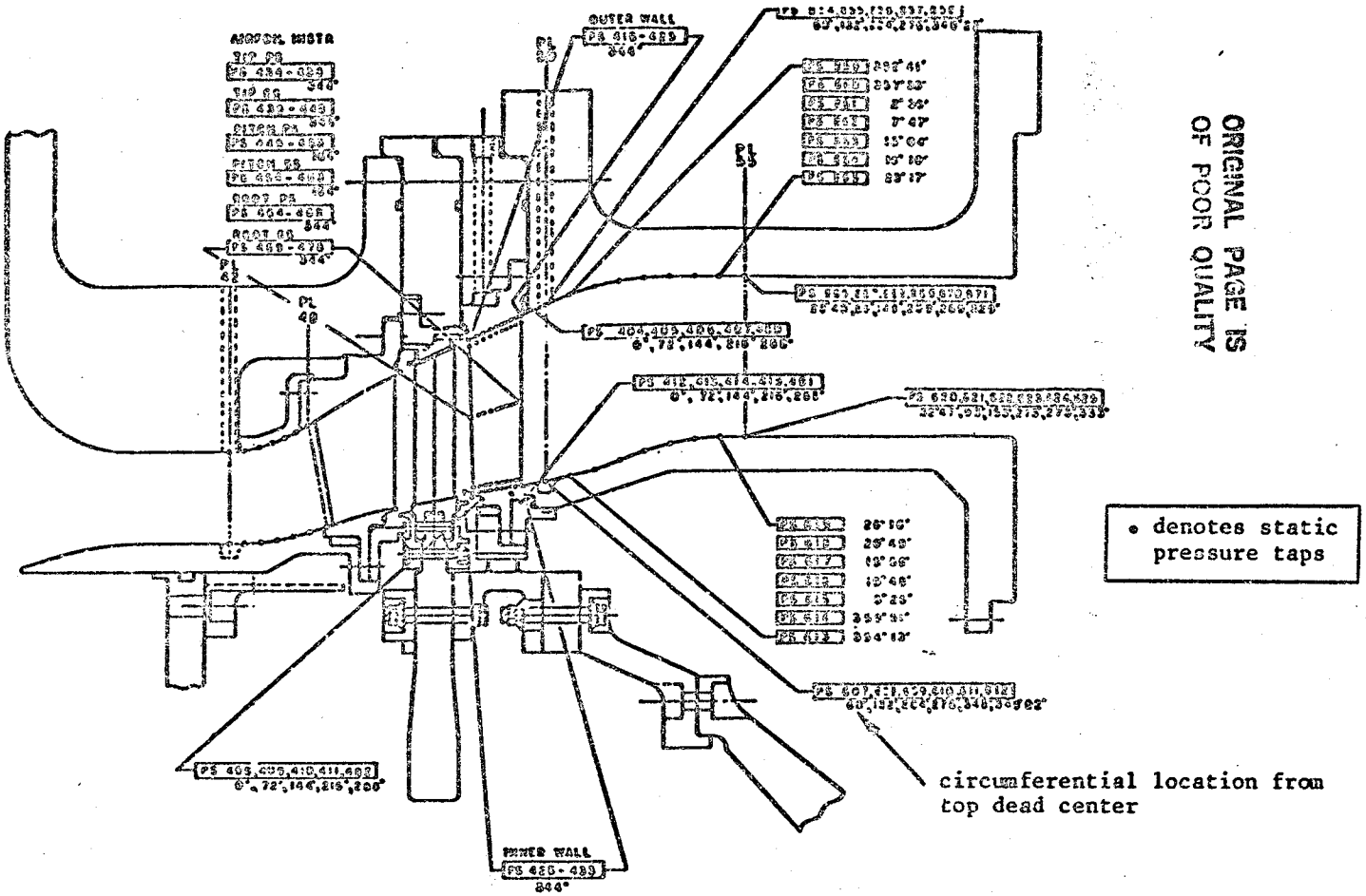

ORIGINAL PAGE IS
OF POOR QUALITY

Figure 27. Block I Configuration 3 Instrumentation.

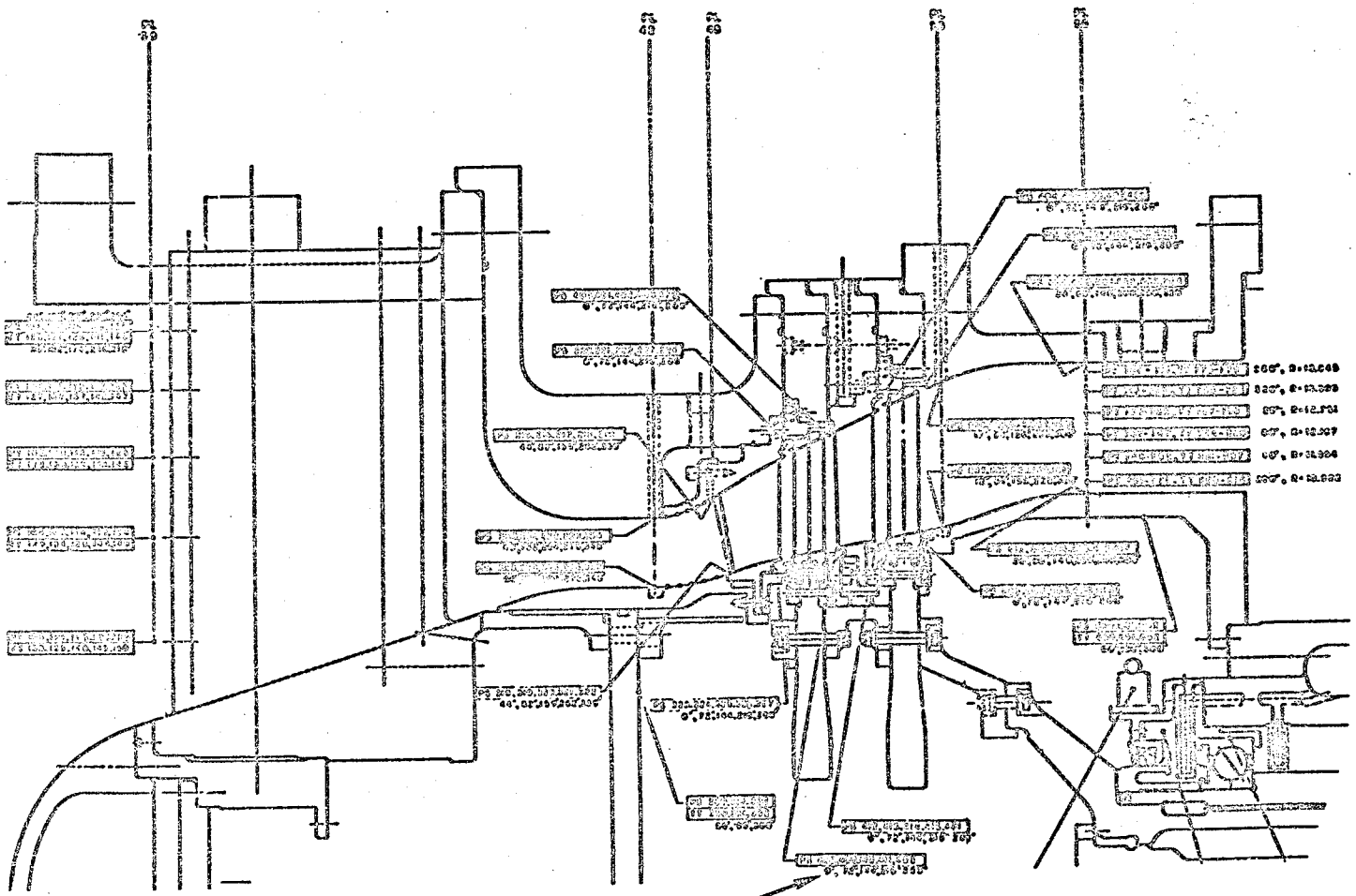

Figure 28. Block I Configuration 4 Instrumentation.

Figure 29. Block II Configuration 5 Instrumentation.

ORIGINAL PAGE IS
OF POOR QUALITY

Table VI. Block I Configuration 1 Instrumentation List

Type	Parameter	Number	Total	Item Numbers	Location
Fixed	Total Temperature	25	25	126-150	PL39 - Inlet Strut
	Total Pressure	25	37	101-125	PL39 - Inlet Strut
		6		291-296	PL48 - EL Rake, outer
		6		328-333	PL48 - El Rake, inner
	Static Pressure	5		200-204	PL42 - Duct Inlet, outer wall
		5		303-307	PL42 - Duct Inlet, inner wall
		10		205-214	Duct Wall, outer
		10		308-317	Duct Wall, inner
		5		125-219	PL48 - Nozzle Inlet, outer wall
		5		318-322	PL48 - Nozzle Inlet, inner wall
		10		225-234	Nozzle Band, outer
		10		235-244	Nozzle Band, inner
		45		245-289	Airfoil Surfaces
		5		220-224	Inter-Stage (Nozzle 1), tip
		5		323-327	Inter-Stage (Nozzle 1), hub
		5		850,864-867	PL50 - Traverse Plane, outer wall
		5		603,617-620	PL50 - Traverse Plane, inner wall
		7		851-857	Exhaust Casing, outer wall
		7		604-610	Exhaust Casing, inner wall
		6		858-863	PL55 - outer wall
		6	151	611-616	PL55 - inner wall
Traverse	Total Temperature Total Pressure Flow Angle				PL42 - Duct Inlet PL50 - Stator Exit

Table VII. Block I Configuration 2 Instrumentation List

Type	Parameter	Number	Total	Item Numbers	Location
Fixed	Total Temperature	25	67	126-150	FL39 - Inlet Strut
		42		772-814	FL55 - Stage Exit Arc Rakes
	Total Pressures	25	91	101-125	FL39 - Inlet Strut
		66		701-771 (not sequential)	FL55 - Stage Exit Arc Rakes
	Static Pressure	5	82	200-204	FL42 - Duct Inlet, outer wall
		5		303-307	FL42 - Duct Inlet, inner wall
		10		205-214	Duct Wall, outer
		10		308-317	Duct Wall, inner
		5		215-219	FL48 - Nozzle Inlet, outer wall
		5		318-322	FL48 - Nozzle Inlet, inner wall
		5		220-224	Inter-Stage (Nozzle 1), tip
		5		323-327	Inter-Stage (Nozzle 1), hub
		5		850-853,865	Inter-Stage (Rotor 1), tip
		5		603-606,618	Inter-Stage (Rotor 1), hub
		5		854-858	FL50 - Traverse Plane, outer wall
		5		607-611	FL50 - Traverse Plane, inner wall
		5		859-864	FL55 - Rake Plane, outer wall
		6		612-617	FL55 - Rake Plane, inner wall
		6			FL50 - Rotor Exit
Traverse	Total Temperature Total Pressure Flow Angle				

Table VIII. Block I Configuration 3 Instrumentation List

Type	Parameter	Number	Total	Item Numbers	Location
Fixed	Total Temperature	25	25	126-150	PL33 - Inlet Strut
	Total Pressure	25	25	101-125	PL39 - Inlet Strut
	Static Pressure	5		200-204	PL42 - Duct Inlet, outer wall
		5		303-307	PL42 - Duct Inlet, inner wall
		10		205-214	Duct Wall, outer
		10		308-317	Duct Wall, inner
		5		215-219	PL48 - Nozzle Inlet, outer wall
		5		318-322	PL48 - Nozzle Inlet, inner wall
		5		220-224	Inter-Stage (Nozzle 1), tip
		5		323-327	Inter-Stage (Nozzle 1), hub
		5		401-403,479	Inter-Stage (Rotor 1), tip
		5		408-411,482	Inter-Stage (Rotor 1), hub
		10		416-425	Nozzle Band (Stg 2), outer
		10		426-433	Nozzle Band (Stg 2), inner
		45		434-478	Airfoil Surfaces (Nozzle 2)
		5		404-407,480	Inter-Stage (Nozzle 2), tip
		5		412-415,481	Inter-Stage (Nozzle 2), hub
		5		854-858	PL50 - Traverse Plane, outer wall
		5		607-612	PL50 - Traverse Plane, inner wall
		7		859-865	Exhaust Casing, outer wall
		7		613-619	Exhaust Casing, inner wall
		6		866-871	PL55 - outer wall
		6	171	620-625	PL55 - inner wall
Traverse	Total Temperature Total Pressure Flow Angle				PL50 - Stator Exit

Table IX. Block I Configuration 4 Instrumentation List

Type	Parameter	Number	Total	Item Numbers	Location
Fixed	Total Temperature	25		126-150	FL39 - Inlet Strut
		42	67	773-814	FL55 - Stage Exit Arc Rakes
	Total Pressures	25		101-125	FL39 - Inlet Strut
		66	91	701-771 (not sequential)	FL55 - Stage Exit Arc Rakes
	Static Pressure	5		200-204	FL42 - Duct Inlet, outer wall
		5		303-307	FL42 - Duct Inlet, inner wall
		10		205-214	Duct Wall, outer
		10		308-317	Duct Wall, inner
		5		215-219	FL48 - Nozzle Inlet, outer wall
		5		318-322	FL48 - Nozzle Inlet, inner wall
		5		220-224	Inter-Stage (Nozzle 1), tip
		5		323-327	Inter-Stage (Nozzle 1), hub
		5		401-403,479	Inter-Stage (Rotor 1), tip
		5		408-411,482	Inter-Stage (Rotor 1), hub
		5		404-407,480	Inter-Stage (Nozzle 2), tip
		5		412-415,481	Inter-Stage (Nozzle 2), hub
		5		850-853,865	Inter-Stage (Rotor 2), tip
		5		603-606,618	Inter-Stage (Rotor 2), hub
		5		854-858	FL50 - Traverse Plane, outer wall
		5		607-611	FL50 - Traverse Plane, inner wall
		5		859-864	FL55 - Rake Plane, outer wall
		6		612-617	FL55 - Rake Plane, inner wall
		6	102		
Traverse	Total Temperature Total Pressure Flow Angle				FL50 - Rotor Exit

Table X. Block II Configuration 5 Instrumentation List

TYPE	PARAMETER	NUMBER	TOTAL	ITEM NUMBERS	LOCATION
Fixed	Total Temperature	25		126-150	PL39 - Inlet Strut
		42	67	773-814	PL55 - Stage Exit Arc Rakes
	Total Pressures	25		101-125	PL39 - Inlet Strut
		6		291-296	PL40 - Outer B.L. Rake
		6		328-333	PL48 - Inner B.L. Rake
		66	103	701-771 (not sequential)	PL55 - Stage Exit Arc Rakes
	Static Pressure	5		200-204	PL42 - Duct Inlet, outer wall
		5		303-307	PL42 - Duct Inlet, inner wall
		10		205-214	Duct Wall, outer
		10		308-317	Duct Wall, inner
		5		215-219	PL48 - Nozzle Inlet, outer wall
		5		318-322	PL48 - Nozzle Inlet, inner wall
		5		220-224	Inter-Stage (Nozzle 1), tip
		5		323-327	Inter-Stage (Nozzle 1), hub
		5		401-403,479	Inter-Stage (Rotor 1), tip
		5		408-411,482	Inter-Stage (Rotor 1), hub
		5		404-407,480	Inter-Stage (Nozzle 2), tip
		5		412-415,481	Inter-Stage (Nozzle 2), hub
		5		491-495	Inter-Stage (Rotor 2), tip
		5		496-500	Inter-Stage (Rotor 2), hub
		5		501-505	Inter-Stage (Nozzle 3), tip
		5		506-510	Inter-Stage (Nozzle 3), hub
		5		511-515	Inter-Stage (Rotor 3), tip
		5		516-520	Inter-Stage (Rotor 3), hub
		5		521-525	Inter-Stage (Nozzle 4), tip
		5		526-530	Inter-Stage (Nozzle 4), hub
		5		531-535	Inter-Stage (Rotor 4), tip
		5		536-540	Inter-Stage (Rotor 4), hub
		5		541-545	Inter-Stage (Nozzle 5), tip
		5		546-550	Inter-Stage (Nozzle 5), hub
		5		850-853,865	Inter-Stage (Rotor 5), tip
		5		603-606,618	Inter-Stage (Rotor 5), hub
		5		854-858	PL50 - Traverse Plane, outer wall
		5		607-611	PL50 - Traverse Plane, inner wall
		6		859-864	PL55 - Rake Plane, outer wall
		6	162	612-617	PL55 - Rake Plane, inner wall
Traverse	Total Temperature Total Pressure Flow Angle				PL50 - Rotor Exit

layers. Figures 31 and 32 present two views of one of the rakes, which were present for tests of the Stage 1 nozzle cascades only.

Five static pressure taps were located in the same plane as the boundary layer rake leading edges on both inner and outer walls, with one tap aligned circumferentially with the duct wall taps. There was some deviation from equal circumferential spacing for these five taps since each was centered between adjacent nozzle leading edges.

Intra-Vane (Stage 1 and 2 Nozzles)

In order to verify the inviscid cascade analyses for the Block I Stage 1 and Stage 2 vane airfoils, fifteen surface static pressure taps were installed along each of three streamsurfaces corresponding approximately to hub, pitch, and tip sections. Ten of the fifteen were on each of the suction surfaces, with remaining five on the pressure surfaces.

In the Block II tests, only the stage 1 vane airfoil was instrumented.

Appendix B presents streamsurface coordinates for each of the instrumentated sections. Location of the static pressure taps on the airfoil surfaces are noted on Figures 44, 67, and 91 along with the data.

Ten static pressure taps were located along the mid-channel streamline on the inner and on the outer bands to monitor wall pressure distributions. The wall taps for the Block I and Block II stage 1 vanes were in a continuous line behind one set of transition duct wall taps and the stator leading edge tap, thus providing a continuous survey of wall pressures from the duct inlet to the vane 1 exit plane.

Inter-Stage

Five static pressure taps, equally spaced circumferentially, were installed approximately in the leading and trailing edge planes of each vane assembly (actual location was in the shroud/wheel-space cavities on the inner and outer band flanges) and on the forward edges of the inner and outer exhaust casings. These taps allowed the measurement of what are, based on past GE rig test experience, very good approximations to the rotor inlet and exit static pressures.

Plane 50 - Stator/Rotor Exit Traverse Planes

Detailed radial and circumferential traverse surveys were conducted at an axial plane just downstream of the trailing edge of the last blade row in each of the configurations to measure absolute levels of total temperature, total pressure, and flow angle. A combination probe similar to that shown in Figure 30 was used. A fast response pressure differential servosystem was used to align the probe with the flow and provide an electrical output proportional to the flow angle. Total temperature, total pressure, and flow angle was recorded on an X-Y chart for in-cell inspection and, simultaneously, on a computer file for automatic mass averaging and contour plotting.

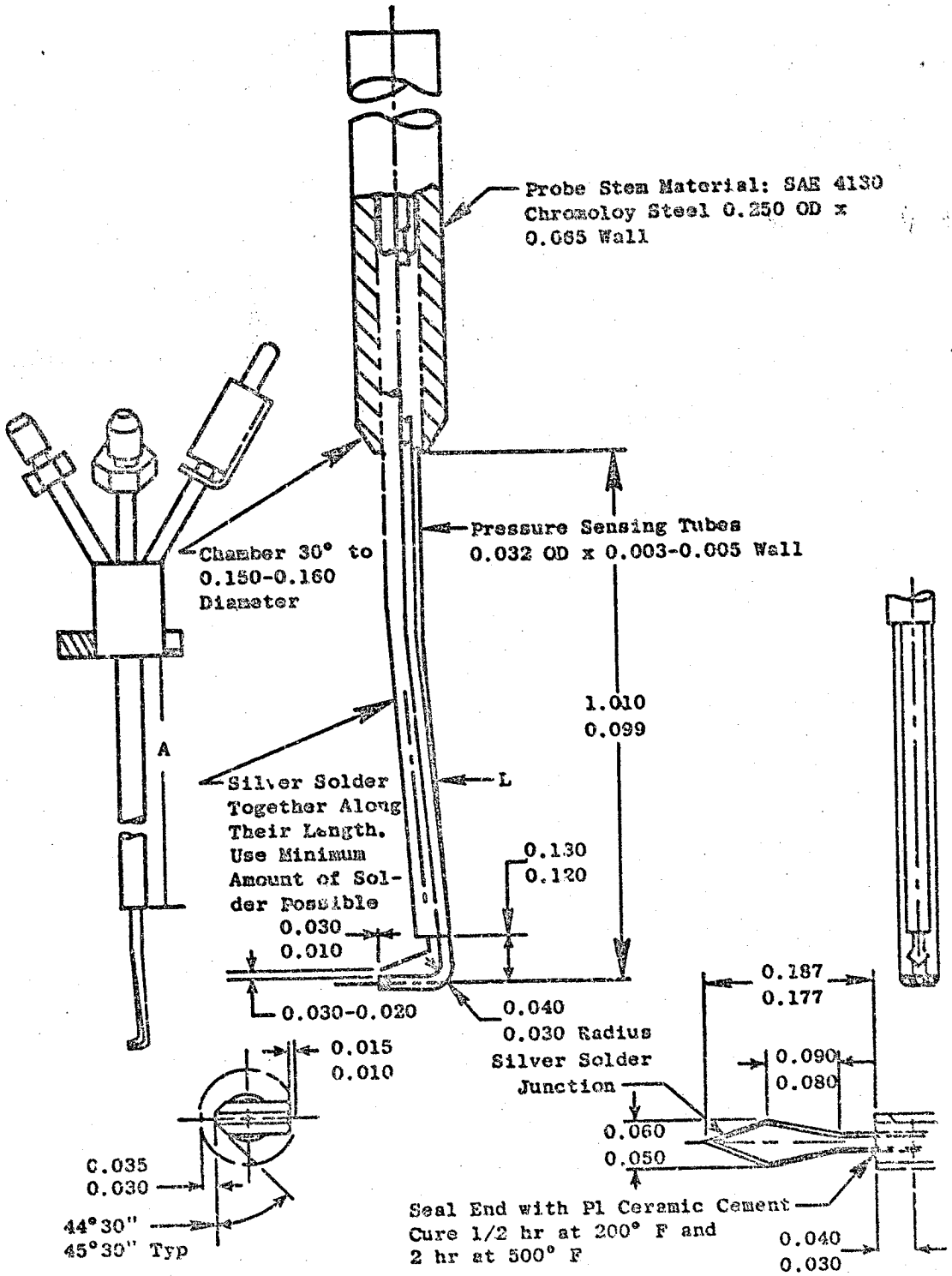

Figure 30. Details of Plane 50 Combination (Cobra) Traverse Probe Construction.

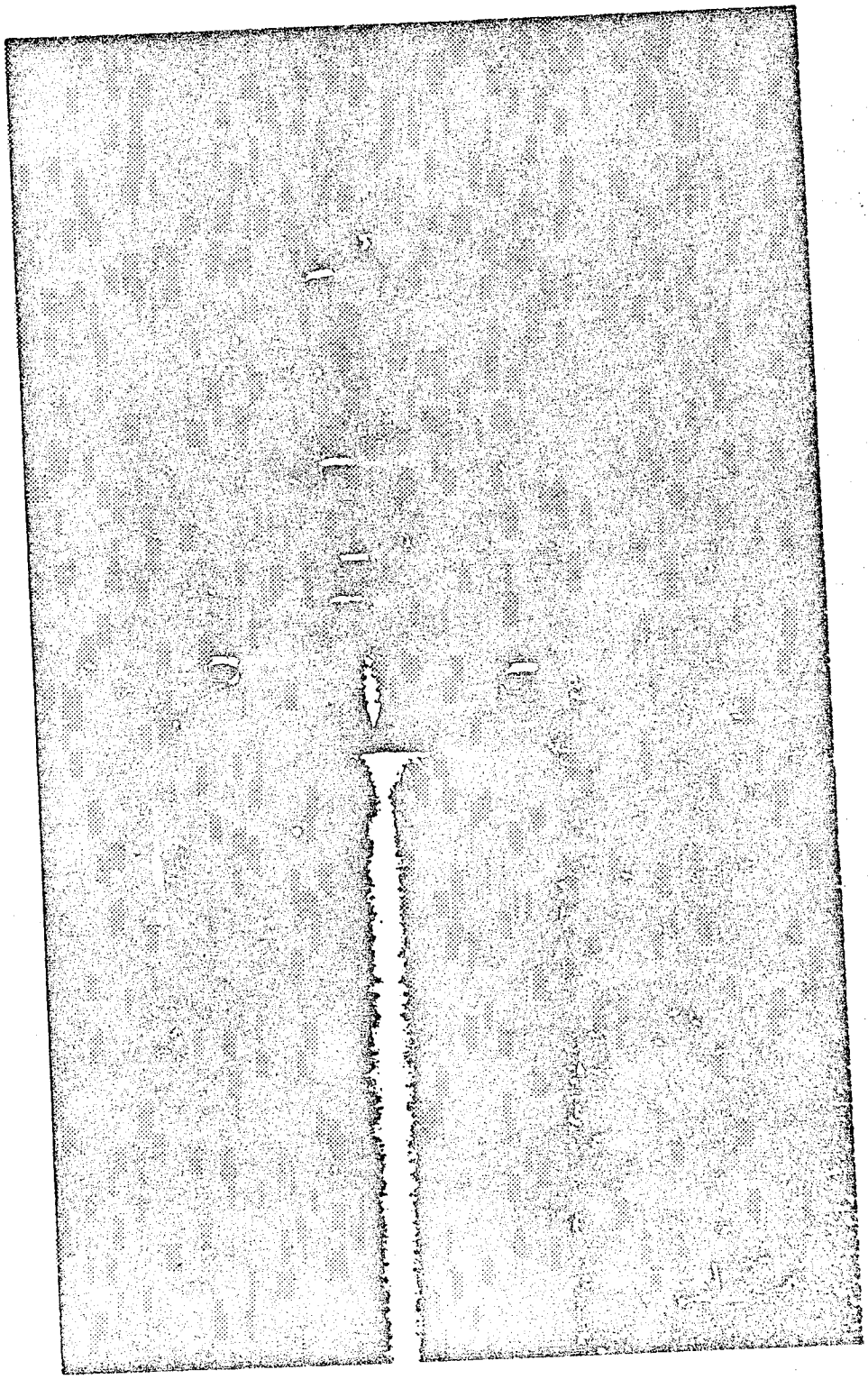

Figure 31. Typical Boundary Layer Rake - Front View.

ORIGINAL PAGE IS
OF POOR QUALITY

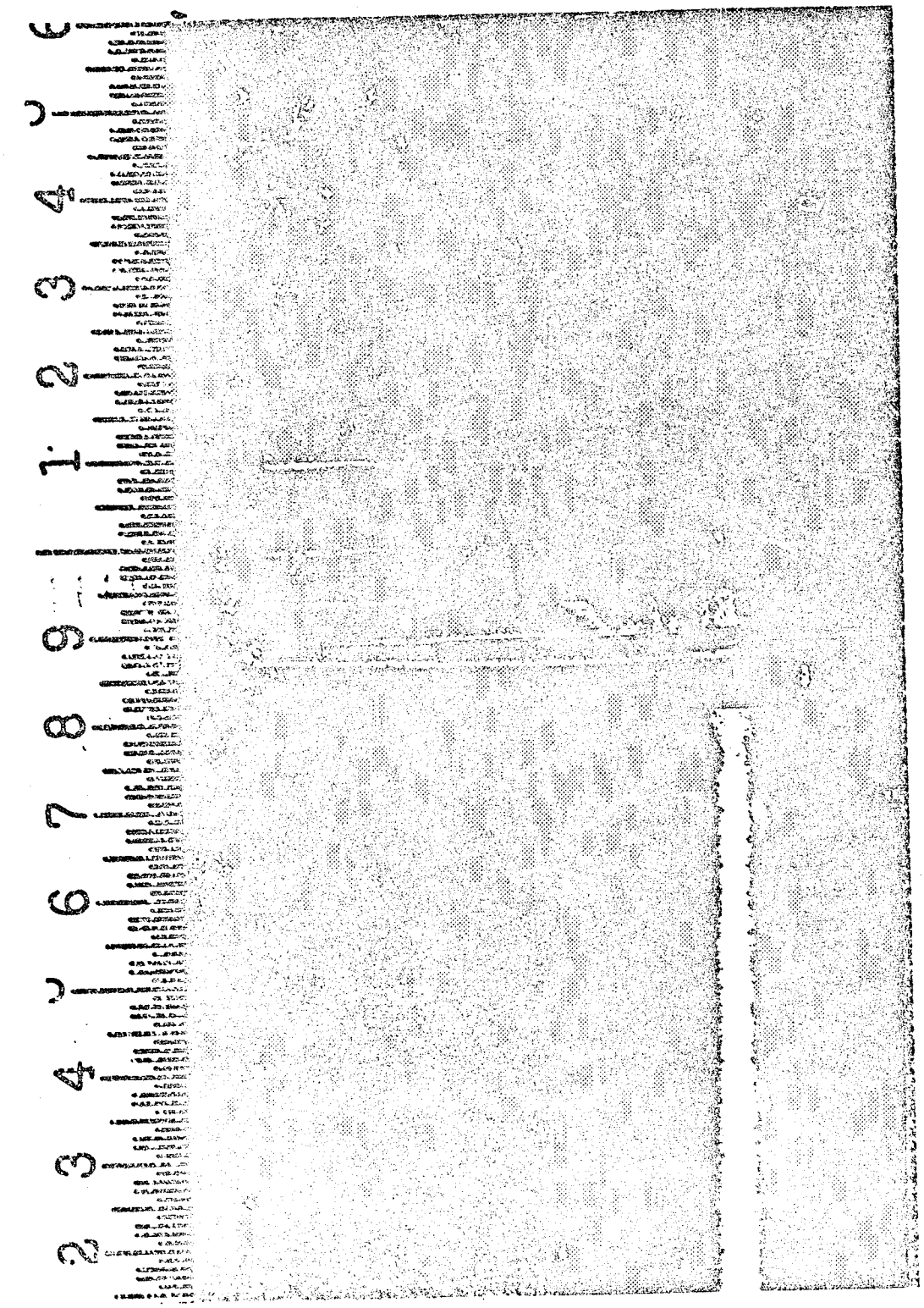

Figure 32. Typical Boundary Layer Rake - Side View.

Maximum circumferential travel of the probe was 22° of arc. This assured coverage of at least three full nozzle passage widths for any of the configurations tested.

Five static pressure taps, equally spaced circumferentially, were located on the inner and outer walls in the plane of the traverse probe. These were used to define a linear distribution of static pressure from hub to tip in the profile mass averaging.

Plane 55 - Stage Discharge Rake Planes

Plane 55 was 11.43 cm (4.5 in.) downstream of the last bladerow in each of the configurations. Six static pressure taps, equally spaced circumferentially, were installed on the inner and outer walls at Plane 55 on all of the configurations. For rotating rig tests only, turbine outlet total temperature and total pressure were measured with six circumferential arc rakes 60 degrees apart, located radially at the centers of six equal annular areas. A total of 42 total temperatures and 66 total pressures were measured. Each rake contained eleven Kiel-type pressure elements located side-by-side and seven shielded thermocouple probes side-by-side. Arc rake specifications are shown in Figure 33.

Exhaust Casings

The exhaust casings for all configurations were designed to meet the following aerodynamic requirements:

- The presence of the casings should not significantly alter the radial distribution of static pressure or flow angle at the bladerow exit plane relative to the distributions expected at the same plane in the five-stage build.
- Excessive diffusion of the exhaust flow should be avoided.

The casing contours designed to meet these requirements for each configuration can be seen in the instrumentation drawings in Figure 25 through 29.

Note from Figure 25 and 27 that a single line of static pressure taps were installed on the inner and outer casing walls of Configurations 1, 3, and lay between Plane 50 and Plane 55 to monitor the exhaust flow from these high-swirl configurations for the purpose of detecting flow separation. The taps were arranged to follow a mid-passage streamline from the stator exit planes.

4.2 TEST FACILITY

4.2.1 Facility Description

Turbine component testing was conducted in the General Electric Company's Evendale Warm Air Turbine Test Facility, Cell A7. This facility, shown in

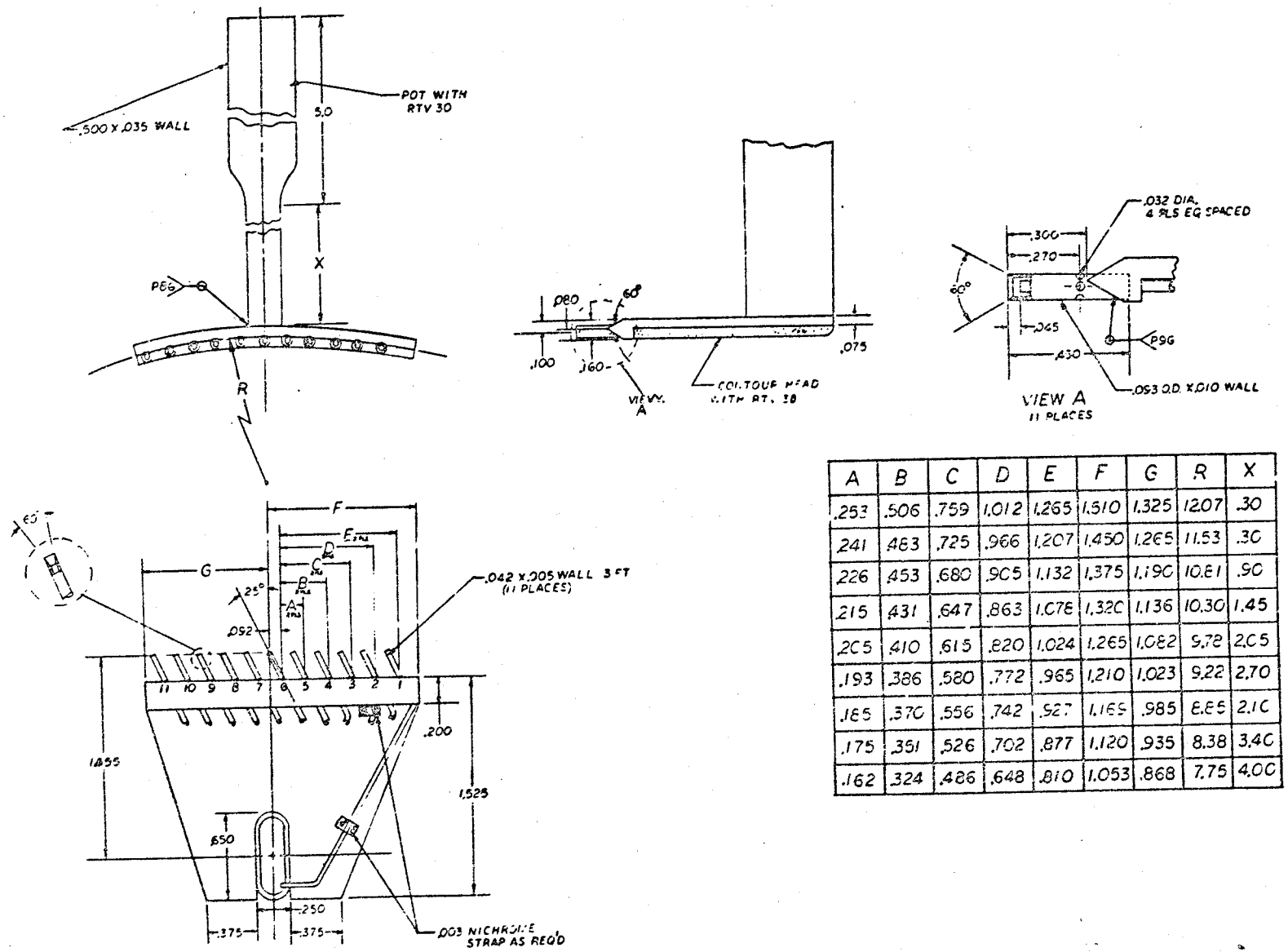

A	B	C	D	E	F	G	R	X
.253	.506	.759	1.012	1.265	1.510	1.325	12.07	.30
.241	.483	.725	.966	1.207	1.450	1.265	11.53	.30
.226	.453	.680	.905	1.132	1.375	1.190	10.81	.90
.215	.431	.647	.863	1.078	1.320	1.136	10.30	1.45
.205	.410	.615	.820	1.024	1.265	1.082	9.78	2.05
.193	.386	.580	.772	.965	1.210	1.023	9.22	2.70
.185	.370	.556	.742	.927	1.165	.985	8.85	2.10
.175	.351	.526	.702	.877	1.120	.935	8.38	3.40
.162	.324	.486	.648	.810	1.053	.868	7.75	4.00

Figure 33. Details of Plane 55 Arc Rake Construction.

Figure 34, will accommodate turbine configurations ranging from a minimum hub diameter of 35.56 cm (14 in.) up to a maximum tip diameter of 81.28 cm (32 in.), with operational capabilities of up to 15,000 horsepower at 15,000 rpm. A plan view of the test facility layout is presented as Figure 35.

Flow enters the test section through an inlet plenum with screens which smooth out any flow disturbances and provide a uniform stream to the test vehicle. Air enters the first-stage nozzle through a convergent bellmouth section which transitions to a constant annular passage (see Figure 24). Turbine discharge air leaves through a constant annular passage and expands into a discharge plenum designed to provide a uniform circumferential pressure distribution.

The turbine horsepower is absorbed by a water brake coupled to the turbine shaft through a strain gage torque sensor mounted between two flexible couplings. This water brake provides excellent speed stability throughout the entire turbine operating map.

A two-level trip system is used for protection against overspeed and excessive temperature or vibrations. The level-1 trip is an overspeed indication. The level-2 trip is signaled by excessive bearing temperature or vibrations or critical support system temperatures or pressures.

The turbine facility control console is located in the Test Cell Control Room. All necessary controls and critical turbine or facility monitoring instruments are strategically located to enable two-man control of the entire test facility. This feature is a direct result of the utilization of analog closed-loop control circuits for setting and maintaining all prime turbine variables. Turbine parameters of inlet temperature, inlet pressure, speed, discharge pressure, and rotor net thrust can all be maintained automatically at preset values.

Air is supplied to the test facility by an arrangement of five multistage centrifugal compressors driven by synchronous motors through speed-increase gears. Flexibility of operation is obtained by the ability to stage the compressors in series or in parallel in various combinations for a wide range of pressure and flows or for use as exhausters. This system provides up to 45.36 Kg/S (100 PPS) of airflow at pressures up to 2068 KPa (300 psig) continuously.

Auxiliary equipment in the air-distribution network further extends the capability of the system by providing air that can be filtered to 10-micron particle size, dried to minus 39 K (70° F) dewpoint, heated to 922 K (1200° F), or cooled to minus 39 K (70° F) for specified conditions for various test cells. High temperature air is provided to the facility by an indirect, natural gas-fired heater.

4.2.2 Facility Instrumentation

Airflow Measurement

Airflow measurement is accomplished through the use of a circular arc venturi operated at critical flow conditions. Design and calibration have

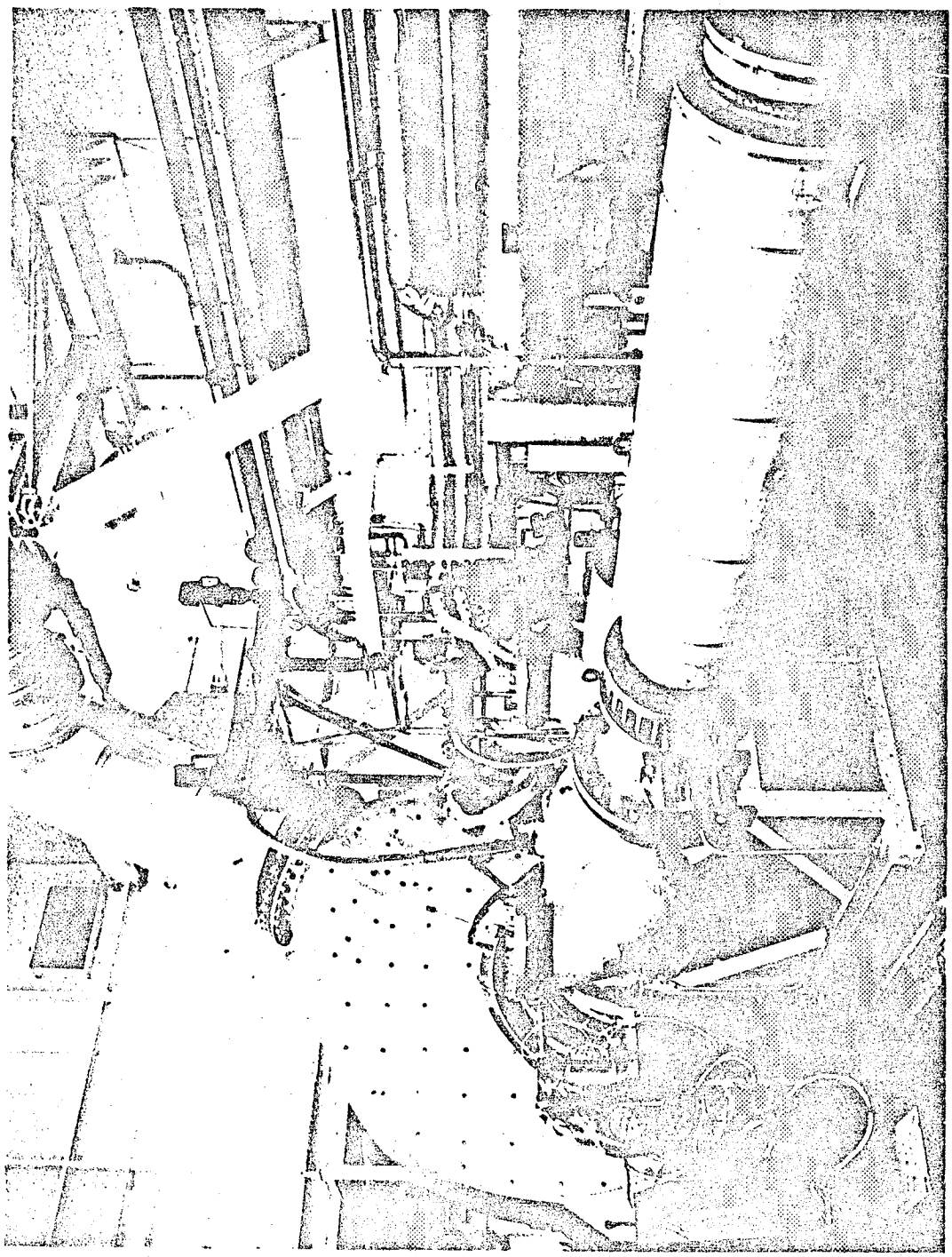

Figure 34. General Electric's Warm Air Turbine Test Facility, Evendale, Ohio.

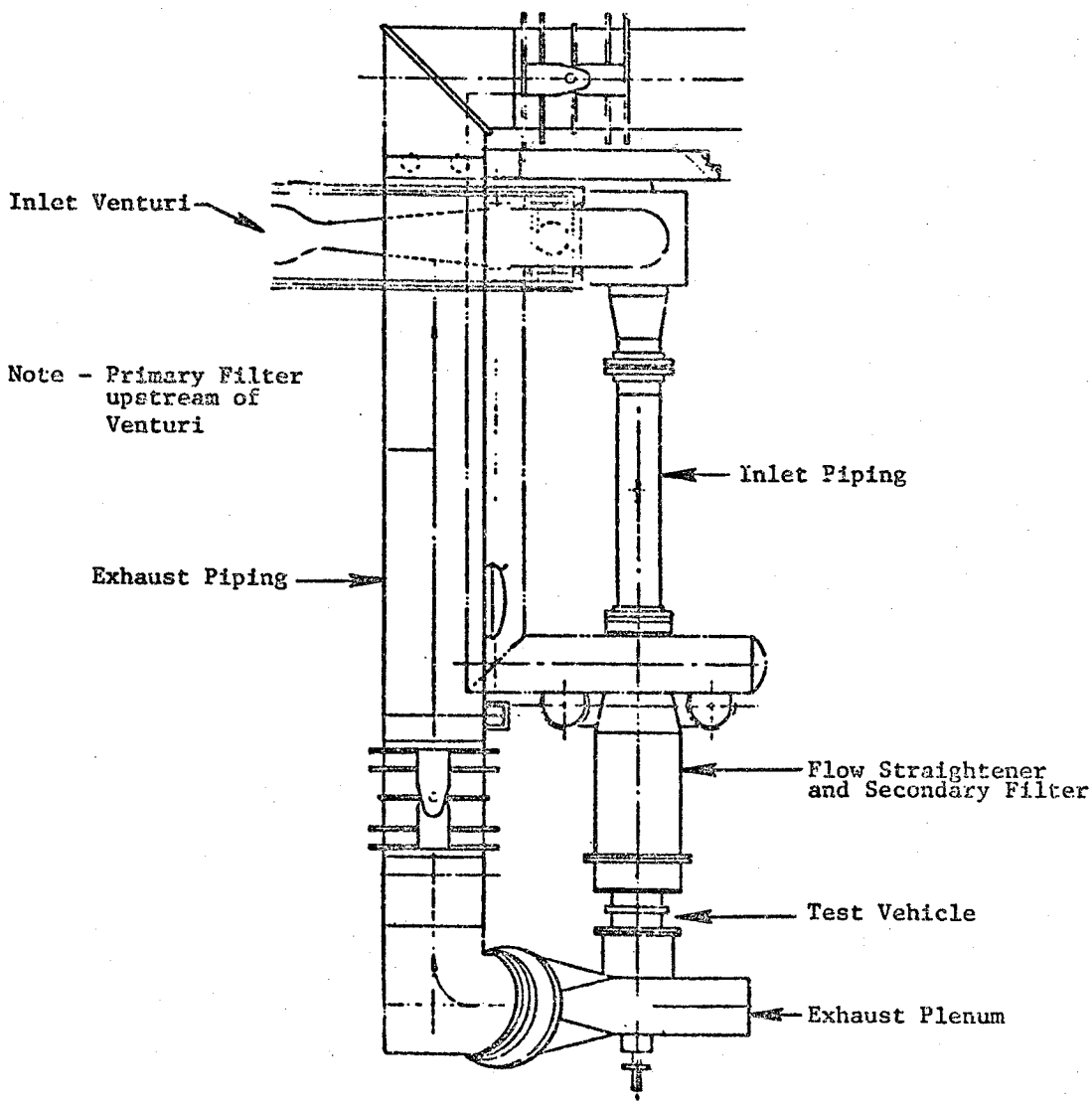

Figure 35. Plan View Schematic of Air Turbine Test Facility.

been completely described by R.E. Smith, Jr., and R.J. Maty in "A Theoretical Method of Determining Discharge Coefficients for Venturis Operating at Critical Flow Conditions," ASME Paper Number 61-WA-211. Critical flow conditions are maintained for all expected operating levels. Accuracy of the flow measurement is ± 0 15 percent.

Speed Measurement

Speed measurements are provided by an indicating system consisting of a 60-tooth gear attached to the turbine drive shaft and a stationary magnetic sensor mounted with its sensing head very close to the gear teeth. Electrical impulses resulting from the passing of each tooth will provide an electrical frequency proportional to engine speed. When integrated over a one-second time period, this system provides speed indication, accurate to within one rpm. In cases where analog readout is required, electronic equipment is available for converting the signal frequency to a proportional d.c. signal. For both types of readout, speed measurement accuracy is 0.25 percent.

Torque Measurement

Two independent strain gage torque meters mounted in the turbine shafting for direct readout are used as the primary torque measurement. The meters provide a readout accuracy of ± 0.25 percent. A secondary measurement of torque is made by a calculation based on measured temperature drop and weight flow.

The strain gage torquemeters are statically calibrated before testing using a precision torque arm and dead weights. Experience with this calibration has shown variations less than 0.1% between calibrations. Torque zeroes (i.e., strain gage output at no load) are recorded before and after each run. Effects of temperature variation on torque zero within the operational range of temperatures has been extensively investigated and is factored into the quoted 0.25 percent torque measurement accuracy.

Data Acquisition System

The data acquisition system consists of a digital recording system capable of recording up to 200 temperature and 264 pressures in addition to other specific turbine performance parameters. The standard sample rate is two to five channels each second.

Temperature measurements are obtained with precision manufactured chromel-constantan (Type E) Thermocouple wire. Sensors in any one plane of measurement use wire from one spool. Calibration samples of wire are cut from each sensor load. The wire samples are then calibrated over the expected temperature range against a platinum resistance thermocouple which is traceable to the National Bureau of Standards, resulting in correction curves which are applied to the temperature measurements in the data reduction program.

Calibration curves are also established to determine temperature recovery at various expected Mach number ranges and flow incidence angles using a specially designed calibration stand with a 6.35 cm (2.5-in.) free jet nozzle capable of a Mach number range from 0.2 to 1.0. Corrections are made in the data reduction program using the calibration curves.

The thermocouple leads terminate in a Copper Alloy Thermal Sink (CATS), which is thermally insulted to minimize temperature gradients. To arrive at the absolute value of any temperature sensor, the absolute temperature of the CATS block is measured, using both a water-ice bath reference and an electronic Ice Point Reference System. The latter is used to determine absolute temperature levels, but both systems are continually compared. The electrical output of each thermocouple is measured at this CATS block and the signal is amplified and directed to the digital recorder. The accuracy of the temperature measurement is ± 0.55 K (1° F).

Turbine rig pressure measurements are obtained by the use of precision gage pressure transducers which convert pneumatic signals to electrical outputs. The pressures enter the control room pneumatically and terminate in electrically controlled scanner which systematically direct each pressure signal to a transducer. The transducer electrical outputs are amplified and directed to the digital recorder. All transducers of this type have a common excitation and output amplification. Each data reading contains the excitation voltage sensed at the transducer, the transducer zero, and a known calibration signal which is recorded through all its associated electrical circuitry. The repeatability of these parameters is continually monitored to preclude any measurement errors. Overall accuracy in the measurement of total pressure is ± 0.1 percent of reading. Accuracy of static pressure is ± 0.2 percent of reading.

Pressure calibrations are performed prior to each test run using a precision deadweight tester for above-atmospheric calibrations and a quartz manometer for sub-atmospheric calibration. Both units are frequently calibrated and are directly traceable to the National Bureau of Standards. All pressure transducers used have characteristic curves compiled in a computer library file, to which each prerun calibration is compared for discrepancies.

The digital recording system is linked to the General Electric computer System by means of a General Electric Terminet 1200 located in the Control Room. This feature enables reduced data to be printed out in the Control Room within five minutes of the reading of a test point.

4.3 TEST PROCEDURES

4.3.1 Test Plans

Test Conditions

Rig inlet temperature was set at 417 K (750° R), which allowed the facility to be run in a closed-loop configuration with the air heated by an indirect

steam heat exchanger (gas fired heater not required). Inlet pressure was set to 310 KPa (45 psia), which allowed attainment of all pressure ratios (with some sub-atmospheric exhaust pressures for the five-stage build) at moderate flow rates.

Reynolds number excursions, to be detailed later in this section, were accomplished by reducing inlet pressure while maintaining the 417 K (750° R) inlet temperature.

Equivalent Design Point

The equivalent aerodynamic design point for each of the rotating rig configurations was selected as that point where the configuration would operate in the five-stage rig with the five-stage rig running at design values of equivalent energy extraction, $\Delta h/T_T$, and equivalent speed, $ND/\sqrt{T_T}$. A comparison of design point parameters for the full-size ICLS turbine with those for the five-stage rig operating at facility inlet conditions is provided in Table XI. The ICLS design point is the M0.8/10.67 Km (35,000 ft.) max climb condition. Note that two sets of ICLS vs. rig data are provided in Table XI, documenting the change in cycle parameters incorporated between Block I and Block II mentioned in Section 3.1.

Note from Table XI that the equivalent flow function, $W\sqrt{T_T}/P_T D^2$, is higher for the rig than for the ICLS turbine. This is due to a positive shift in the flow function vs Mach number characteristic at the higher rig value of specific heat ratio.

Table XII shows that, in the five-stage rig, the pitchline value of inlet gas angle to each bladerow is within 0.2 degree of its respective value in the full-size ICLS turbine. Further, the pitchline reaction for each of the five rig stages is reasonably close to its respective ICLS value. This attests to the validity of the method used to set the equivalent design point for the rig.

Mapping the Air Turbine Configurations

Test plans for the air turbine configurations were defined in terms of group total-to-static pressure ratio, P_T/P_S, and group blade-jet speed ratio, u/C_o. The definition and significance of the blade-to-jet speed ratio is presented as Appendix D.

Figure 36 presents the selected test maps for the one-stage, two-stage, and five-stage rigs as functions of energy extraction and corrected speed (at rig size). A test point is defined by each intersection of a line of constant pressure ratio with a line of constant blade-jet speed ratio.

The following key operating points have been spotted on the five-stage map: max climb (MXCL), max cruise (MXCR), takeoff (TKOF), min and max loiter, approach, and flight-idle (F-IDLE). Note that the max climb condition is the aero design point.

Table XI. Equivalent Design Point Parameters Compared, ICLS vs. Rig - Five Stage Configuration.

Item	Symbol	Block I		Block II	
		ICLS	Rig	ICLS	Rig
Inlet Total Temperature, K (° R)	T_T	1104.8 (1988.6)	416.7 (750.0)	1111.9 (2001.4)	416.7 (750.0)
Inlet Total Pressure, mPa (psia)	P_T	0.262 (38.0)	0.310 (45.0)	0.255 (36.94)	0.310 (45.0)
Scale Factor	D	1.00	0.67	1.00	0.67
Equivalent Energy Extracton, J/Kg K (Btu/lbm ° R)	$\Delta h/T_T$	322.8 (0.0771)	322.8 (0.0771)	318.2 (0.0760)	318.2 (0.0760)
Energy Extraction, J/g (Btu/lbm)	Δh	356.6 (153.3)	134.5 (57.8)	353.8 (152.11)	132.6 (57.0)
Equivalent Speed, Rad/Sec $\sqrt{°K}$ (RPM/$\sqrt{°R}$)	$ND/\sqrt{T_T}$	11.08 (78.88)	11.08 (78.88)	11.03 (78.50)	11.03 (78.50)
Corrected Speed, Rad/Sec $\sqrt{°K}$ (RPM/$\sqrt{°R}$)	$N/\sqrt{T_T}$	11.08 (78.88)	16.54 (117.73)	11.03 (78.50)	16.46 (117.17)
Rotative Speed, RPM	N	3517.6	3224.2	3511.9	3208.7
Equivalent Flow Function (Kg $\sqrt{°K}$/Sec Pa; lbm $\sqrt{°R}$/Sec psia)	$W\sqrt{T_T}/P_T D^2$	0.00395 (80.55)	0.00401 (81.84)	0.00409 (83.40)	0.00416 (84.83)
Flow Function (Kg$\sqrt{°K}$/Sec Pa; lbm $\sqrt{°R}$/Sec psia)	$W\sqrt{T_T}/P_T$	0.00395 (80.55)	0.00180 (36.74)	0.00409 (83.40)	0.00187 (38.08)
Flow, Kg/Sec (lbm/sec)	W	31.1 (68.6)	27.4 (60.36)	31.2 (68.86)	24.4 (62.58)
Pressure Ratio, total-to-total	P_{T_1}/P_{T_2}	4.36	4.56	4.22	4.37
Pressure Ratio, total to static	P_{T_1}/P_{S_2}	4.71	4.95	4.57	4.76
Pitchline Aerodynamic Loading, = $gJ\Delta h/2U^2$	ψ_P	1.295	1.295	1.292	1.292

Table XII. Comparison of Free Vortex Values of Inlet Gas Angle and Reaction for Five-Stage Configurations ICLS vs. Rig.

	Inlet Gas Angle at Pitchline (degrees)		Stage Hub Reaction Rx *	
Bladerow	IC/LS	Rig	IC/LS	Rig
S1	0	0	-	-
R1	46.93	47.09	.182	.176
S2	45.74	45.86	-	-
R2	47.79	47.84	.194	.190
S3	46.20	46.18	-	-
R3	45.81	45.71	.186	.183
S4	43.68	43.52	-	-
R4	36.44	36.23	.156	.157
S5	32.44	32.24	-	-
R5	20.60	20.46	.078	.081

$$* Rx = 1 - \left\{ \left[1 - \left(\frac{P_{S,1}}{P_{T,0}} \right)^{\frac{\gamma-1}{\gamma}} \right] \Big/ \left[1 - \left(\frac{P_{S,2}}{P_{T,0}} \right)^{\frac{\gamma-1}{\gamma}} \right] \right\}$$

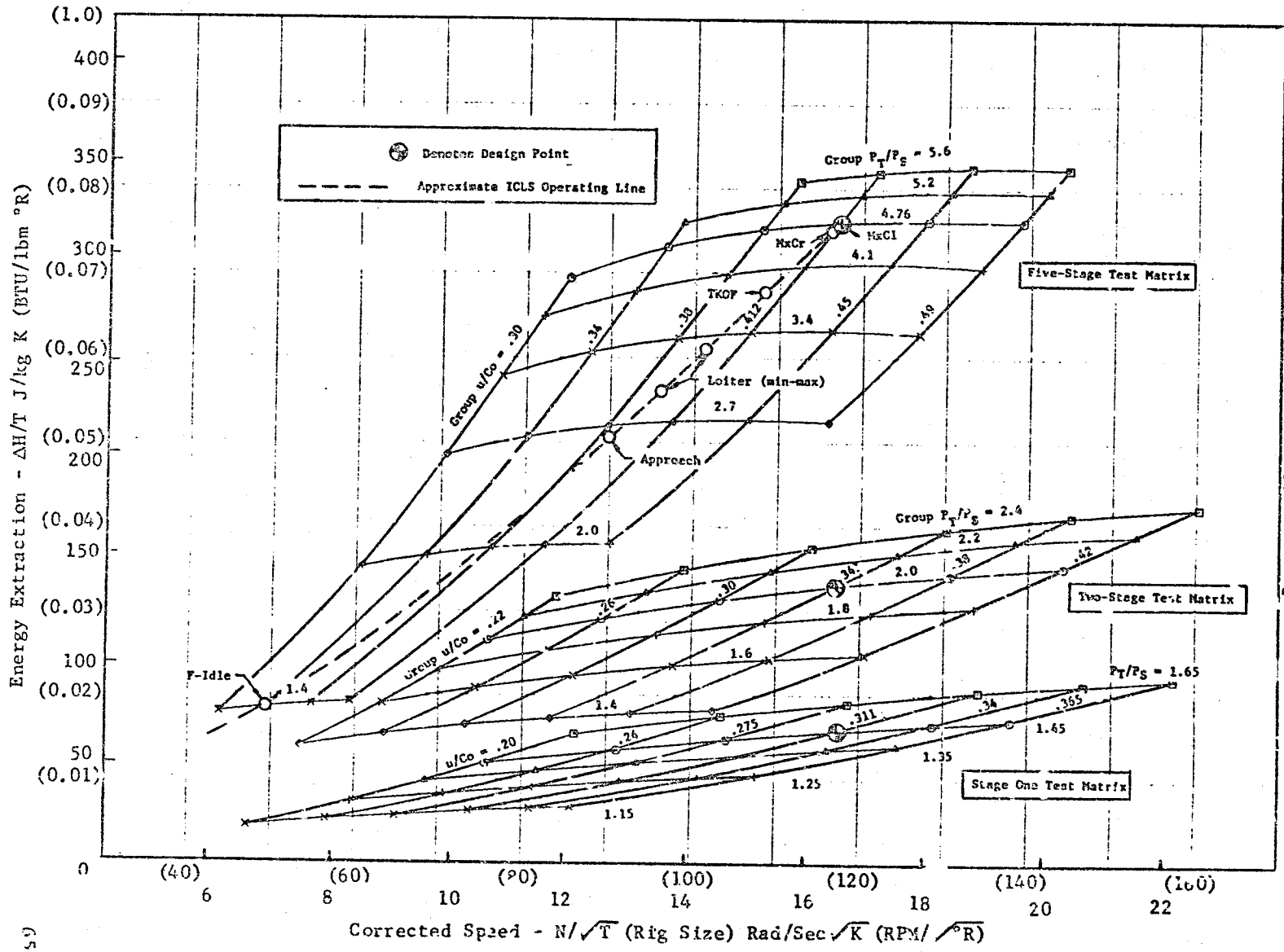

Figure 36. Intended Test Matrices For Rotating Rig Tests

Test Point Schedules

Tables XIII through XVII define the test point schedules for all rotating rig and annular cascade configurations. Small differences between Block I and Block II point settings are evident here, for reasons noted previously (see Section 4.3.1).

Configurations 1 and 1a, the stage one stator cascades, were tested over a range of seven pressure ratios, Table XIII, including the design pressure ratio.

Configuration 2, the stage one build, was tested at five pressure ratios for six values of the blade-jet speed ratio, thus defining a 30-point test matrix, Table XIV.

Configuration 3, the stage-and-a-half build, was tested over the 15-point test matrix defined in Table XV. Six blade-jet ratios were set at the stage one design pressure ratio. Three blade-jet ratios were set at each of three additional pressure ratios, one above and two below the stage one design pressure ratio.

Configurations 4 and 4a, the two stage builds, were tested at six pressure ratios for six values of blade-jet speed ratio, thus providing a 36-point test matrix, Table XVI. Note that an additional five point test matrix has been defined in Table XVI for evaluation of the loss characteristics of 14 inter-turbine PT/TT probes to be installed in the ICLS. These probes were simulated in the Block II 2-stage group using 14 steel dowels, which were immersed into the transition duct upon completion of the nominal 36-point test matrix. These probes are called out in Figure 23.

Configuration 5, the five-stage rig, was tested over a range of eight pressure ratios from a maximum of 5.60 to a minimum of 1.40. Note that this covers the entire range of 5-stage operation, from max climb through flight-idle. Table XVII defines a basic matrix of 42 discrete points for the five-stage rig.

Supplemental to the test points defined in Tables XIII thru XVII were several repeat design points (see Section 4.3.2) for each configuration and, for the stage tests, several design points set with reduced inlet pressure to evaluate the effects of Reynolds number (see Appendix E).

4.3.2 Test Operation

Instrumentation Verification

Each rig configuration was pressurized to a pretest pressure level to check for vehicle leaks and to verify pressure line continuity to the transducers.

Point	$\frac{P_{T_0}}{P_{S_1}}$	$\frac{W\sqrt{T_{T_0}}}{P_{T_0}}$	Traverse Type
11	1.11	26.60	B
15	1.155	30.35	C
21	1.210	33.60	B
28*	1.284	36.87	C
35	1.35	38.88	B
42	1.425	40.55	C
50	1.50	41.72	B

* Denotes design point conditions

Traverse types defined:
A. 1 circumferential + 1 radial
B. 7 circumferential + 1 radial
C. 12 circumferential + 1 radial

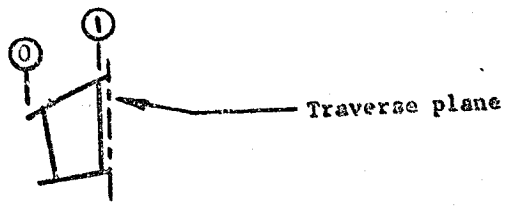

Table XIII. Test Point Schedule - Block I Configuration 1 and Block II Configuration 1a.

Table XIV. Test Point Schedule - Block I Configuration 2.

Point	$\frac{P_{T_0}}{P_{S_2}}$	$\frac{U}{C_0}$	$\frac{N}{\sqrt{T_{T_0}}}$	N, RPM	$\frac{\Delta h}{T_{T_0}}$	Δh, BTU/lbm	$\frac{W\sqrt{T_{T_0}}}{P_{T_0}}$	Traverse Type
1423	1.65	.20	86.2	2360.7	.0154	11.55	40.55	A
1428		.24	103.6	2837.2	.0175	13.13	40.09	
1432		.275	118.7	3250.7	.0190	14.25	39.64	
1436		.311	134.2	3675.2	.0204	15.30	39.26	
1440		.34	146.7	4017.5	.0212	15.90	38.87	
1443		.365	157.4	4310.6	.0219	16.43	38.61	
1421	1.45	.20	75.6	2070.4	.0219			
1425		.24	91.2	2497.6	.0135	10.13	37.72	
1429		.275	104.2	2853.6	.0147	11.03	37.32	
1433*		.311	117.7	3224.3	.0157	11.78	36.87	C
1435		.34	128.7	3524.6	.0164	12.30	36.52	A
1438		.365	138.0	3779.3	.0169	12.68	36.19	
1318	1.35	.20	68.5	1875.9	.0098	7.35	39.26	
1322		.24	81.7	2237.4	.0118	8.85	35.65	
1325		.275	93.6	2563.3	.0120	9.00	35.26	
1328		.311	106.0	2902.9	.0128	9.60	34.74	
1331		.34	116.2	3182.3	.0135	10.13	34.50	
1334		.365	124.5	3409.6	.0139	10.43	34.15	
1216	1.25	.20	59.6	1632.2	.0073	5.48	32.76	
1219		.24	70.7	1936.2	.0083	6.23	32.51	
1222		.275	81.3	2226.5	.0091	6.83	32.16	
1225		.311	91.6	2508.6	.0098	7.35	31.88	
1227		.34	100.9	2763.3	.0102	7.65	31.34	
1229		.365	107.7	2949.5	.0105	7.87	31.04	
1113	1.15	.20	47.2	1292.6	.0044	3.30	26.50	
1115		.24	56.7	1552.8	.0052	3.90	26.94	
1117		.275	64.9	1777.4	.0057	4.28	26.71	
1120		.311	73.7	2018.4	.0063	4.73	26.83	
1122		.34	80.9	2215.5	.0066	4.95	26.46	
1123		.365	85.7	2347.0	.0068	5.10	26.28	

* Denotes design point conditions

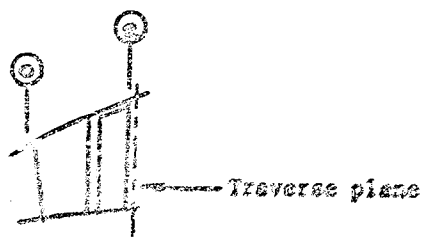

Traverse types defined:

A. 1 circumferential + 1 radial
B. 7 circumferential + 1 radial
C. 12 circumferential + 1 radial

Table XV. Test Point Schedule - Block I Configuration 3.

Point	$\frac{P_{T_2}}{P_{S_2}}$	$\frac{U}{C_0}$	$\frac{N}{\sqrt{T_{T_0}}}$	$\frac{\Delta h}{T_{T_0}}$	$\frac{W\sqrt{T_{T_0}}}{P_{T_0}}$	Traverse Type
1628	1.65	.24	103.6	.0175	40.09	B
1636		.311	134.2	.0204	39.26	
1643		.365	157.4	.0219	38.61	
1421	1.45	.20	75.6	.0118	38.13	C
1425		.24	91.2	.0135	37.72	B
1429		.275		.0147	37.33	C
1432*		.311	117.7	.0157	36.87	B
1435		.34	128.7	.0164	36.52	C
1438		.365	138.0	.0169	36.19	B
1322	1.35	.24	81.7	.0110	35.65	
1329		.311	106.0	.0128	34.74	
1334		.365	124.5	.0139	34.15	
1219	1.25	.24	70.7	.0083	32.51	
1225		.311	91.6	.0098	31.88	
1229		.365	107.7	.0105	31.04	

* Denotes design point conditions

Traverse types defined:
A. 1 circumferential + 1 radial
B. 7 circumferential + 1 radial
C. 12 circumferential + 1 radial

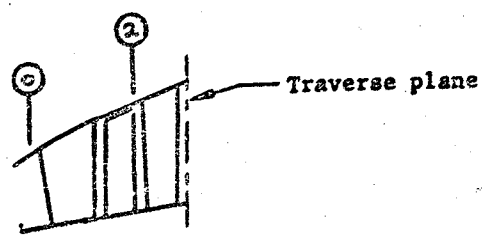

Table XVI. Test Point Schedule - Block I Configuration 4 and Block II Configuration 4a.

Point	$\frac{P_{T_0}}{P_{s_2}}$	$\frac{U}{C_0}$	$\frac{N}{\sqrt{T_{T_0}}}$	N,RPM	$\frac{\Delta h}{T_{T_0}}$	Δh, BTU/lbm	$\frac{W\sqrt{T_{T_0}}}{P_{T_0}}$	Traverse Type
2422	2.40	.22	83.89	2297.4	.0317	23.78	41.43	A
2427		.26	99.01	2711.5	.0349	26.17	40.53	
2431		.30	114.24	3128.6	.0375	28.10	39.72	
2435		.341	130.16	3564.6	.0394	29.67	38.82	
2439		.38	145.09	3973.9	.0412	30.86	38.08	
2443		.42	160.31	4390.6	.0423	31.76	37.38	
2221	2.20	.22	80.11	2193.9	.0293	21.99	41.23	
2225		.26	94.54	2589.1	.0322	24.15	40.34	
2229		.30	109.26	2992.2	.0347	26.03	39.48	
2234		.341	124.39	3406.6	.0367	27.51	38.60	
2237		.38	138.42	3790.8	.0382	28.68	37.80	
2241		.42	152.85	4186.0	.0390	29.22	37.07	
2010	2.00	.22	75.83	3076.7	.0265	19.90	40.82	
2024		.26	89.26	2644.5	.0291	21.84	39.92	
2028		.30	103.39	2828.7	.0313	23.48	39.00	
2032 *		.341	117.16	3208.7	.0330	24.75	38.11	B
2035		.38	130.66	3578.3	.0342	25.64	37.28	A
2039		.42	144.29	3951.5	.0352	26.39	36.56	
1819	1.80	.22	70.16	1921.6	.0230	17.22	39.99	
1822		.26	82.79	2267.3	.0253	19.01	39.09	
1826		.30	95.83	2624.6	.0272	20.43	38.13	
1829		.341	109.57	2976.6	.0287	21.54	37.23	
1833		.38	121.31	3322.2	.0296	22.22	36.31	
1836		.42	133.55	3657.6	.0304	22.81	35.60	
1617	1.60	.22	63.29	1733.3	.0189	14.16	38.50	
1620		.26	74.64	2038.6	.0208	15.58	37.57	
1623		.30	85.98	2354.7	.0223	16.70	36.56	
1626		.341	97.82	2678.9	.0235	17.59	35.59	
1629		.38	109.27	2992.5	.0243	18.19	34.69	
1633		.42	120.61	3303.0	.0248	18.64	33.92	
1414	1.40	.22	53.54	1466.3	.0138	10.36	35.60	
1417		.26	63.49	1738.7	.0153	11.48	34.65	
1420		.30	73.24	2005.8	.0164	12.30	33.65	
1422		.341	83.29	2281.0	.0172	12.90	32.62	
1425		.38	92.75	2540.1	.0178	13.34	31.77	
1428		.42	102.59	2809.8	.0182	13.64	30.97	
2439	2.40	.341	130.16	3564.6	.0196	39.67	38.82	A
2020	2.00	.22	75.83	2076.7	.0265	19.90	40.82	
2032 ** *		.341	117.16	3208.7	.0330	24.75	38.11	
2039		.42	144.29	3951.5	.0352	26.39	36.56	
1414	1.40	.341	53.54	1466.3	.0138	10.36	39.60	

* Denotes design point conditions

Traverse types defined:
A. 1 circumferential + 1 radial
B. 15 circumferential + 1 radial

** { Reduced Test Point Schedule for Evaluation of Inter-Turbine Instrumentation for ICLS

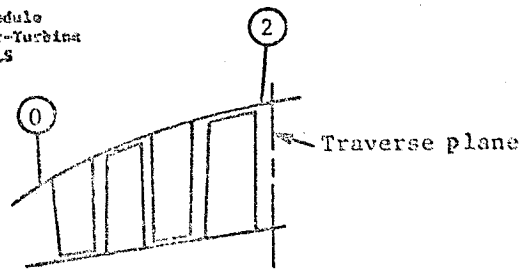

Table XVII. Test Point Schedule - Block II Configuration 5.

Point	$\frac{P_{T_e}}{P_{g_2}}$	$\frac{U}{C_0}$	$\frac{N}{\sqrt{T_{T_0}}}$	H.EFM	$\frac{\Delta h}{T_{T_0}}$	Δh, Btu/lbm	$\frac{W\sqrt{T_{T_0}}}{F_{T_0}}$	Traverse Type
5630	5.6	.38	112.4	3078.2	.03085	60.64	38.73	A
5633		.412	121.8	3335.6	.03193	61.45	37.98	
5636		.45	132.9	3639.6	.03250	61.88	37.14	
5639		.49	144.5	3957.3	.03240	61.89	36.33	
5227	5.2	.34	98.6	2709.3	.07600	57.00	39.78	
5230		.38	110.5	3026.2	.07830	58.73	38.79	
5232		.412	119.8	3280.8	.07923	59.42	38.03	
5235		.45	130.6	3576.6	.07960	59.70	37.17	
5238		.49	142.1	3891.6	.07955	59.66	36.35	
4723	4.76	.30	85.1	2330.6	.06930	51.98	40.68	
4726		.34	96.6	2645.5	.07305	54.79	39.80	
4729		.38	108.0	2957.7	.07515	56.36	38.86	
4732 *		.412	117.2	3209.6	.07600	57.00	38.09	
4734		.45	127.7	3497.2	.07620	57.15	37.22	
4738		.49	139.1	3809.4	.07610	57.08	36.38	
4122	4.1	.30	82.0	2245.7	.06480	48.60	40.74	
4125		.34	92.9	2544.2	.06780	50.85	39.85	
4128		.38	104.0	2848.1	.06990	52.43	38.91	
4130		.412	113.1	3097.4	.07080	53.10	38.11	
4133		.45	123.4	3379.4	.07110	53.33	37.23	
4136		.49	134.2	3675.2	.07060	52.95	36.36	
3421	3.4	.30	77.1	2111.5	.05780	43.35	40.74	
3424		.34	87.7	2401.8	.06065	45.49	39.80	
3426		.38	98.0	2646.6	.06223	46.67	38.83	
3429		.412	106.7	2922.1	.06300	47.25	38.02	
3431		.43	116.3	3185.0	.06319	47.39	37.12	
3434		.49	126.8	3472.5	.06280	47.10	36.21	
2719	2.7	.30	70.6	1933.5	.04845	36.34	40.48	
2721		.34	80.2	2196.4	.05060	37.95	39.39	
2724		.38	89.8	2459.3	.05193	38.95	38.36	
2726		.412	97.5	2670.1	.05250	39.38	37.55	
2729		.45	106.6	2919.9	.05265	39.49	36.61	
2931		.49	116.9	3179.8	.05245	39.36	35.70	
2016	2.0	.30	60.7	1662.3	.03515	26.36	38.80	
2018		.34	68.4	1873.2	.03650	27.28	37.73	
2020		.38	76.2	2086.8	.03745	28.09	36.70	
2022		.412	82.5	2259.4	.03780	28.35	35.85	
2024		.45	90.2	2470.2	.03793	28.45	34.89	
1411	1.4	.30	43.8	1199.5	.01780	13.35	33.65	
1413		.34	49.5	1355.6	.01843	13.82	31.47	
1415		.38	54.8	1500.8	.01883	14.12	30.49	
1416		.412	59.4	1626.7	.01910	14.33	29.77	

* Denotes design point conditions

Traverse types defined:
A. 1 circumferential + 1 radial
B. 15 circumferential + 1 radial

The pressure transducers, thermocouple, and torque meters were calibrated prior to testing each configuration.

Traverse probes had been calibrated in the exit of a free-jet nozzle over a Mach number range which adequately covered the Mach numbers expected in the test program.

In-Test Vehicle Operation

The desired test point was set by the cell operator by adjusting the ratio of $P_{T_{39}}$ to $P_{S_{55}}$ (ref. Figures 25 thru 29) to a pre-specified value which yielded the proper total-to-static pressure ratio. The turbine rotational speed (for the rotating rig tests) which yielded the proper blade-jet speed ratio at this pressure ratio was then set by adjusting the flow to the water brake. Once the vehicle stabilized on point, all fixed instrumentation was scanned automatically and recorded by the data acquisition system. Upon completion of the steady-state reading, the traverse probe, which had been fully retracted for that reading, was traversed radially and circumferentially as specified by the test schedule. Traverse data was automatically digitized and stored for data reduction.

The speed was then re-adjusted to set the next value of blade-jet speed ratio. At the completion of a line of constant pressure ratio, the next pressure ratio was set.

In order to monitor and assure stability of test measurements, repeat design points were taken at the start of every run and approximately after every second pressure ratio thereafter. A minimum of two steady state readings were recorded at each point setting.

4.4 DATA REDUCTION PROCEDURES

Appendix F has been provided to define cascade efficiency, stage efficiency, and various other performance parameters to be presented in Section 4.5. Procedures as to how data from various measurement devices are reduced are included.

Since the range in value of measured parameters for the rotating rig tests varied appreciably from the single-stage to the five-stage test, Appendix G has been provided to give the reader an estimate of the accuracy of the stage efficiency calculation for each of the builds based on the known accuracy of the measuring devices. From the error analysis of Appendix G, the uncertainty in design point efficiency level induced by the inaccuracies of the measurement devices is 0.49 percent for the single stage build, 0.28 percent for the two-stage build, and 0.22 for the five-stage build.

4.5 EXPERIMENTAL RESULTS AND DISCUSSION

This section will present results of all testing on the E^3 LP turbine scaled test vehicle. Appendix H is a tabulation of steady state data for the Block I and Block II rotating rig configurations.

4.5.1 Block I Test Results

Inlet Traverse

Extensive traverse data was taken at the duct inlet plane to evaluate the pressure losses associated with scrubbing on the walls of the inlet casings and the 10 struts of the inlet frame. Figure 37 presents the spanwise distribution of ΔP_T at the inlet plane based on 21 circumferential traverses. Integration of this profile yielded a 0.37 KPa (0.054 psia) pressure loss, relative to the plane 39 strut-mounted impact element, at the 310 KPa (45 psia) inlet pressure level. This corresponds to an average inlet loss coefficient, $\bar{\omega}$, of 0.0137, where $\bar{\omega} = (P_{T39}-P_{T42})/(P_{T39}-P_{S42})$ and P_{S42} is the average between the hub and tip static pressures at plane 42. This was added to the data reduction program, thus giving the turbines credit for loss incurred in the inlet spool as a function of the inlet head.

Configuration 1

The test configuration for the Block I Stage 1 nozzle annular cascade is shown in Figure 25. The transition duct inlet (Plane 42) corresponds to the HPT exit in the engine layout.

The test plan for this configuration, Table XIII, was completed early in the test program; however, post-test inspection of the cascade revealed that some of the epoxy used to seal between the transition duct outer wall and the outer band had curled into the flowpath, acting as a flow disturbance on the diffusing portion of the duct outer wall. This problem was subsequently eliminated and the cascade was reinstalled and retested at test point 28 only. Consequently, only Point 28 traverse data will be reviewed herein.

Design point data for the transition duct is presented in Figure 38. The plot on the left presents static pressure rise coefficient, $\Delta P_s/q$, as a function of duct axial length for inner and outer walls. The reference static pressure and the dynamic head, q, are defined as inlet average. The solid lines represent an axisymmetric pre-test prediction and the symbols are data from static taps. The dashed line and the dotted line represent, respectively, the stagnation streamline and the mid-channel streamline from a blade-to-blade analysis of the stator tip section. Note that the data taken on the duct outer wall matches the dotted line very closely, as one would expect considering that the taps were located circumferentially between leading edges. The steep pressure rise exhibited by the stagnation streamline would lead one to expect a locally separated region right in front of the leading edge and the eventual formation of a "horseshoe" vortex. The second plot in Figure 38 presents total pressure loss profiles for the inner and outer walls measured by boundary layer rakes at the duct exit/stator inlet. Note that no significant loss is incurred beyond 4% of annulus height from either wall.

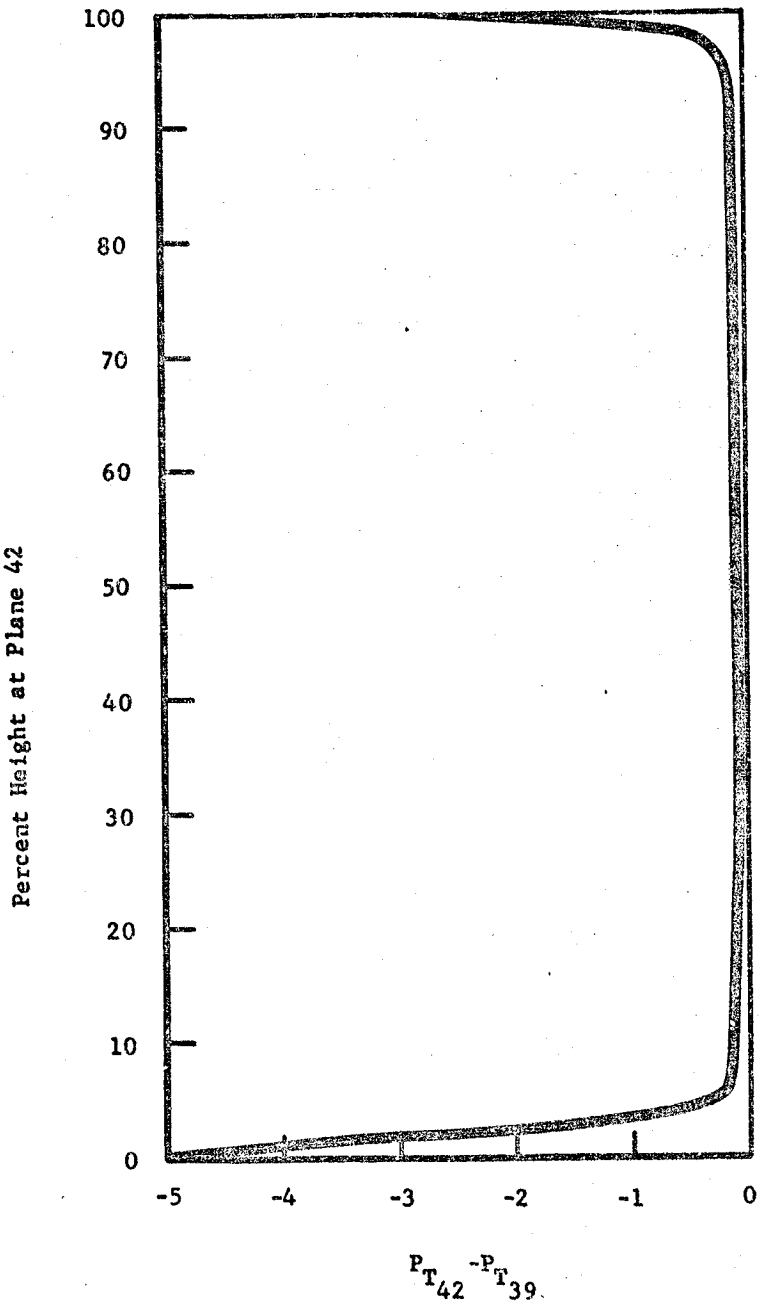

Figure 37. Inlet Pressure Drop Based on Inlet Traverse

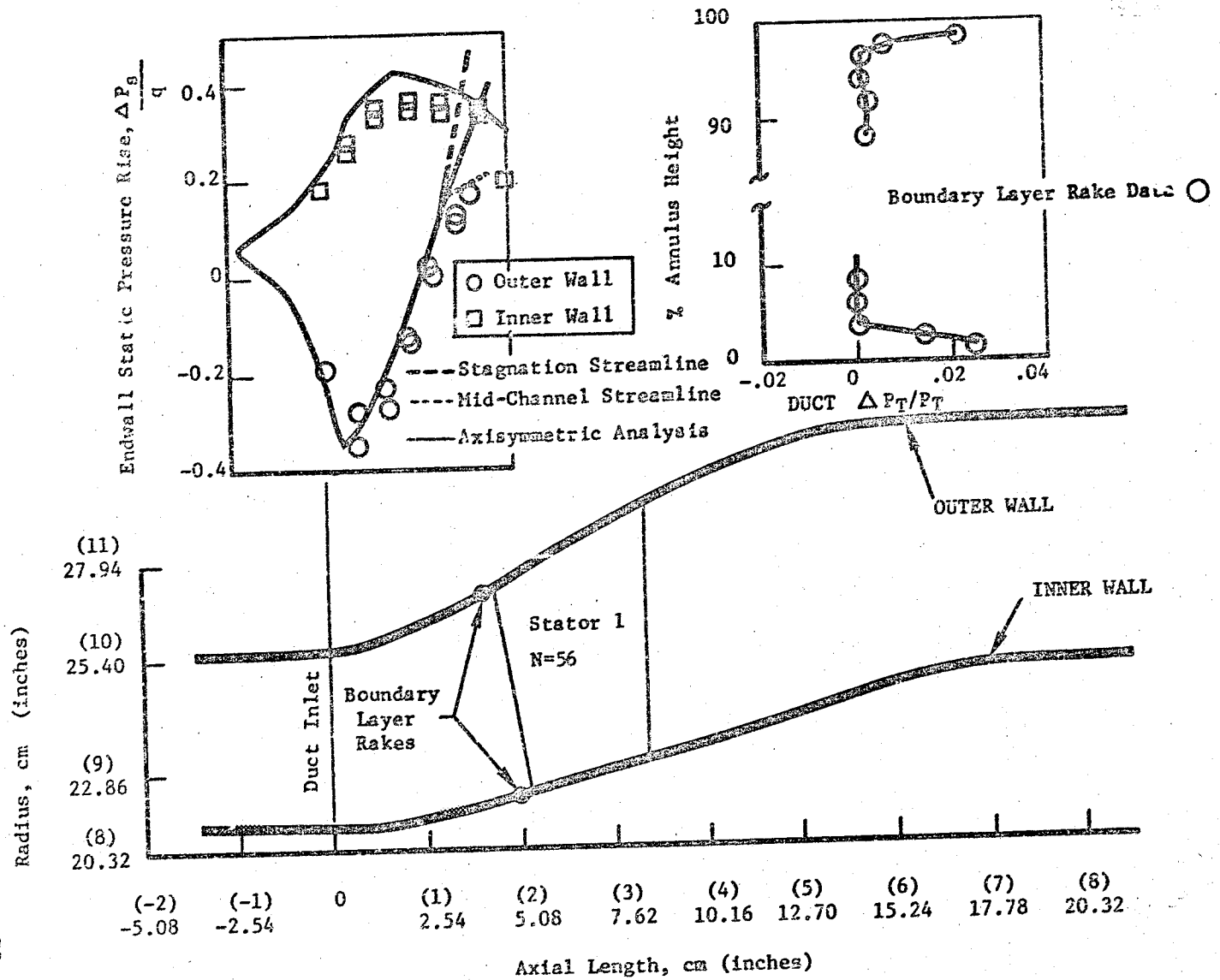

Figure 38. Block I Configuration 1 Transition Duct Data at Design Pressure Ratio.

Figure 39 presents nozzle inlet flow function vs total-to-static pressure ratio $P_{T_{42}}/Ps_{ex}$, where Ps_{ex}, is the average of the hub and tip static pressures at the trailing edge plane (PS220-224 and PS323-327 in Figure 25). Note that the design intent level was exceeded by 1.4%. This is due to the fact that measured nozzle passage areas (throat x height) were approximately 1.6% greater than design intent.

Results of the Run 10 exit traverse survey are presented in Figures 40 thru 43. Spanwise distribution of $P_{T_{50}}/P_{T_{42}}$ and of bladerow kinetic energy efficiency are presented in Figures 40 and 41 respectively. Data is presented at design pressure ratio. Note the large secondary loss core formed on the outer 40% of span, due primarily to the thickened boundary layer from the duct outer wall and the high tip slope of the stator itself. A graphic representation of these loss cores is provided by the contour plot of $P_{T_{50}}/P_{T_{42}}$ in Figure 43, where a large accumulation of low momentum flow can be seen in an area corresponding to the vane suction surface near the tip. Large losses at the hub are also evident and may be due to the low solidity design of the airfoil.

Vane exit angle distribution at design P_T/P_S is presented in Figure 42. Included for reference is the axisymmetric prediction for the cascade flowpath. Note the classical deviation induced by the secondary flow pattern at the stator tip.

Airfoil surface Mach number distributions for pitchline and near tip streamlines are presented in Figure 44. These Mach numbers are calculated using measured surface static pressure normalized by inlet total pressure and therefore represent the isentropic value.

None of the near hub static pressure tap leads survived final machining of the nozzle diaphragm and consequently, that data cannot be presented. Note that, compared to analytical predictions, the tip exhibits a definite loss in circulation due to secondary flow effects, and that even the pitchline seems to be affected somewhat. Coordinates for these stream-surfaces are presented in Appendix B.

Configuration 2

Test data for Block I Configuration 2, the stage one build, are tabulated in Appendix H.

Figure 45, a plot of $\Delta h/\theta_T$ vs $N/\sqrt{\theta_T}$, illustrates that the entire test matrix specified in Table XIV was successfully run.

Efficiency of the Block I first stage is plotted against blade-jet speed ratio, stage loading, and stage total-to-static pressure ratio in Figures 46 thru 48. Note that, at design values of P_T/P_S and u/C_o, the efficiency is 0.885. As noted in Appendix F, this efficiency is based on shaft torque and exhaust rake total pressure. Note further that stage efficiency continues to improve with increasing pressure ratio.

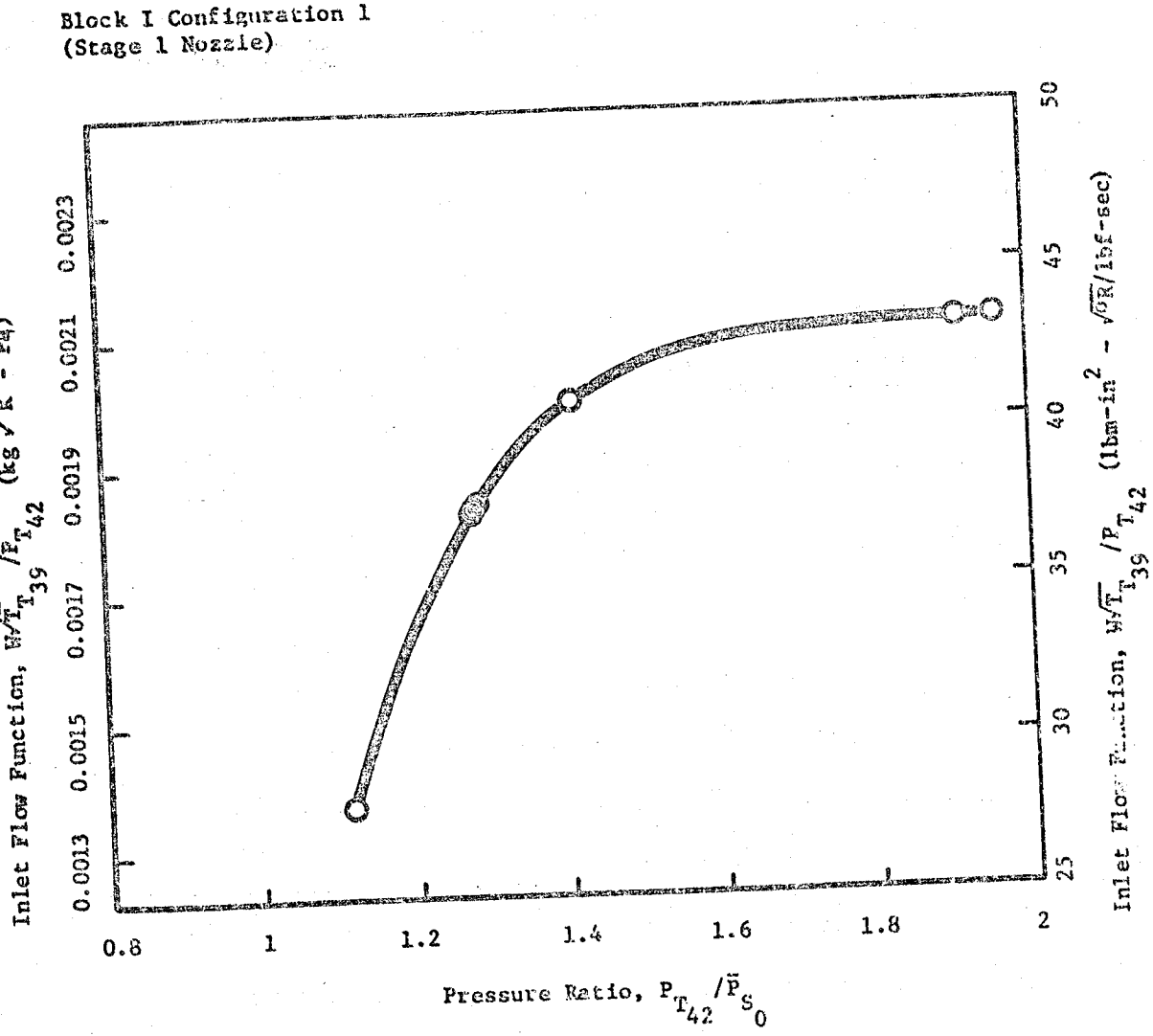

Figure 39. Block I Configuration 1, Inlet Flow Function, $W\sqrt{T}_{T_{39}}/P_{T_{42}}$ VS. Pressure Ratio, $P_{T_{42}}/\bar{P}_{S_0}$

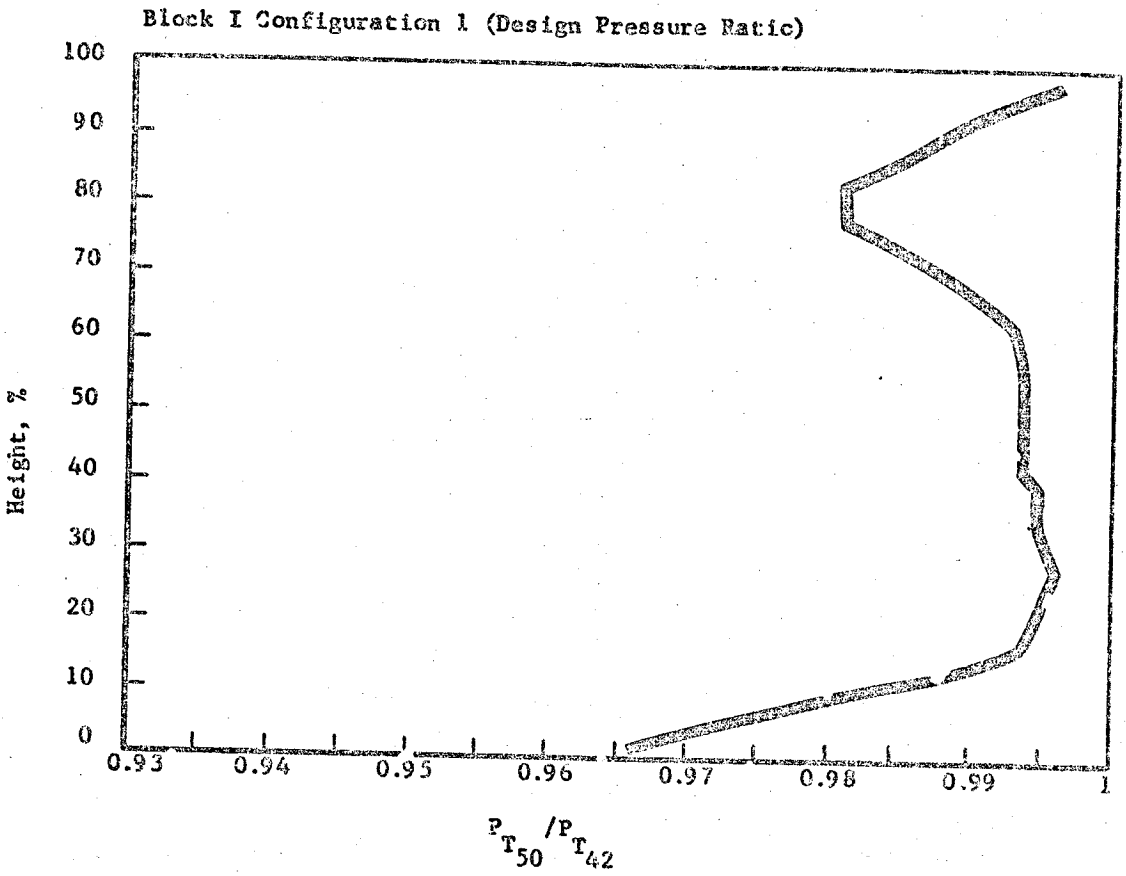

Figure 40. Block I Configuration 1 Exit Survey $P_{T_{50}}/P_{T_{42}}$ vs. % Height.

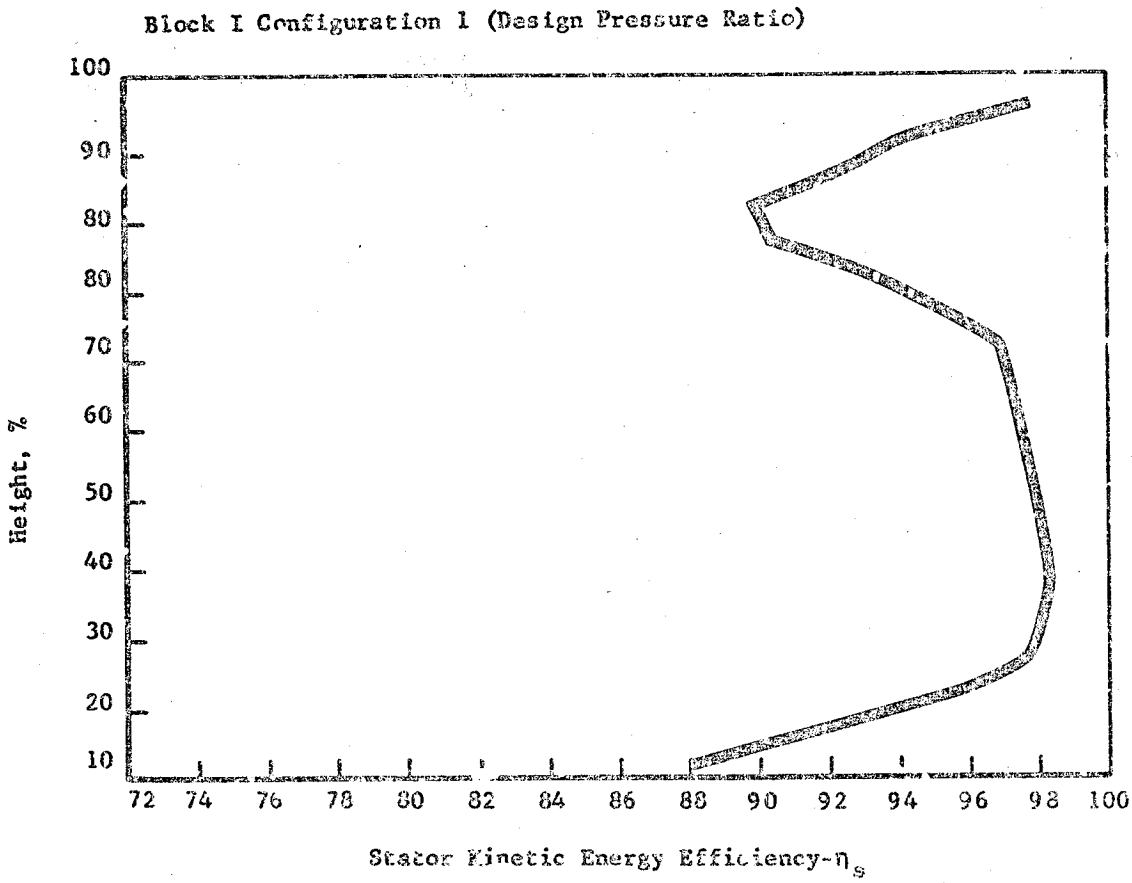

Figure 41. Block 1 Configuration 1 Exit Survey - Efficiency . . % Height

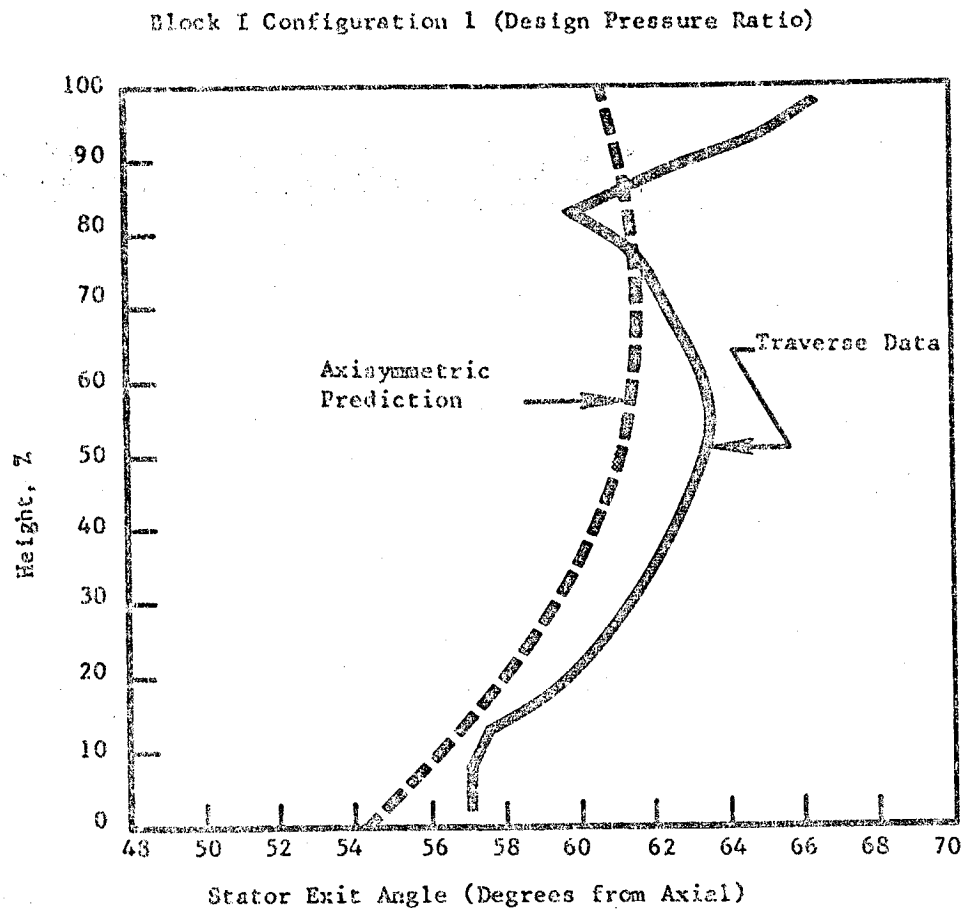

Figure 42. Block I Configuration 1 Exit Survey - Swirl vs. % Height

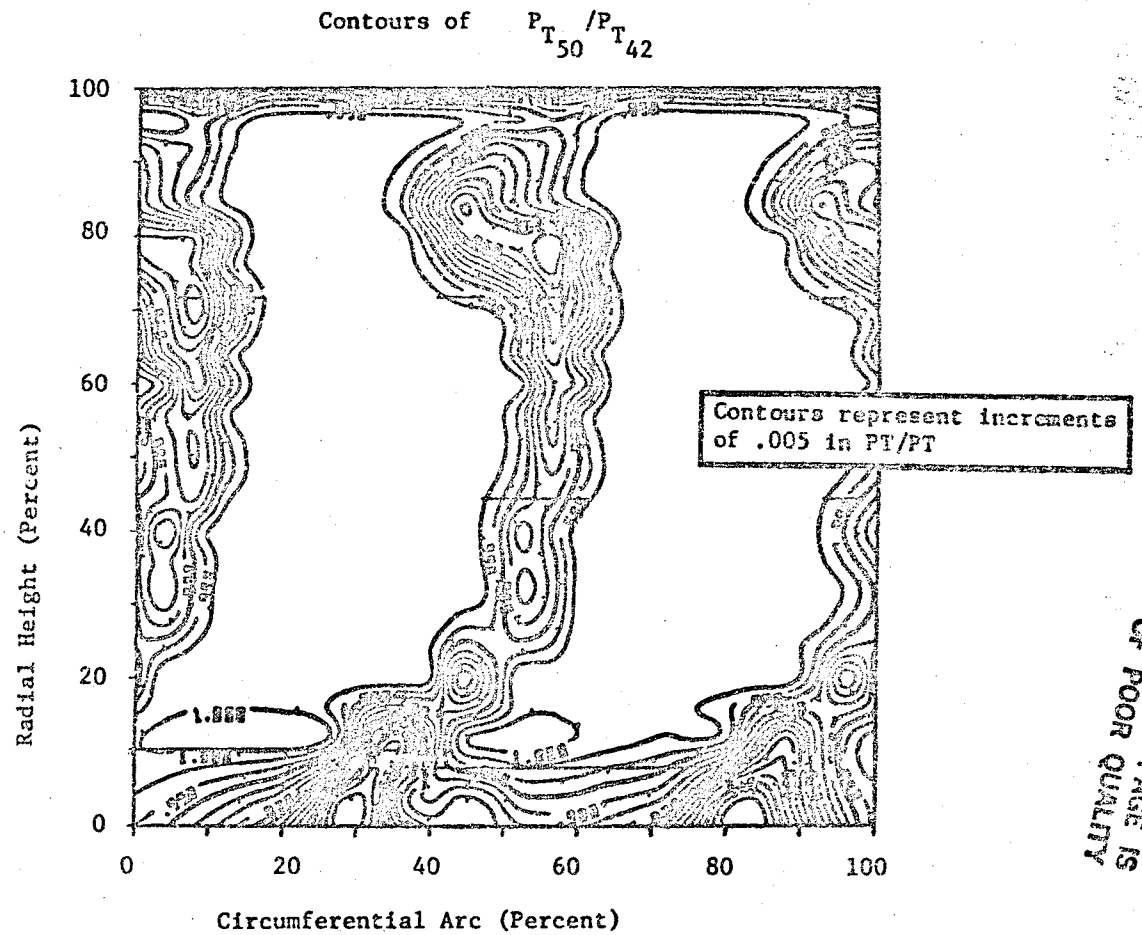

Figure 43. Block I Configuration 1 Exhaust Total Pressure Ratio Contours.

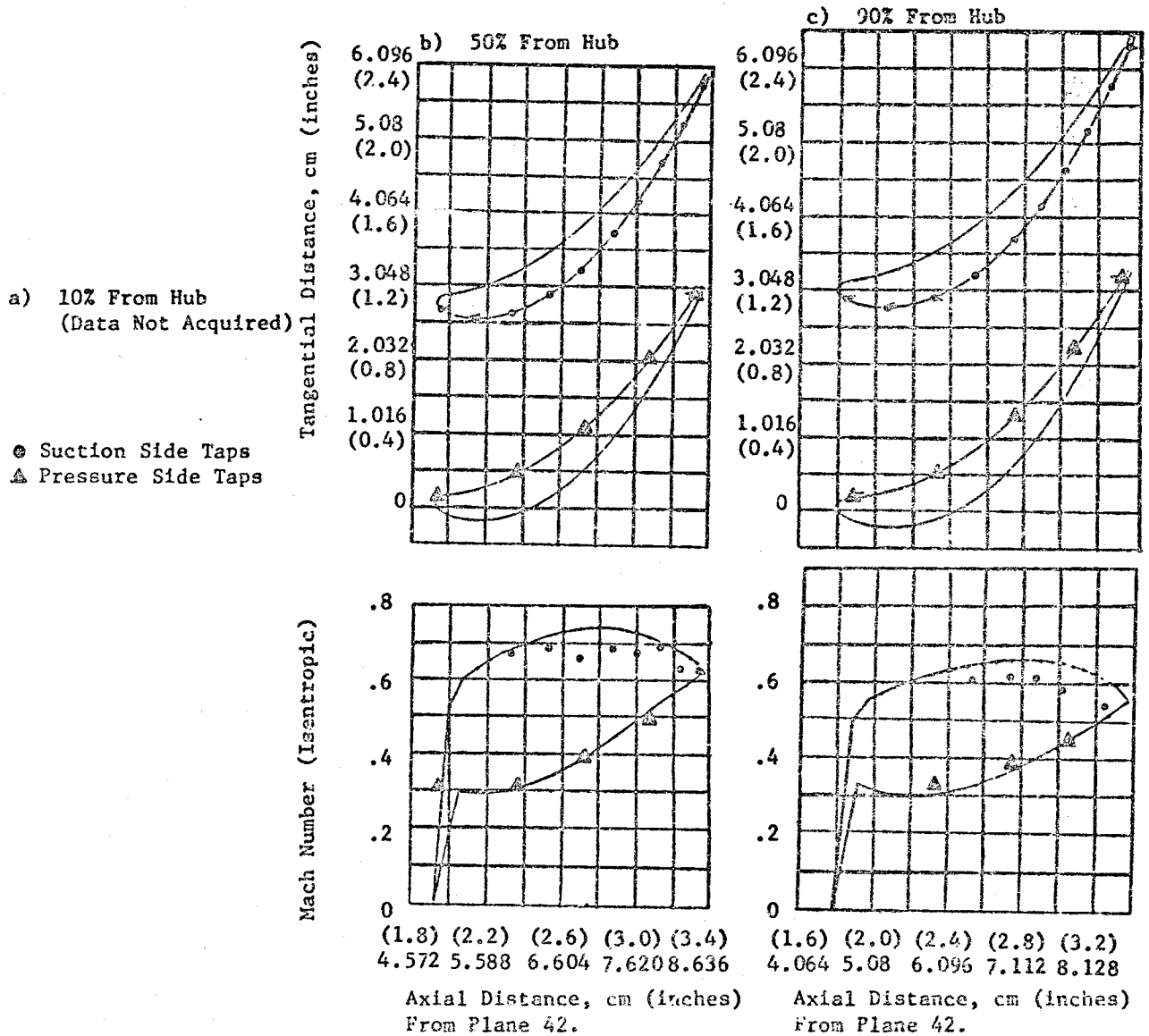

Figure 44. Block I Configuration 1 (Stage 1 Nozzle) Mach Number Distribution (Based On Measured Surface Static Pressure)

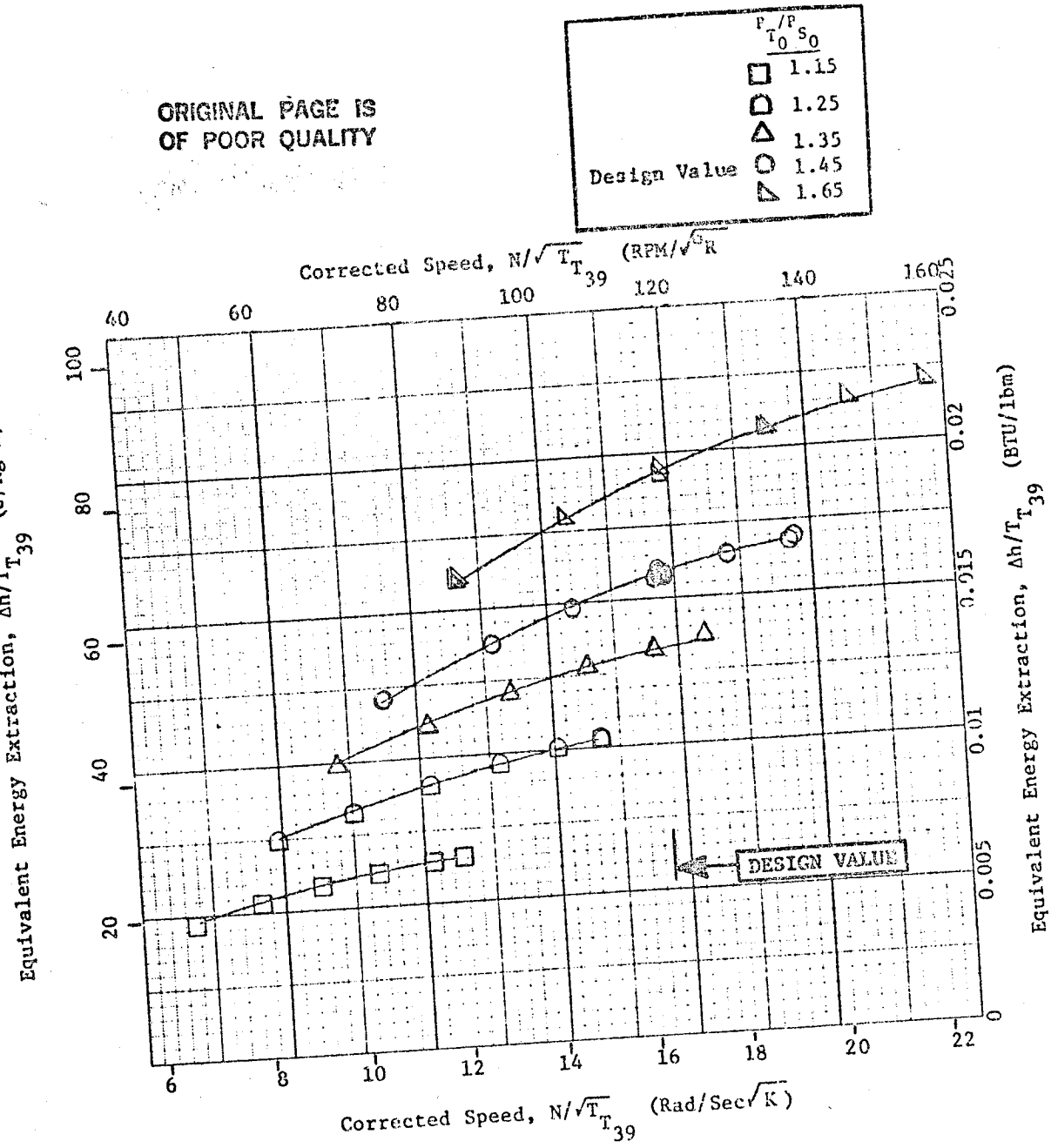

Figure 45. Block I Configuration 2, Equivalent Energy Extraction $,\Delta h/T_{T_{39}}$, Vs. Corrected Speed, $N\sqrt{T_{T_{39}}}$

Block I Configuration 2
(Stage 1)

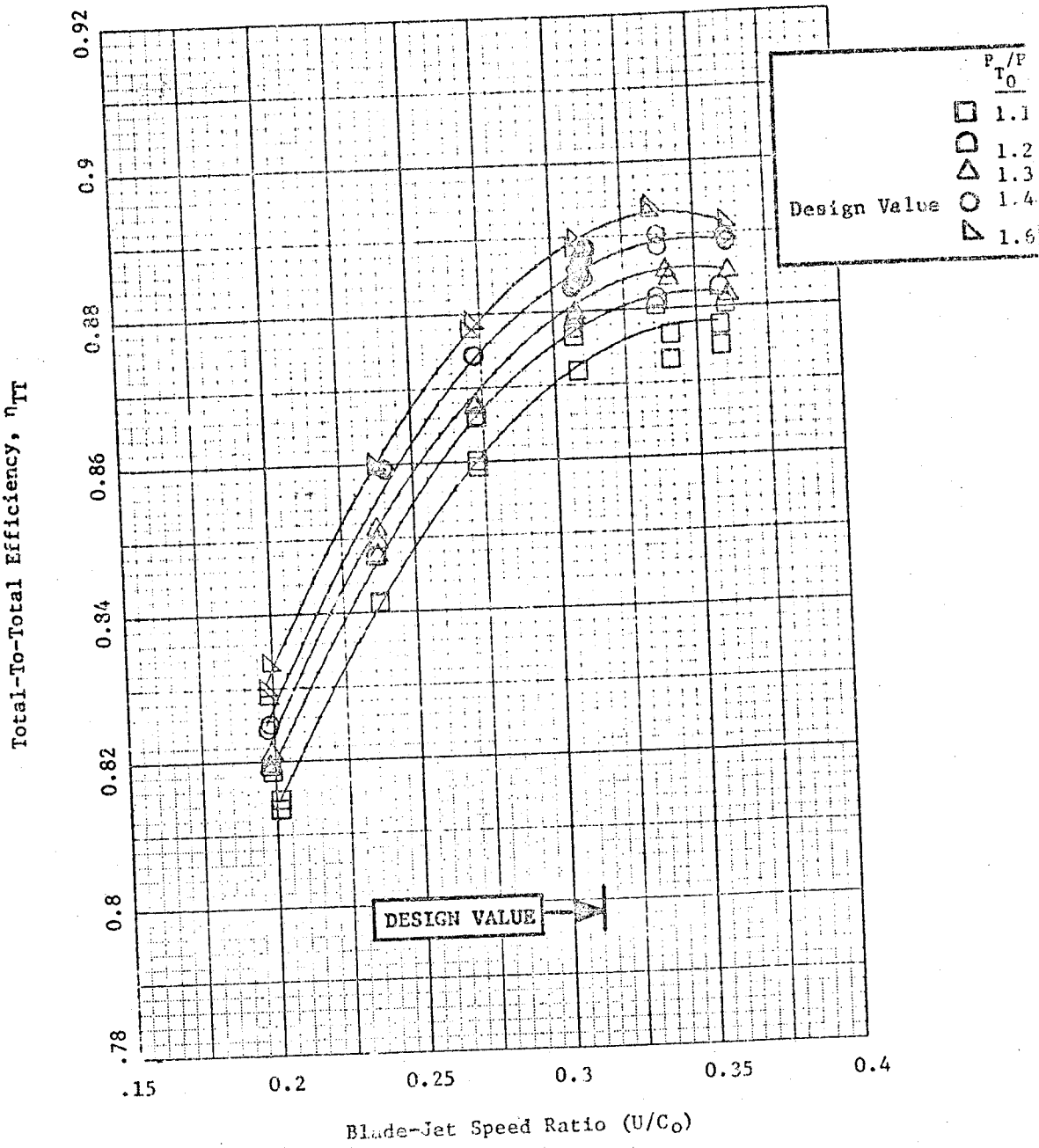

Figure 46. Block I Configuration 2, Total-To-Total Efficiency ,η_{TT}, VS. Blade-Jet Speed Ratio, u/C_o

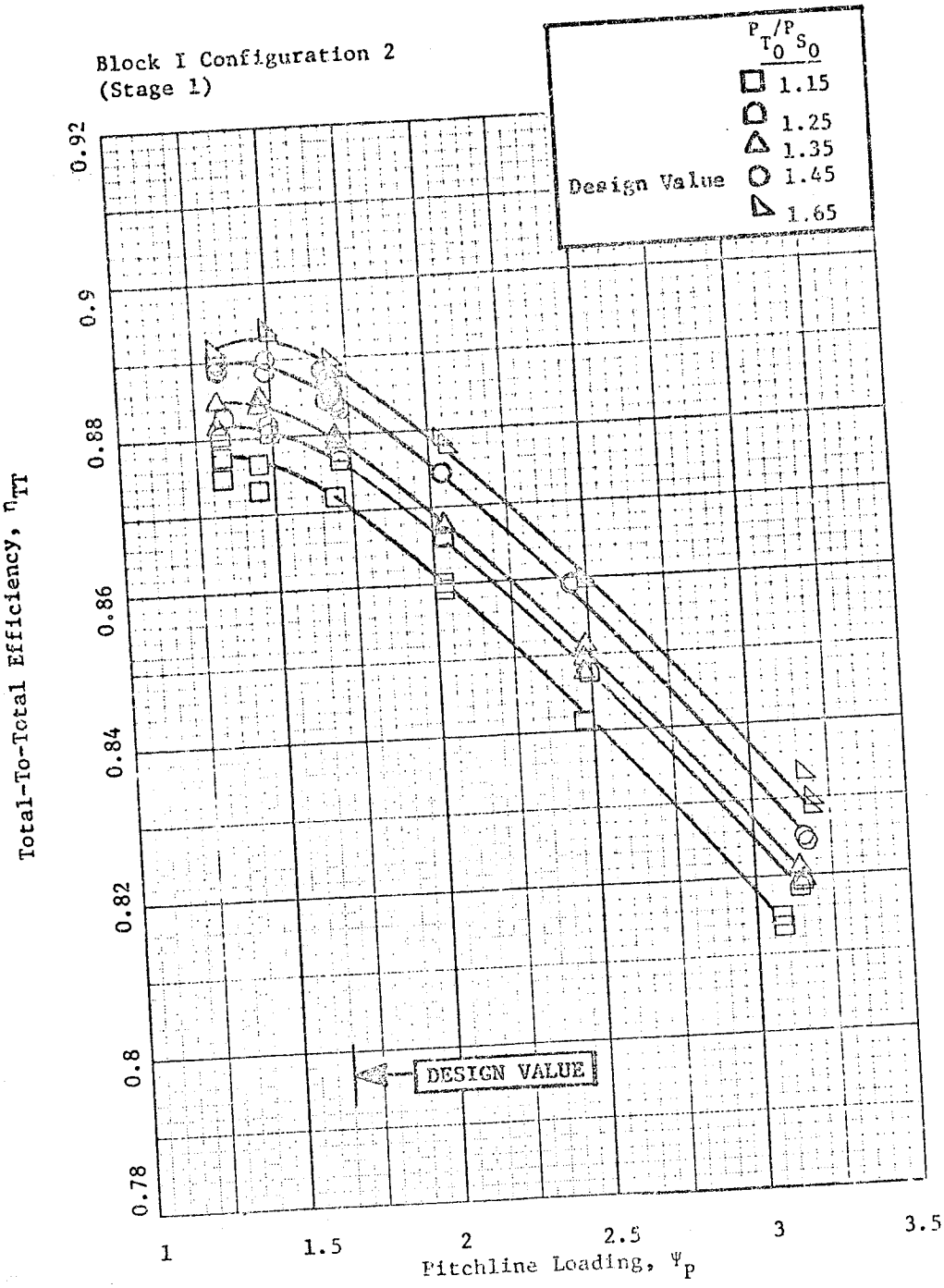

Figure 47. Block I Configuration 2, Total-To-Total Efficiency, η_{TT}, Vs. Pitchline Loading, Ψ_P

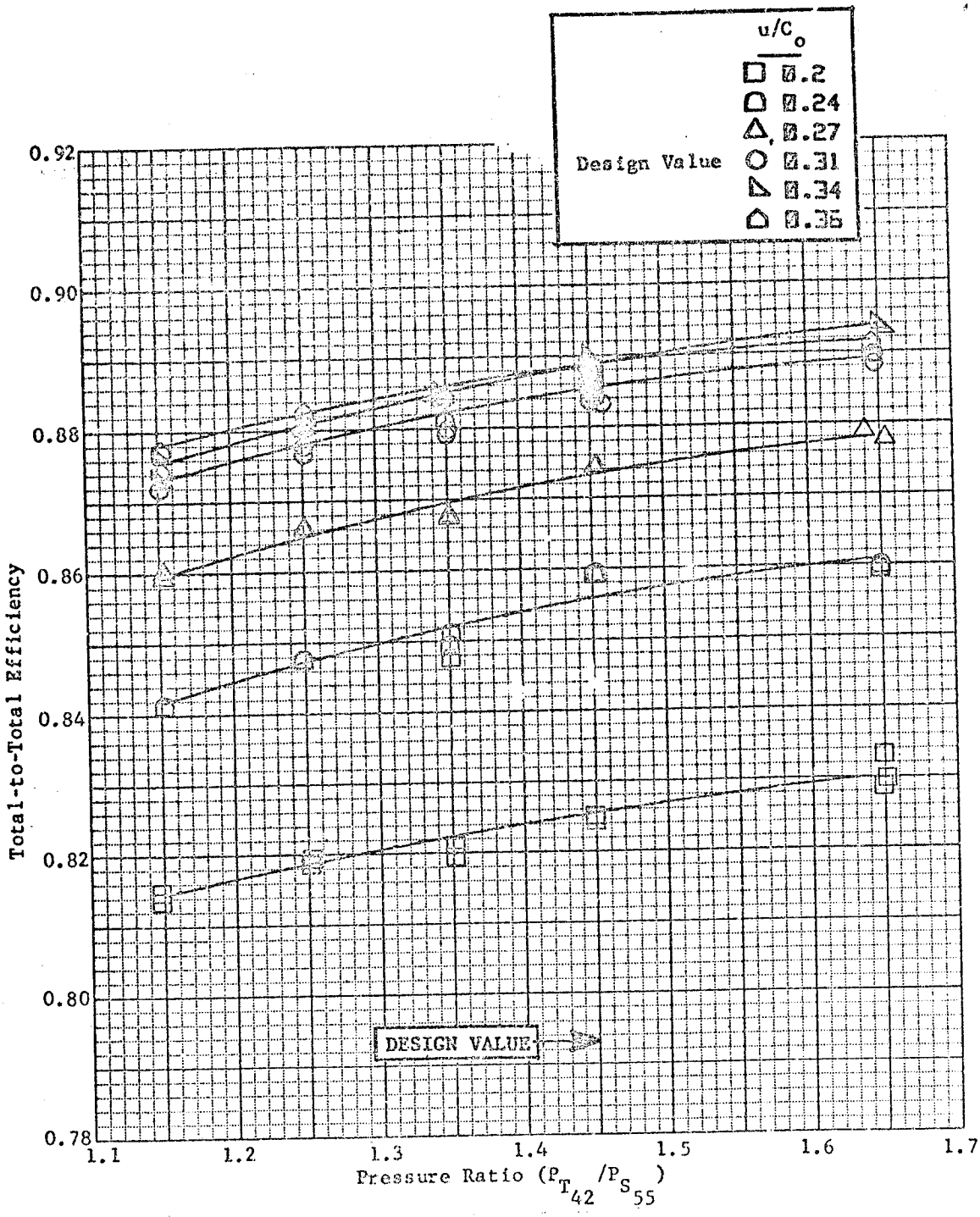

Figure 48. Block I Configuration 2, Total-to-Total Efficiency vs. Pressure Ratio ($P_{T_{42}}/P_{S_{55}}$).

Flow characteristics for this stage are presented as Figures 49 through 52. Note from Figure 50 that, at the design stage total-to-static pressure ratio of 1.45, the flow function was 38.3, or about 2% above the tested value of 37.4 from the annular cascade (Conf. 1) value shown in Figure 39. This is due to the fact that the stage 1 nozzle pressure ratio was higher in the stage test than in the cascade test. The relatively steep slope of the flow function vs. pressure ratio characteristic of Figure 39 suggests that this magnitude of flow shift could occur with a very small change in pressure ratio.

Torque characteristics are presented in Figures 53 and 54.

The stage swirl map is presented in Figure 55.

The row-by-row distribution of measured interstage static pressures, normalized by $P_{T_{42}}$, are presented for the design point in Figure 56 compared to an axisymmetric prediction.

Results of the turbine exit traverse survey are presented in Figures 57 through 60. Figure 57 presents the ratio of exhaust total pressure to inlet total pressure as measured by the traverse probe (solid line) and the arc rakes (asterisks), and as predicted by the axisymmetric analysis (dashed line). For this comparison, the level of the traverse pressure profile has been adjusted slightly to match the average of the arc rakes, since the rake average is used as the exhaust total pressure in the efficiency calculation. Figure 58 presents the ratio of exhaust total temperature to inlet total temperature. In this case, the level of the traverse temperature has been adjusted to yield the temperature drop indicated by the shaft torque measurement.

Figure 59 presents exhaust swirl measured at the traverse plane compared to the axisymmetric prediction. Note the core of underturning and then overturning indicative of secondary flow activity, which is especially strong at the outer wall.

Figure 60 presents the radial distribution of stage efficiency as calculated from the pressure and temperature profiles of Figures 58 and 59. Since the average of the pressure profile has been set to the arc rake level and the average of the temperature profile has been set to yield the torque indicated temperature drop, the average of the efficiency profile in Figure 61 is at the quoted level of 0.885, based on a spanwise mass average. Note that two areas of poor performance are evident. The first, covering an area from 50 to 85 percent span, is probably due directly to the stator tip loss so evident from Figures 41 and 43. The second is from 0 to 25 percent span. Posttest data match analysis has shown that sub-standard performance (relative to prediction) in both the stator hub and rotor blade hub contributed to the deficiency in this region.

Results of the Reynolds number excursion for Configuration 2 are presented as Figure 61 as normalized efficiency versus normalized Reynolds number. The reader is referred to Appendix E for detail on the Reynolds number excursion.

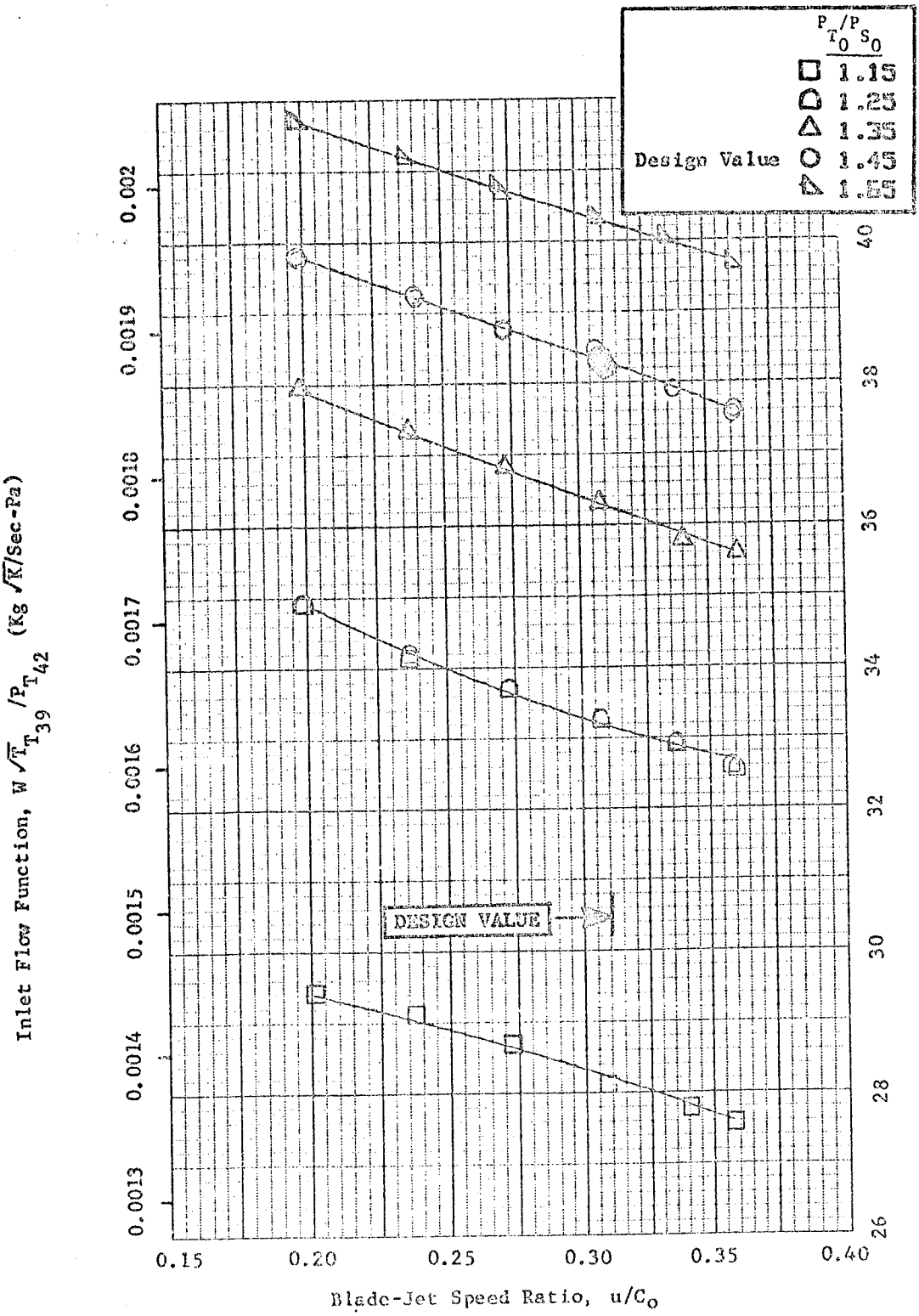

Figure 49. Block I Configuration 2, Inlet Flow Function ($W\sqrt{T_{T_{39}}}/P_{T_{42}}$) vs. Blade-Jet Speed Ratio (u/C_o).

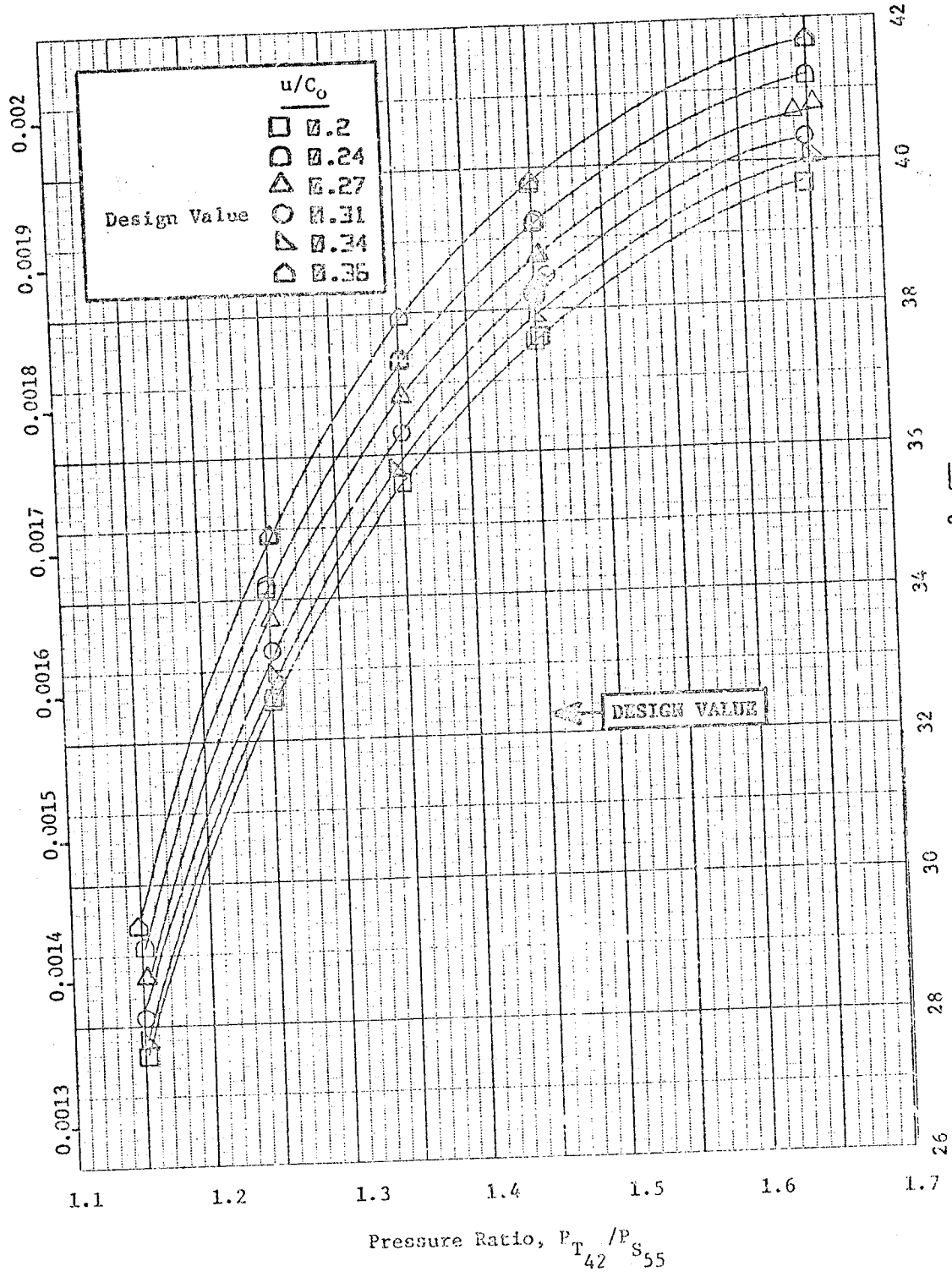

Figure 50. Block I Configuration 2, Inlet Flow Function ($W\sqrt{T}_{T_{39}}/P_{T_{42}}$) vs. Pressure Ratio ($P_{T_{42}}/P_{S_{55}}$).

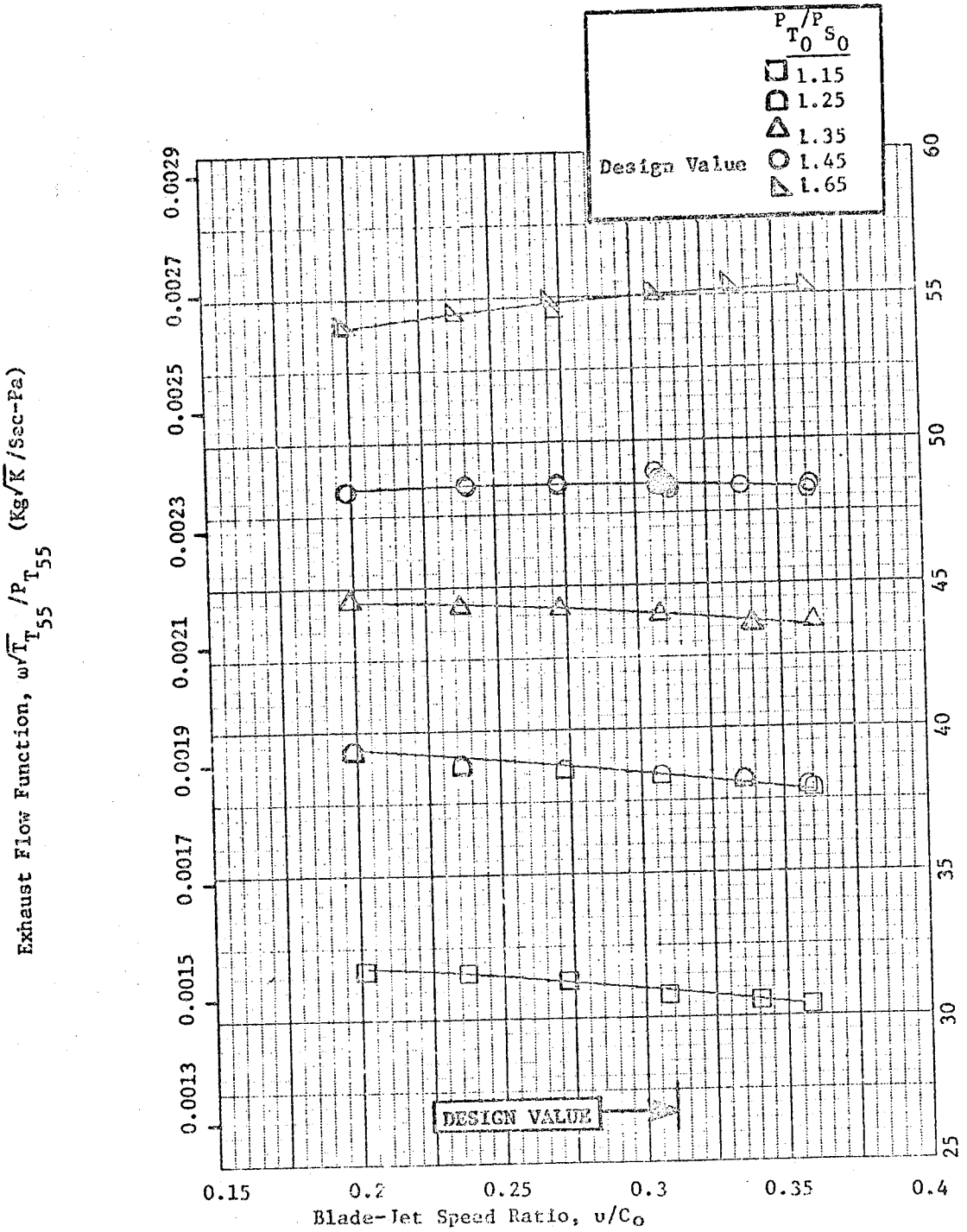

Figure 51. Block I Configuration 2, Exhaust Flow Function, $\omega\sqrt{T_{T_{55}}}/P_{T_{55}}$, vs. Blade-Jet Speed Ratio, u/CO.

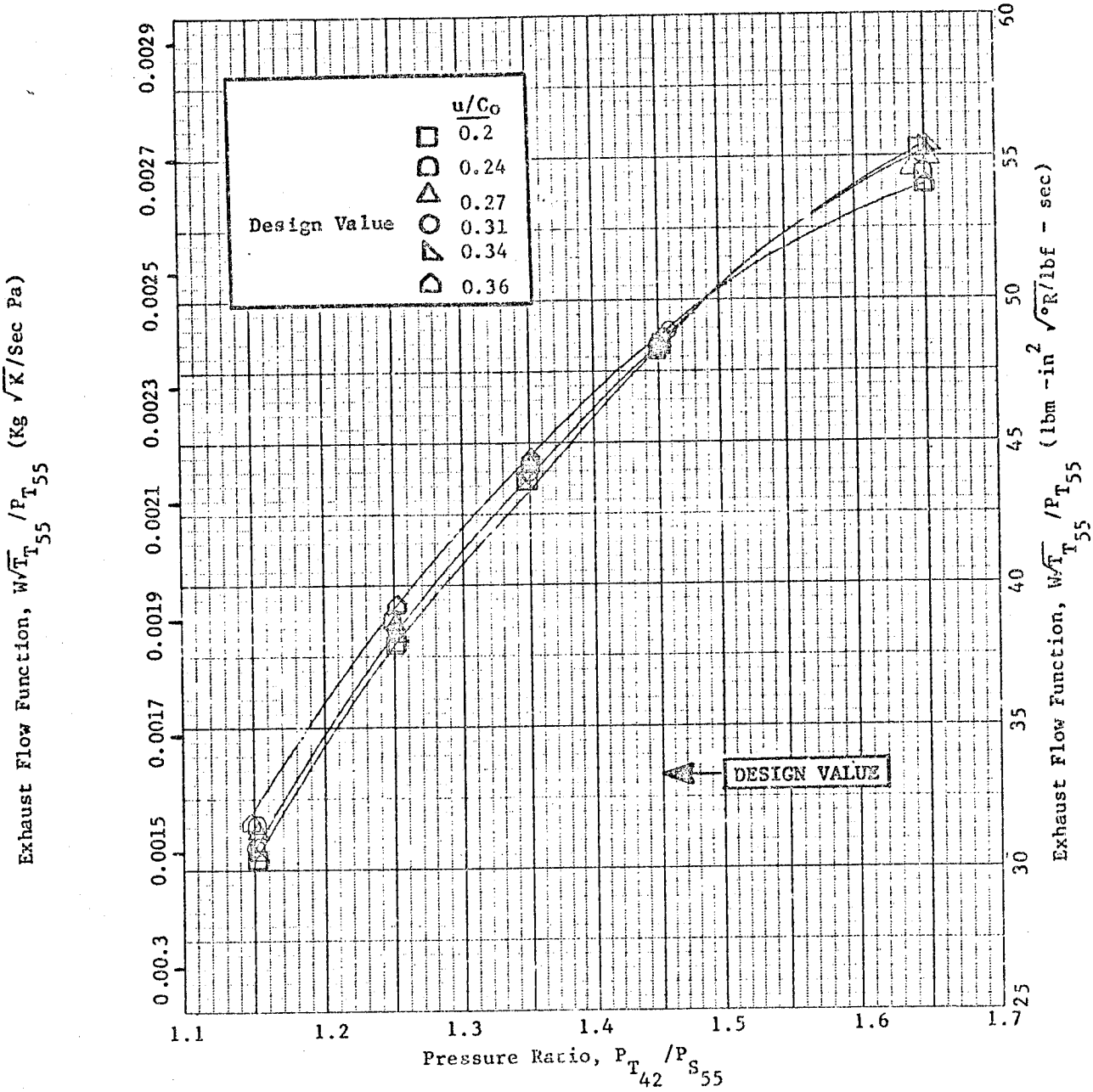

Figure 52. Block 1 Configuration 2. Exhaust Flow Function, $W\sqrt{T}_{T_{55}}/P_{T_{55}}$, vs. Pressure Ratio, $P_{T_{42}}/P_{S_{55}}$.

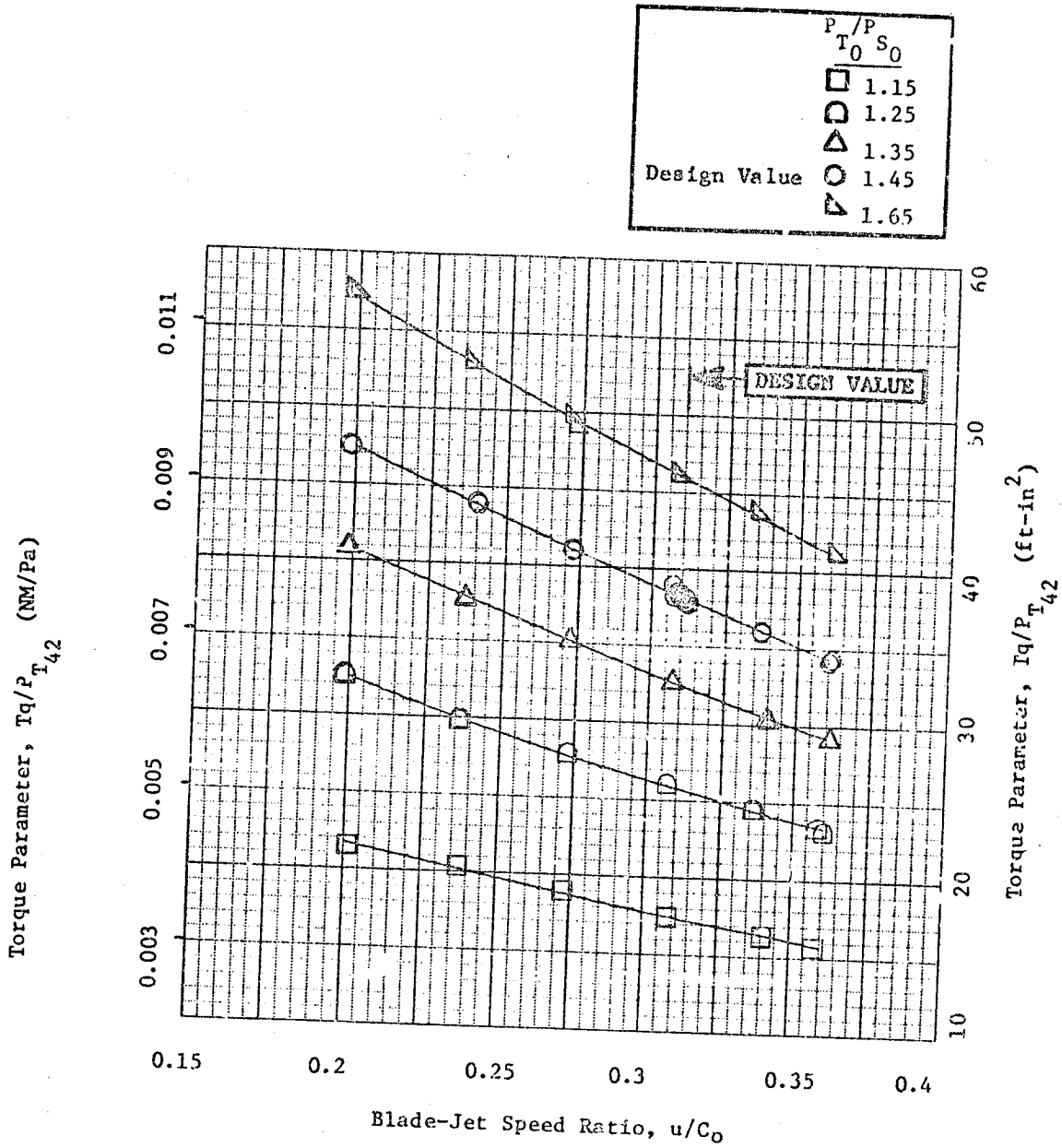

Figure 53. Block I Configuration 2, Torque Parameter, $Tq/P_{T_{42}}$, vs. Blade-Jet Speed Ratio, u/C_o

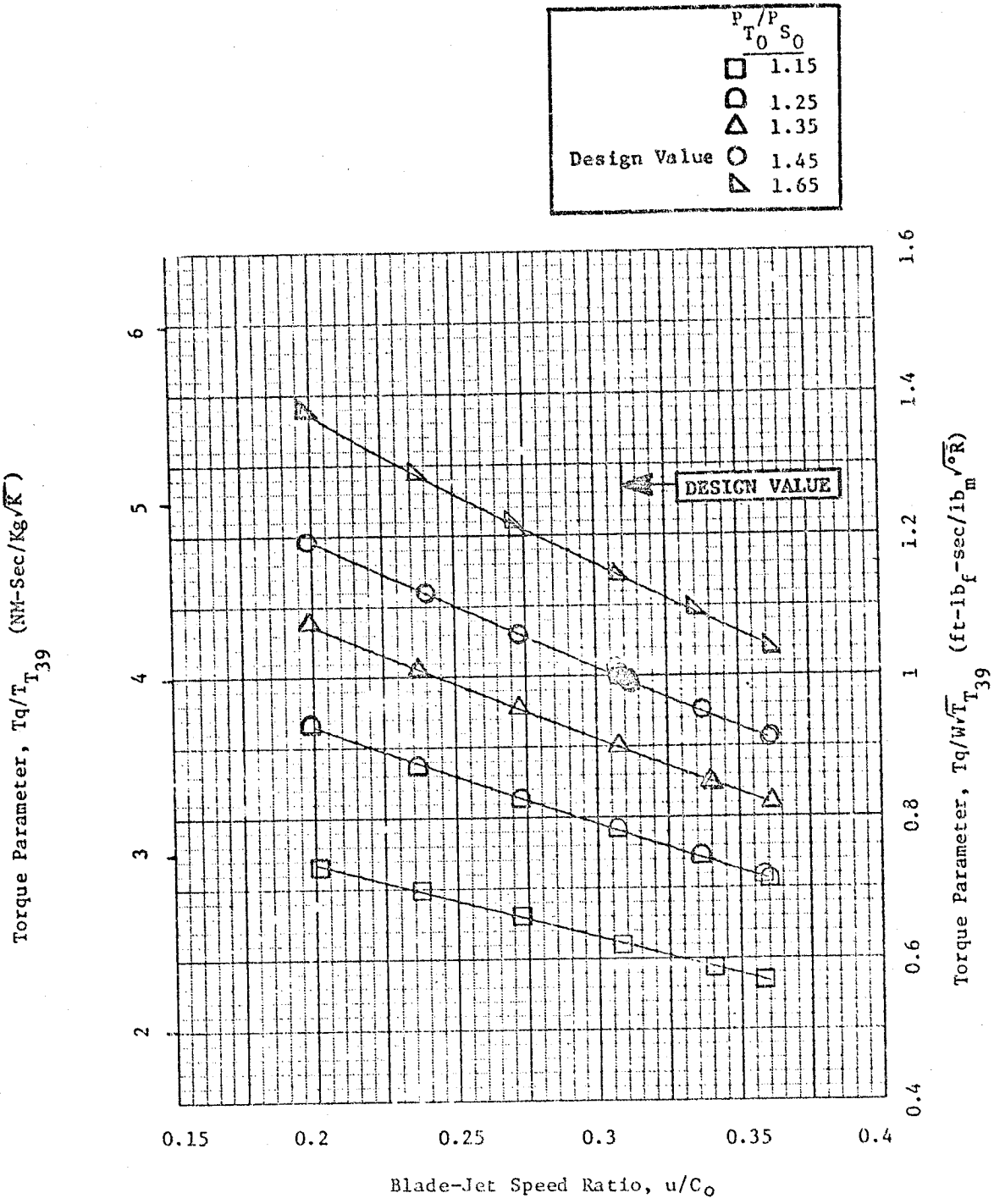

Figure 54. Block I Configuration 2, Torque Parameter, $Tq/W\sqrt{T}_{T_{39}}$, Vs. Blade-Jet Speed Ratio, u/C_o

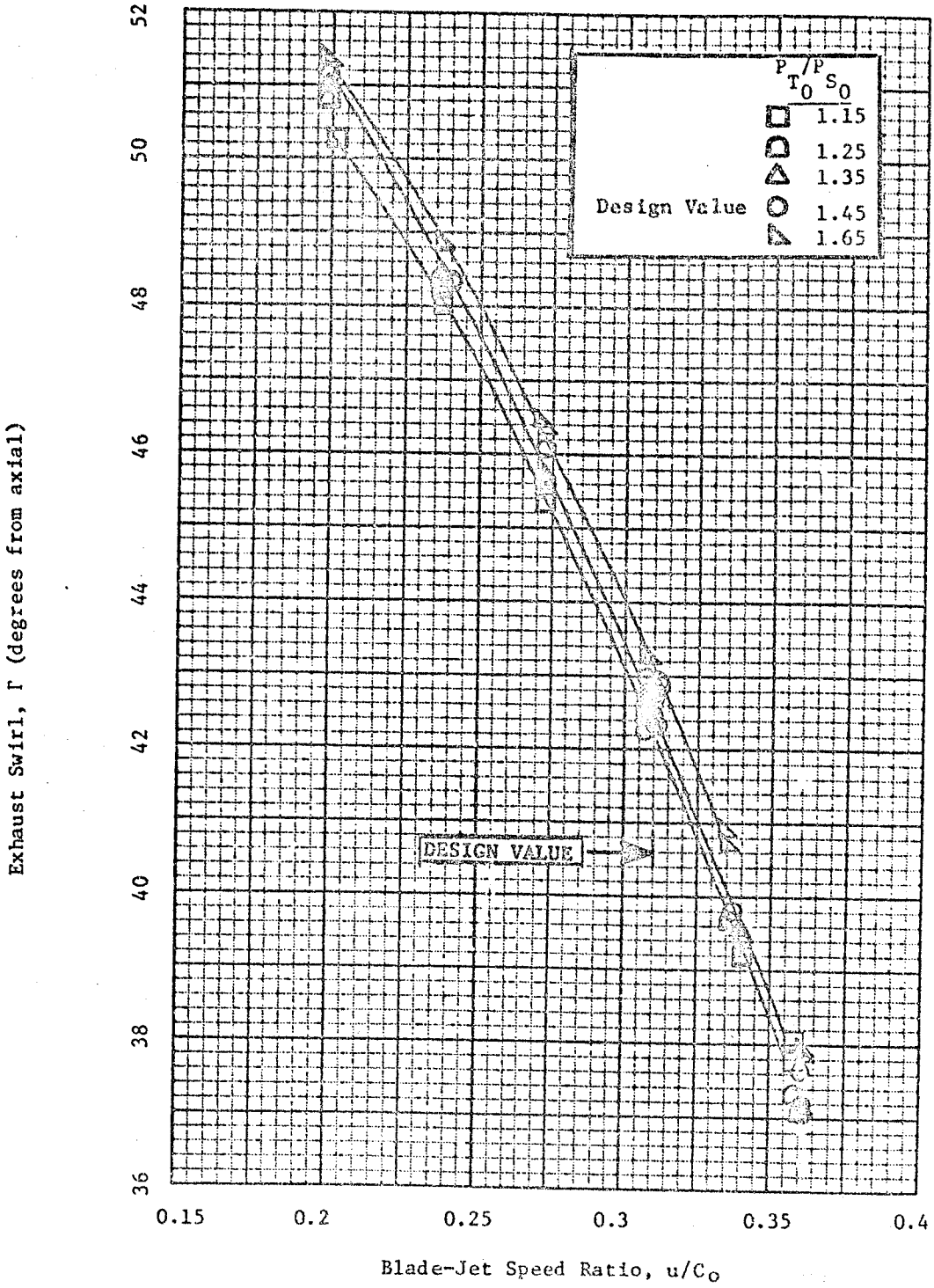

Figure 55. Block I Configuration 2, Exhaust Swirl, Γ, Vs. Blade-Jet Speed Ratio, u/C_o.

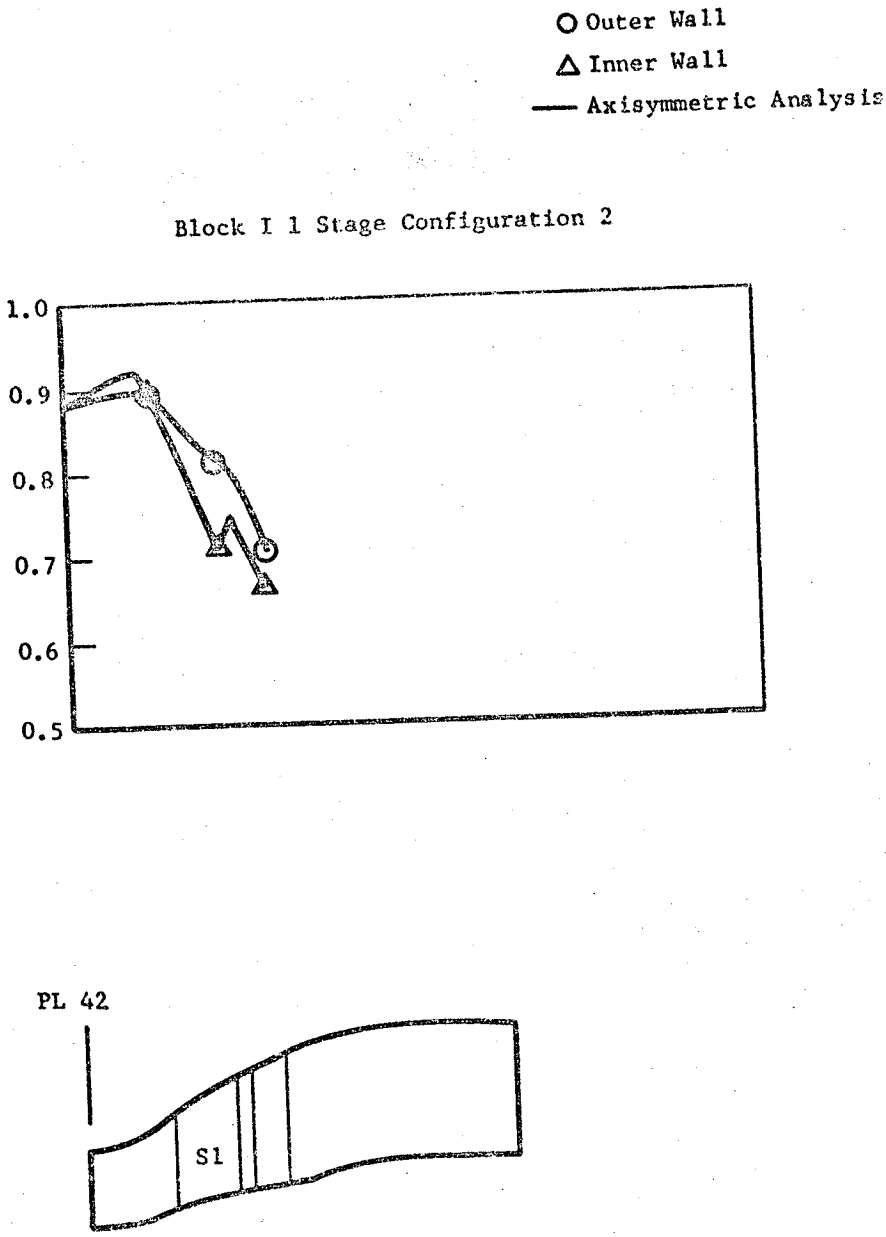

Figure 56. Interstage Static Pressures, Predicted Versus Test (Design Point Data)

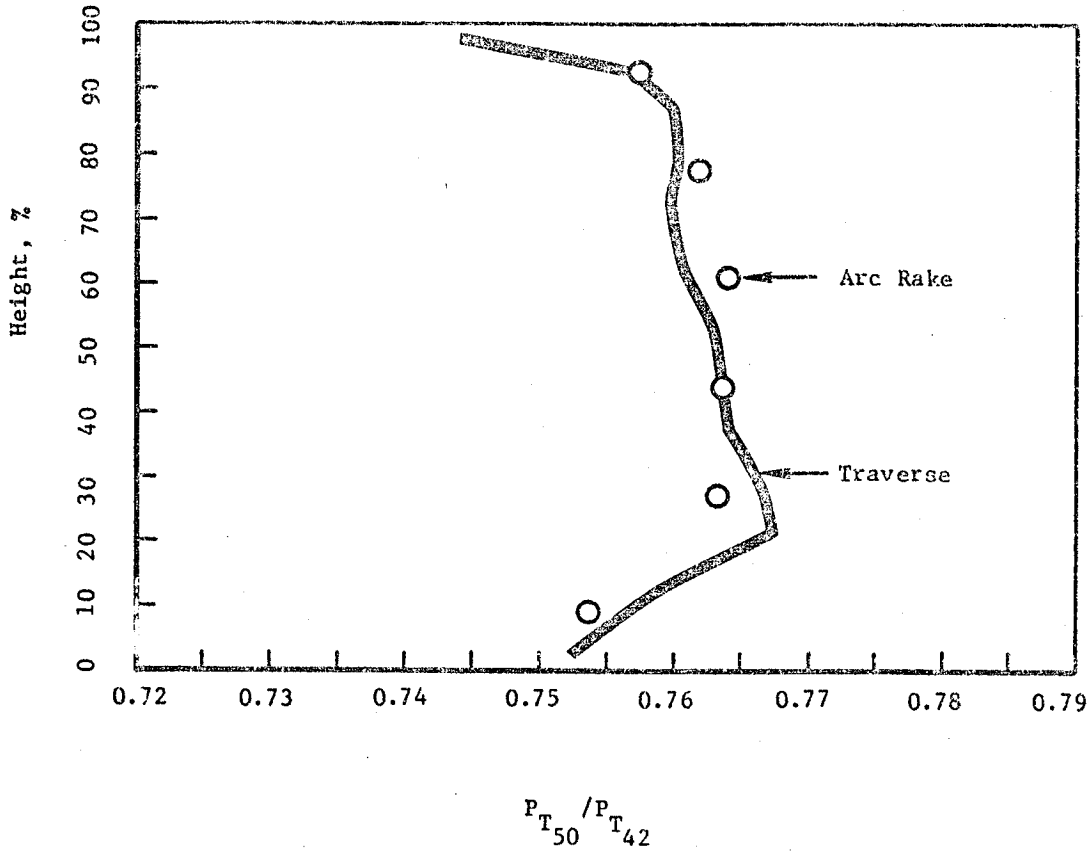

Figure 57. Block I Configuration 2 Exit Survey-$P_{T_{50}}/P_{T_{42}}$ Vs. % Height

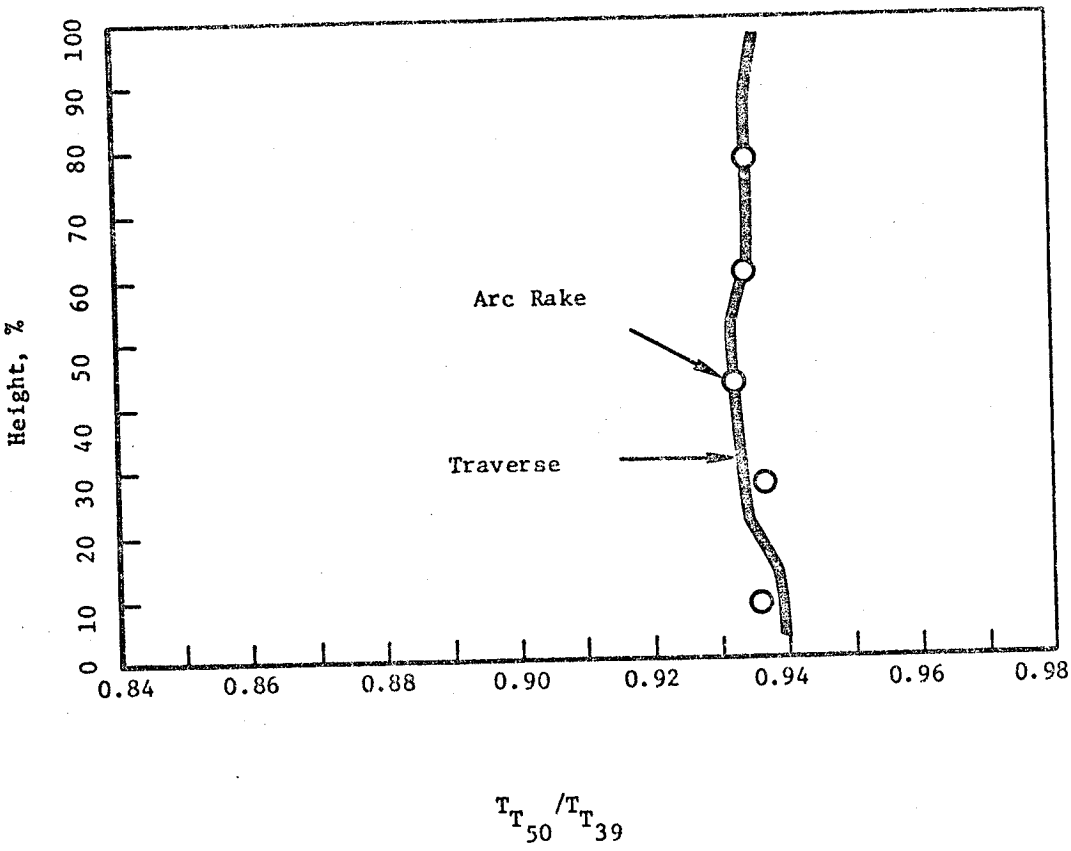

Figure 58. Block I Configuration 2 Exit Survey-$T_{T_{50}}/T_{T_{39}}$ VS. % Height.

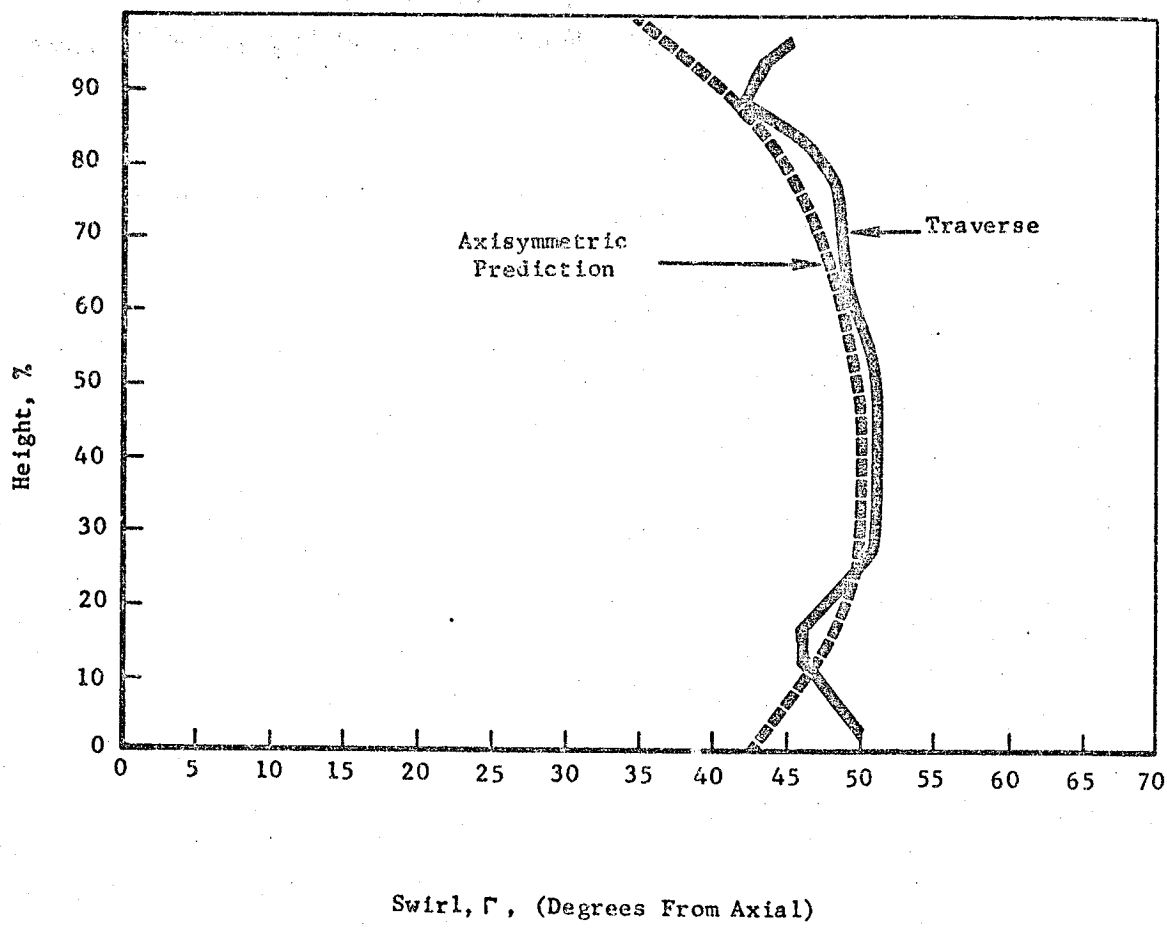

Figure 59. Block I Configuration 2 Exit Survey - Swirl vs. % Height.

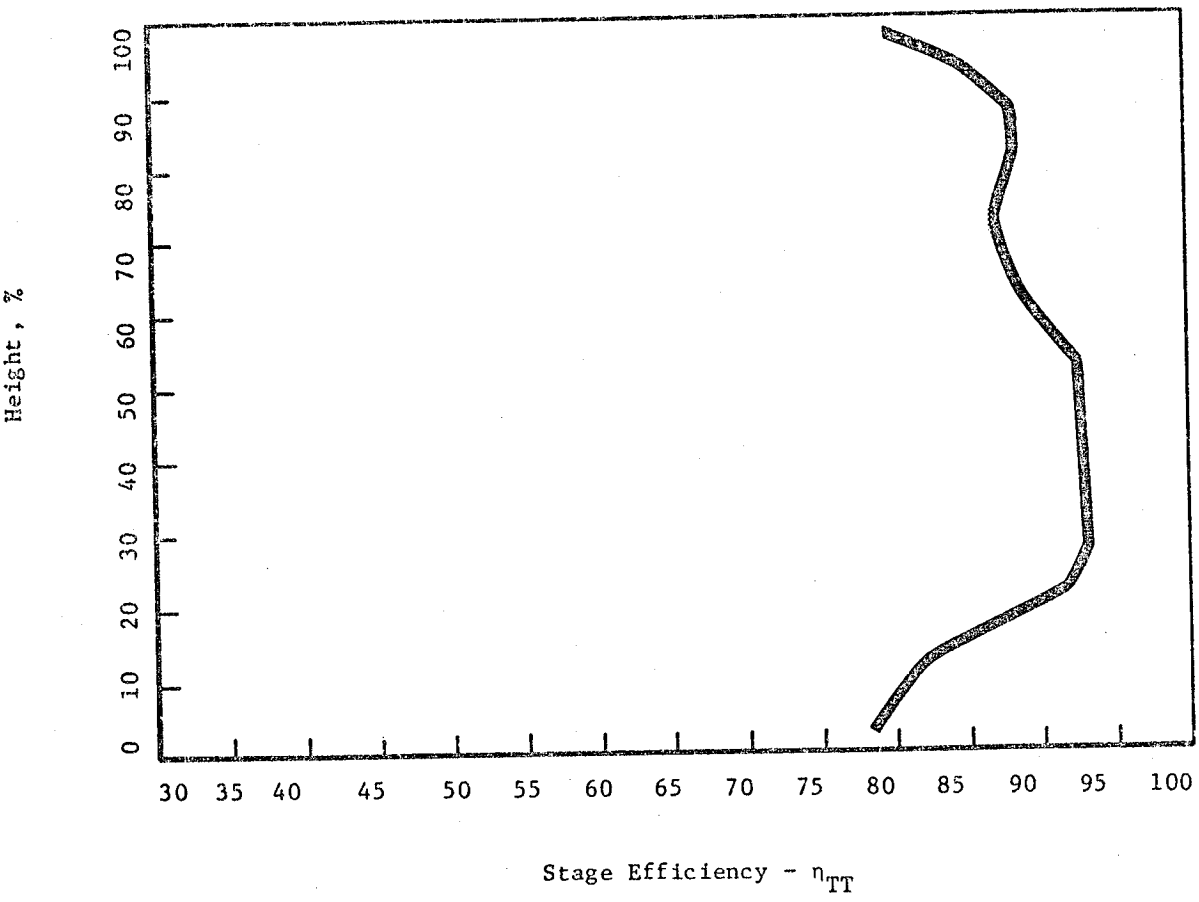

Figure 60. Block I Configuration 2 Exit Survey - Efficiency Vs. % Height

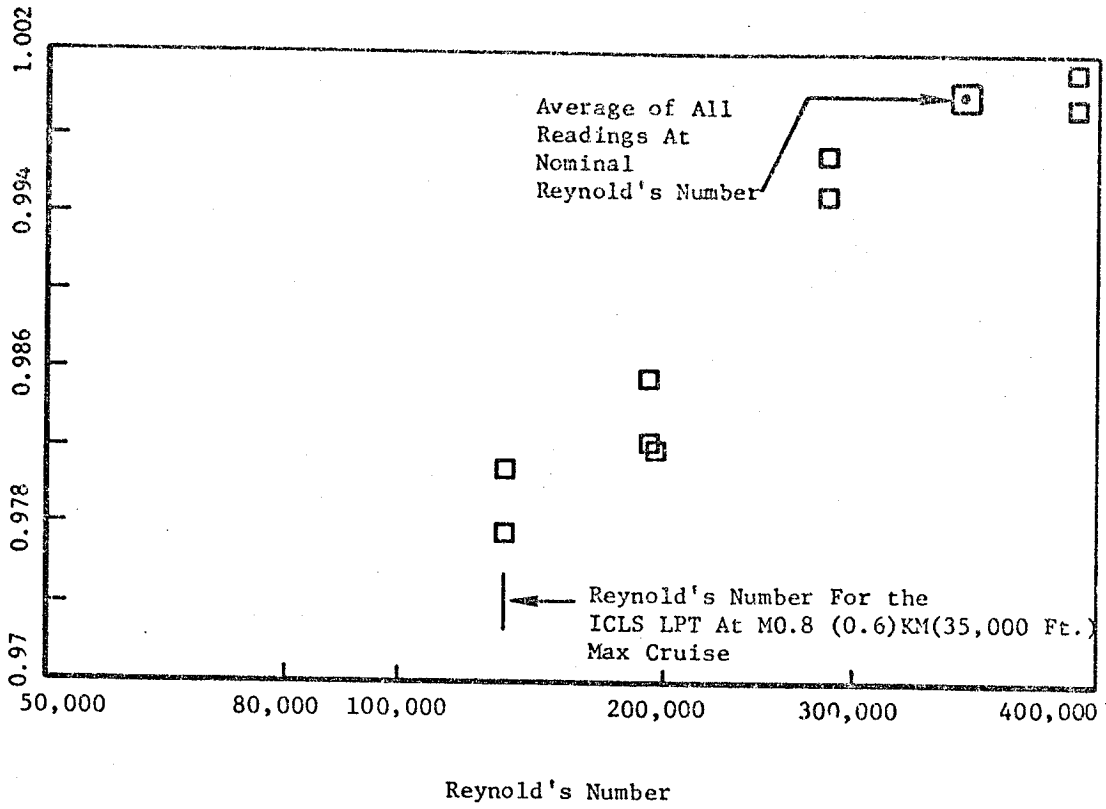

Figure 61. Block I Configuration 2 Reynolds Number Excursion

Configuration 3

Figure 27 presents the rig flowpath for the Block I stage-and-a-half, or stage 2 nozzle annular cascade, test. Test points, per Table XV, were set by running to the same $N/\sqrt{T_T}$ and torque/inlet pressure as set for corresponding points in the Configuration 2 test. The test points are shown on the basis of Stage 1 $\Delta h/T_T$ vs $N/\sqrt{T_T}$ in Figure 62.

Results of the design point exit traverse survey are presented in Figures 63 through 66. Figure 63 presents the spanwise distribution of Nozzle 2 exit pressure normalized by stage inlet pressure at the design point. Added for reference are Configuration 2 stage exit P_T distributions measured by the traverse probe and the arc rakes in the stage one only test.

Stator 2 design point efficiency, Figure 64, was calculated using Equation F1 of Appendix F. Quantitatively, use of the stage one traverse pressure as $P_{T_{50}}$ (rather than the rake pressure, Figure 63) gave a more realistic level of cascade efficiency for this high turning bladerow. Note once again the large secondary loss core formed at the highly-sloped tip of this bladerow. The depth of the core is similar to that measured for Nozzle 1, however, the penetration from the outer wall is reduced due to higher aspect ratio in this bladerow.

Figure 66 presents contours of P_T exit/P_T inlet for Nozzle 2 which show suction side loss accumulation at the tip similar to that for Nozzle 1, Figure 43. Also evident are loss cores formed near the hub.

Airfoil surface Mach numbers calculated from static pressures measured on near hub, pitchline, and near tip streamlines are presented in Figure 67. Note that, compared to analytical predictions, the hub and tip exhibit decreased circulation due to secondary flow effects, while the pitchline shows relatively good agreement. Coordinates for these streamsurfaces are presented in Appendix B.

Configuration 4

Test data for Block I Configuration 4, the 2-stage group, are tabulated in Appendix H. The flowpath and instrumentation layout for this build was shown in Figure 28.

Figure 68, a plot of $\Delta h/T_T$ vs $N/\sqrt{T_T}$ illustrates that the entire test matrix specified in Table XVI was successfully run.

Efficiency of the Block I 2-stage group is plotted against blade-jet speed ratio, group loading, and stage total-to-static pressure ratio in Figures 69, 70, and 71. Note from Figure 69 that, at design values of P_T/P_S and u/C_o, the group total-to-total efficiency was 0.884 based on measured shaft torque and arc rake exhaust pressure. This was approximately 0.007 below the pre-test prediction based on ALFT technology. Note further from Figure 69 that, at pressure ratios at and above design, the efficiency begins a drop off as soon as design u/C_o is exceeded. This phenomenon, possibly indicative of a

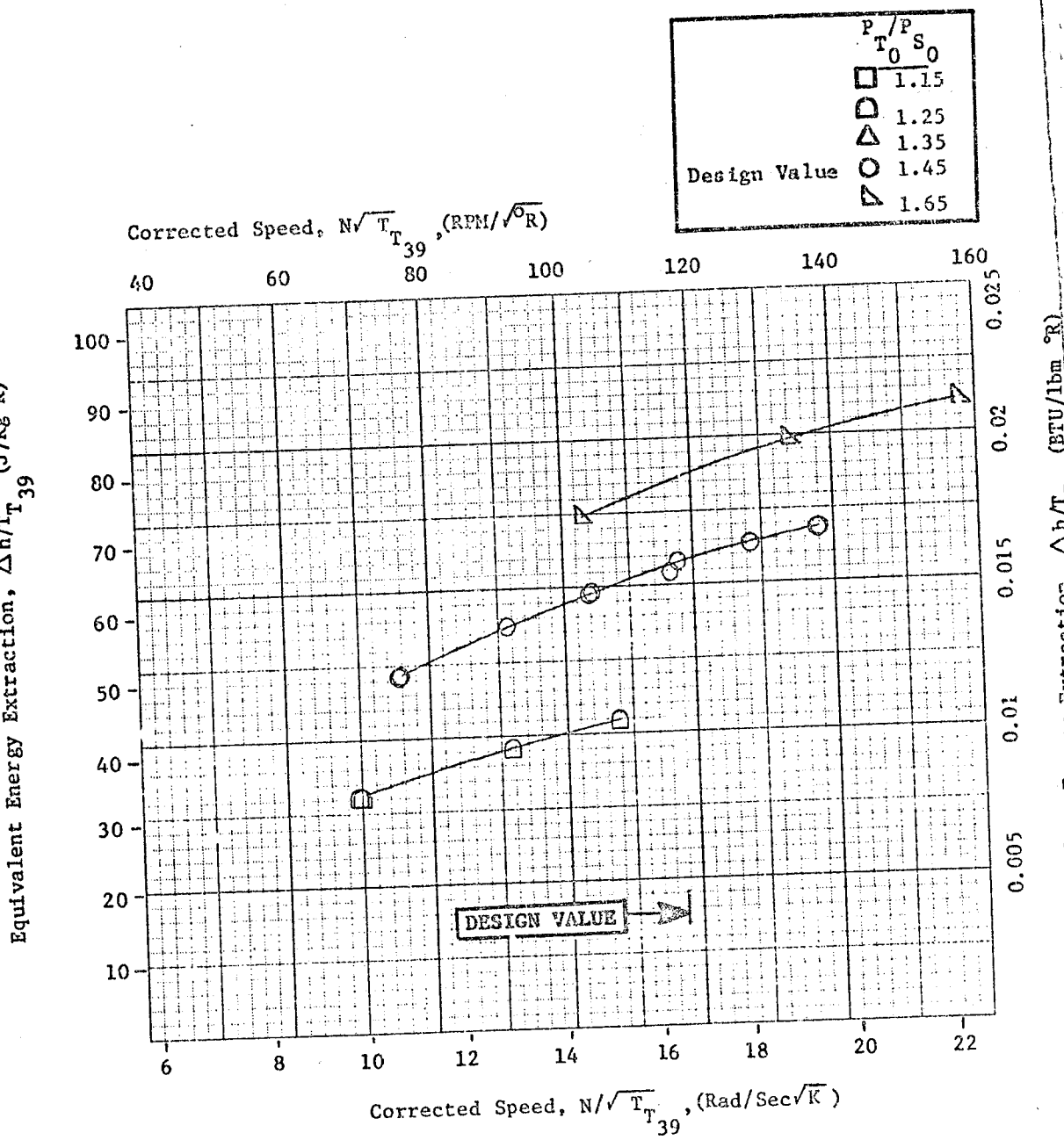

Figure 62. Block I Configuration 3, Equivalent Energy Extraction, $\Delta h/T_{T_{39}}$, Vs. Corrected Speed, $N/\sqrt{T_{T_{39}}}$

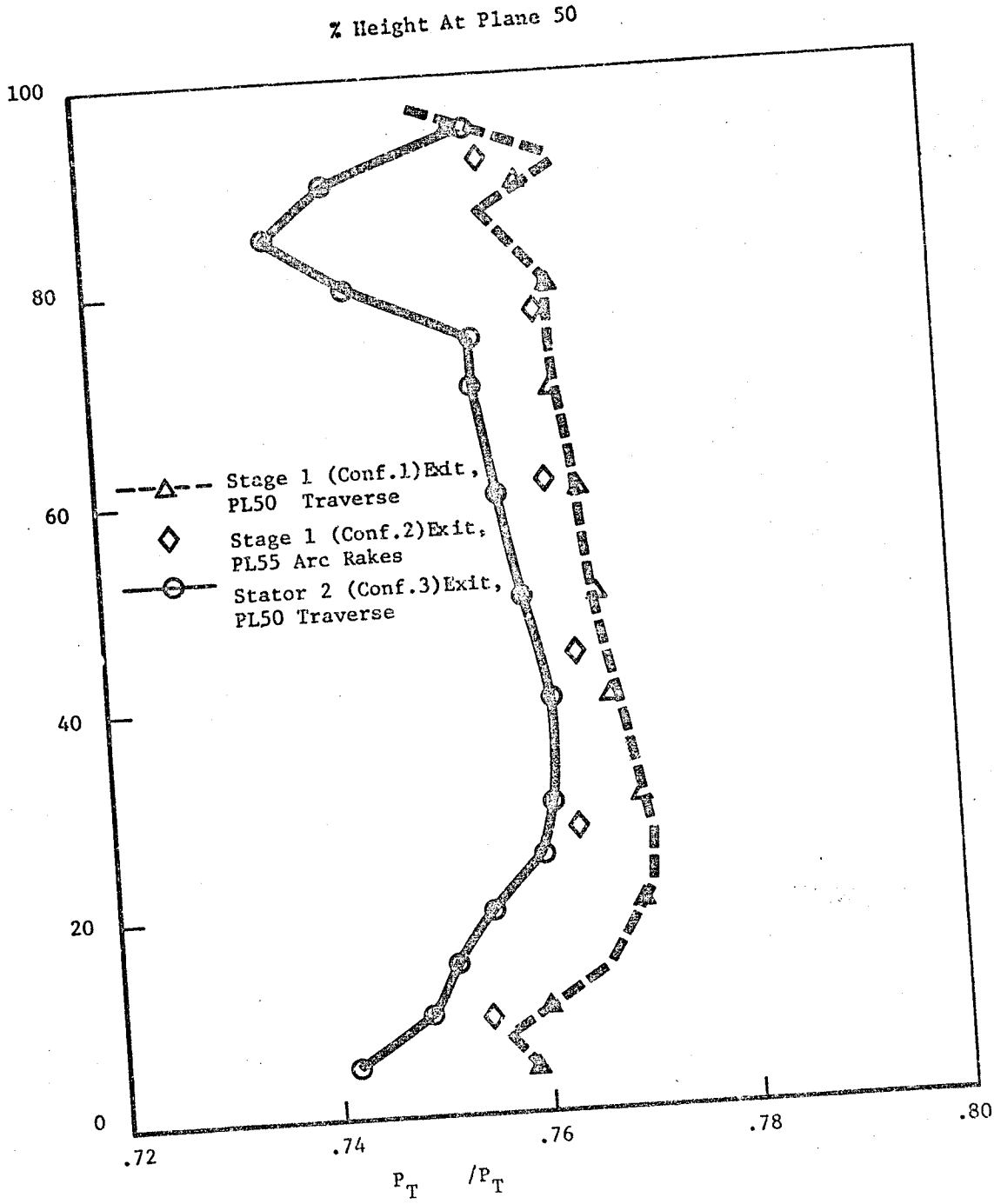

Figure 63. Local Total Pressure Normalized by Stage Inlet Total Pressure, Stage 1 Exit and Stator 2 Exit.

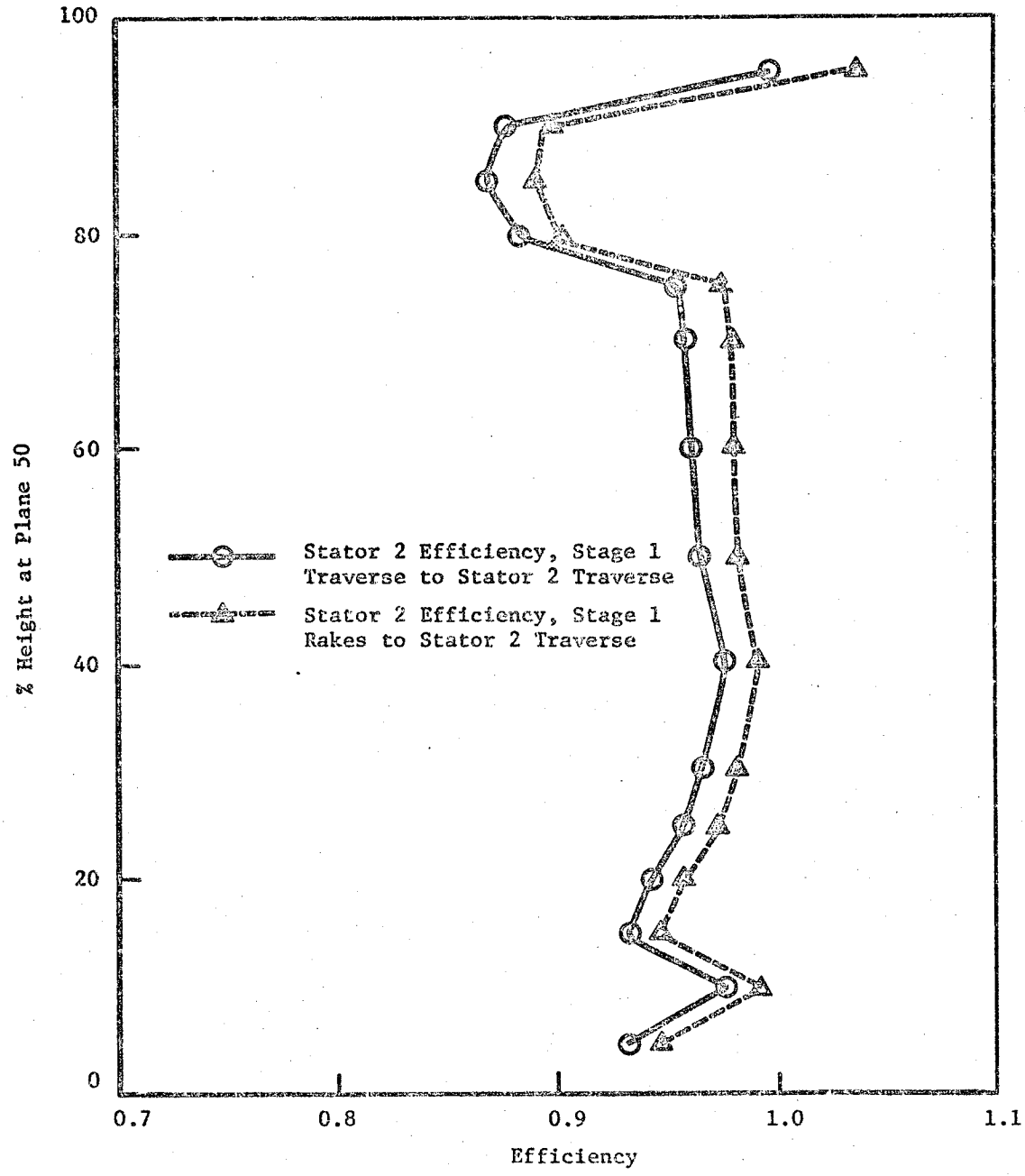

Figure 64. Stator 2 Efficiency Deduced from Total Pressure Distributions of Figure 63.

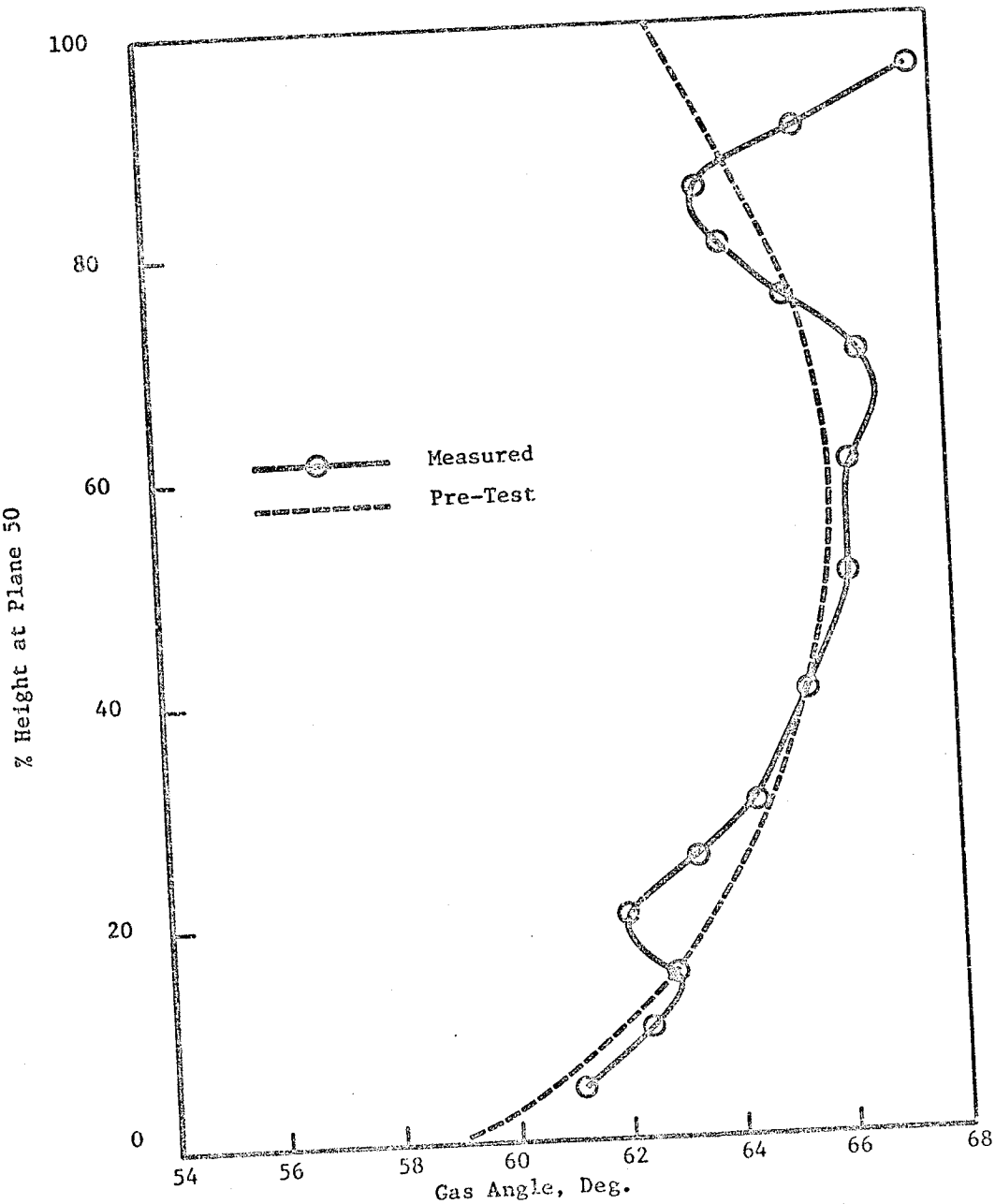

Figure 65. Gas Angle at Stator 2 Exit Traverse Plane, (PL 50), Measured vs. Pre-Test.

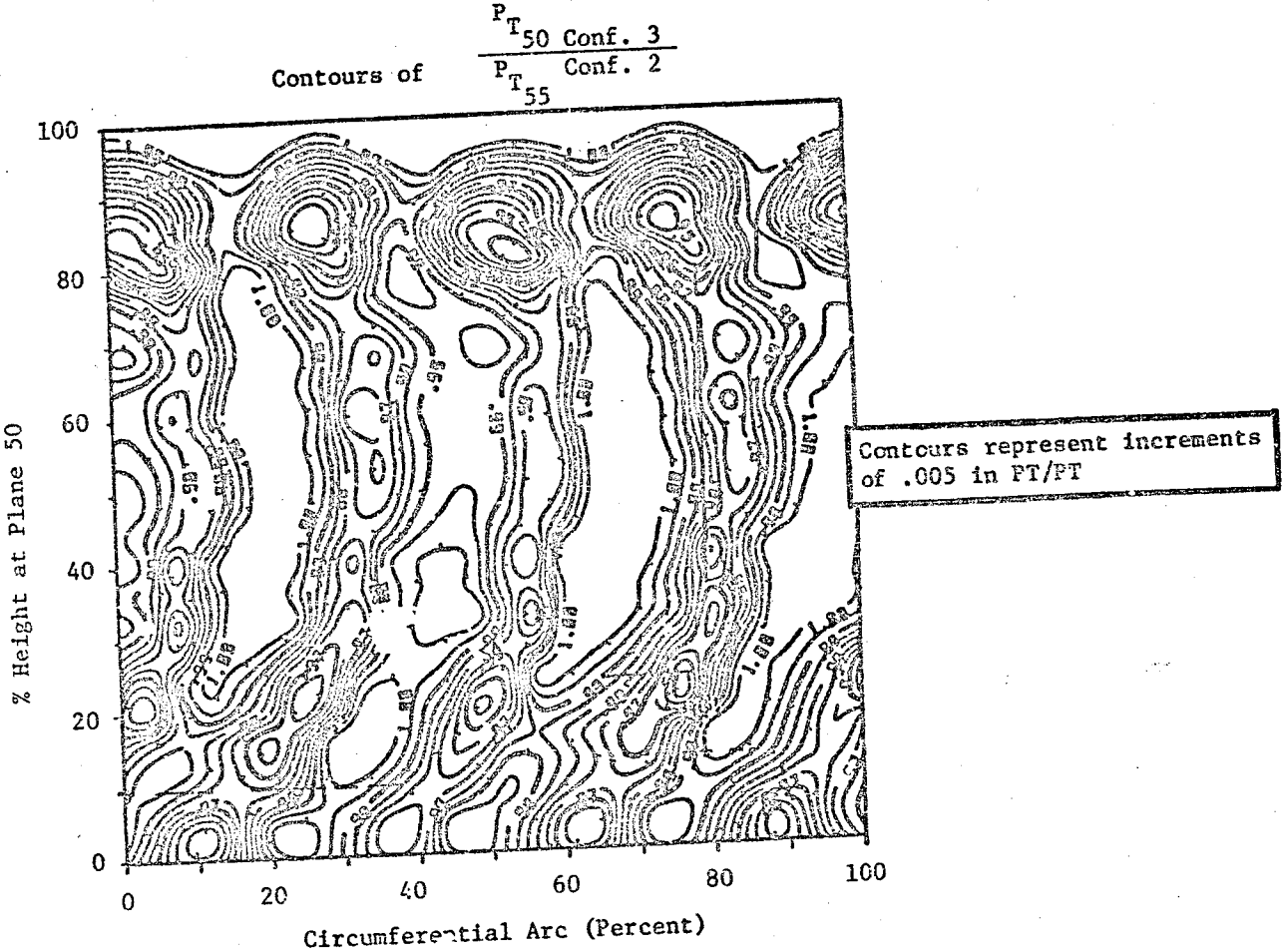

Figure 66. Block I Configuration 3 (Stage Two Stator Cascade) Exhaust Total Pressure Ratio Contours.

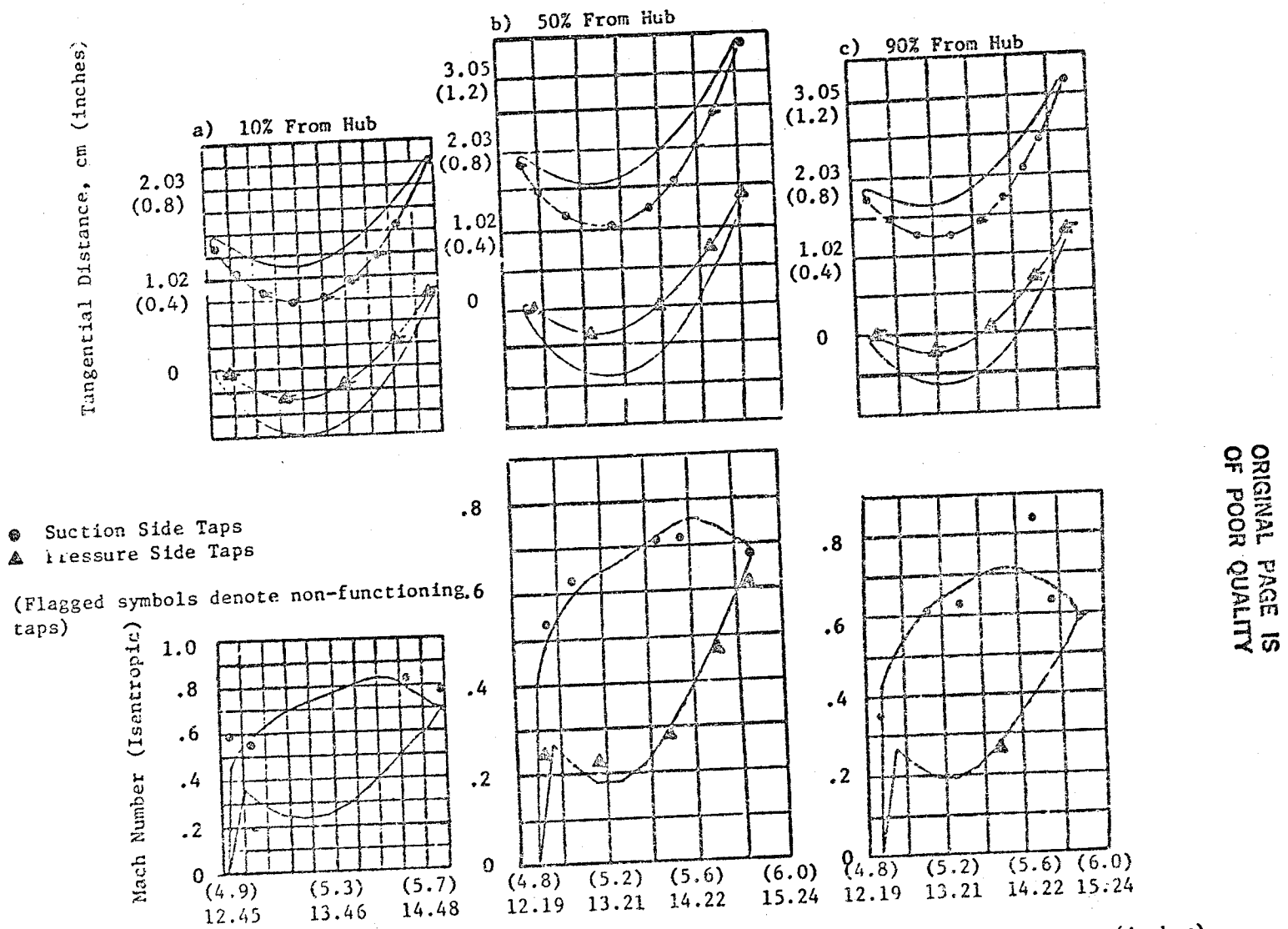

Figure 67. Block I Configuration 3 (Stage 2 Nozzle) Mach Number Distribution (Based On Measured Surface Static Pressures) Compared To Prediction.

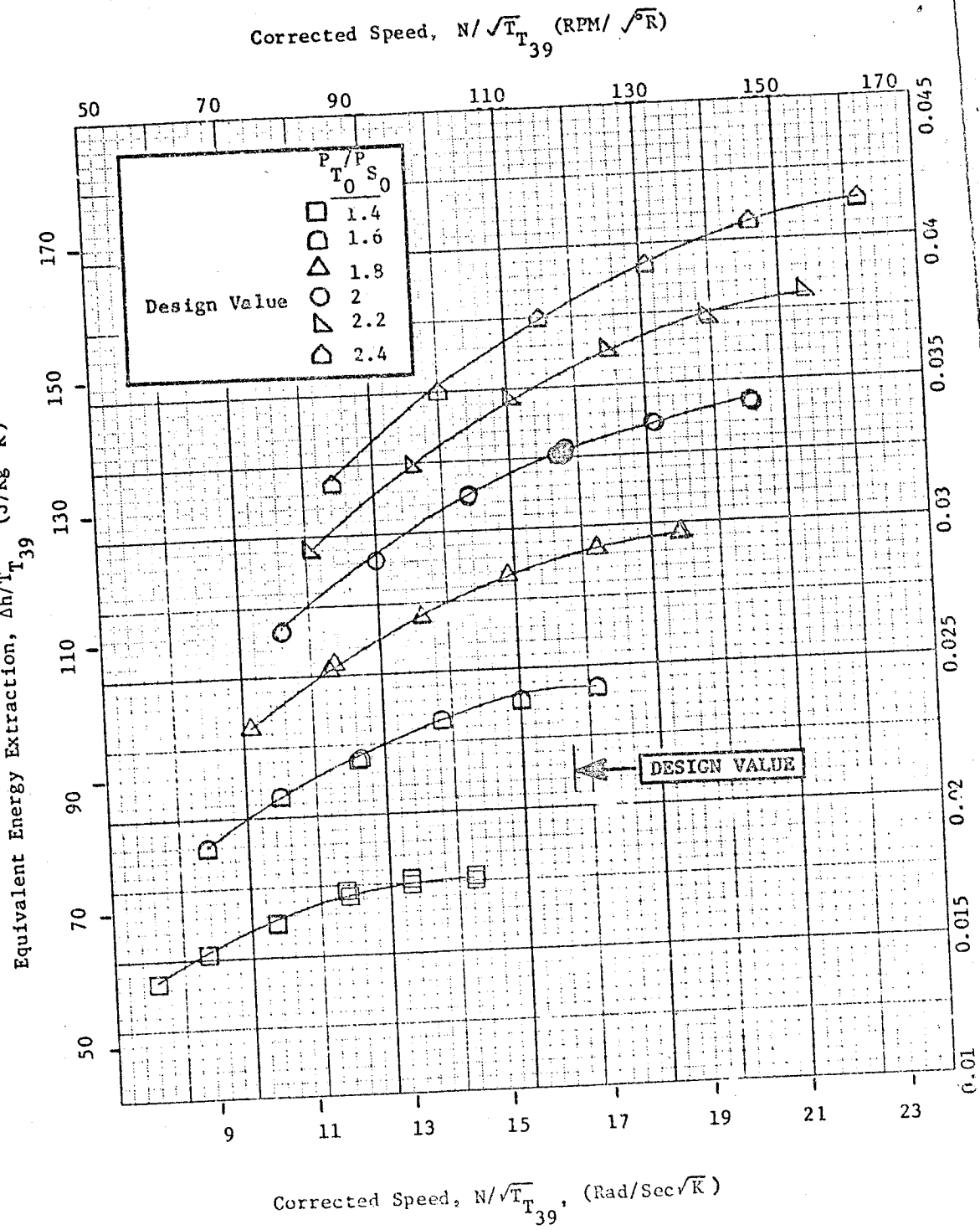

Figure 68. Block I Configuration 4, Equivalent Energy Extraction $\Delta h/T_{T_{39}}$, Vs. Corrected Speed, $N/\sqrt{T_{T_{39}}}$

ORIGINAL PAGE IS
OF POOR QUALITY

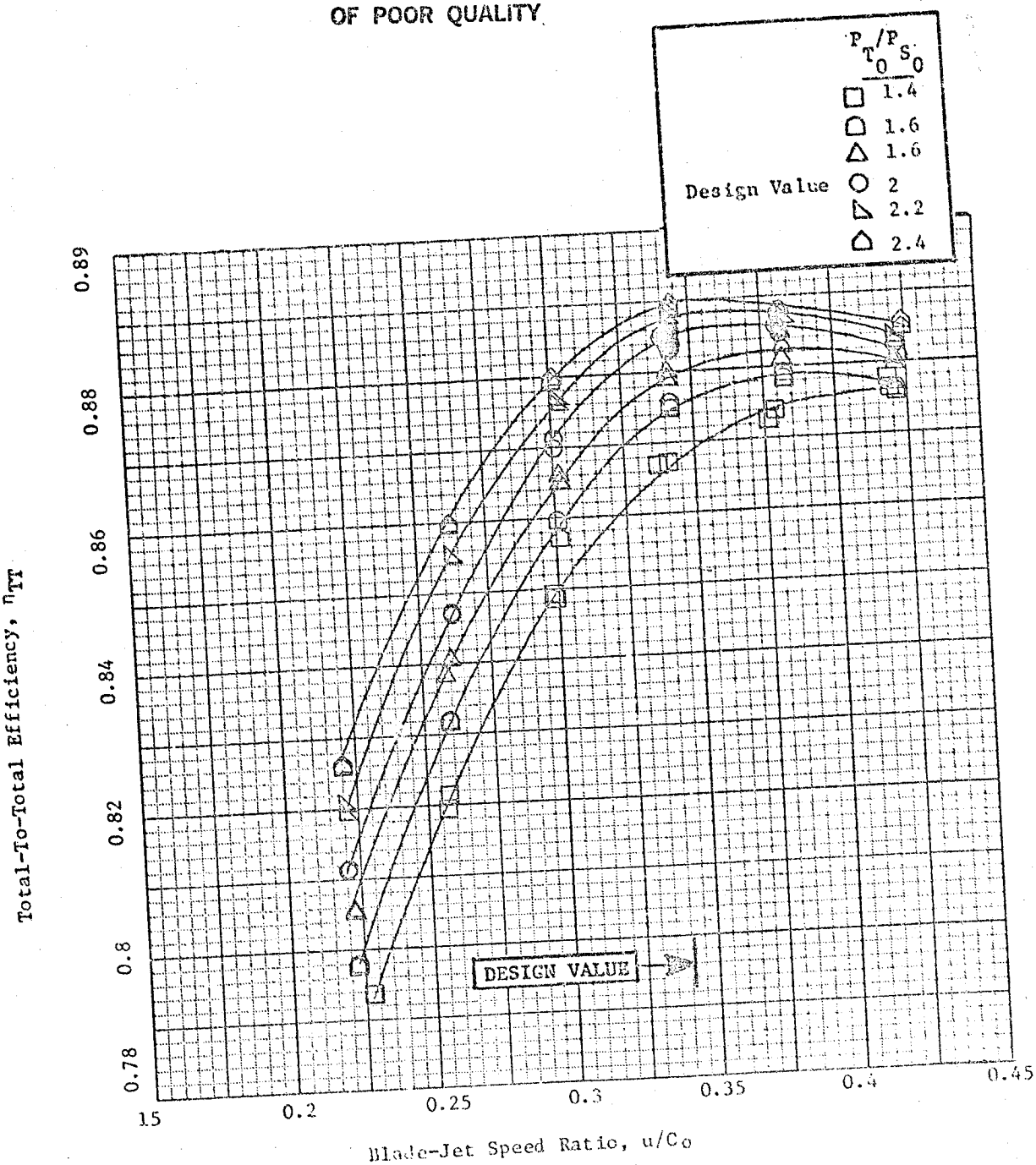

Figure 69. Block I Configuration 4, Total-To-Total Efficiency, η_{TT}, VS. Blade-Jet Ratio, u/Co

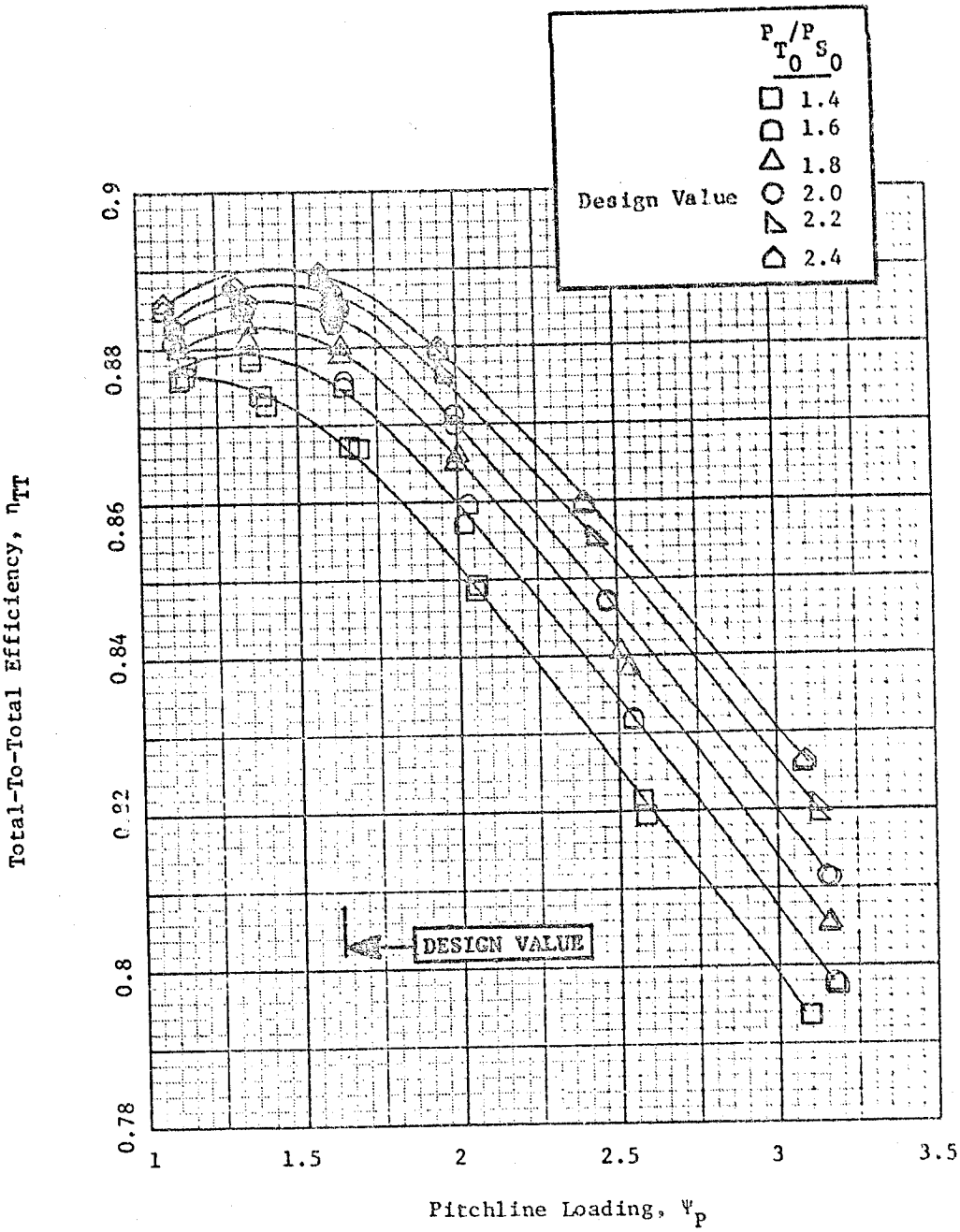

Figure 70. Block I Configuration 4, Total-To-Total Efficiency, η_{TT}, VS. Pitchline Loading, ψ_p

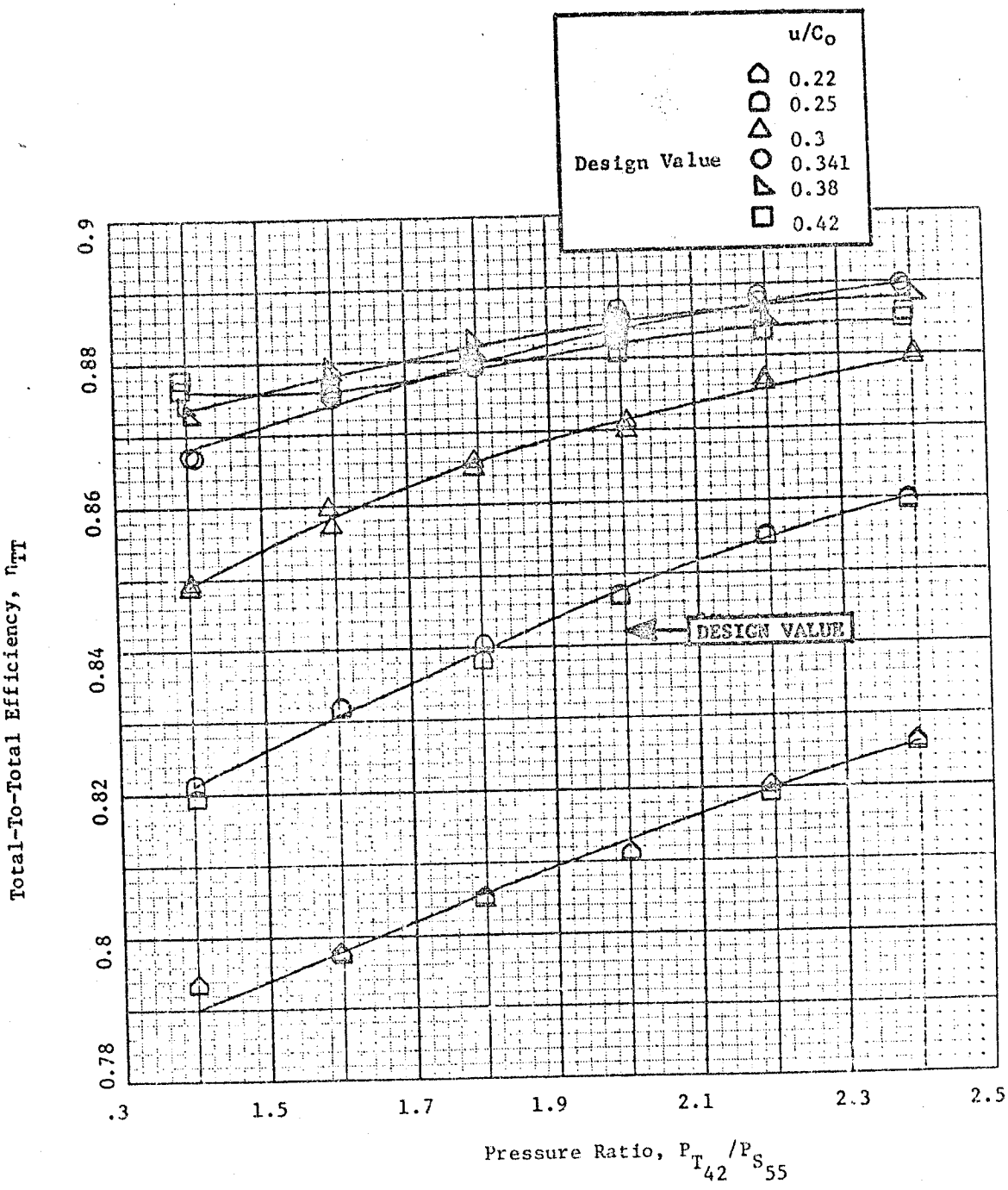

Figure 71. Block I Configuration 4, Total-To-Total Efficiency, n_{TT}, Vs. Pressure Ratio, $P_{T_{42}}/P_{S_{55}}$

negative incidence problem, will be discussed in more detail once results from Block II Configuration 4a have been presented.

Flow characteristics for this build are presented as Figures 72 through 75.

Torque characteristics are presented as Figures 76 and 77.

The 2-stage group swirl map is presented as Γ vs u/C_o in Figure 78.

The row-by-row distribution of measured interstage static pressures, normalized by $P_{T_{42}}$, are presented for the design point in Figure 79 compared to an axisymmetric prediction.

Spanwise distributions of stage exit pressure (normalized), temperature (normalized), swirl, and group total-to-total efficiency based on results of the design point exit traverse survey are presented in Figures 80 through 83.

Note from Figure 83 that the tip losses, so prominent in the Stage 1 profile, have been attenuated somewhat for the group. Losses at the hub, however, are just as servere and penetrate somewhat further from the inner wall than those for Stage 1. As in the case of Configuration 2, posttest data match analysis shows that the blade (stage 2 in this case) is deficient near the hub relative to design prediction and does contribute to the poor hub performance.

Results of the Reynolds number excursion for Configuration 4 are presented as Figure 84.

4.5.2 Block II Test Results

Configuration 1a

The detailed differences between Configurations 1 and 1a are shown in Figure 6; otherwise, the test setup, including instrumentation, was the same as that shown for Configuration 1 in Figure 25.

Design point data for the transition duct is presented in Figure 85. Static pressure rise coefficient, $\Delta P_S/q$, from the duct wall taps and total pressure loss profiles from the boundary layer rakes show that the Block II transition duct performance was similar to the Block I, Figure 38.

Figure 86 presents nozzle inlet flow function vs total-to-static pressure ratio, $P_{T_{42}}/P_{S_{ex}}$, where $P_{S_{ex}}$ is the average of the hub and tip static pressures at the trailing edge plane (PS220-224 and PS323-327 in Figure 25).

Results of the exit traverse survey are presented in Figures 87 through 90. Spanwise distribution of $P_{T_{50}}/P_{T_{42}}$ and of bladerow kinetic efficiency are presented in Figure 87 and 88 respectively. Note that the Block I profile

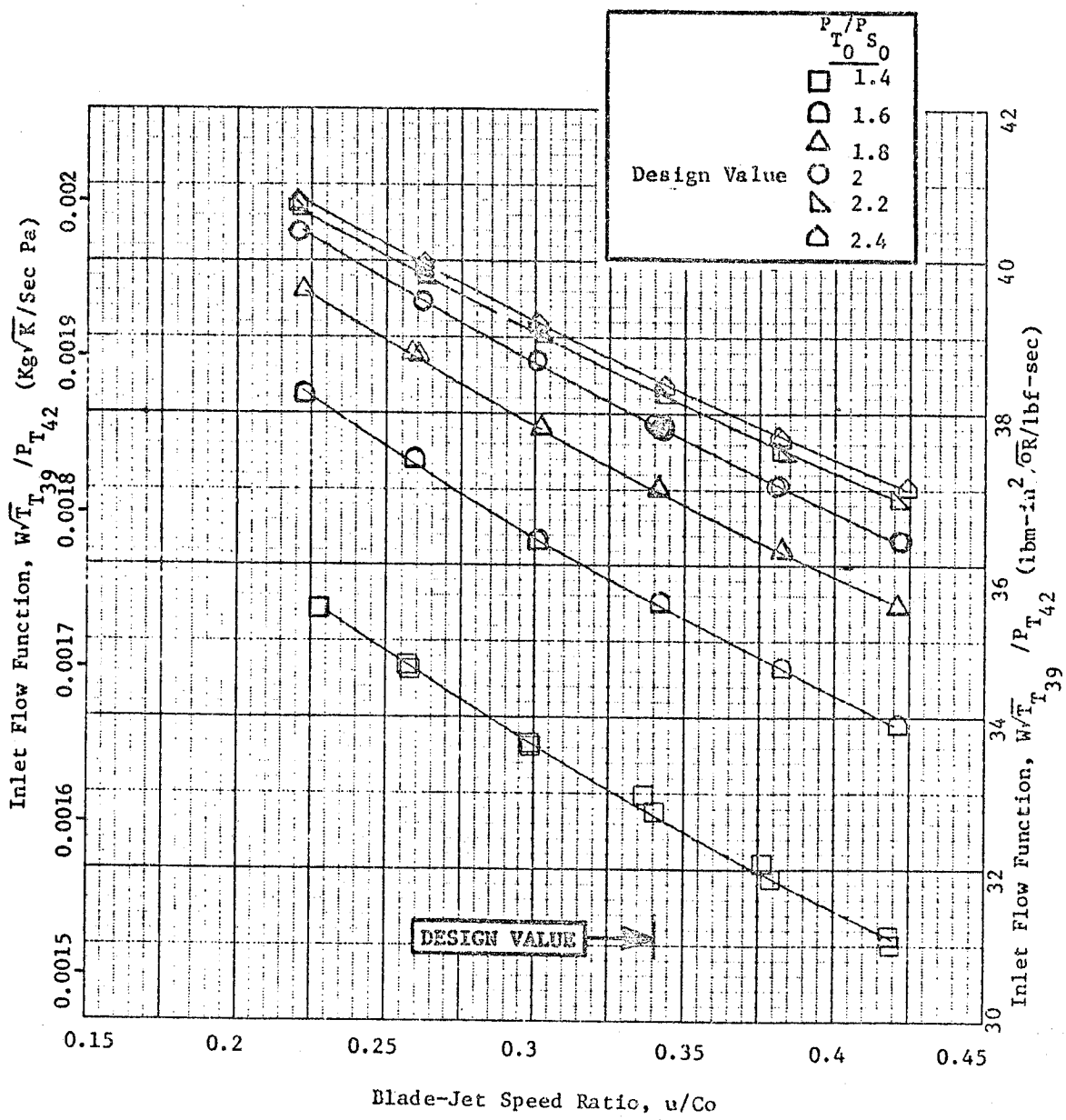

Figure 72. Block I Configuration 4, Inlet Flow Function, $W\sqrt{T_{T_{39}}}/P_{T_{42}}$, Vs. Blade-Jet Speed Ratio, u/C_o

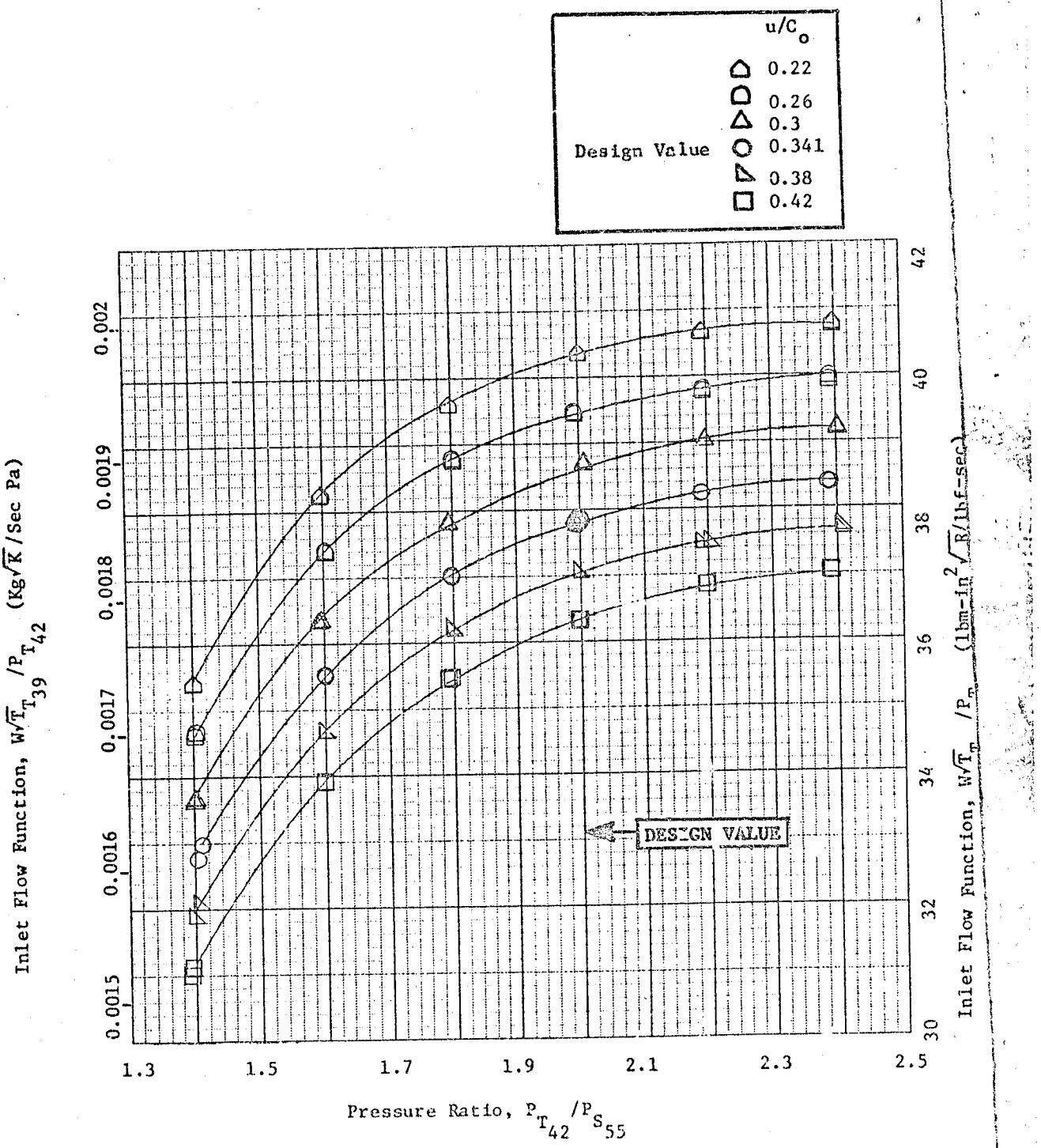

Figure 73. Block I Configuration 4, Inlet Flow Function $,W\sqrt{T_{T_{39}}}/P_{T_{42}}$, VS. Pressure Ratio, $P_{T_{42}}/P_{S_{55}}$

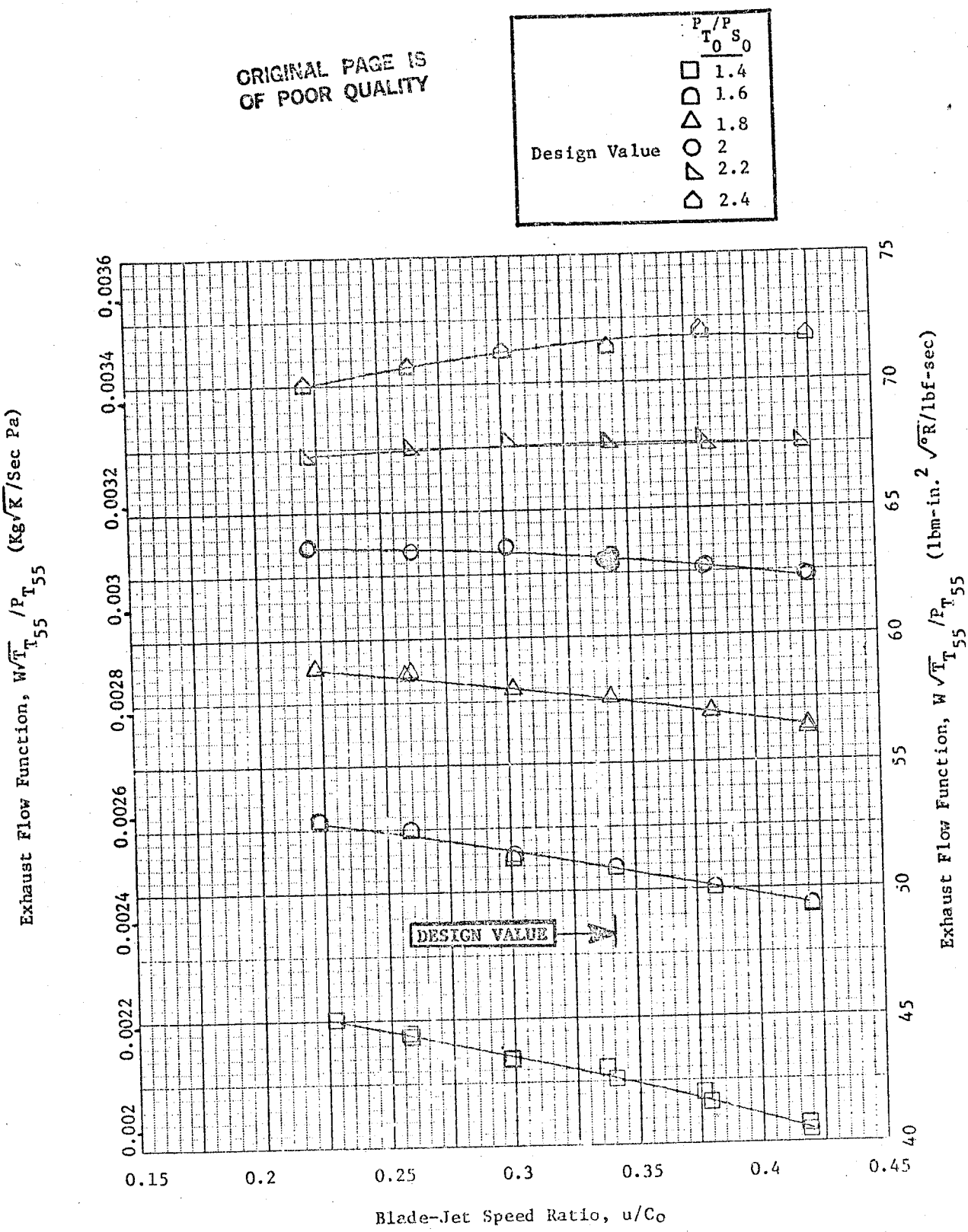

Figure 74. Block I Configuration 4, Exhaust Flow Function, $W\sqrt{T}_{T_{55}}/P_{T_{55}}$, VS. Blade-Jet Speed Ratio, u/C_o

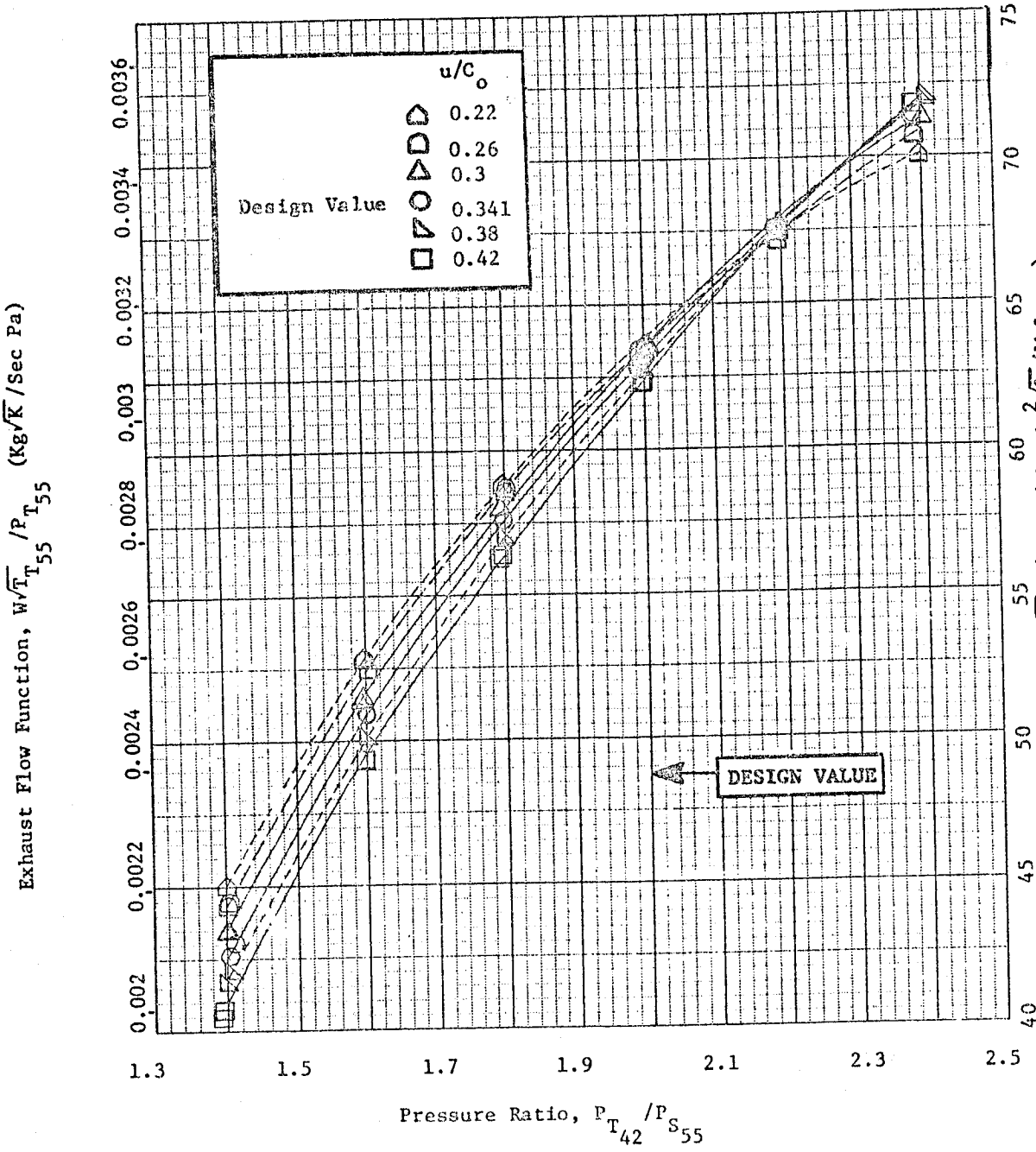

Figure 75. Block I Configuration 4, Exhaust Flow Function, $W\sqrt{T}_{T_{55}}/P_{T_{55}}$, VS. Pressure Ratio, $P_{T_{42}}/P_{S_{55}}$

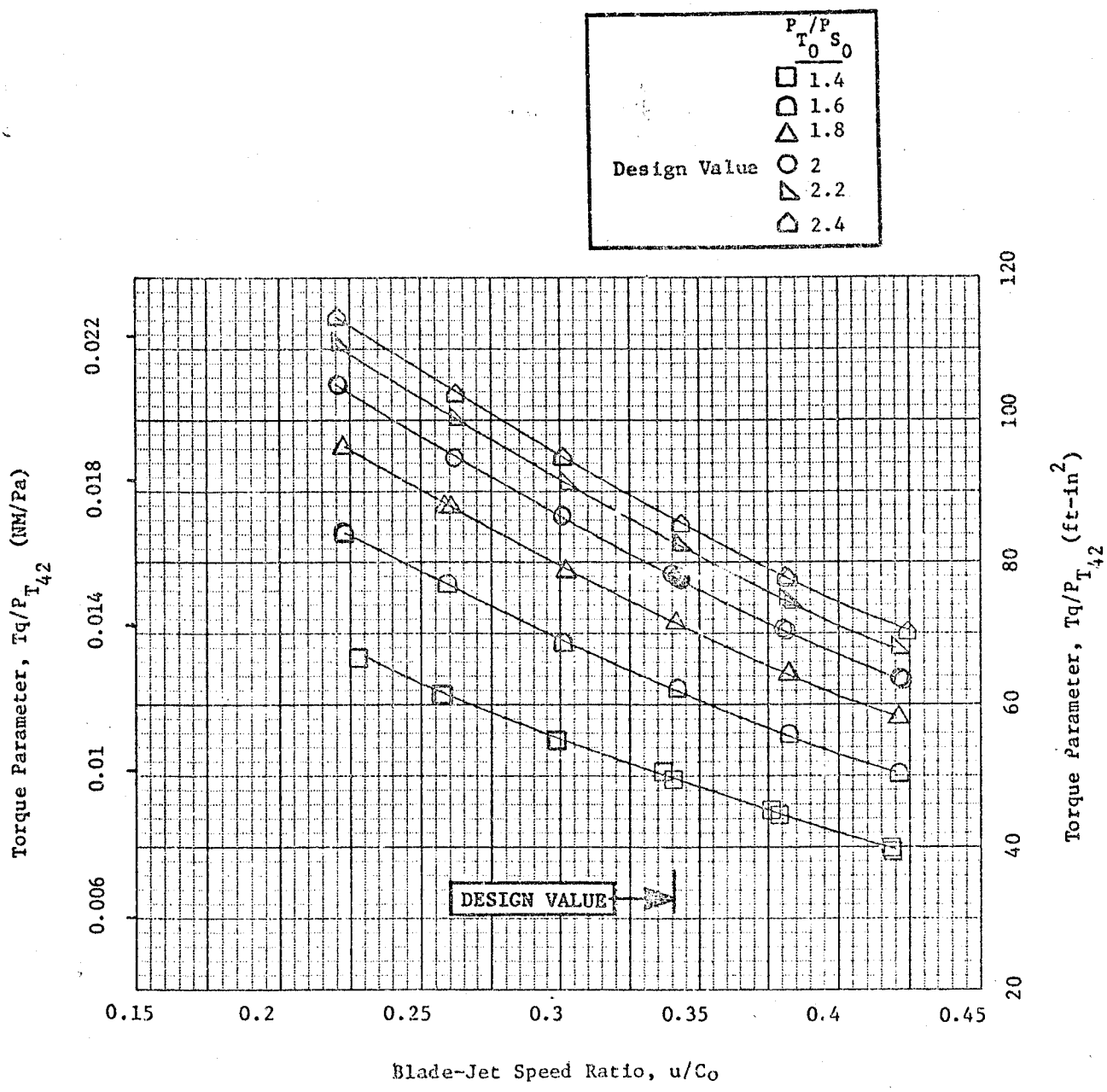

Figure 76. Block I Configuration 4, Torque Parameter, $Tq/P_{T_{42}}$, Vs. Blade-Jet Speed Ratio, u/C_o

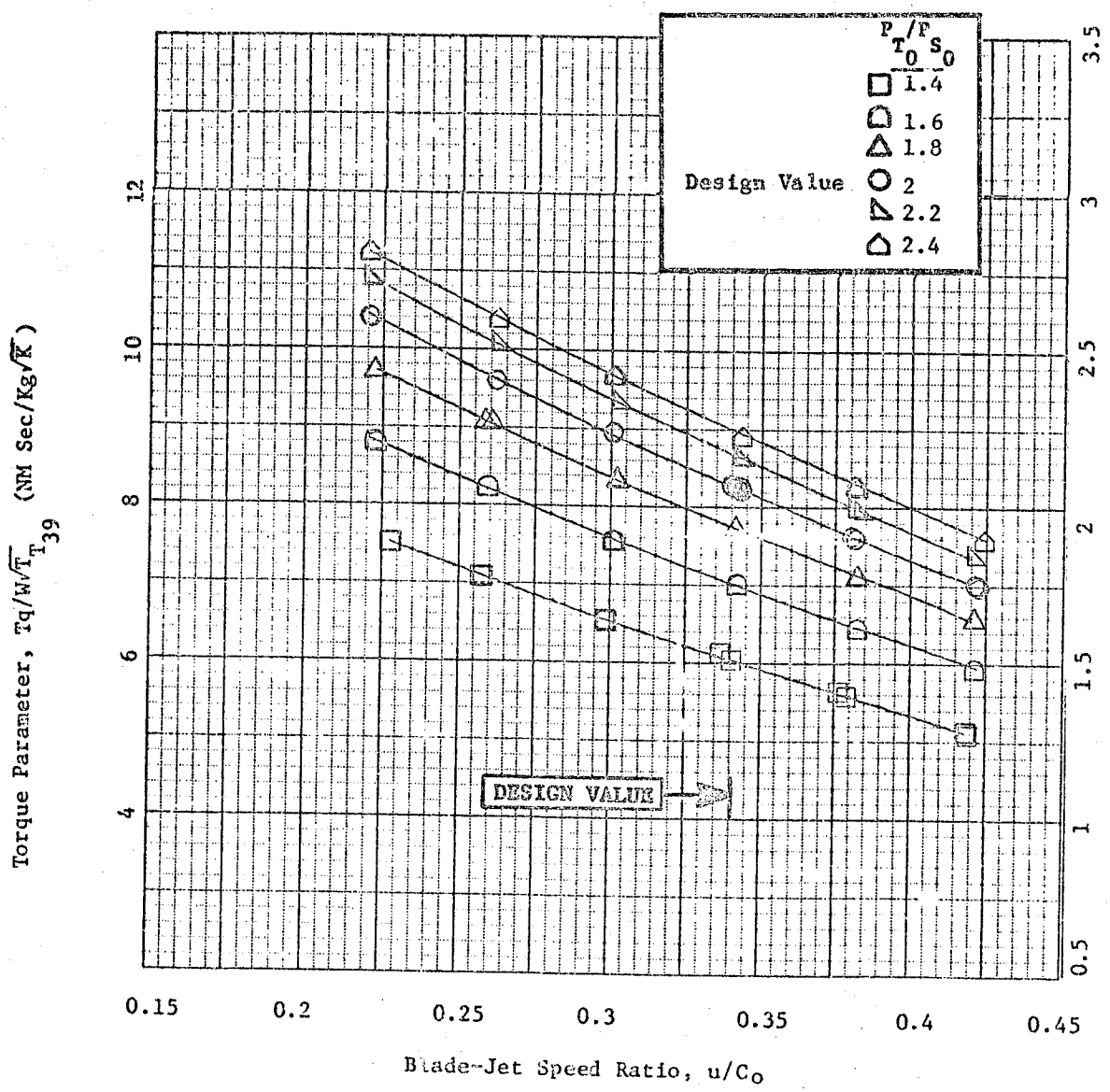

Figure 77. Block I Configuration 4, Torque Parameter, $Tq/W\sqrt{T}_{T_{39}}$ Vs. Blade-Jet Speed Ratio, u/C_o

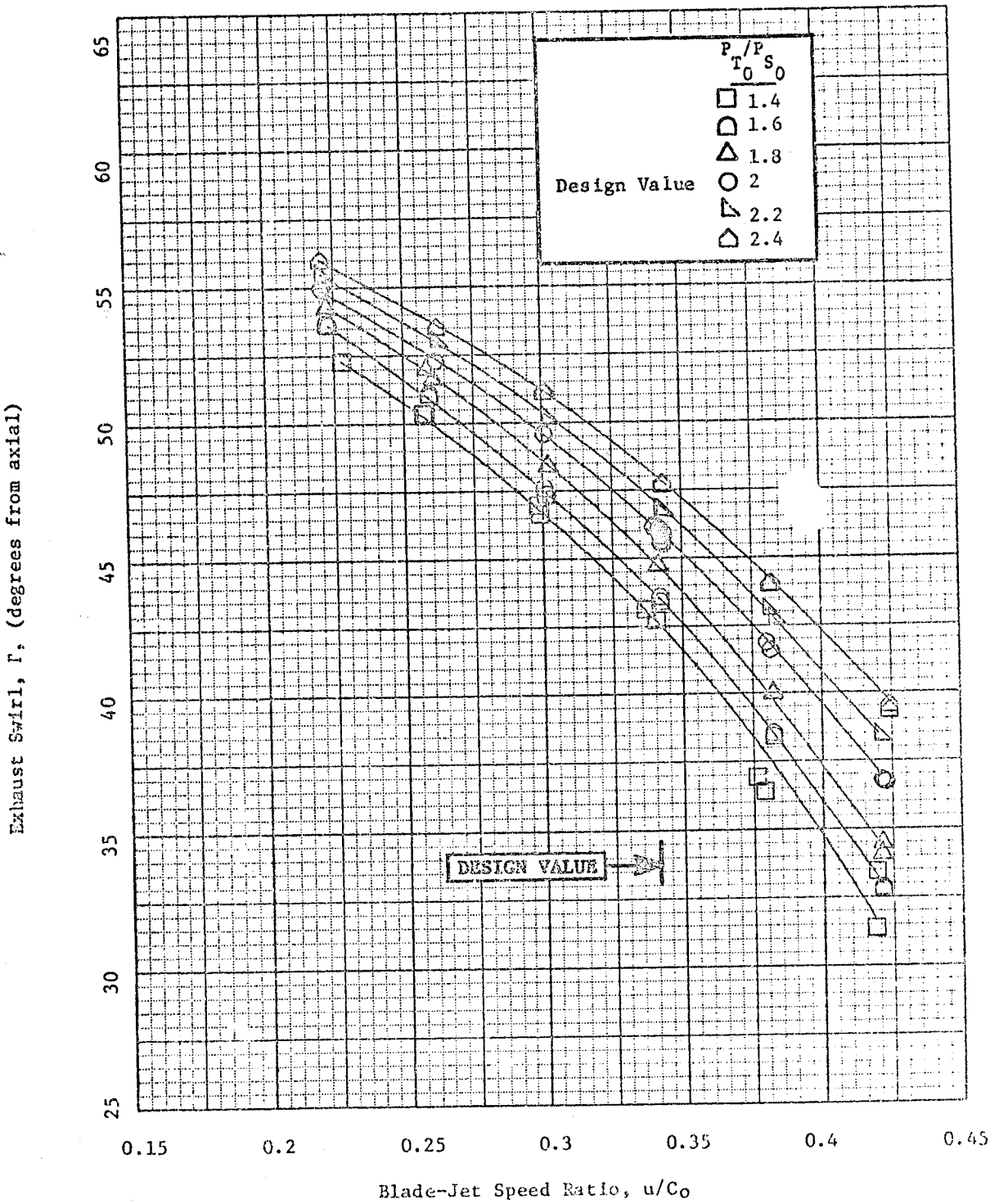

Figure 78. Block I Configuration 4, Exhaust Swirl, Γ, Vs. Blade-Jet Speed Ratio, u/C_o

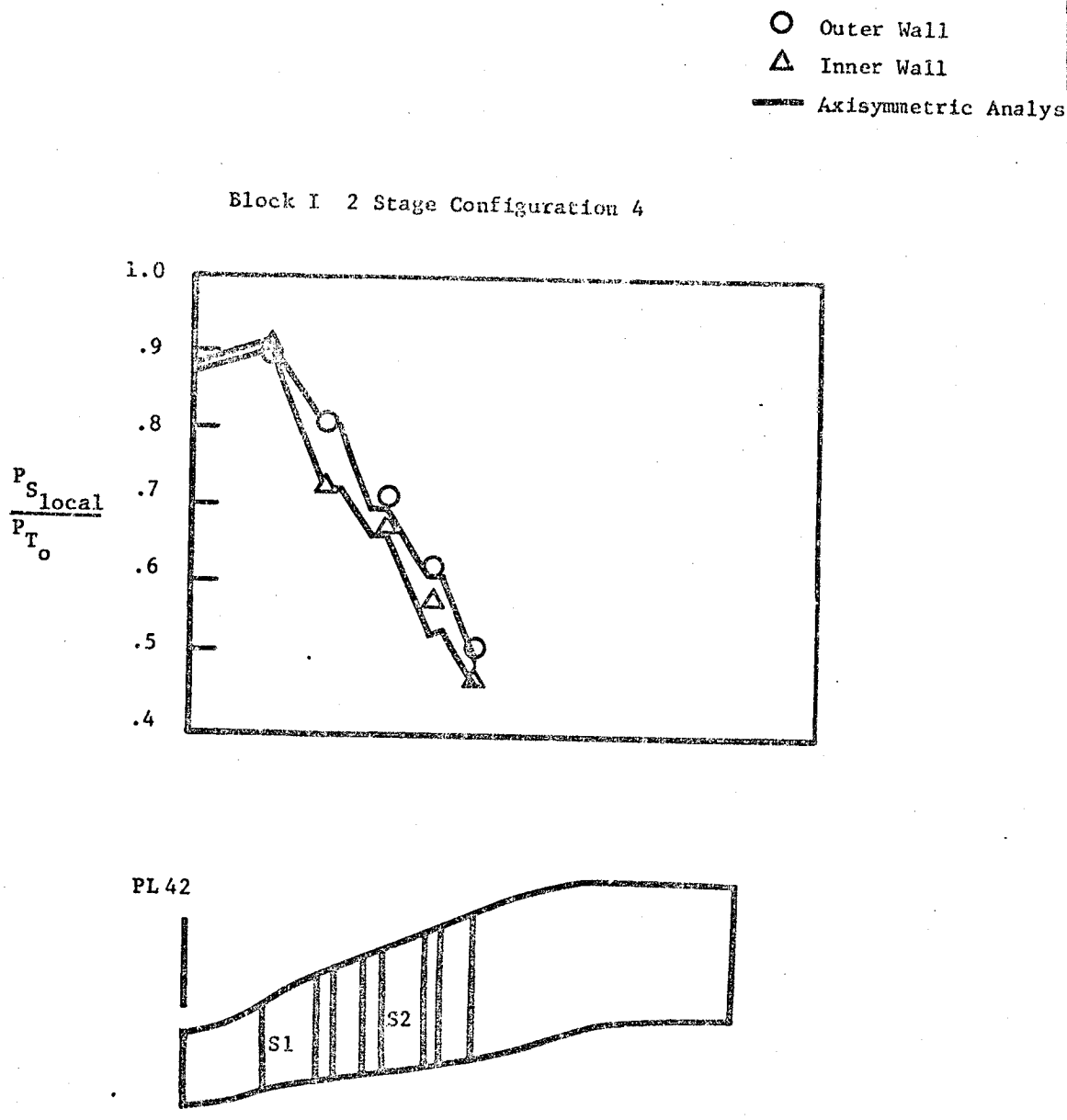

Figure 79. Interstage Static Pressures, Predicted Versus Test (Design Point Data)

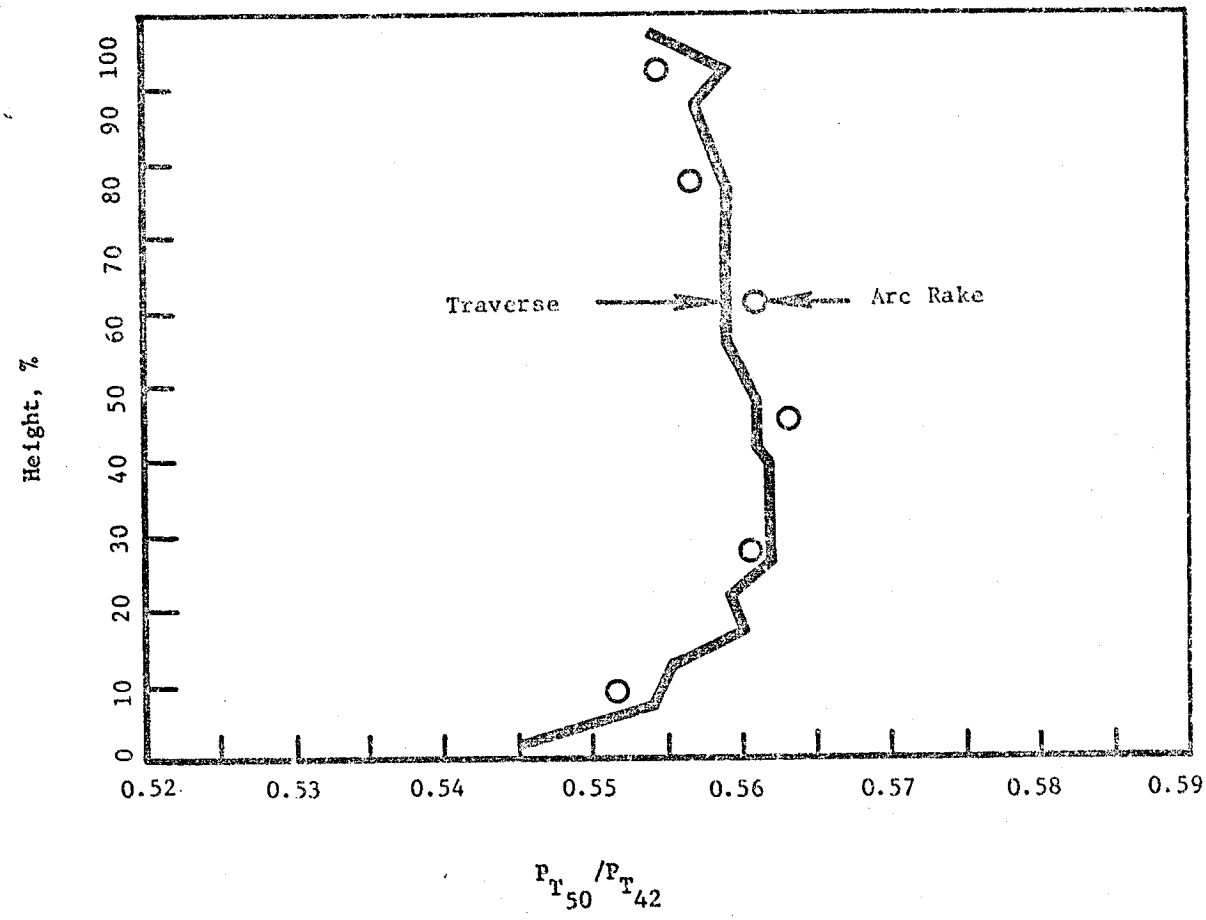

Figure 80. Block I Configuration 4 Exit Survey - $P_{T_{50}}/P_{T_{42}}$ Vs. % Height

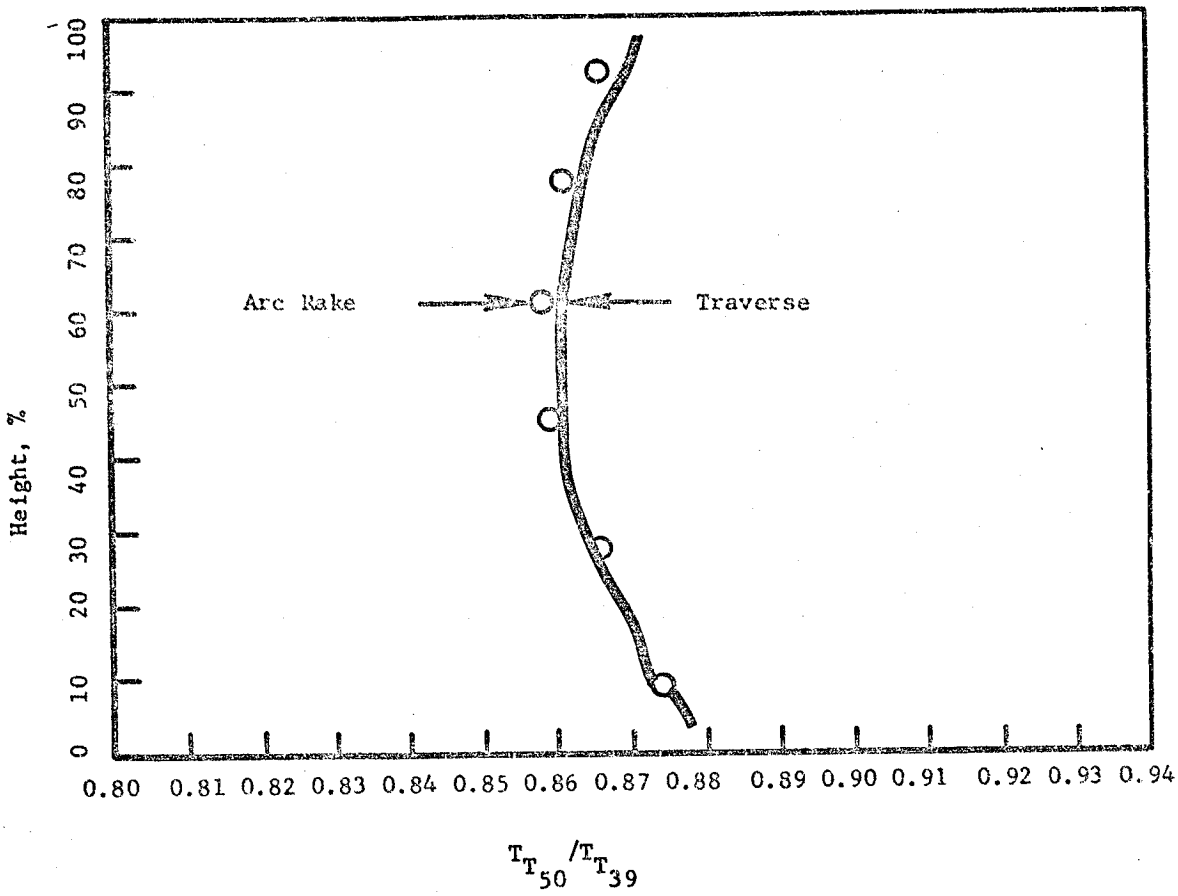

Figure 81. Block I Configuration 4 Exit Survey - $T_{T_{50}}/T_{T_{39}}$ Vs. % Height

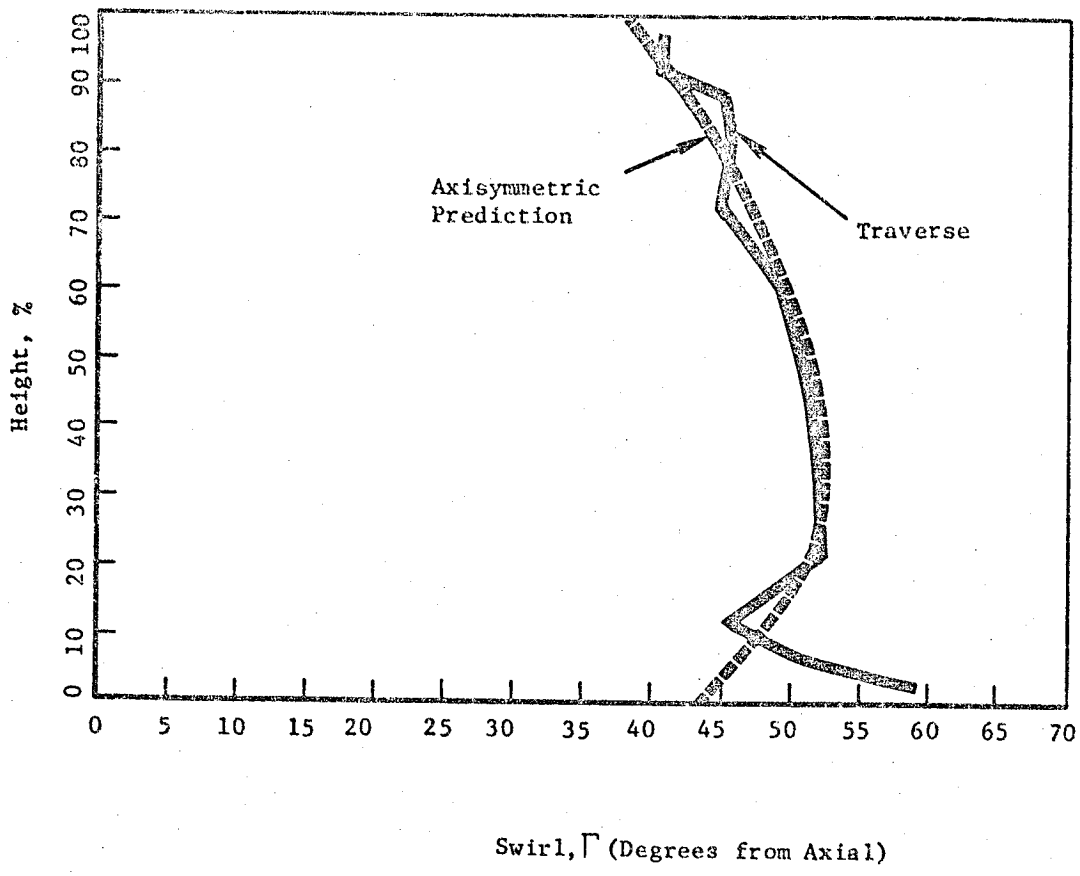

Figure 82. Block I Configuration 4 Exit Survey - Swirl, Γ, Vs. % Height

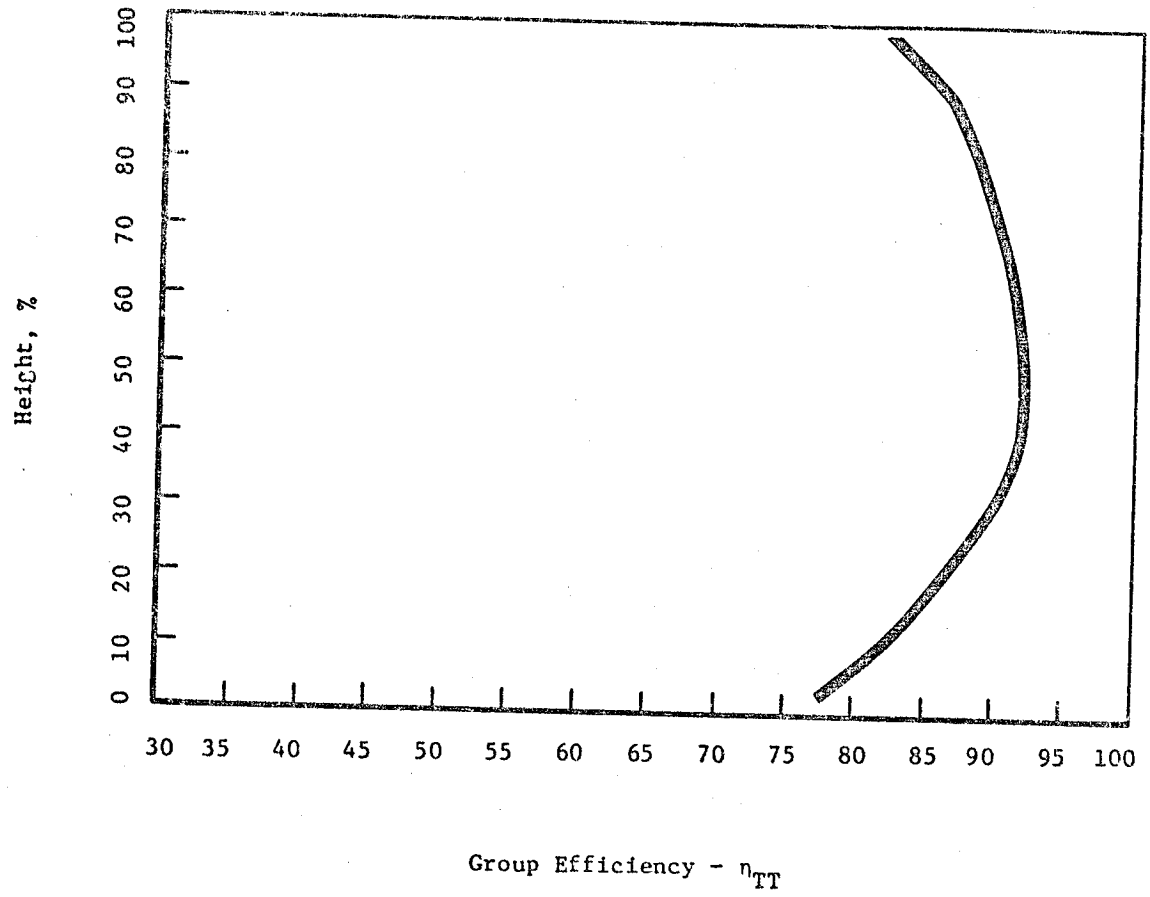

Figure 83. Block I Configuration 4 Exit Survey - Efficiency Vs. % Height

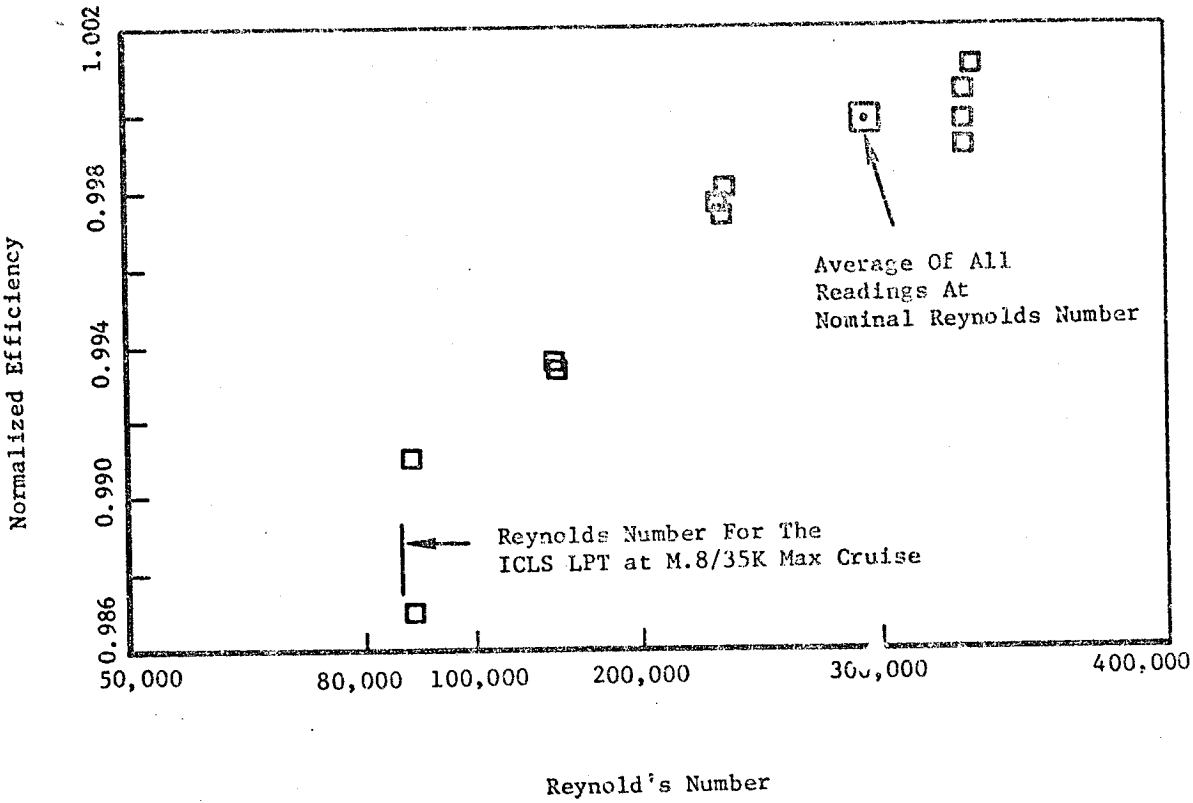

Figure 84. Block I Configuration 4 Reynolds Number Excursion – Efficiency Vs. Reynold's Number.

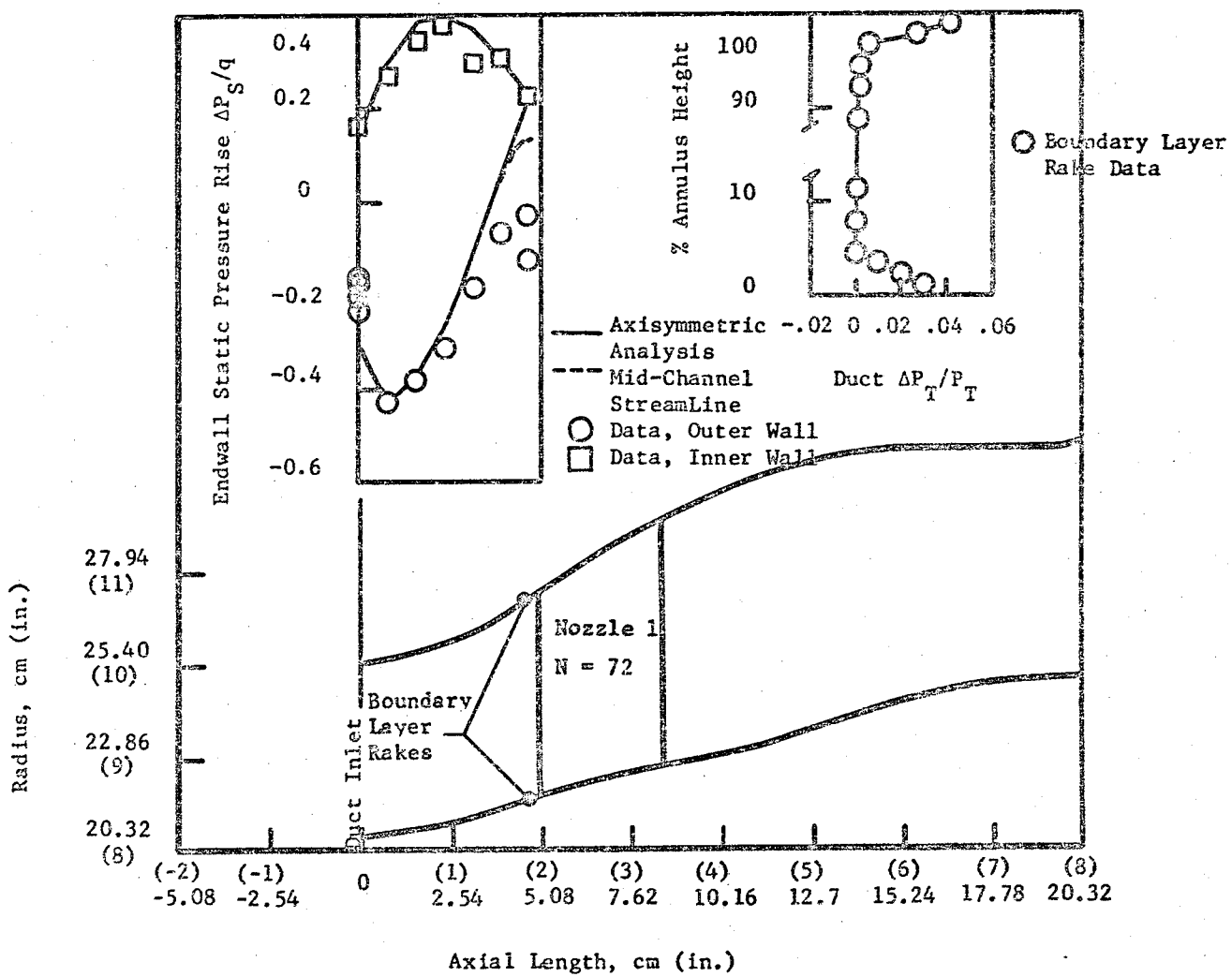

Figure 85. Block II Configuration 1a Transition Duct Data at Design Pressure Ratio

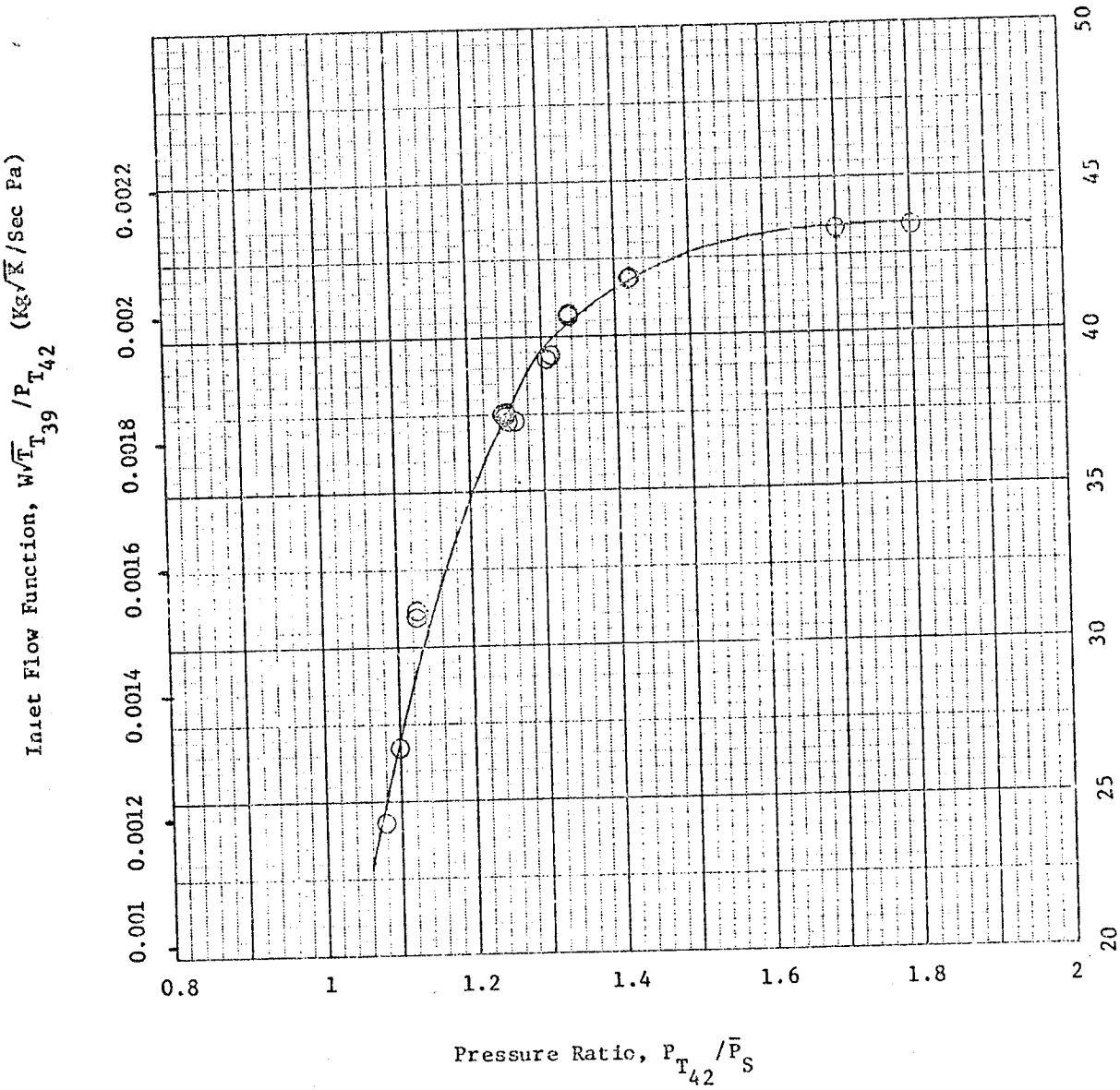

Figure 86. Block II Configuration 1a, Inlet Flow Function, $W\sqrt{T}_{T_{39}}/P_{T_{42}}$ Vs. Pressure Ratio, $P_{T_{42}}/\bar{P}_S$.

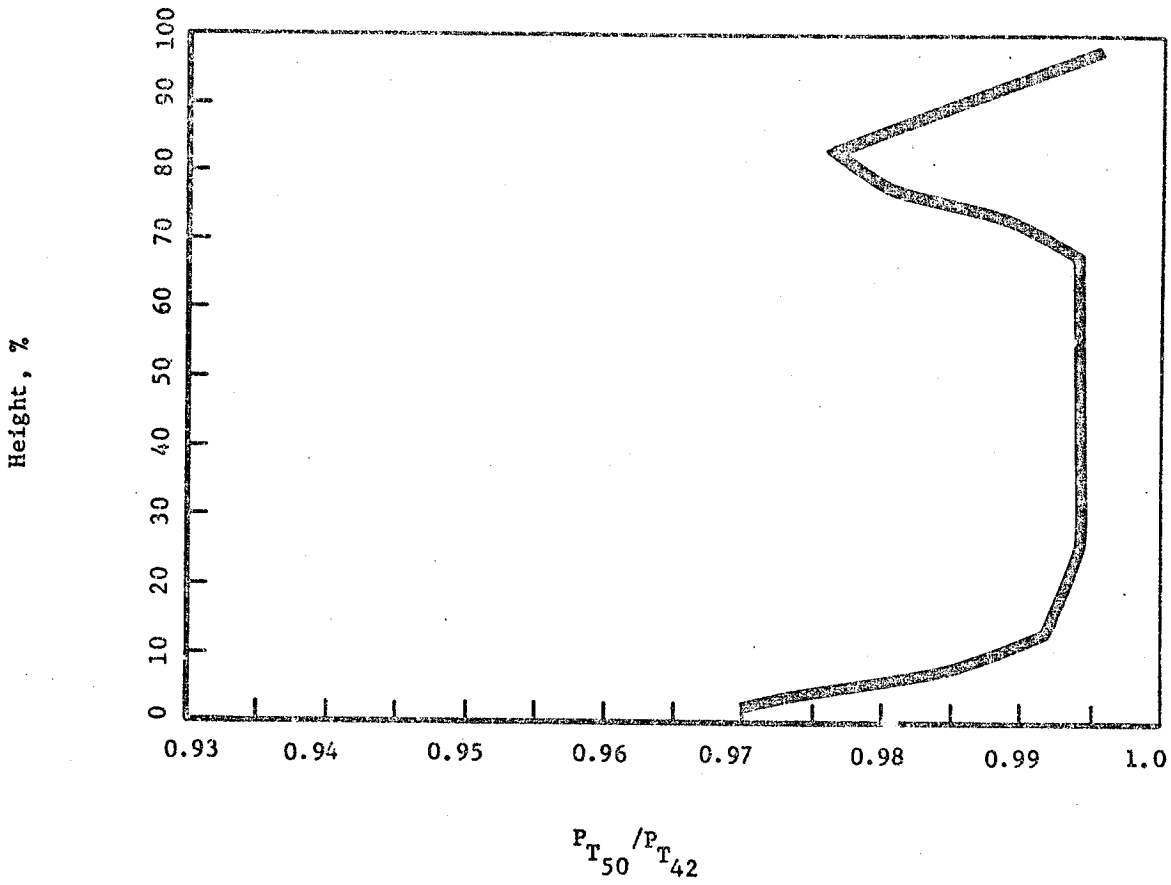

Figure 87. Block II Configuration 1a, Exit Survey-$P_{T_{50}}/P_{T_{42}}$ Vs. % Height.

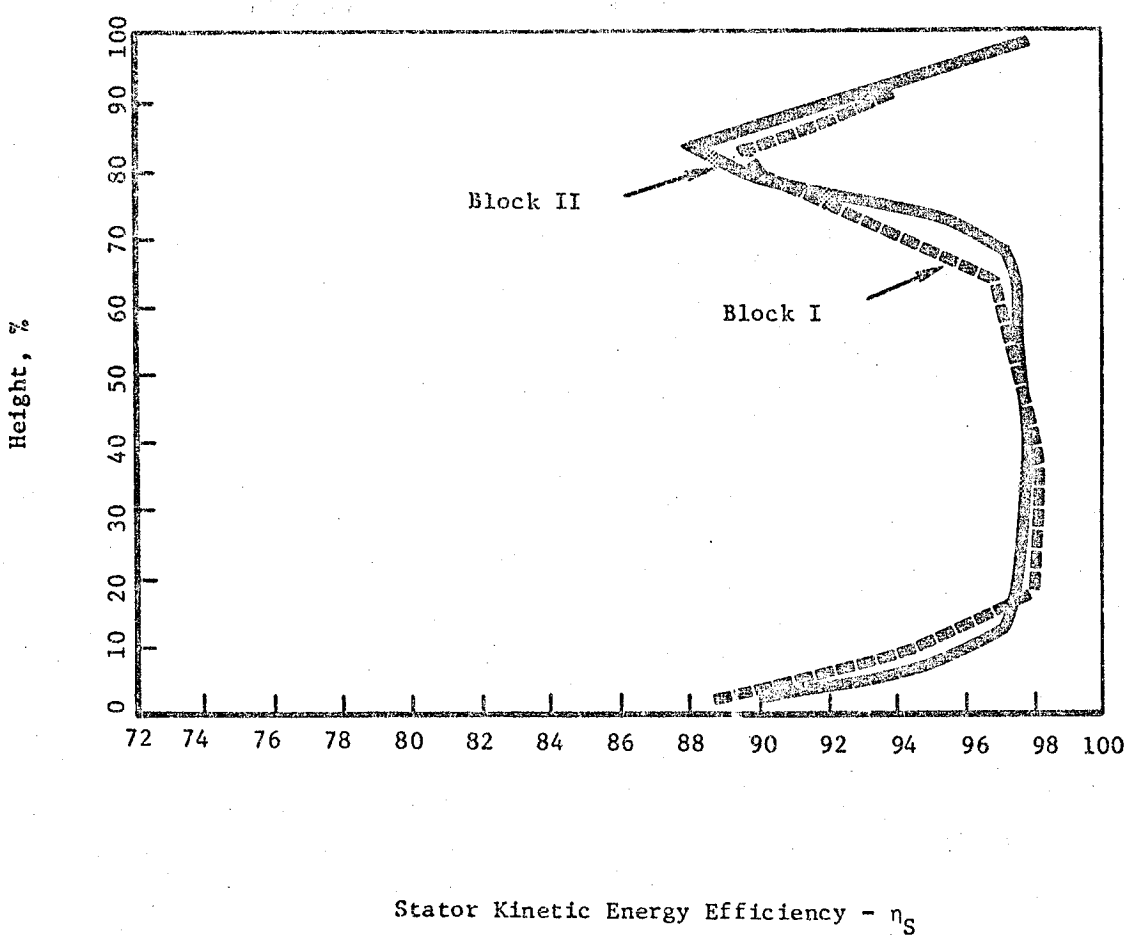

Figure 88. Block II Configuration 1a Exit Survey-Efficiency Vs. % Height (Comparison with Block I)

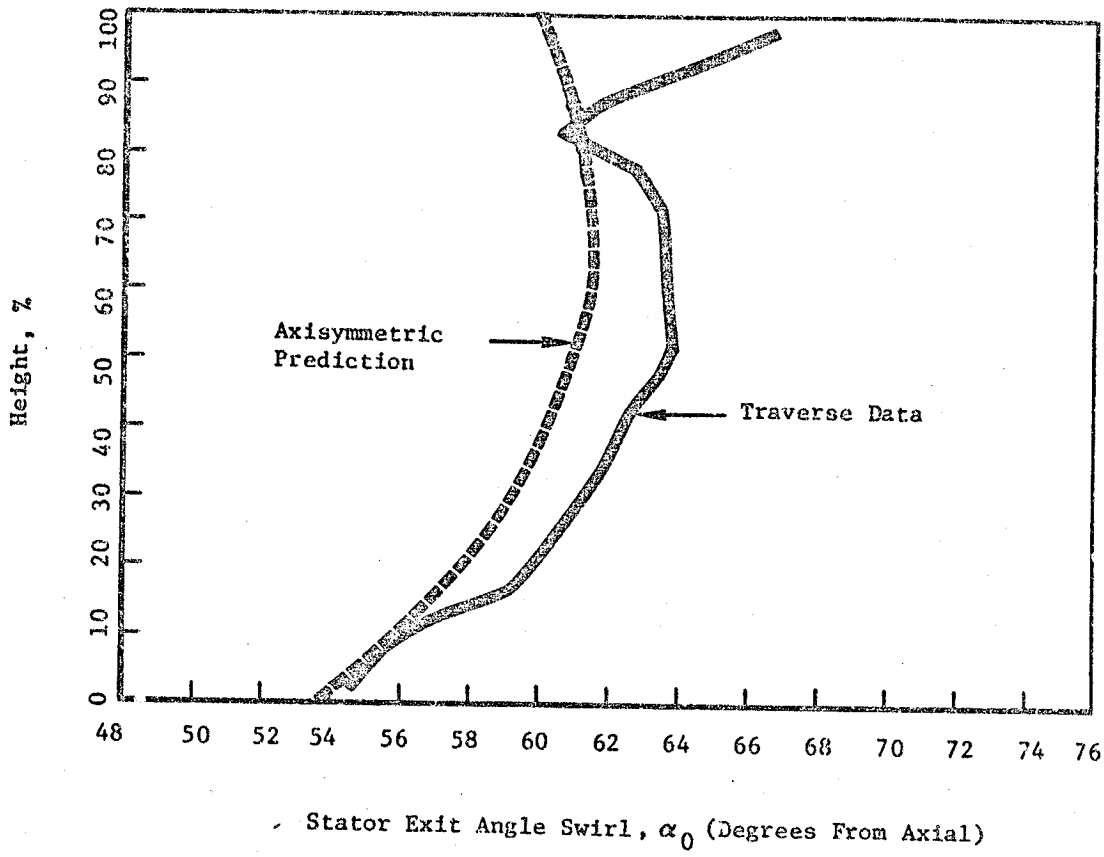

Figure 89. Block II Configuration 1a Exit Survey-Swirl Vs. % Height

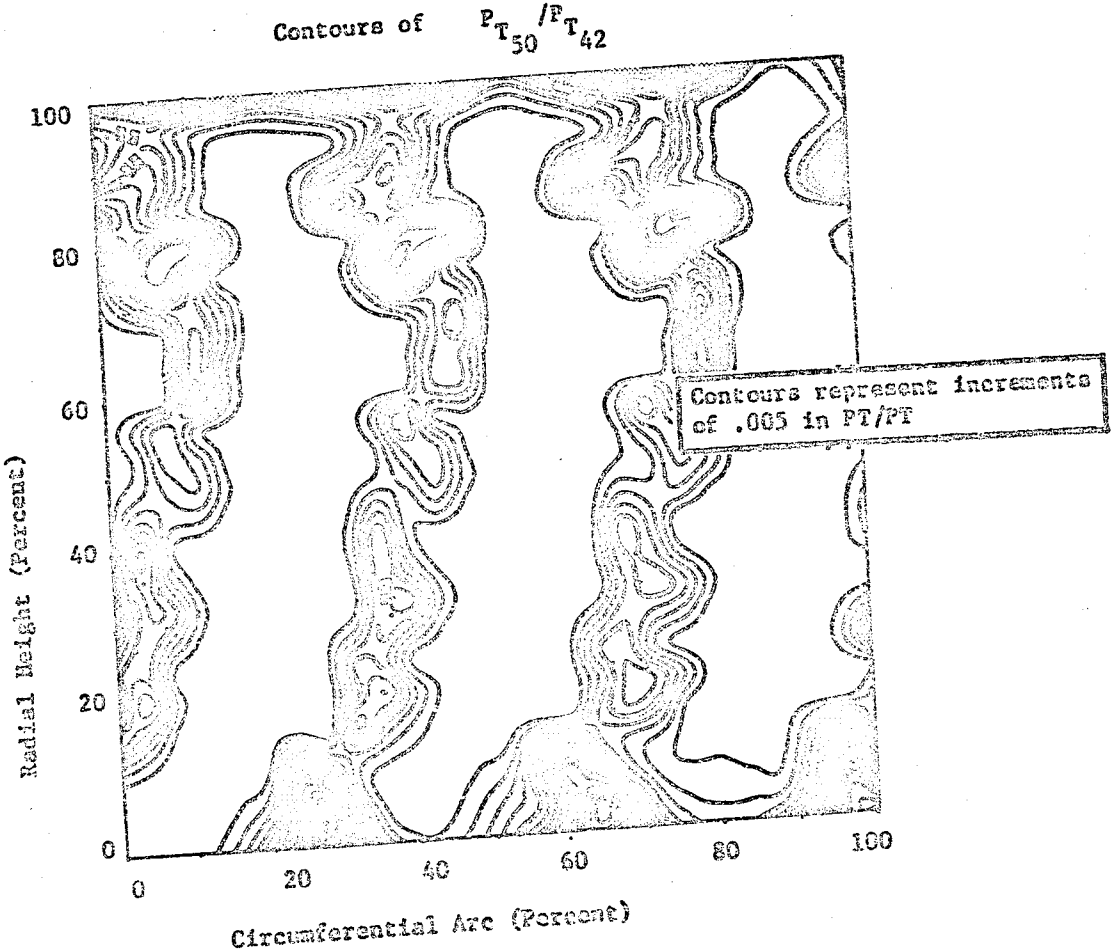

Figure 90. Block II Configuration 1a Exhaust Total Pressure Ratio Contours.

has been added to Figure 88 for comparison and that, although the Block II nozzle exhibits an improvement of 0.4% in integrated efficiency, the performance hole near the tip is still present to the same degree. The higher throat aspect ratio, h/d_o, near the tip of the Block II nozzle had only limited effect in confining the tip vortex. The higher hub solidity, however, did improve the performance near the inner wall.

Vane exit angle is presented in Figure 89 and, as in Figure 43, reflects the deep loss core near the tip.

Contours of P_{T50}/P_{T42} are provided in Figure 90, and once again illustrate the loss cores near the walls.

Further graphic evidence of the vortex near the tip (and of general flow traces through the channel of the Block II nozzle) is provided by lampblack and oil traces included in Appendix I.

Airfoil surface Mach numbers calculated from static pressures measured on near hub, pitchline, and near tip streamlines are presented in Figure 91. Note that, compared to analytical prediction, the tip exhibits decreased circulation due to secondary flow effects, while the pitchline and near hub sections show relatively good agreement. Recall (from Figure 44) that Configuration 1 exhibited the same defect at the tip and, to a degree, at the pitchline as well. Coordinates for these streamsurfaces are presented in Appendix B.

Configuration 4a

Test data for Block II Configuration 4a, the two-stage group redesign, are tabulated in Appendix H. The instrumentation was identical to that for Configuration 4 shown in Figure 28.

Figure 92, a plot of $\Delta h/T_T$ vs $N/\sqrt{T_T}$, illustrates that the entire test matrix specified in Table XVIII was successfully run.

Efficiency of the Block II 2-stage group is plotted against blade-jet speed ratio, group loading, and stage total-to-static pressure ratio in Figures 93, 94 and 95. From a comparison of Figures 94 and 70, it is evident that the value of 0.892 for Configuration 4a η_{TT} (at design ψ_p and P_T/P_S) represents an improvement of 0.008 in group efficiency over Block I at ψ_p = 1.68. This improvement is attributable to the modifications incorporated into Block II as outlined in Section 3.4, namely:

1. higher aspect ratio and solidity in stage 1 vane,
2. improved flowpath overlap geometry, and
3. improved airfoil design (decrease in pressure surface diffusion).

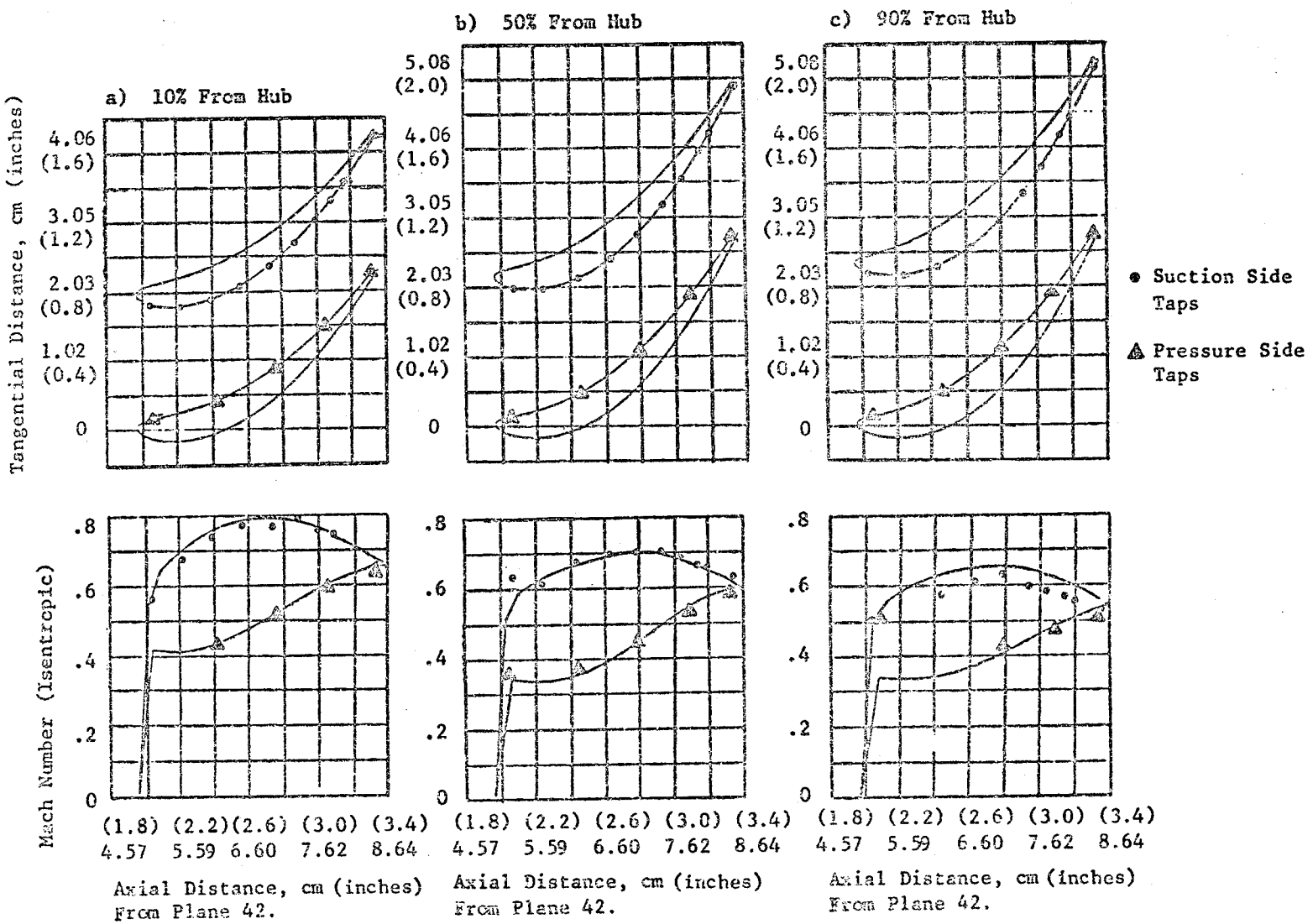

Figure 91. Block II Configuration 1a (Stage 1 Nozzle) Mach Number Distribution (Based On Measured Surface Static Pressures) Compared To Prediction.

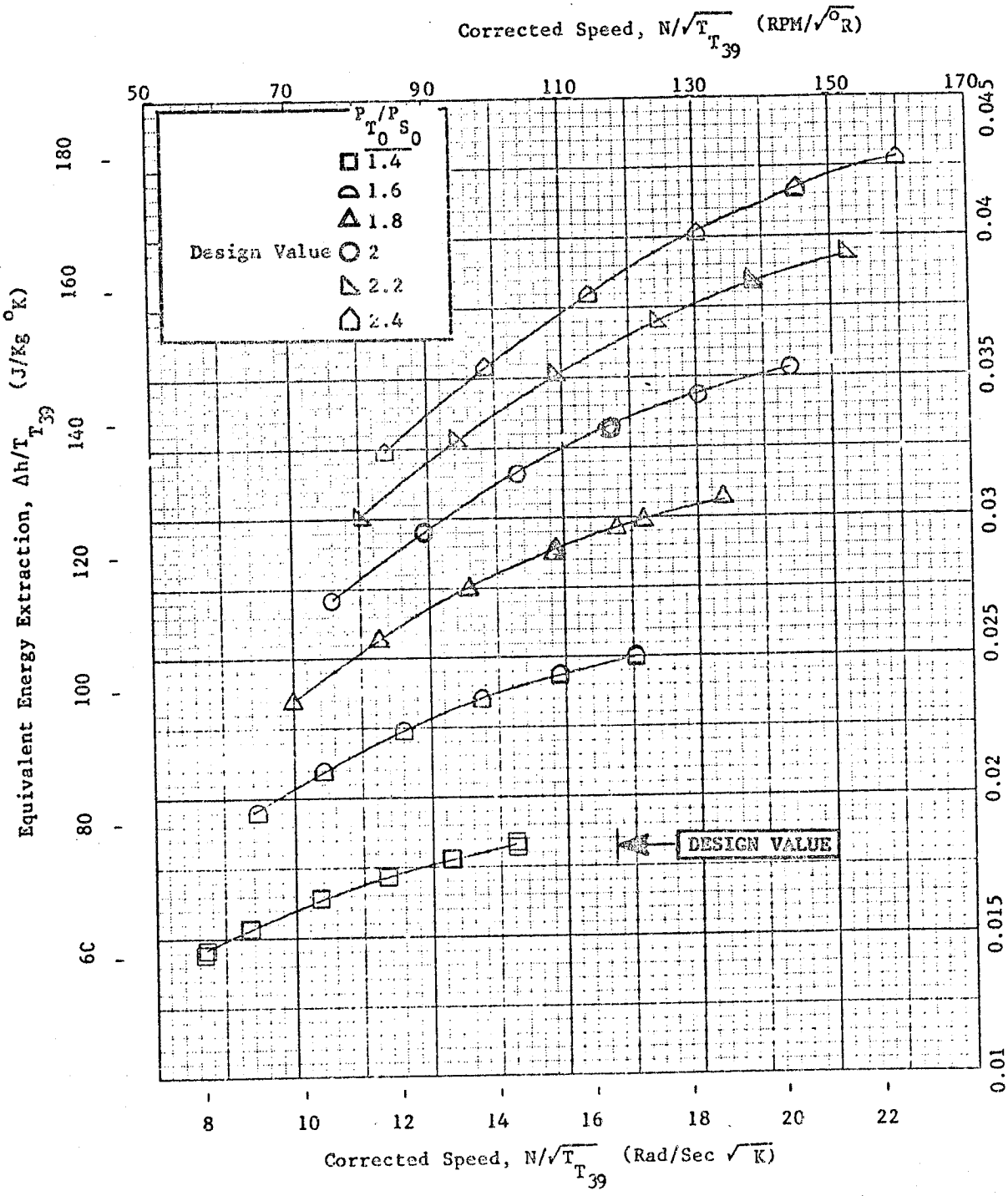

Figure 92. Block 11 Configuration 4a, Equivalent Energy Extraction, $\Delta h/T_{T_{39}}$, vs. Corrected Speed, $N/\sqrt{T_{T_{39}}}$.

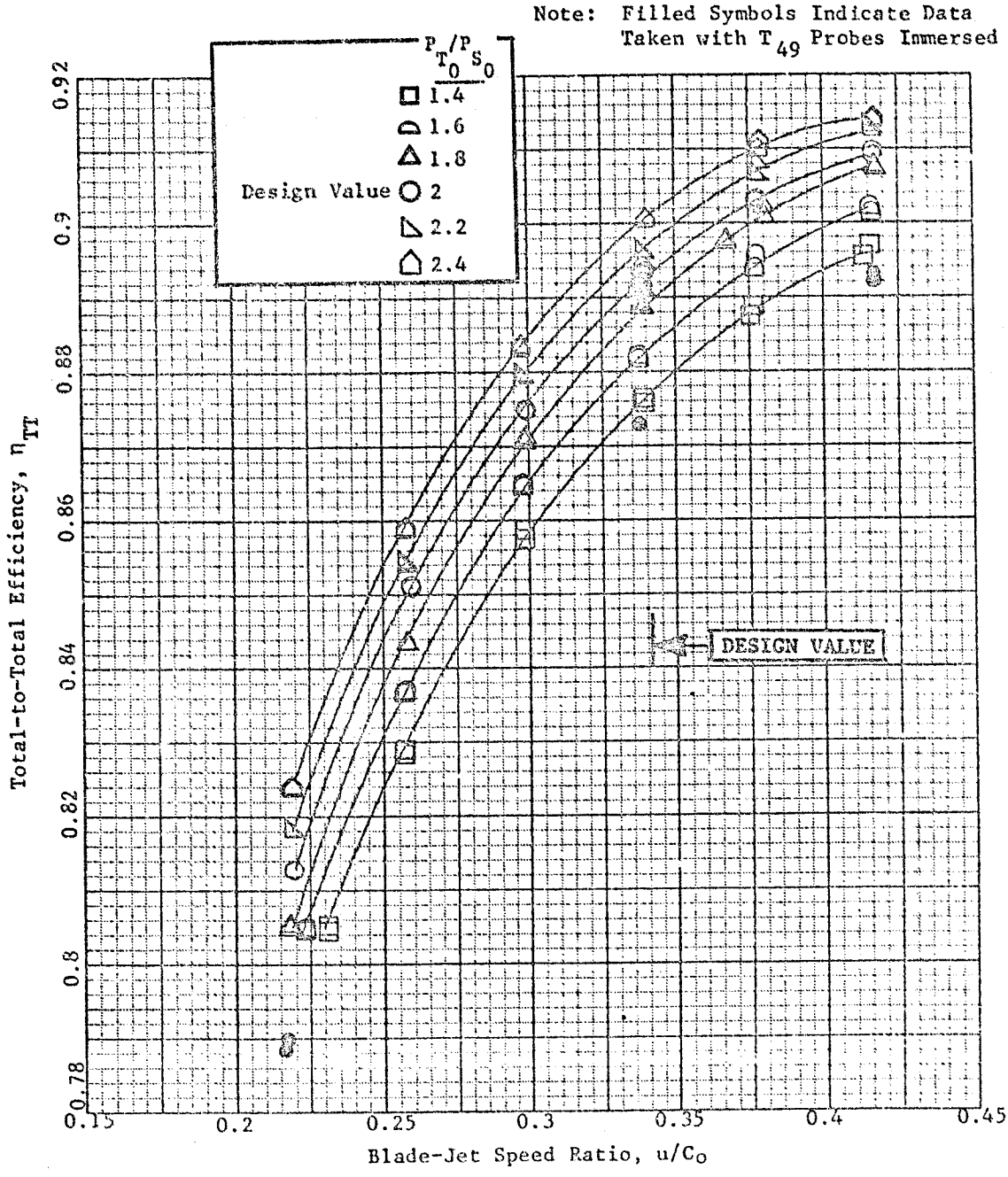

Figure 93. Block 11 Configuration 4a. Total-to-Total Efficiency, η_{TT}, vs. Blade-Jet Speed Ratio, u/C_o.

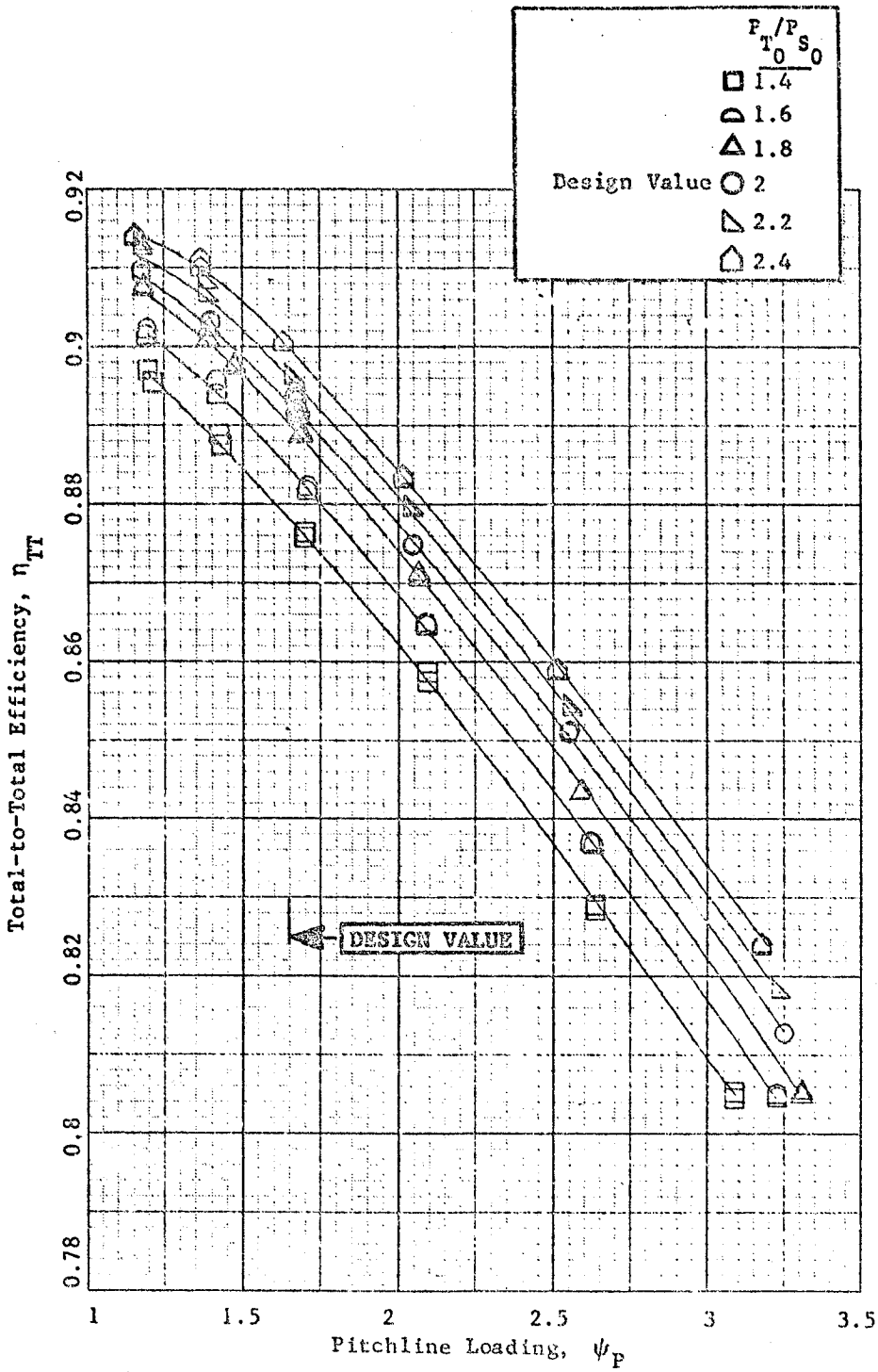

Figure 94. Block II Configuration 4a. Total-to-Total Efficiency, η_{TT}, vs. Pitchline Loading ψP.

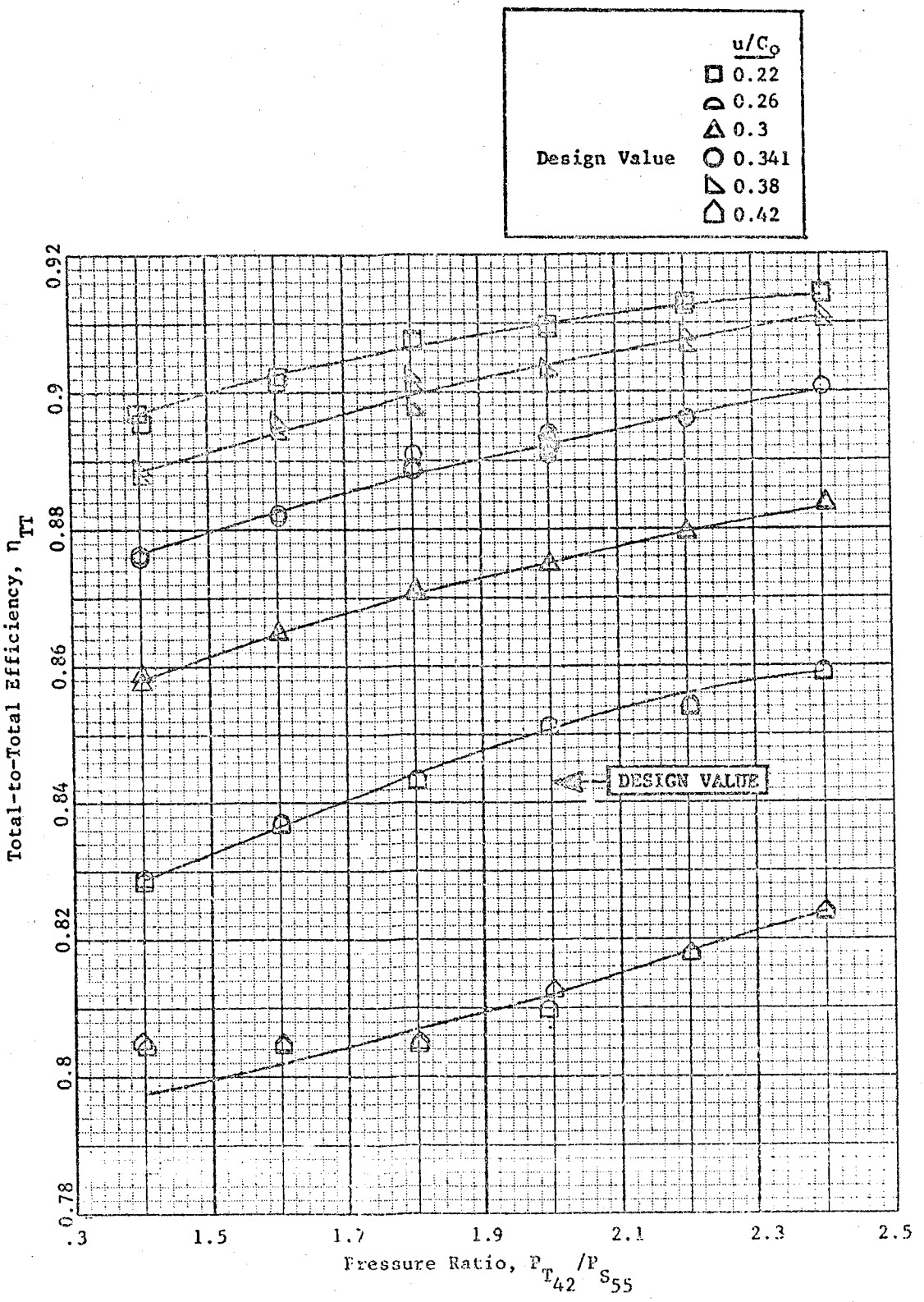

Figure 95. Block II Configuration 4a, Total-to-Total Efficiency, η_{TT}, vs. Pressure Ratio, $P_{T_{42}}/P_{S_{55}}$

It is interesting to note that the improved airfoils (item 3) seem to be more tolerant of negative incidence as evidenced by the relatively larger efficiency gains at loadings less than design loading, Figure 94.

As will be noted in Section 5.0 when the final performance stackup for the ICLS is discussed, all Block II rotor blades were received from the vendor with trailing edge diameters which were, on the average, 0.0127 cm (0.005 in.) oversize 0.0635 cm (0.025 in.) average measured vs. 0.0508 cm (0.02 in.) design intent). It has been calculated that this 25% increase in trailing edge blockage beyond design intent induced an additional loss in Configuration 4a equivalent to 0.001 in efficiency at design point. Consequently, the actual performance gain relative to Block I was 0.009 in efficiency and the absolute efficiency level of Configuration 4a, corrected for edge blockage, was 0.893.

The magnitude of the measured efficiency change is consistent with that anticipated for the Block II improvements, and brought the 2-stage build back to just above the Block I pre-test prediction level.

A loss of 1.8 points in two-stage group efficiency (accompanied by a 1.6 percent drop in inlet flow function) was measured when the 14 simulated P_T/T_T probes were immersed into the flow stream. This corresponds to a loss of 0.77 points in the five-stage group efficiency and about 0.5 percent in ICLS SFC. The data taken with the probes immersed is shown in Figures 93 and 96.

Flow characteristics for this build are presented in Figures 96 through 99.

Torque characteristics are presented as Figures 100 and 101.

The Block II 2-stage group swirl map is presented as Γ vs u/C_o in Figure 102. The row-by-row distribution of measured interstage static pressure, normalized by $P_{T_{42}}$, is presented for the design point in Figure 103 compared to an axisymmetric prediction.

Spanwise distributions of stage exit pressure (normalized), temperature (normalized), swirl, and group total-to-total efficiency based on results of the design point exit traverse survey are presented in Figures 104 through 107.

Note from Figure 107, η_{TT} vs %h for Block II (with Block I added for reference), that the Block II performance gain is over most of the span.

Results of the Reynolds number excursion for Configuration 4a are presented in Figure 108.

Configuration 5

Test data for Block II Configuration 5, the five-stage build, are tabulated in Appendix H.

The following items were accomplished during Block II 5-stage rig testing:

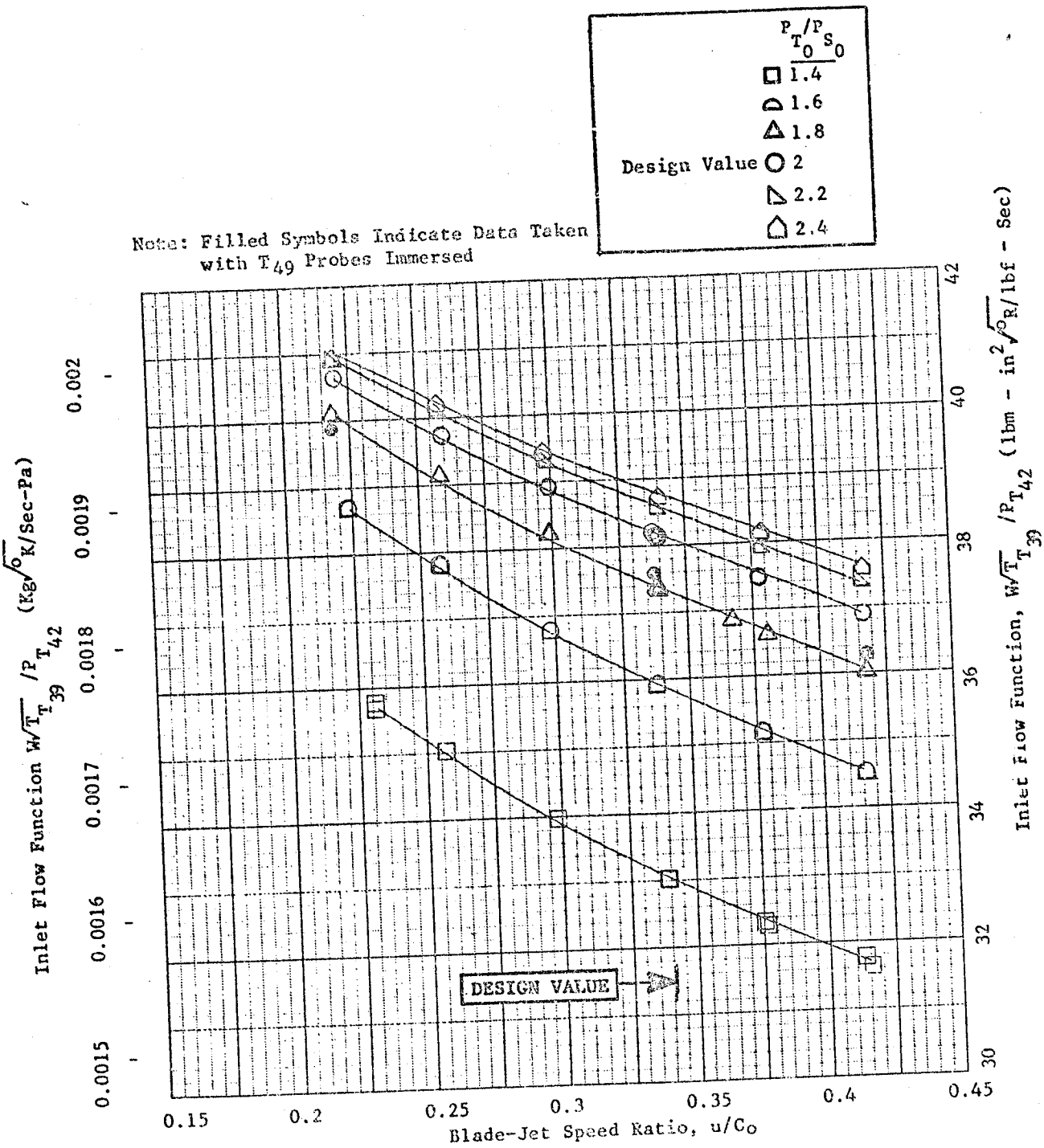

Figure 96. Block II Configuration 4a, Inlet Flow Function, $W\sqrt{T_{T_{39}}}/P_{T_{42}}$, vs. Blade-Jet Speed Ratio, u/Co.

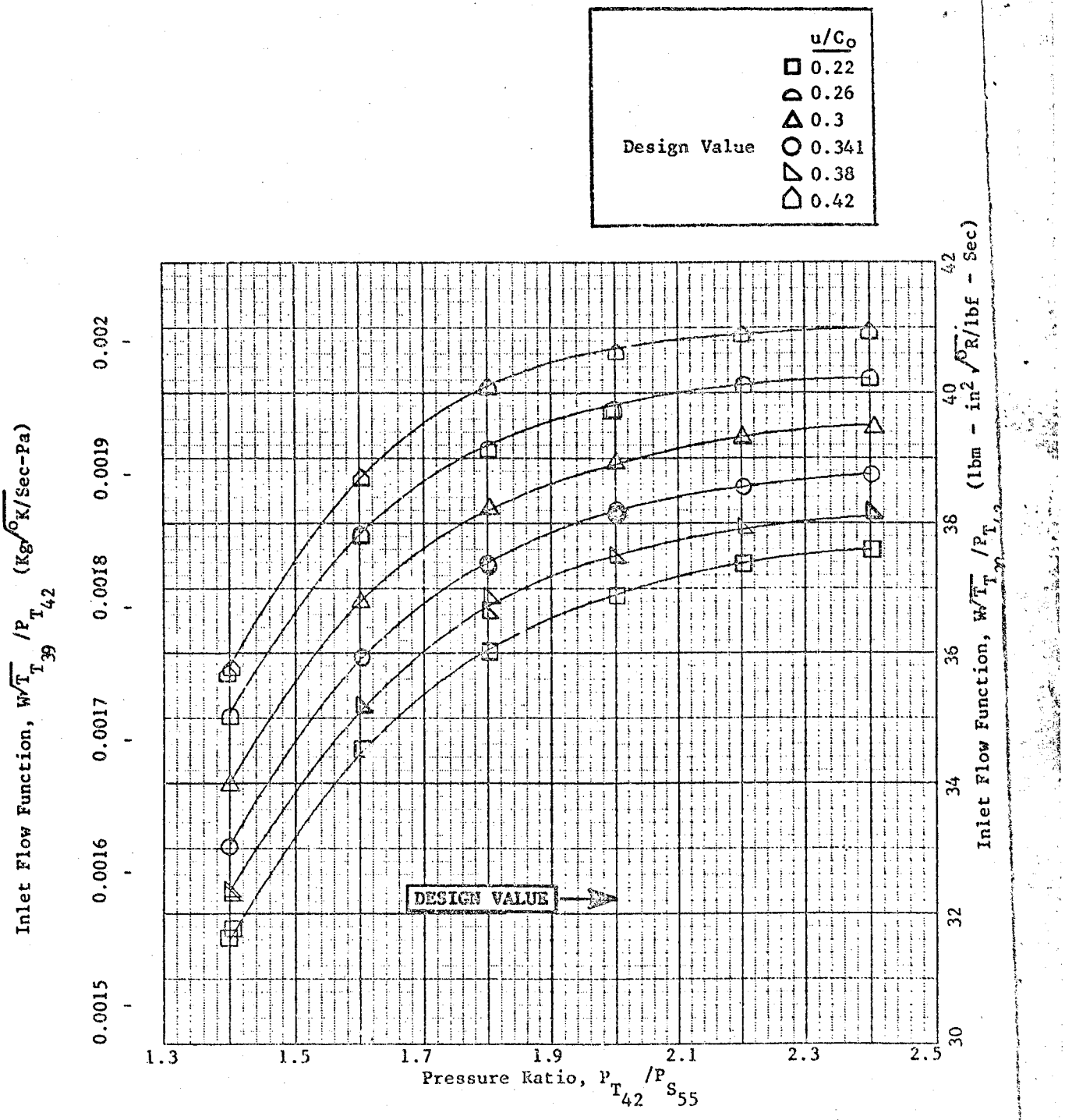

Figure 97. Block II Configuration 4a, Inlet Flow Function, $W\sqrt{T}_{T_{39}}/P_{T_{42}}$, vs, Pressure Ratio, $P_{T_{42}}/P_{S_{55}}$.

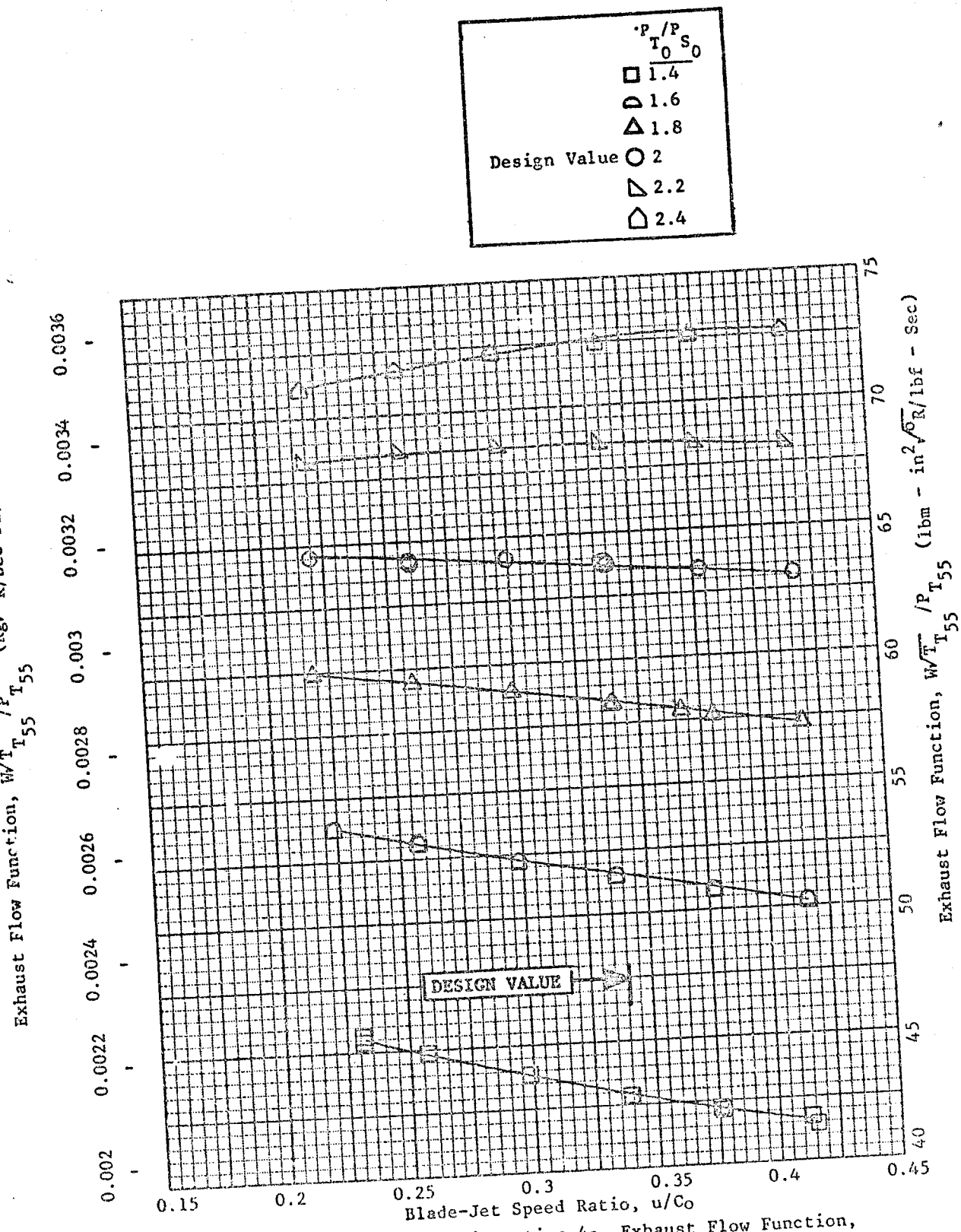

Figure 98. Block II Configuration 4a, Exhaust Flow Function, $W\sqrt{T}_{T_{55}}/P_{T_{55}}$, vs. Blade-Jet Speed Ratio, u/Co.

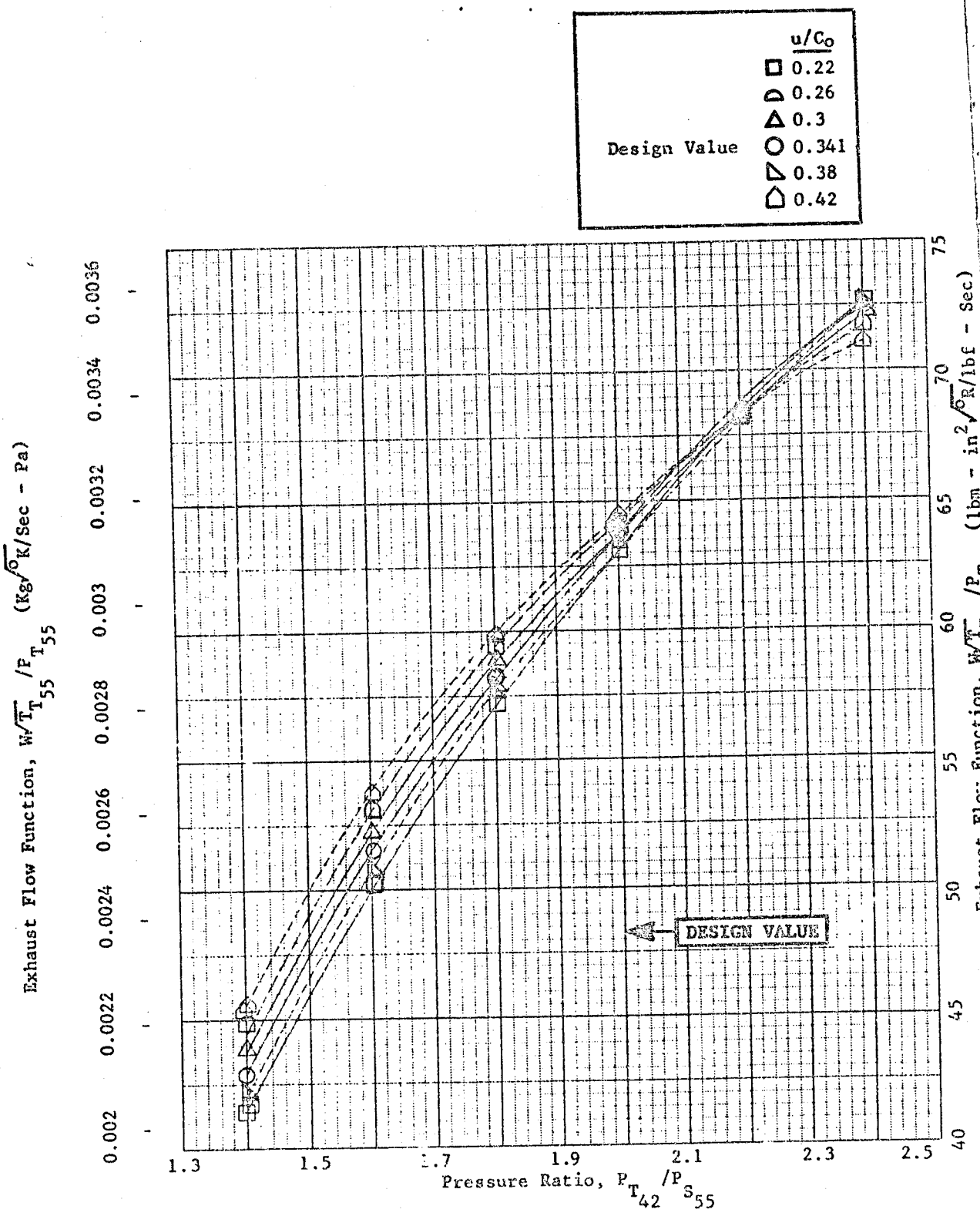

Figure 99. Block II Configuration 4a, Exhaust Flow Function, $W\sqrt{T_{T_{55}}}/P_{T_{55}}$ vs. Pressure Ratio, $P_{T_{42}}/P_{S_{55}}$.

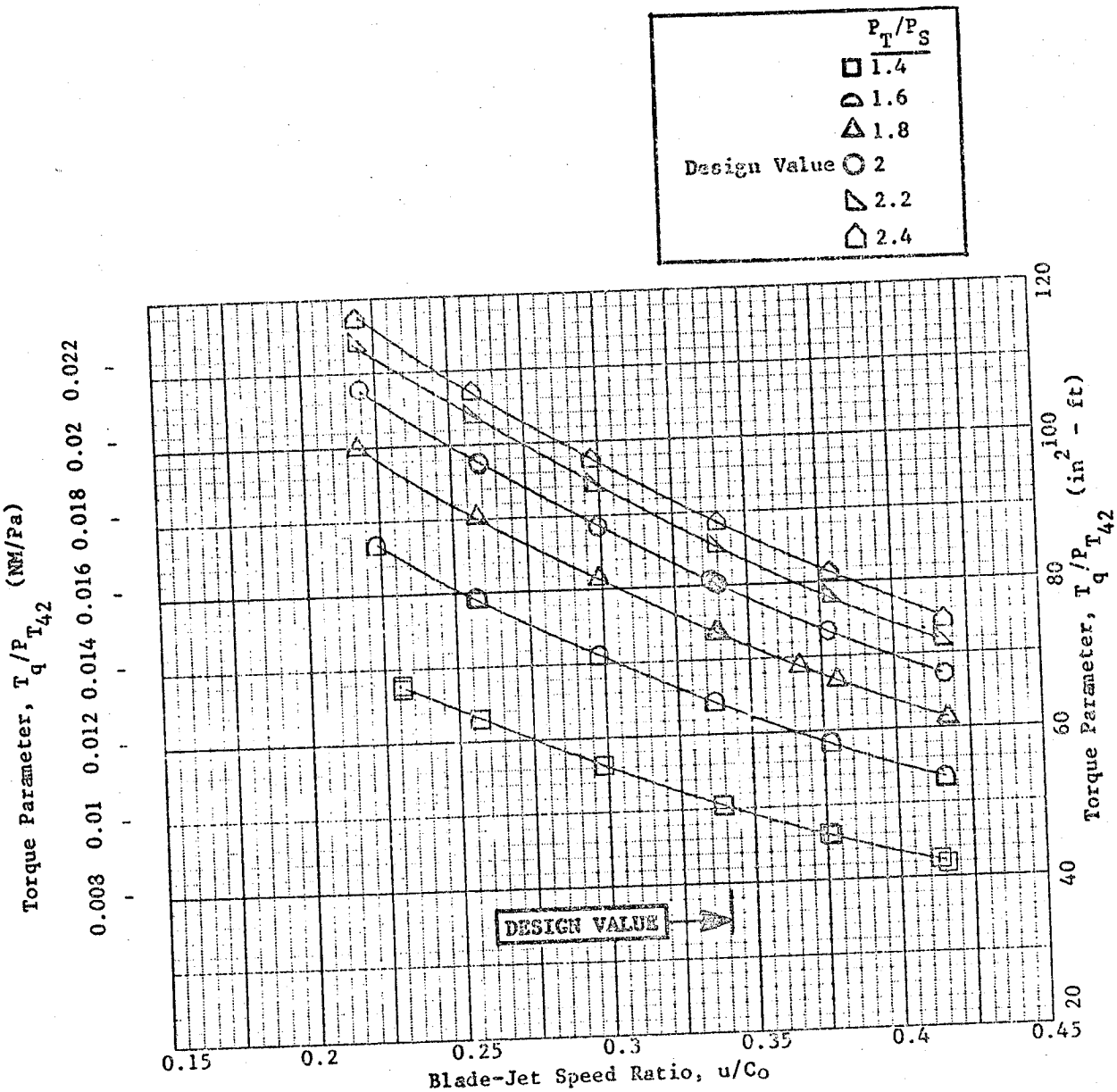

Figure 100. Block II Configuration 4a, Torque Parameter, $Tq/P_{T_{42}}$ vs. Blade-Jet Speed Ratio, u/C_o.

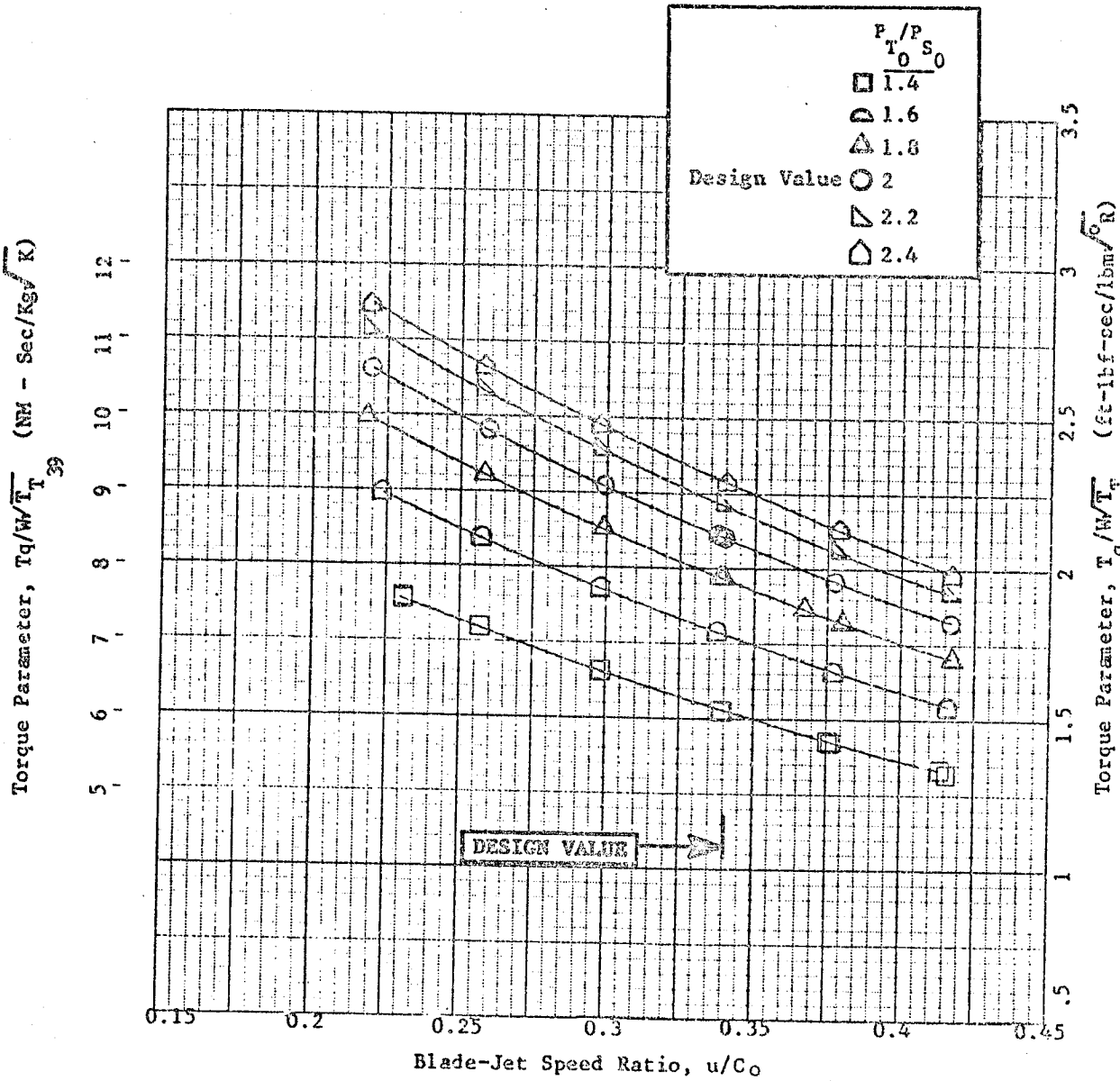

Figure 101. Block II Configuration 4a, Torque Parameter, $Tq/W\sqrt{T_{T_{39}}}$, vs. Blade-Jet Speed Ratio, u/C_o.

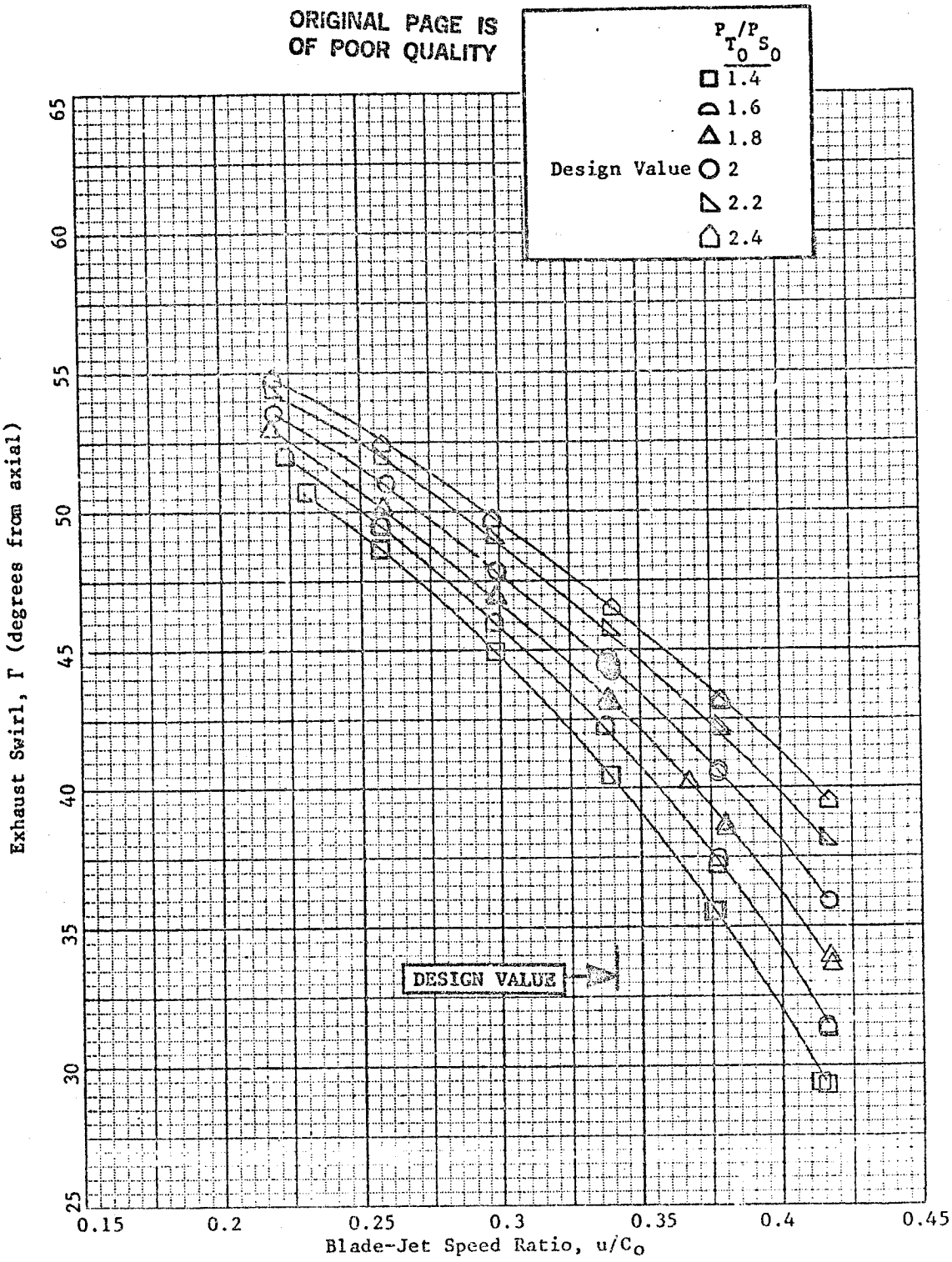

Figure 102. Block II Configuration 4a, Exhaust Swirl, Γ, vs. Blade-Jet Speed Ratio, u/C_o.

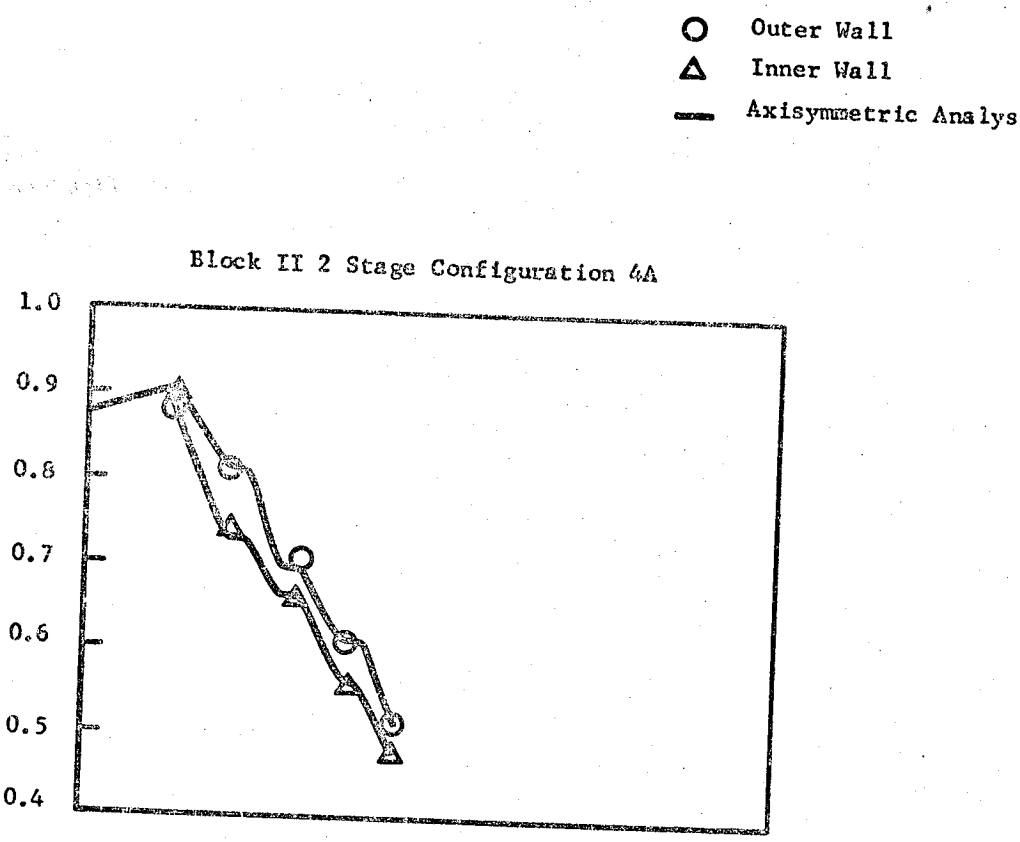

Figure 103. Interstage Static Pressures, Predicted vs. Test (Design Point Data).

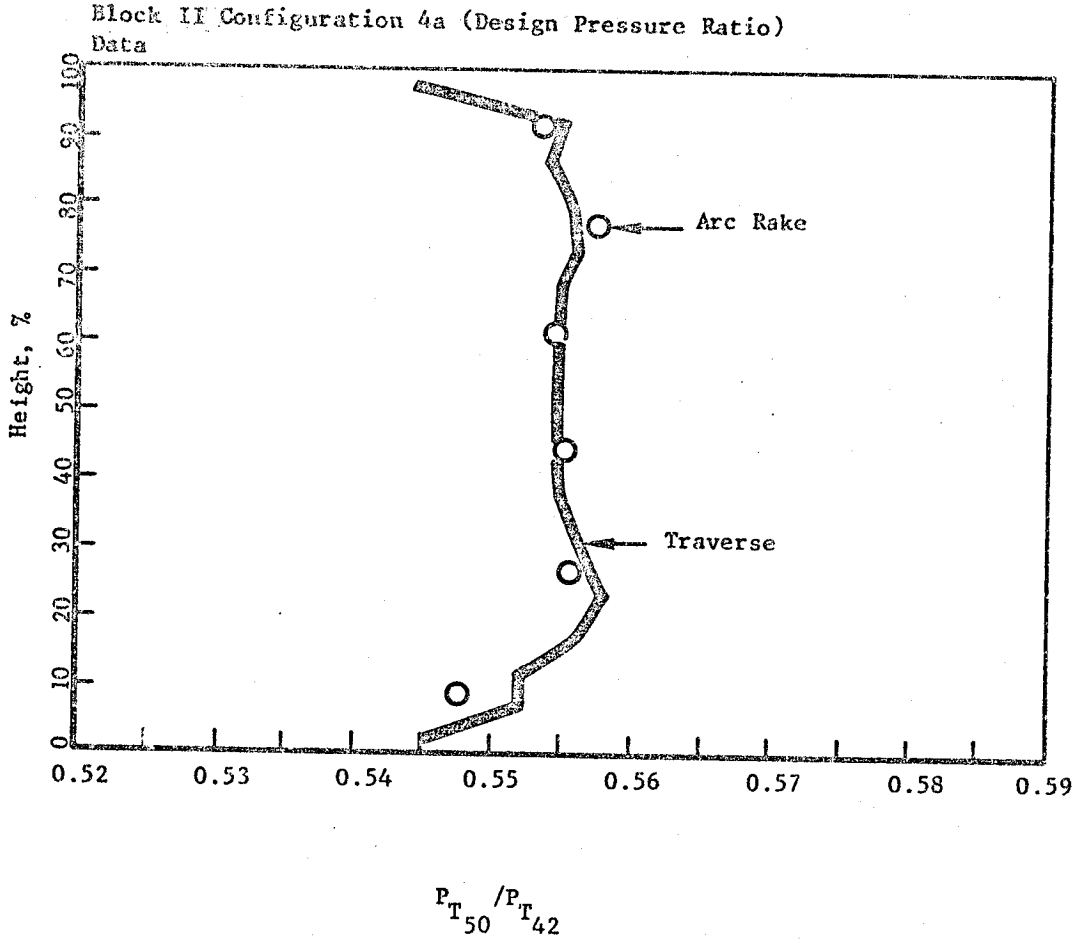

Figure 104. Block II Configuration 4a - $P_{T_{50}}/P_{T_{42}}$ vs. % Height.

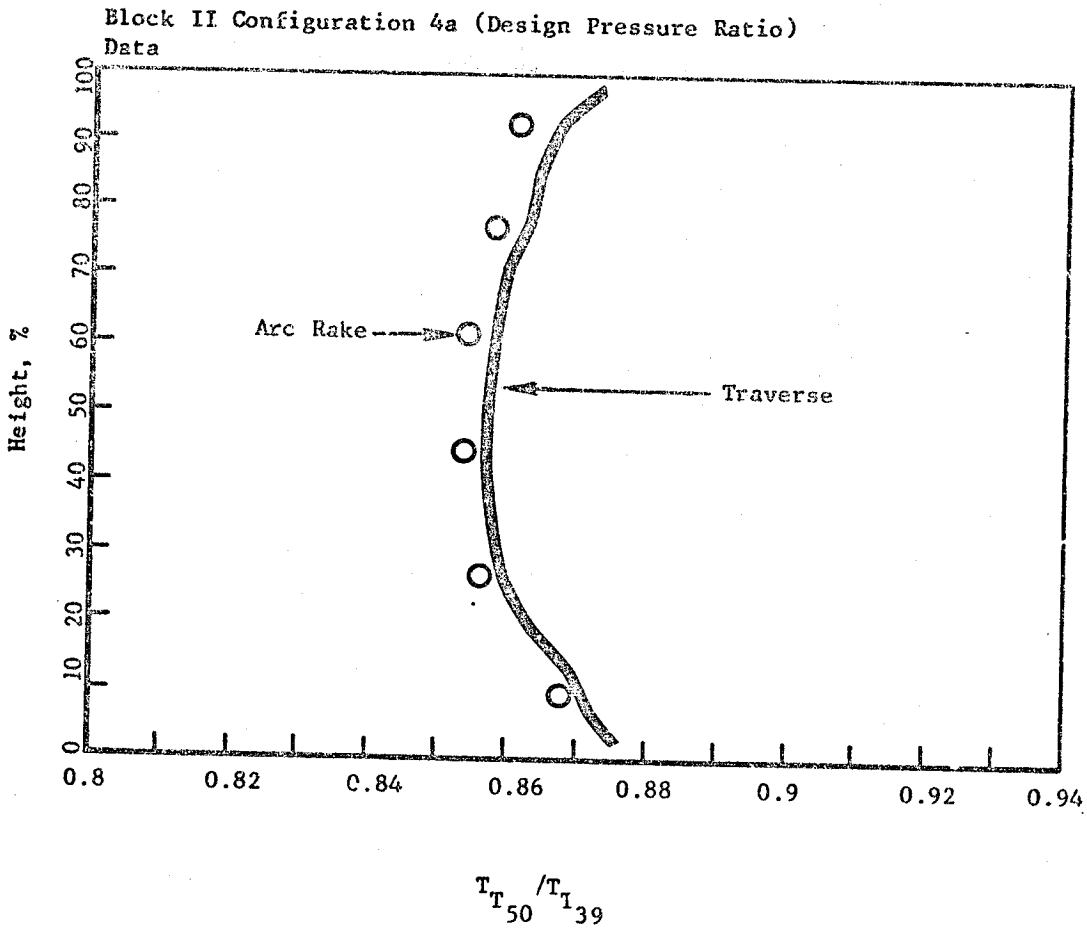

Figure 105. Block II Configuration 4a - $T_{T_{50}}/T_{T_{39}}$ vs. % Height.

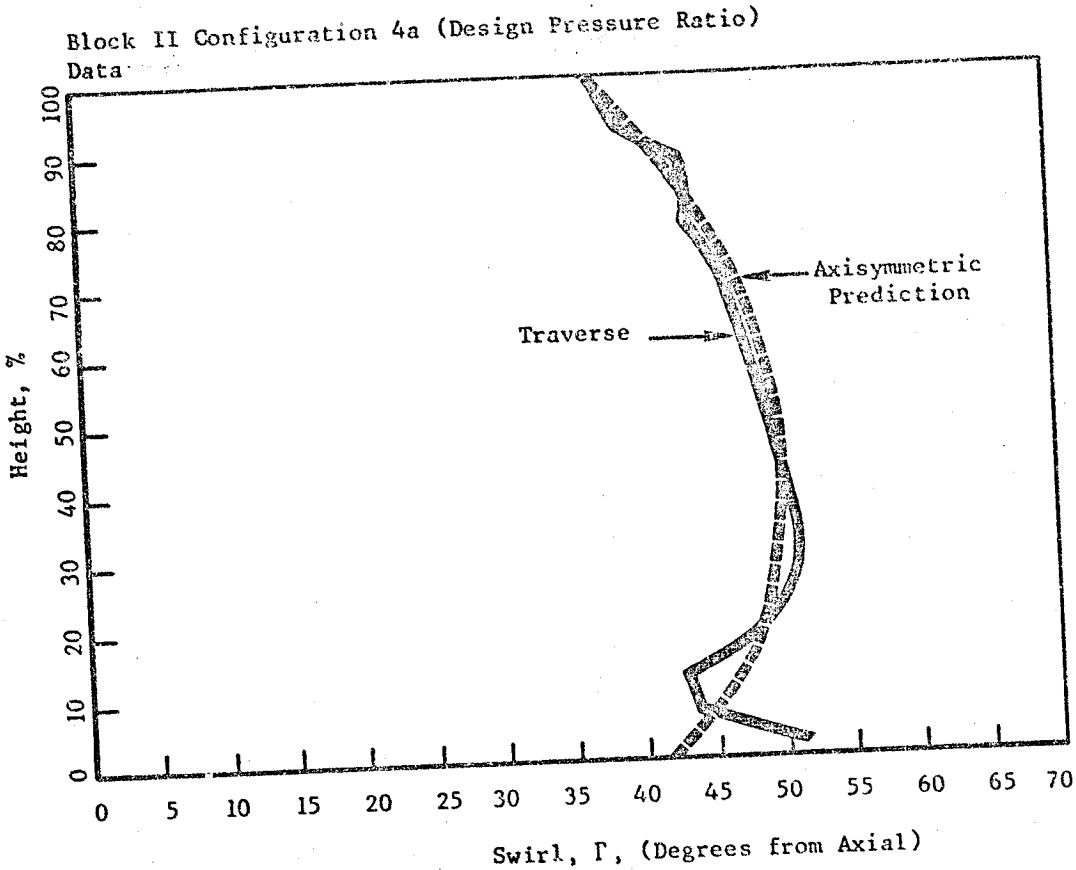

Figure 106. Block II Configuration 4a - Swirl Γ, vs. % Height.

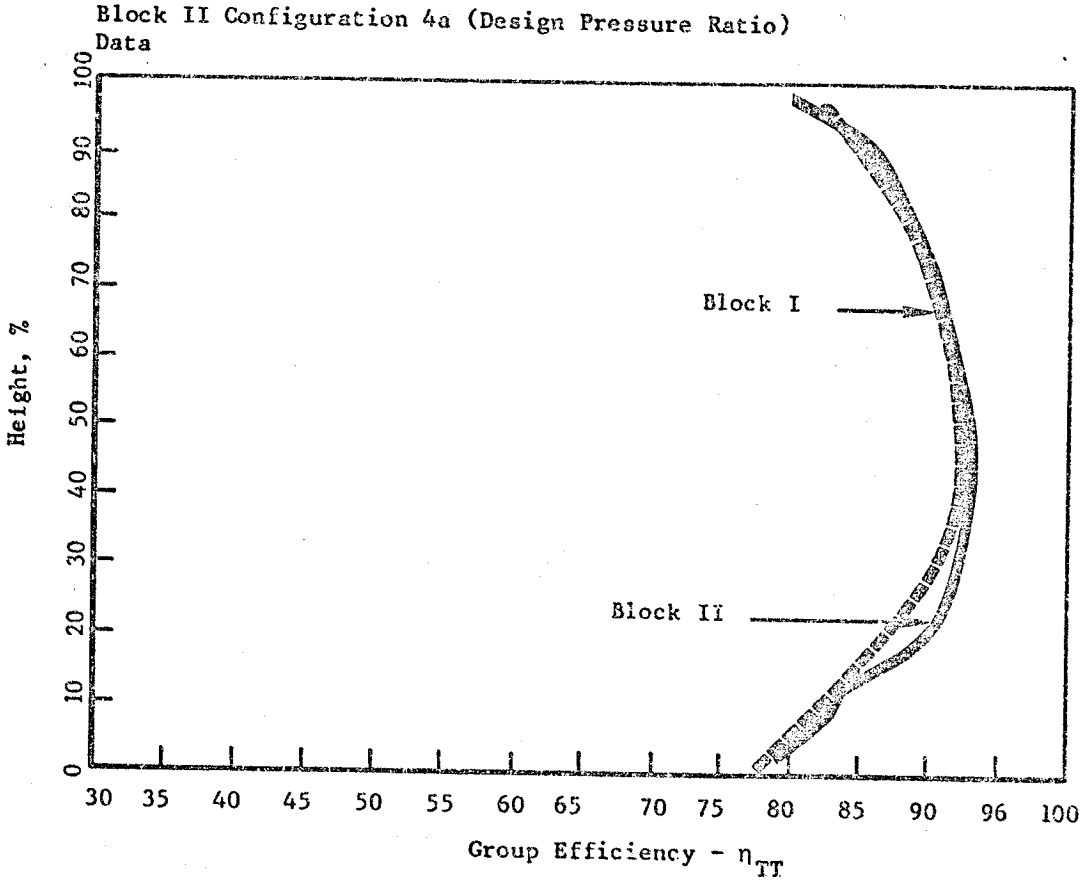

Figure 107. Block II Configuration 4a (Compared with Block I) - Group Efficiency vs. % Height.

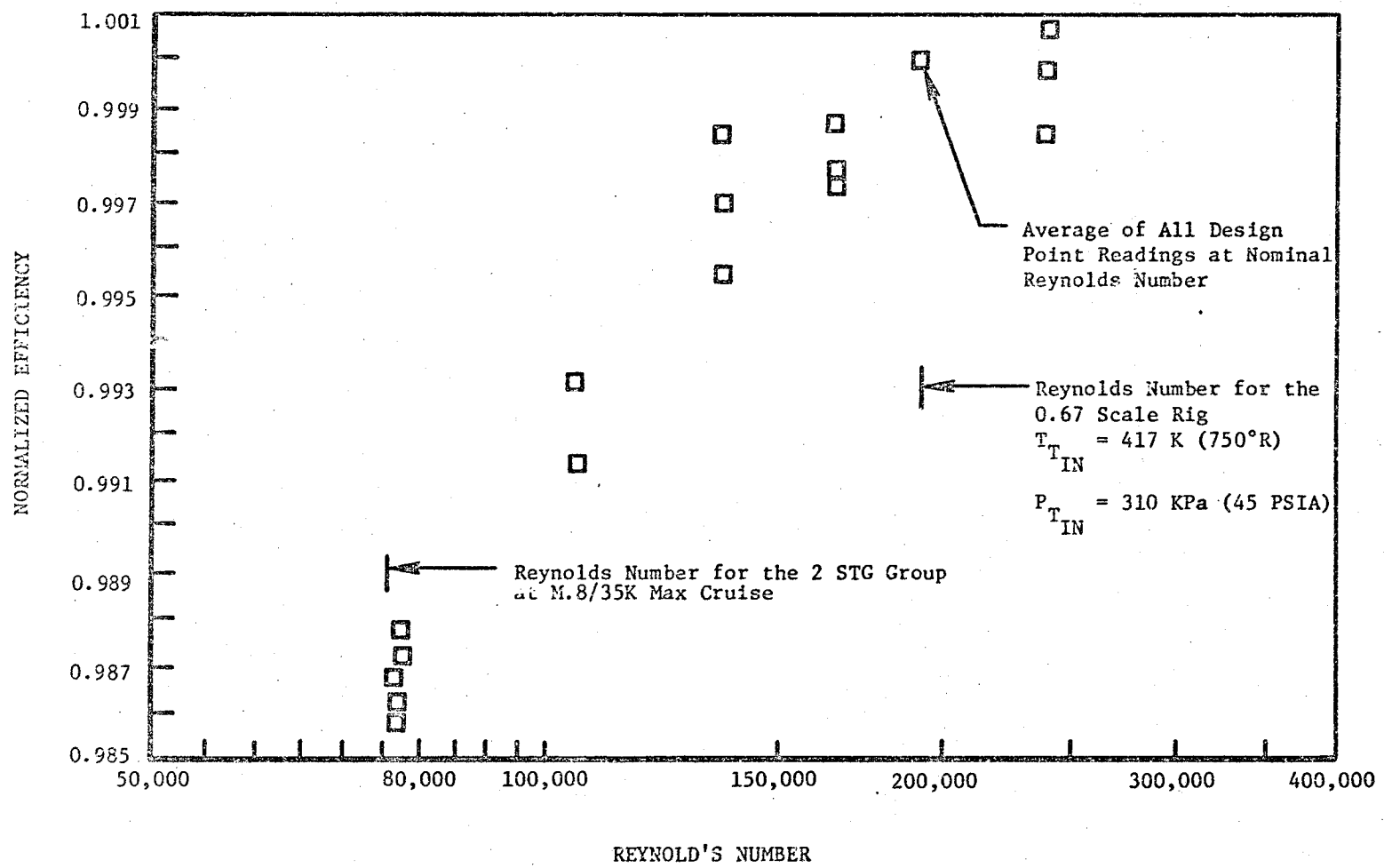

Figure 108. Block II Configuration 4a Reynolds Number Excursion

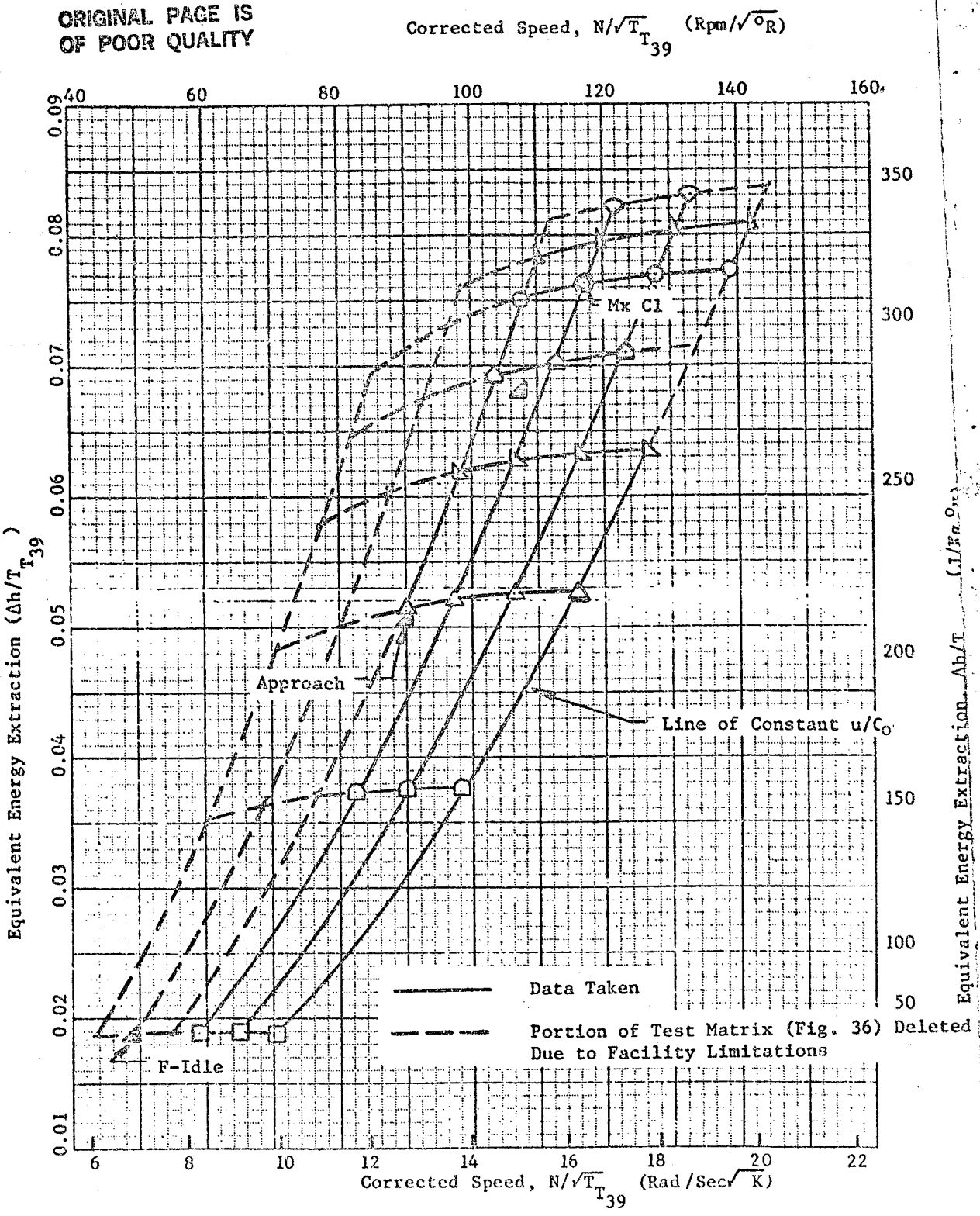

Figure 109. Block II Configuration 5,-Equivalent Energy Extraction, $\Delta h/T_{T_{39}}$, Vs Corrected Speed, $N/\sqrt{T_{T_{39}}}$

- o Performance mapping over a range of pressure ratios and speeds which (within the operational limitations of the test facility) yielded data across the full extent of the ICLS LPT operating line, from maximum climb to flight-idle.

- o Reynolds number excursion, covering a range of Reynolds numbers from one equivalent to the ICLS LPT at sea level takeoff to one equivalent to the ICLS LPT at the Mach 0.8, 10.67 Km (35,000 feet) maximum climb (design point) condition.

- o Detailed Rotor 5 exit survey (traverse) at the aero design point.

Figure 29 shows a cross-section of the five-stage test vehicle, which represents a 0.67 scale of the final ICLS design.

Figure 109 presents the test matrix ($\Delta h/T_T$ vs $N/\sqrt{T_T}$) for the five-stage rig. Each intersection of a line of constant total-to-static pressure ratio with a line of constant blade-jet speed ratio represents an intended test point. Due to facility waterbrake limitations, however, only those points formed by the intersection of the solid lines were actually set. Points on the low speed side of of the test matrix (formed by the intersection of the dashed lines) could not be set because, at the lower pressure ratios, there was not enough viscous torque in the brake to hold at the very low speeds and, at the higher pressure ratios, insufficient flow rate through the brake caused excessive water temperature rise. An approximation to the LPT operating line shows that most of the significant operating points (from maximum climb to approach) are covered by data, but that the very low settings (from approach to flight-idle) have required extrapolation of performance data.

Results of the mapping are presented in Figures 110 through 122. Figure 111 presents five-stage group efficiency, η_{TT}, as a function of group pitchline loading, $gJ\Delta h/2u_D^2$, and group total-to-static pressure ratio, P_T/P_S. Efficiency at the design pressure ratio (4.76) and loading (1.3) is 92.0%. The efficiency calculation is based on measured values of flow, shaft torque, shaft speed, inlet pressure and temperature, and exhaust pressure. No bearing or windage corrections have been added to the torque measurement since they are considered relatively insignificant.

Plots of 5-stage total-to-static efficiency are presented in Figure 113 through 115.

As noted in the discussion of results for Configuration 4a, the Block II rotor blade trailing edge diameters were oversized by, on the average, 25%. Calculations have shown that an additional loss, equivalent to 0.001 in five-stage turbine efficiency, was caused by this deviation. This has not been credited to Configuration 5 in any of the performance plots, which present only "as measured" results. Credit will be assigned for the edge blockage deviation, however, in the ICLS performance stackup, Section 5.0.

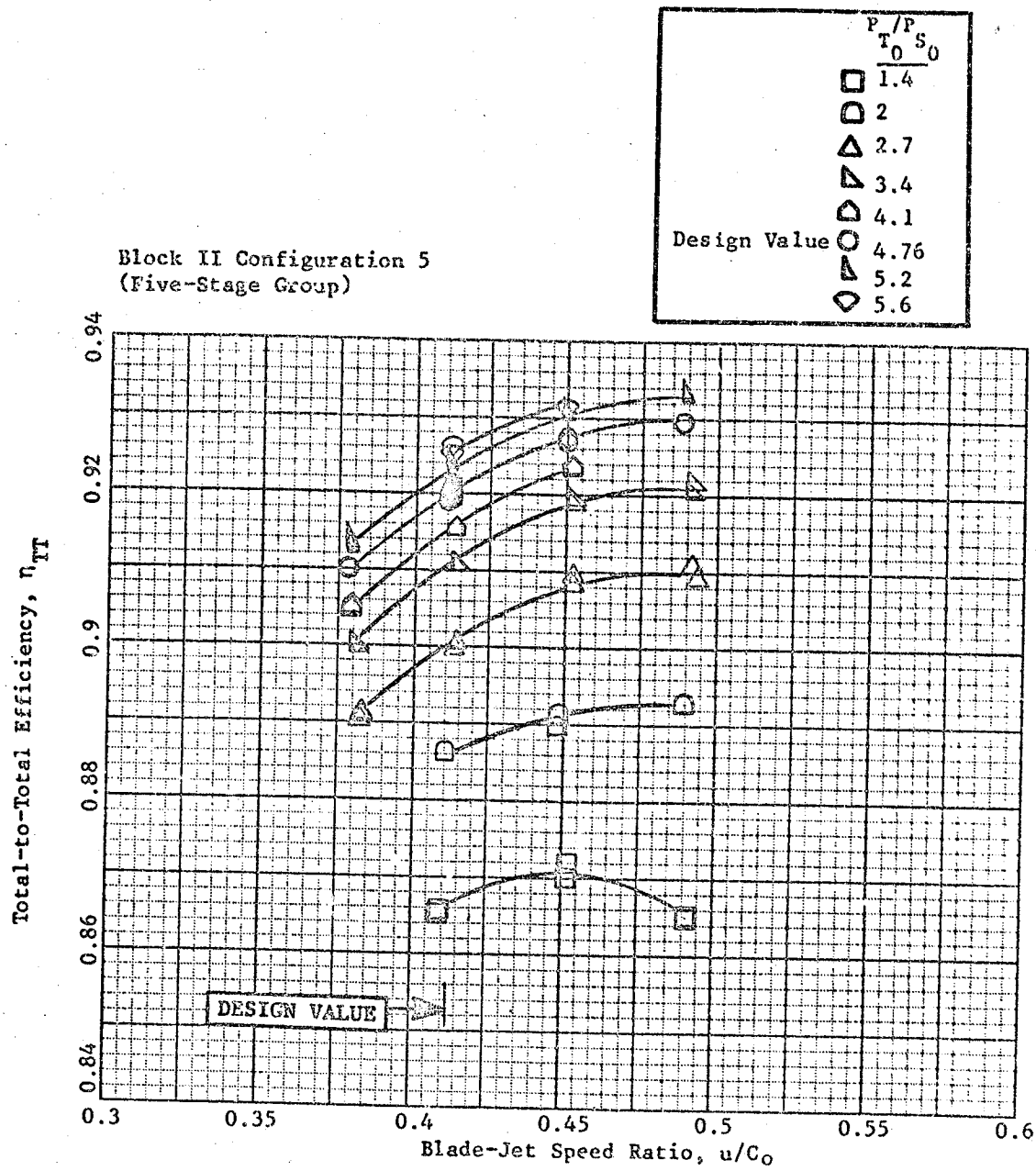

Figure 110. Block II Configuration 5, Total-to-Total Efficiency, η_{TT}, vs. Blade-Jet Speed Ratio, u/C_o

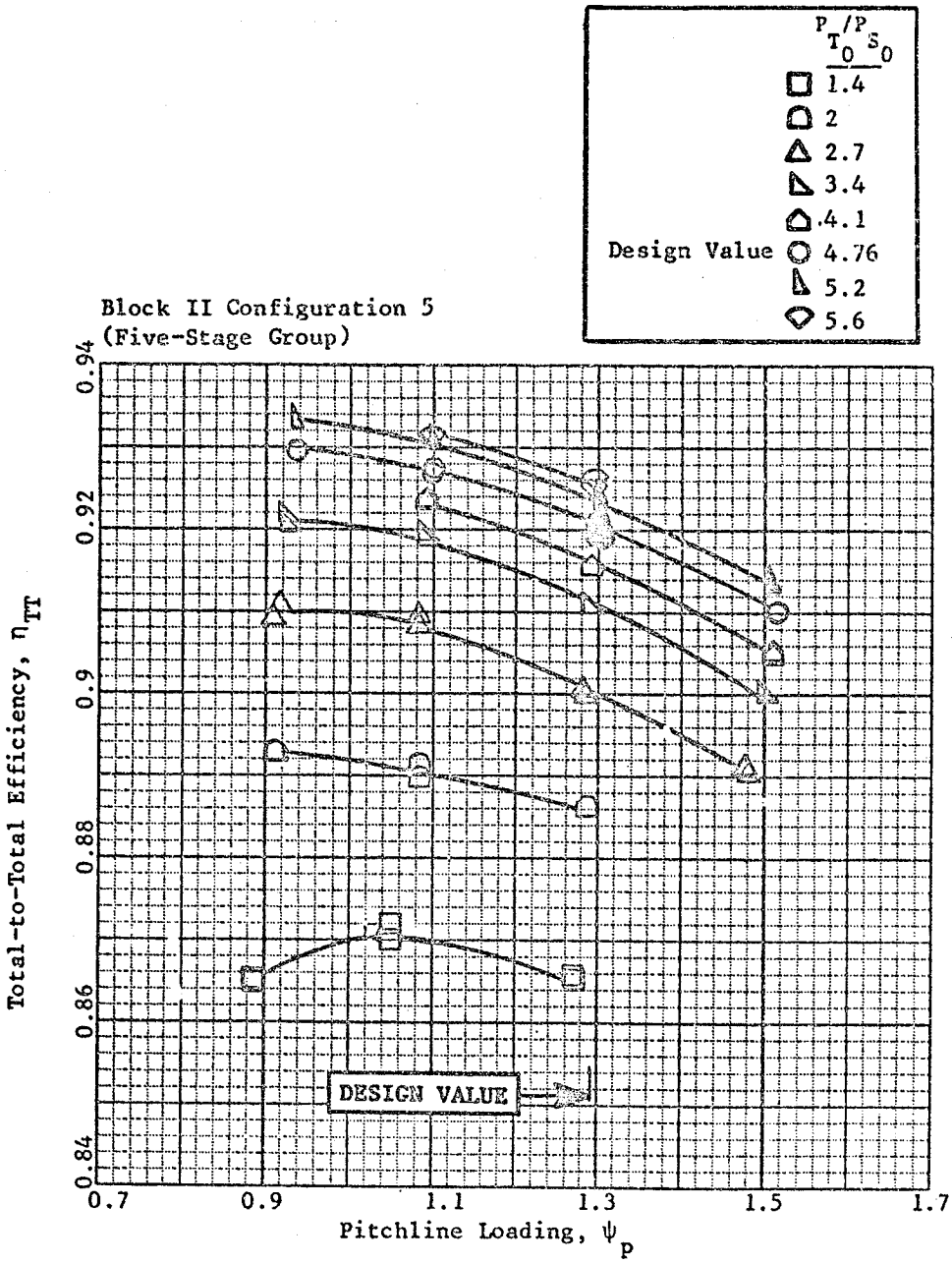

Figure 111. Block 11 Configuration 5, Total-to-Total Efficiency, η_{TT} vs. Pitchline Loading, ψ_p.

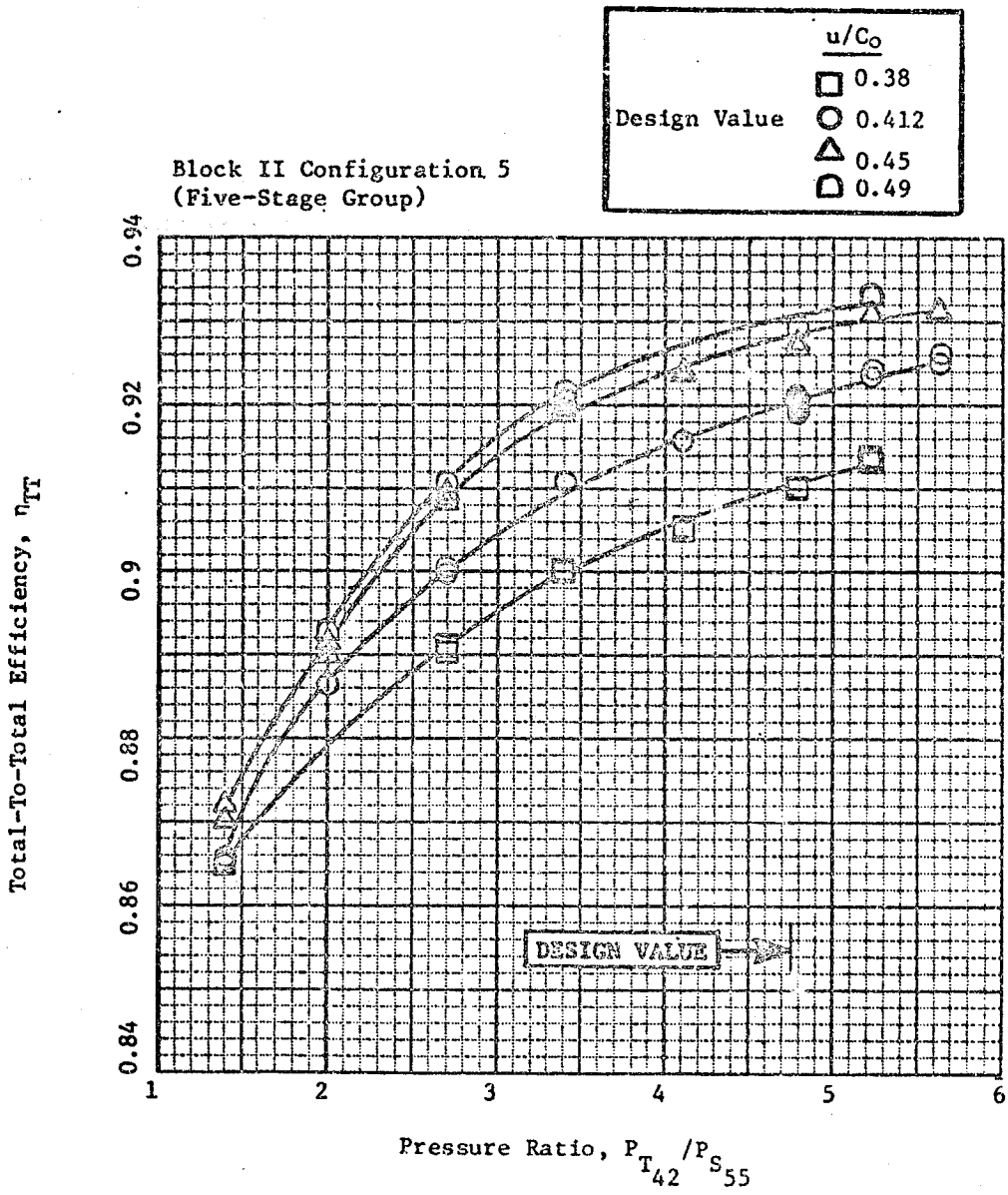

Figure 112. Block II Configuration 5, Total-to-Total Efficiency, η_{TT} vs. Pressure Ratio, $P_{T_{42}}/P_{S_{55}}$.

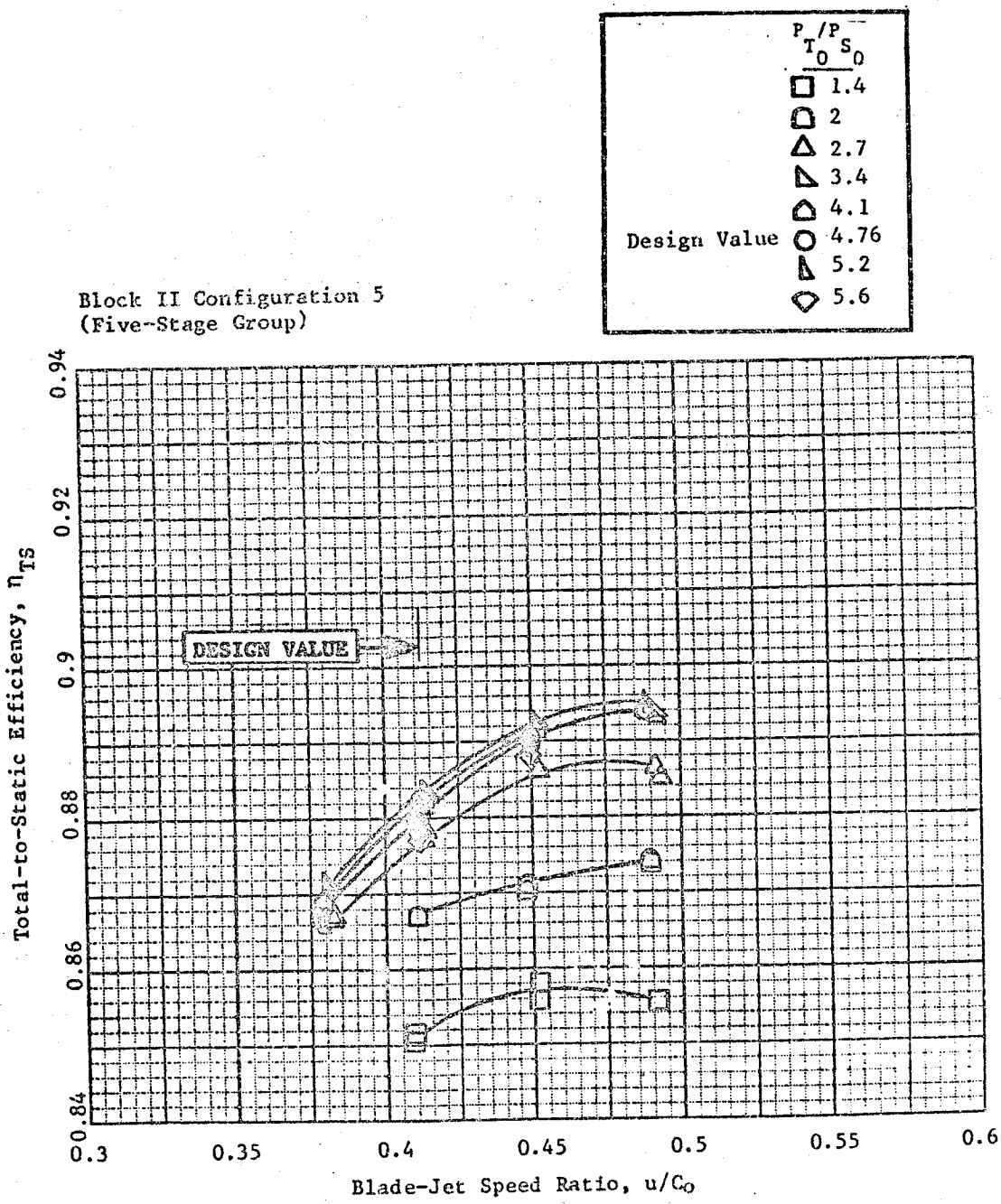

Figure 113. Block II Configuration 5, Total-to-Static Efficiency, η_{TS} vs. Blade-Jet Speed Ratio, u/C_o

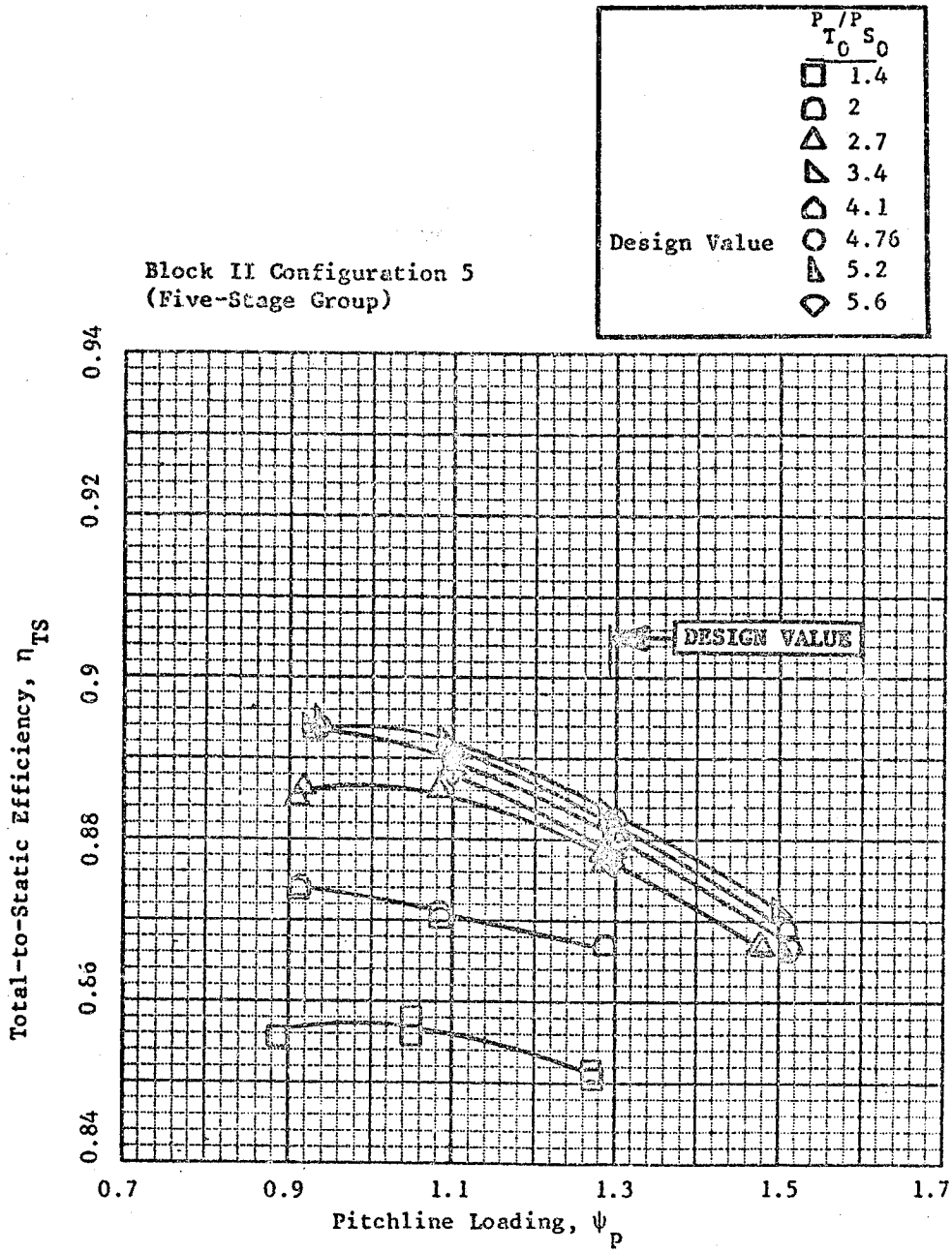

Figure 114. Block II Configuration 5, Total-to-Static Efficiency, η_{TS} vs. Pitchline Loading, ψ_p.

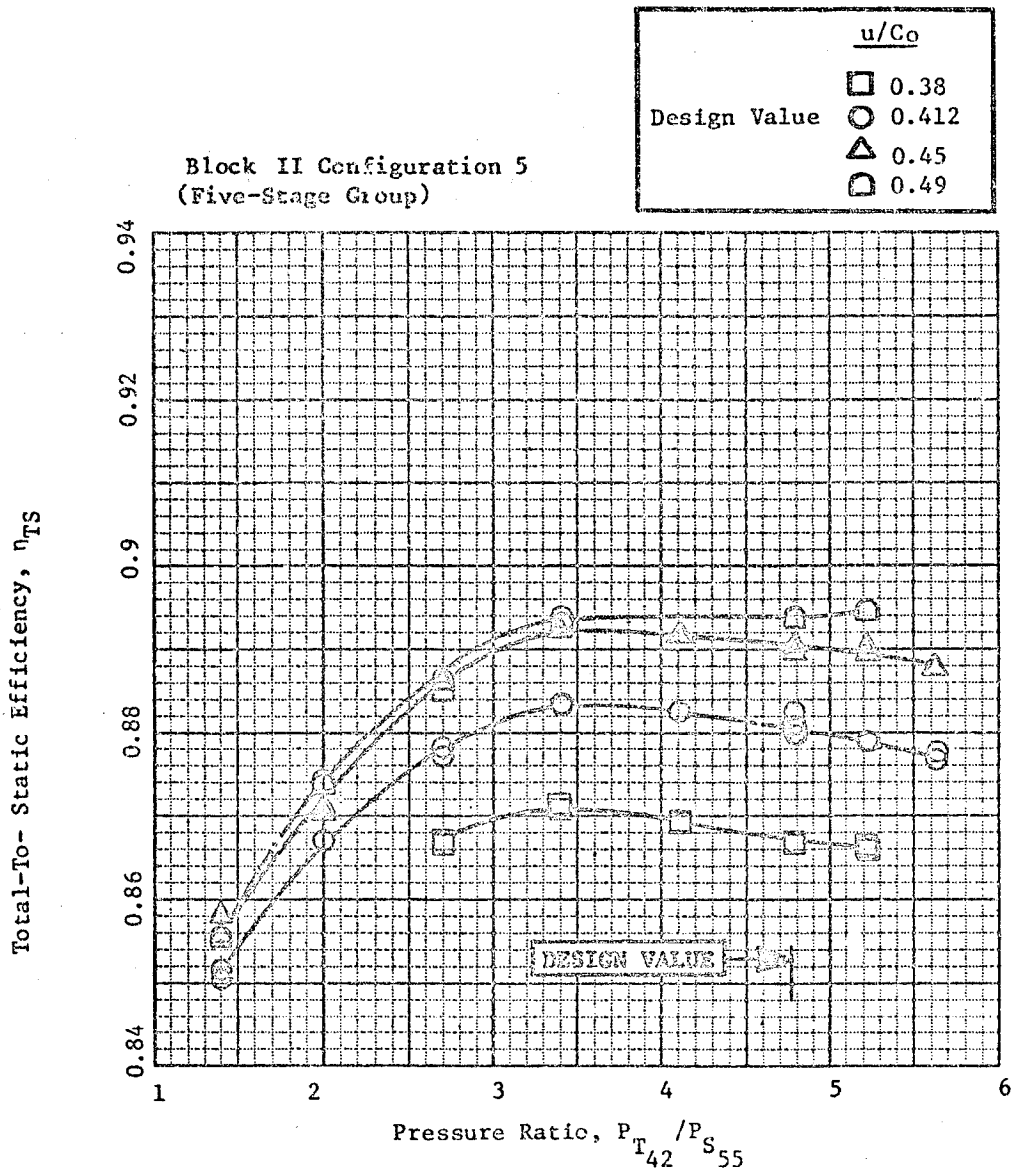

Figure 115. Block II Configuration 5, Total-To-Static Efficiency, η_{TS}, vs. Pressure Ratio, $P_{T_{42}}/P_{S_{55}}$.

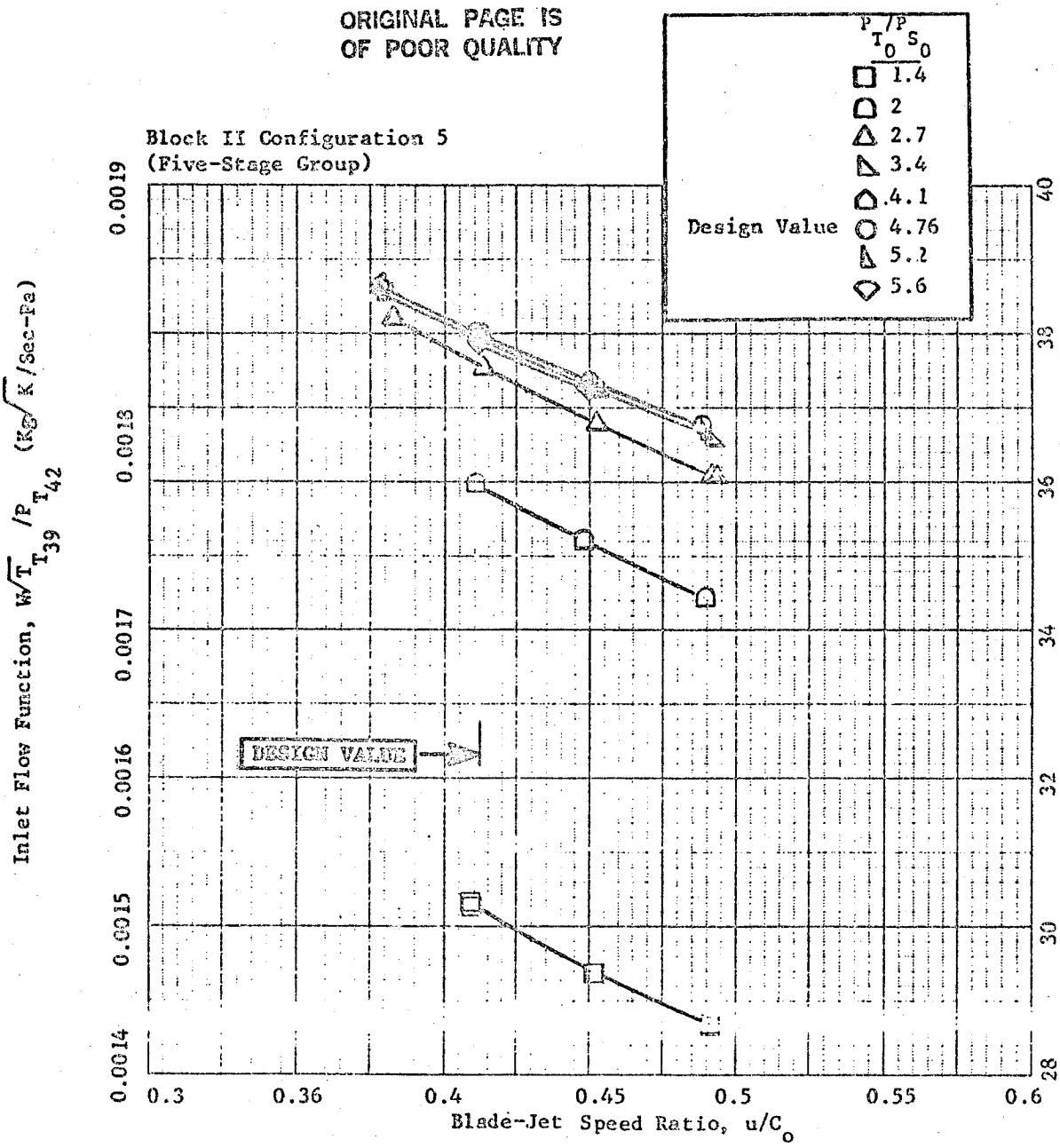

Figure 116. Block II Configuration 5, Inlet Flow Function, $W\sqrt{T}_{T_{39}}/P_{T_{42}}$, vs. Blade-Jet Speed Ratio, u/C_o.

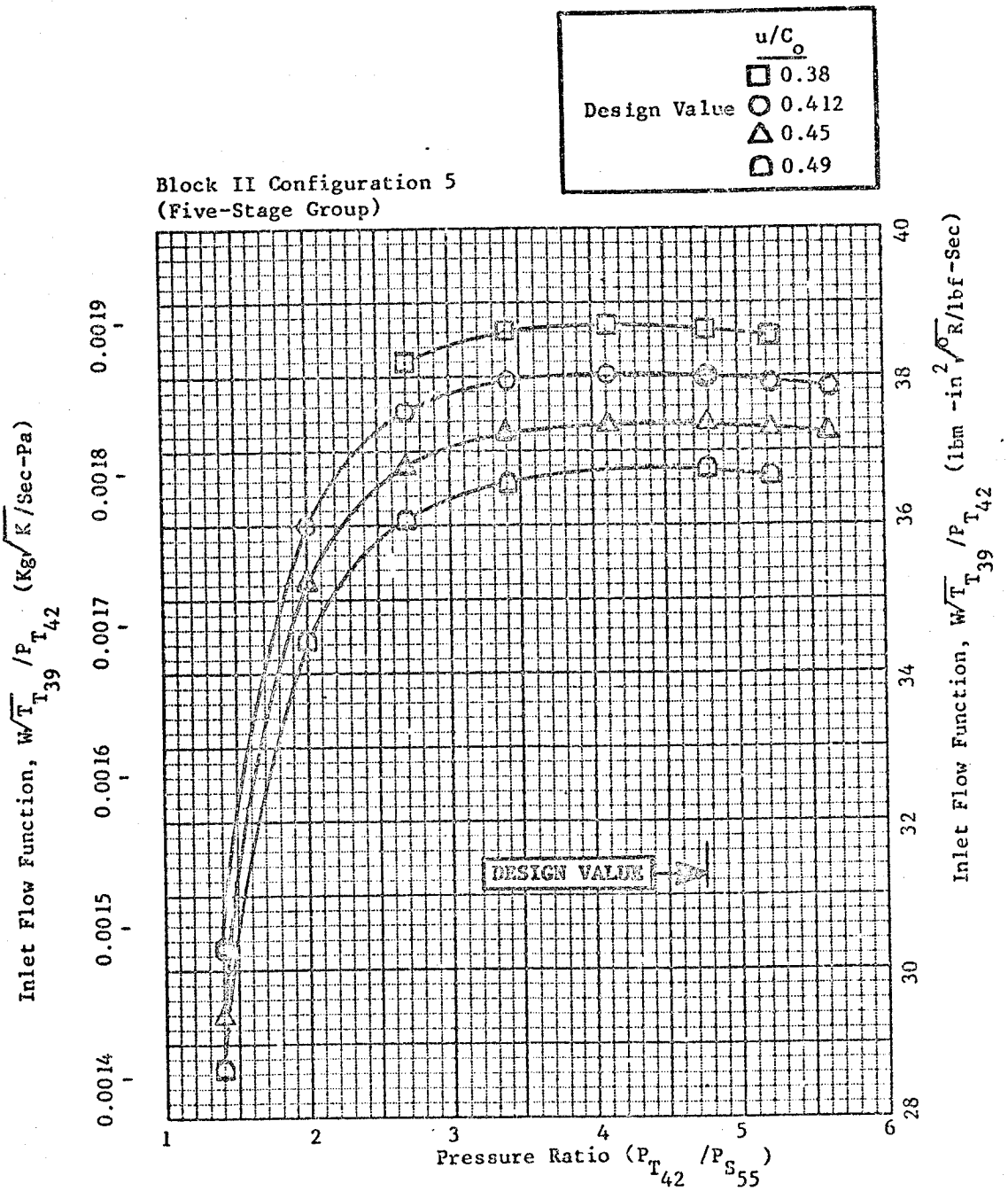

Figure 117. Block II Configuration 5, Inlet Flow Function Efficiency, $W\sqrt{T}_{T_{39}}/P_{T_{42}}$, vs. Pressure Ratio, $P_{T_{42}}/P_{S_{55}}$.

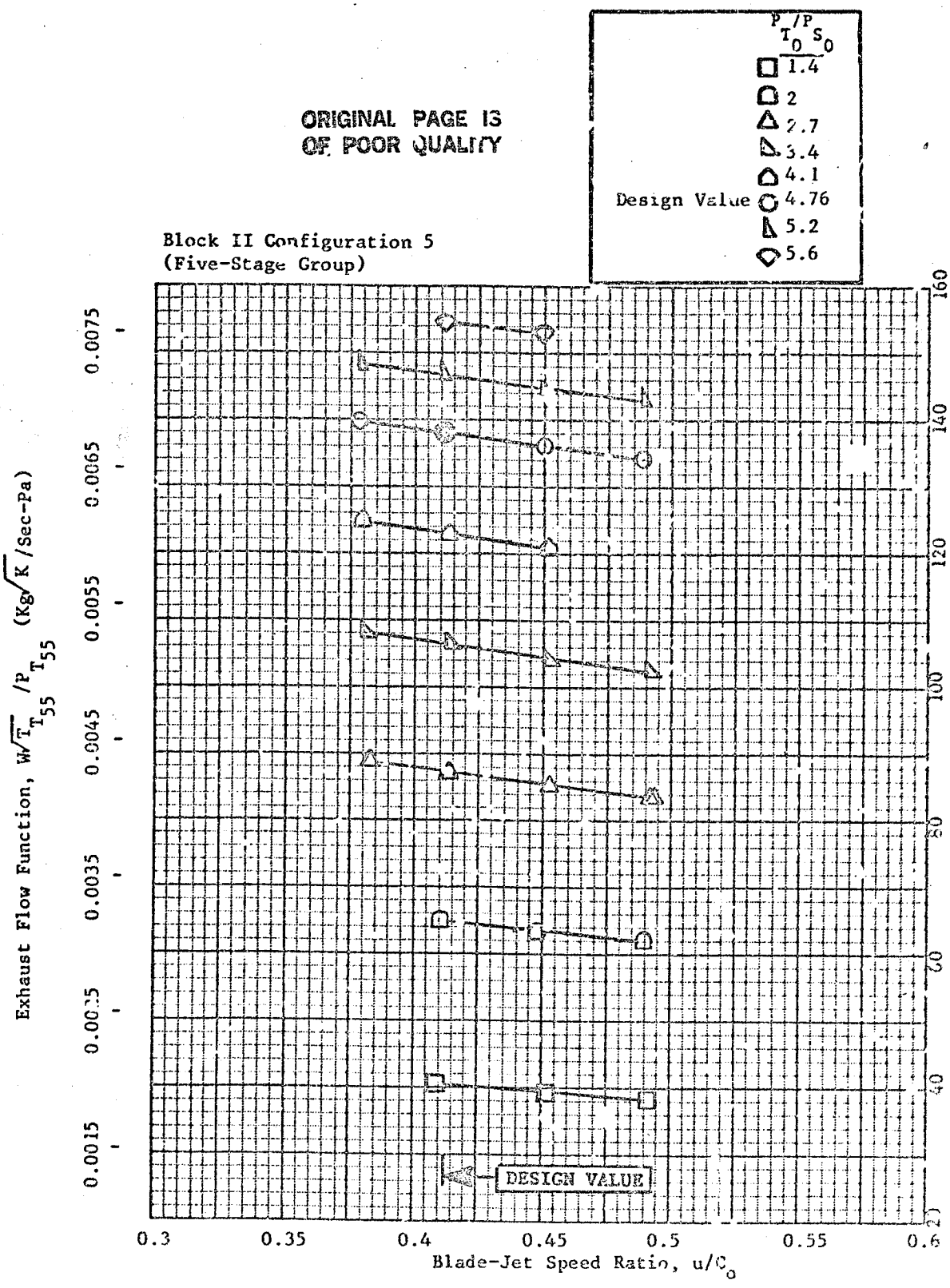

Figure 118. Block II Configuration 5, Exhaust Flow Function, $W\sqrt{T_{T_{55}}}/P_{T_{55}}$, vs. Blade-Jet Speed Ratio, u/C_o.

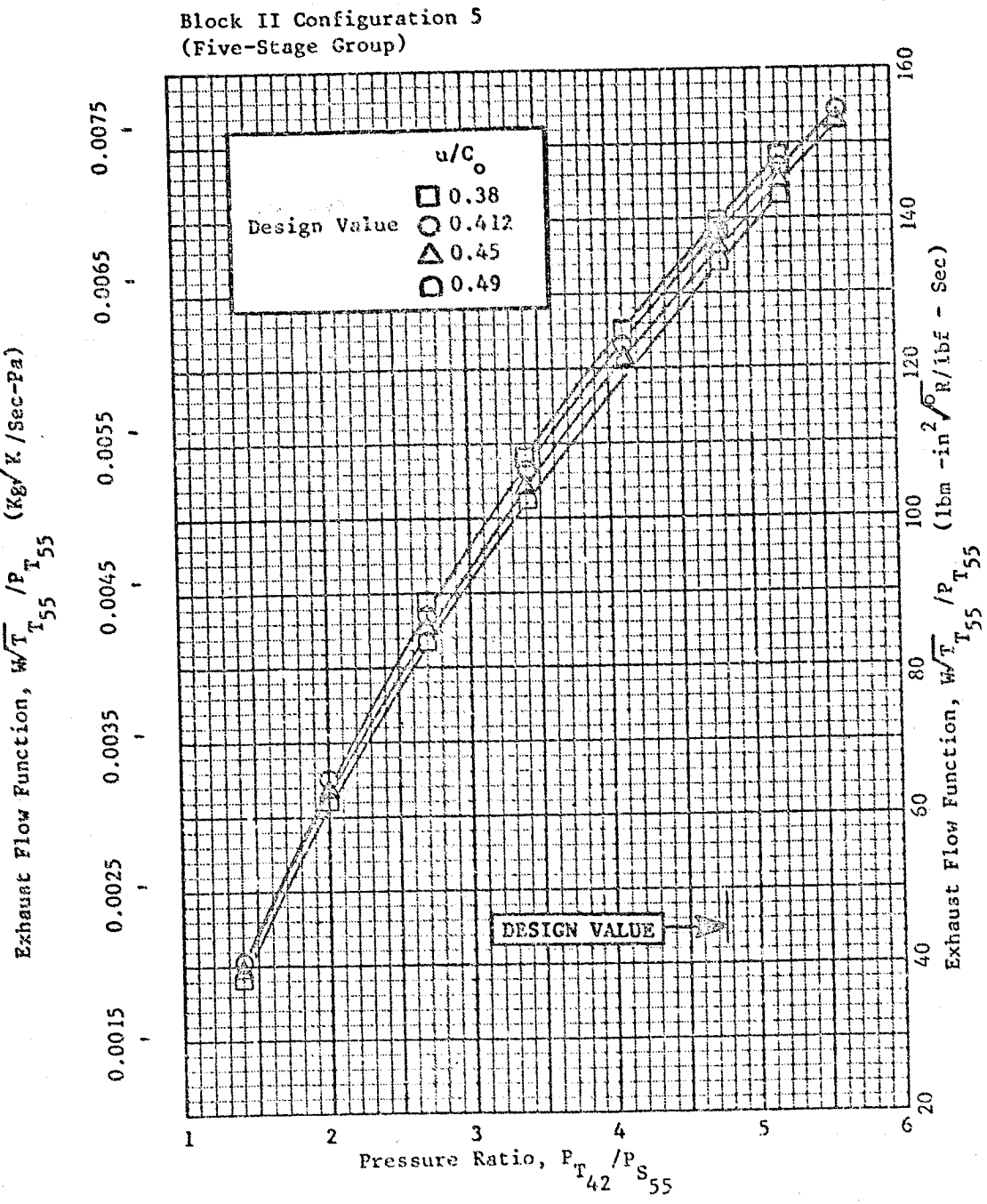

Figure 119. Block II Configuration 5, Exhaust Flow Function $W\sqrt{T}_{T_{55}} / P_{T_{55}}$, vs. Pressure Ratio, $P_{T_{42}} / P_{S_{55}}$.

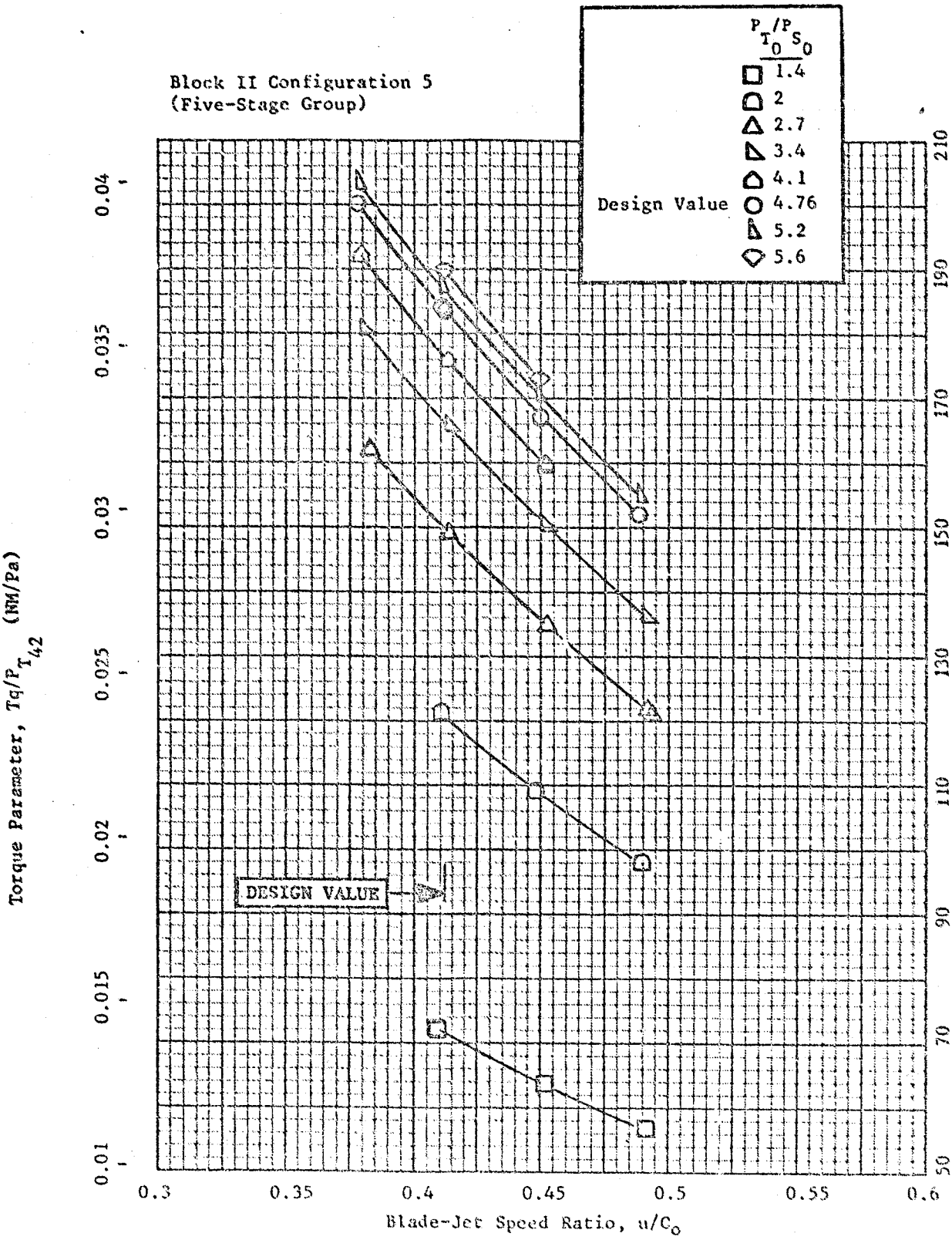

Figure 120. Block II Configuration 5 Torque Parameter, $Tq/P_{T_{42}}$ vs. Blade-Jet Speed Ratio, u/C_o.

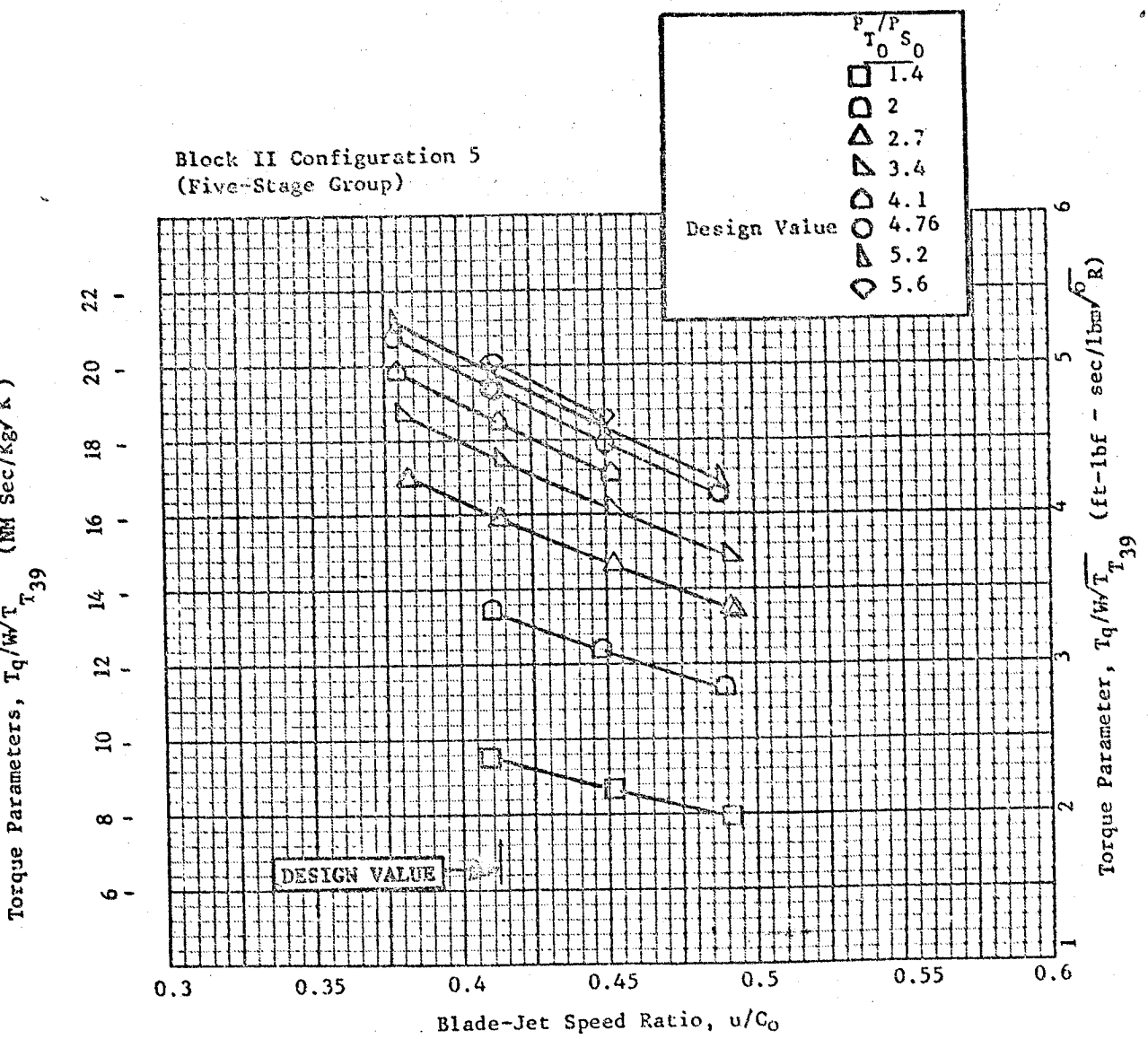

Figure 121. Block II Configuration 5, Torque Parameter, $Tq/W\sqrt{T}_{T_{39}}$ vs. Blade-Jet Speed Ratio, u/C_o.

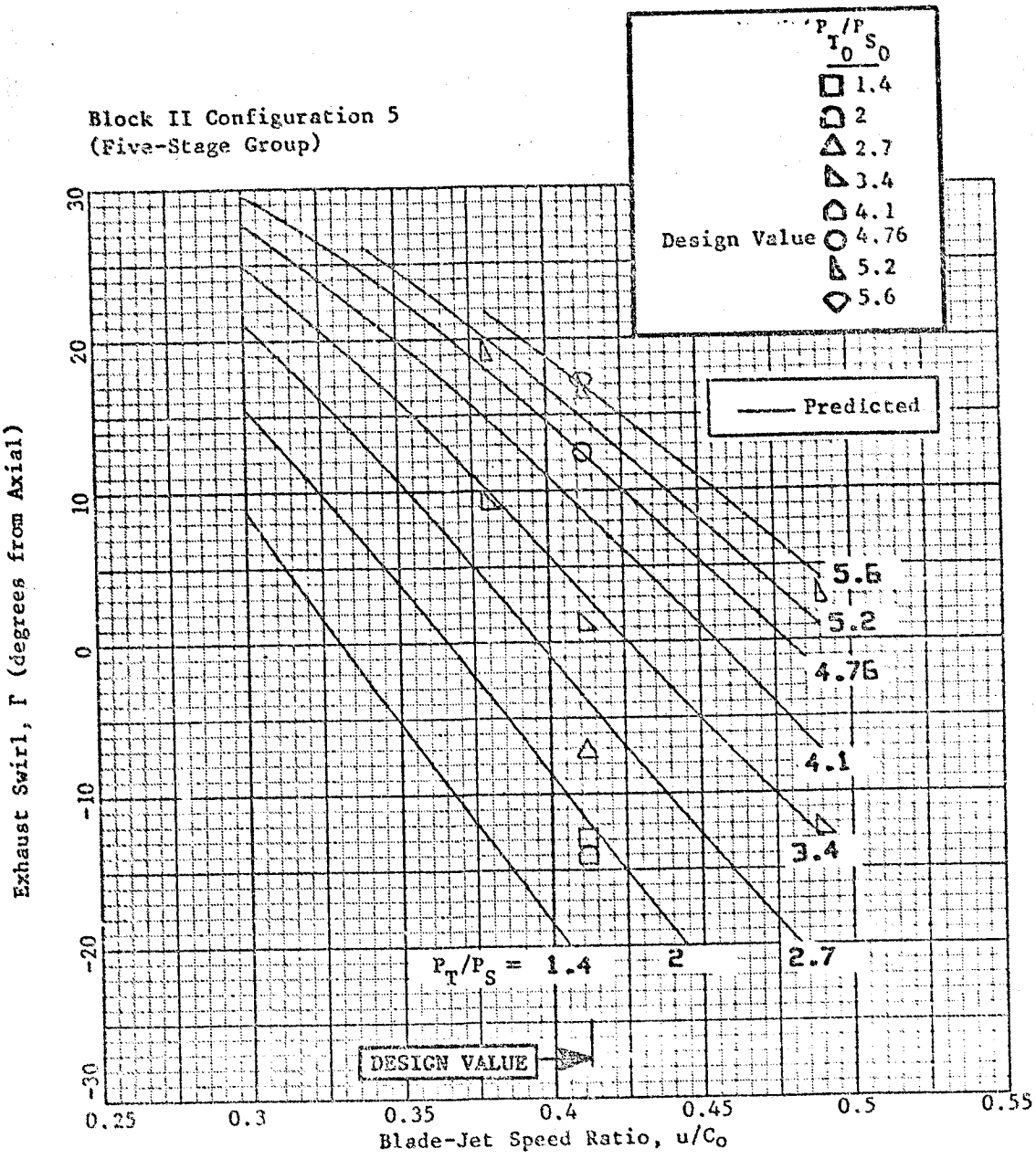

Figure 122. Blade II Configuration 5, Exhaust Swirl, Γ vs. Blade-Jet Speed Ratio, u/C_o.

Flow characteristics of the 5-stage vehicle are presented in Figures 116 thru 119. Figure 117 presents turbine inlet flow function as a function of total-to-static pressure ratio and blade-jet speed ratio. The value of flow function at the design pressure ratio (4.76) and blade-jet speed ratio (0.412) is 38.0 versus a target of 38.08. The corresponding value for the ICLS, then, is 83.2 versus a target of 83.4.

Torque characteristics are presented in Figures 120 and 121.

The 5-stage swirl map is presented as Γ vs u/C_o in Figure 122.

Since the accuracy of the continuity method of calculating exhaust swirl breaks down for swirls very near axial, the 5-stage swirl map consists of several pitchline values from the Plane 50 radial traverse superimposed upon the analytically predicted swirl map.

Figure 123 presents the distribution of inner and outer wheelspace static pressures (normalized by inlet total pressure) throughout the five-stage turbine at the design point. Also included for reference is the pre-test prediction from an axisymmetric analysis at the rig design point. The circles represent data taken during the five-stage rig test. Note that several inner wall static pressures are missing because that instrumentation was damaged in the rig assembly. Where possible, the missing pressures have been supplied using the data from the two-stage rig test and these are denoted by the triangles. Agreement with the pre-test prediction is generally good.

Results of the turbine exit traverse survey are presented in Figures 124 through 127. Figure 124 presents the ratio of exhaust total pressure to inlet total pressure as measured by the traverse probe (solid line) and the arc rakes (asterisks), and as predicted by the axisymmetric analysis (dashed line). For this comparison, the level of the traverse pressure profile has been adjusted slightly to match the average of the arc rakes, since the rake average is used as the exhaust total pressure in the efficiency calculation. Not that measured pressure is actually higher at the hub than the pre-test prediction.

Figure 125 presents the ratio of exhaust total temperature to inlet total temperature. In this case, the level of the traverse temperature has been adjusted to yield the temperature drop indicated by the shaft torque measurement.

Figure 126 presents exhaust swirl measured at the traverse plane compared to design intent. Note the overturning at the inner wall, indicative of secondary flow activity.

Figure 127 presents the radial distribution of five-stage efficiency as calculated from the pressure and temperature profiles of Figures 125 and 124. Since the average of the pressure profile has been set to the arc rake level and the average of the temperature profile has been set to yield the torque indicated temperature drop, the average of the efficiency profile in Figure 127 is at the quoted level of 92.0 percent. Note that mid-span efficiency

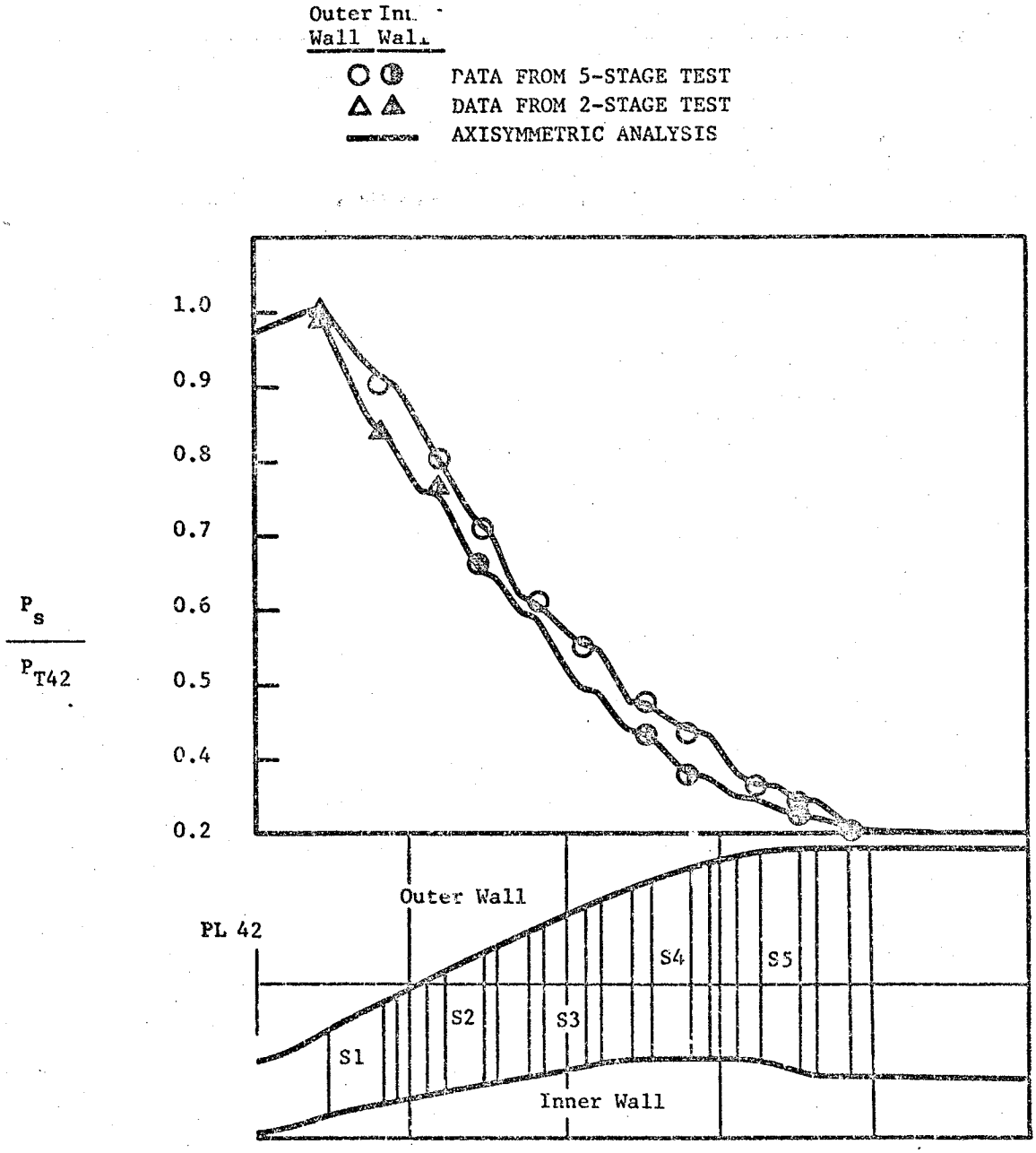

Figure 123. Interstage Static Pressures, Predicted vs. Test. (Design Point Data)

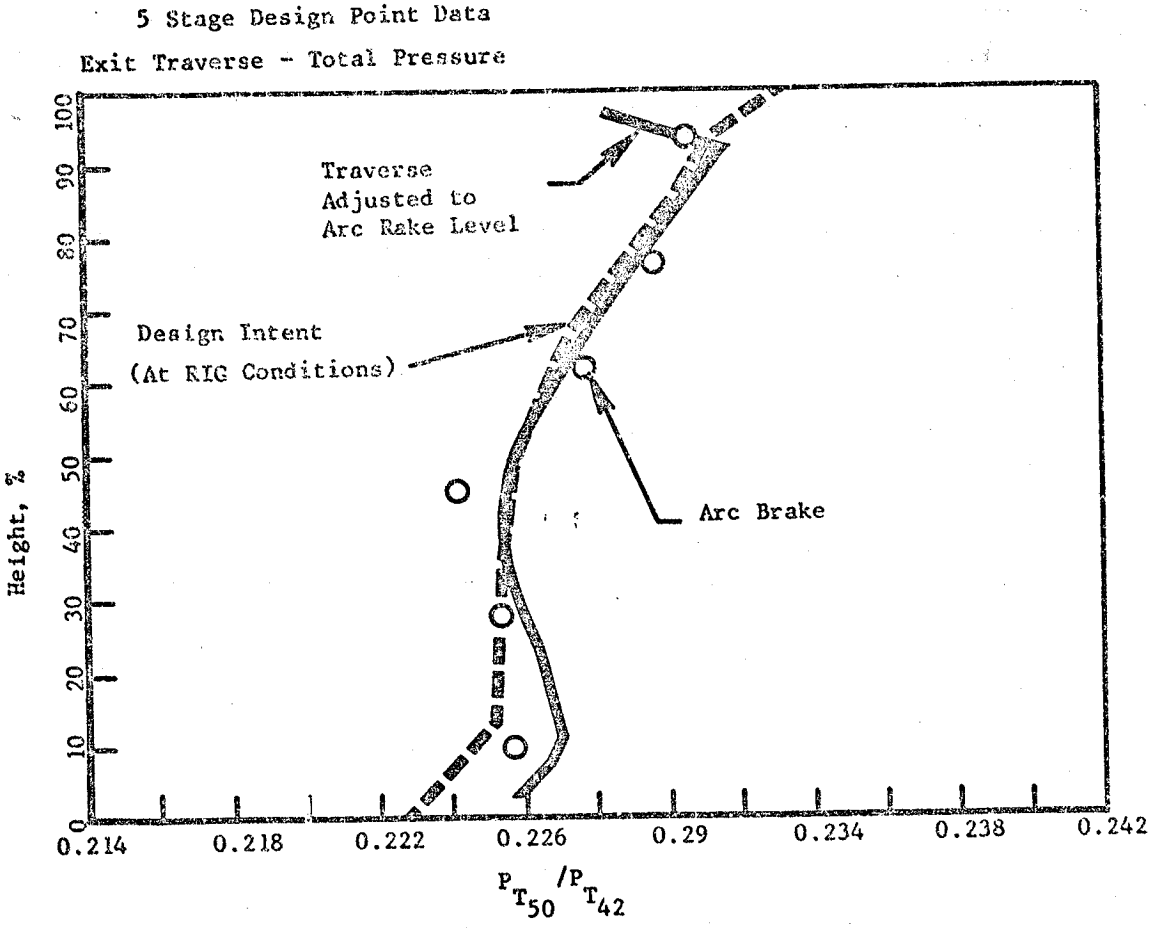

Figure 124. Block II Configuration 5 Exit Survey - $P_{T_{50}}/P_{T_{42}}$ vs. % Height.

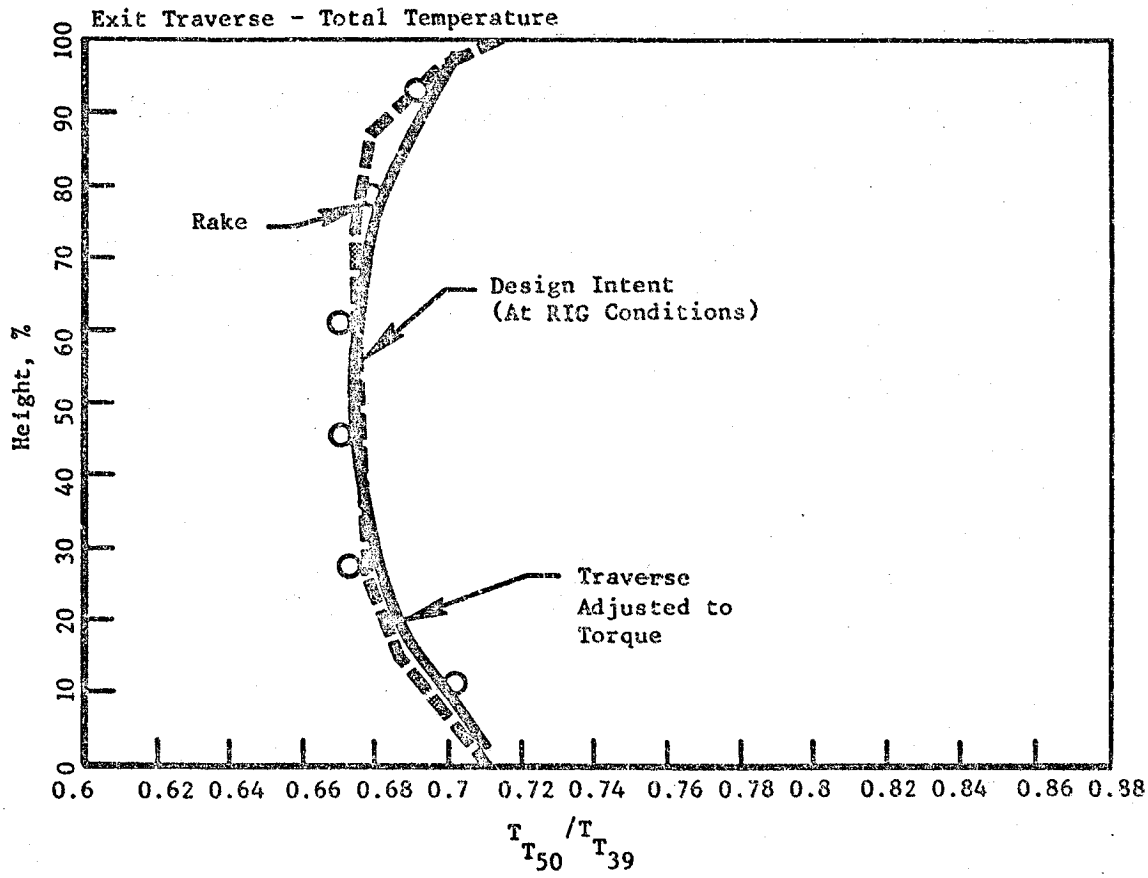

Figure 125. Block II Configuration 5 Exit Survey - $T_{T_{50}}/T_{T_{39}}$ vs. % Height.

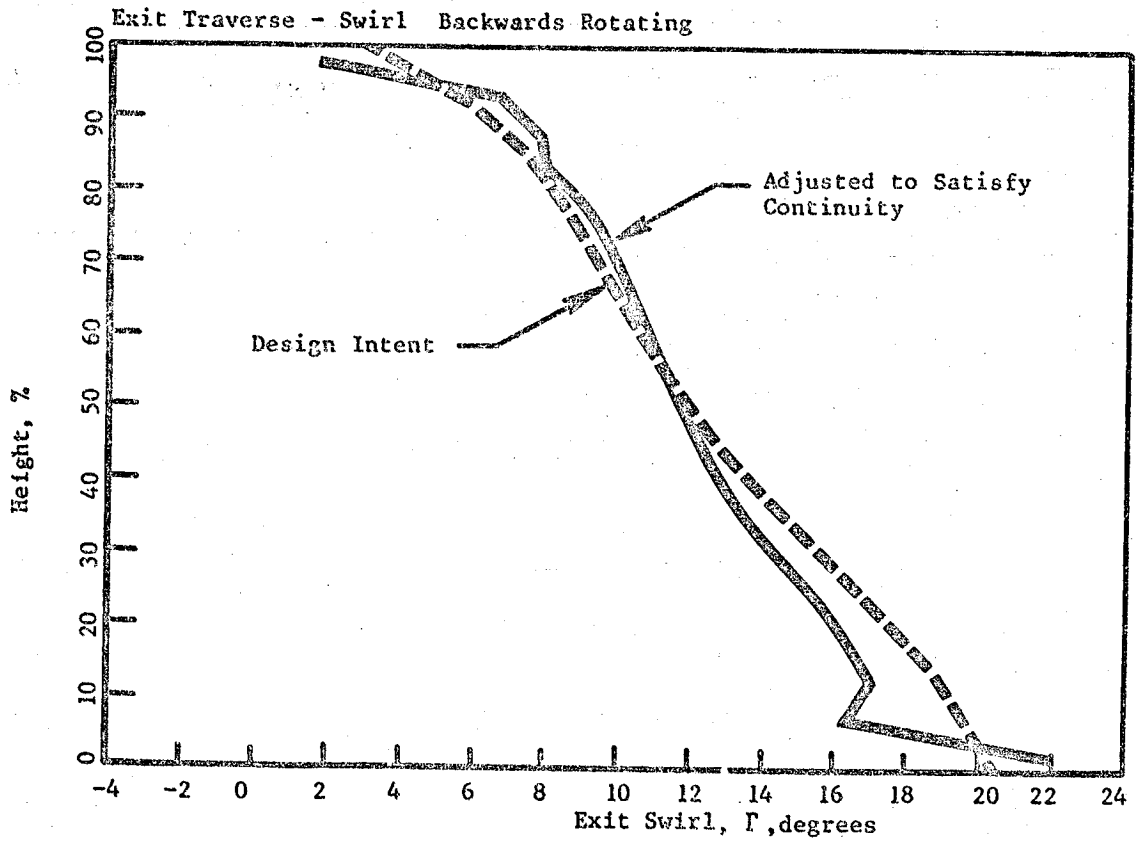

Figure 126. Block II Configuration 5 Exit Survey - Swirl vs. % Height.

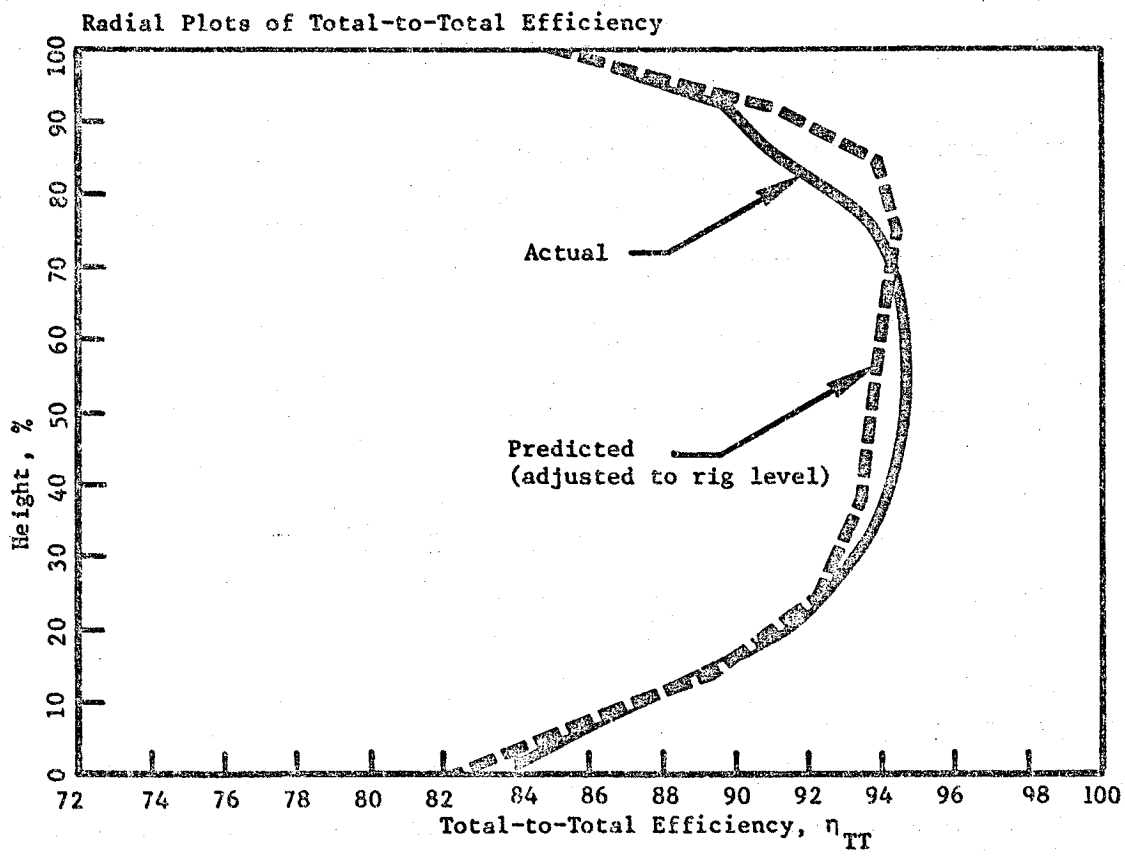

Figure 127. Block II Configuration 5 Exit Survey - Efficiency vs. % Height.

is actually better than predicted while the tip is poorer. The hub portion is very close to design intent.

Results of the Reynolds number testing are presented in Figure 128.

Appendix E defines the Reynolds number calculation used for the five-stage LPT. At the M0.8/10.67 Km (35,000 ft) max climb aero design point, the Reynolds number for the engine (ICLS) turbine is 0.56×10^5. At nominal inlet conditions 310 KPa (45 psia inlet pressure, 417 K (750° R) inlet temperature) the 0.67 scale rig has a Reynolds number of 145×10^5.

One exception to the method described in Appendix E which applied only to Configuration 5 was that, in order to preclude the possibility of condensation in the rear stages or exhaust of the five-stage rig, several additional Reynolds number points were taken at elevated inlet temperatures as well as with reduced inlet pressure. The data taken at these points are flagged in Figure 128.

As previously noted, the quoted turbine efficiency of 92.0 percent does not include bearing or windage corrections to measured torque because, at the power levels attained at the nominal inlet conditions, they represent a very small percentage of total torque (less than 0.1%). However, as the inlet pressure is lowered from its 310 KPa (45 psia) level to achieve the Reynolds number reduction, power output decreases in linear proportion while bearing losses are maintained (since shaft speed is maintained). Thus these losses consume a proportionately larger portion of the gaspath power output which, if not properly compensated for, will yield a steeper Reynolds number loss characteristic (i.e. performance loss with decreasing Reynolds number). Consequently, the ordinate in Figure 128 represents an efficiency to which a calculated bearing power absorption has been added.

The Reynolds number penalty for operation at the M0.8/10.67 Km (35,000 ft.) max climb condition is approximately 0.7 percent, as calculated for a normalized efficiency from Figure 128 of 0.992.

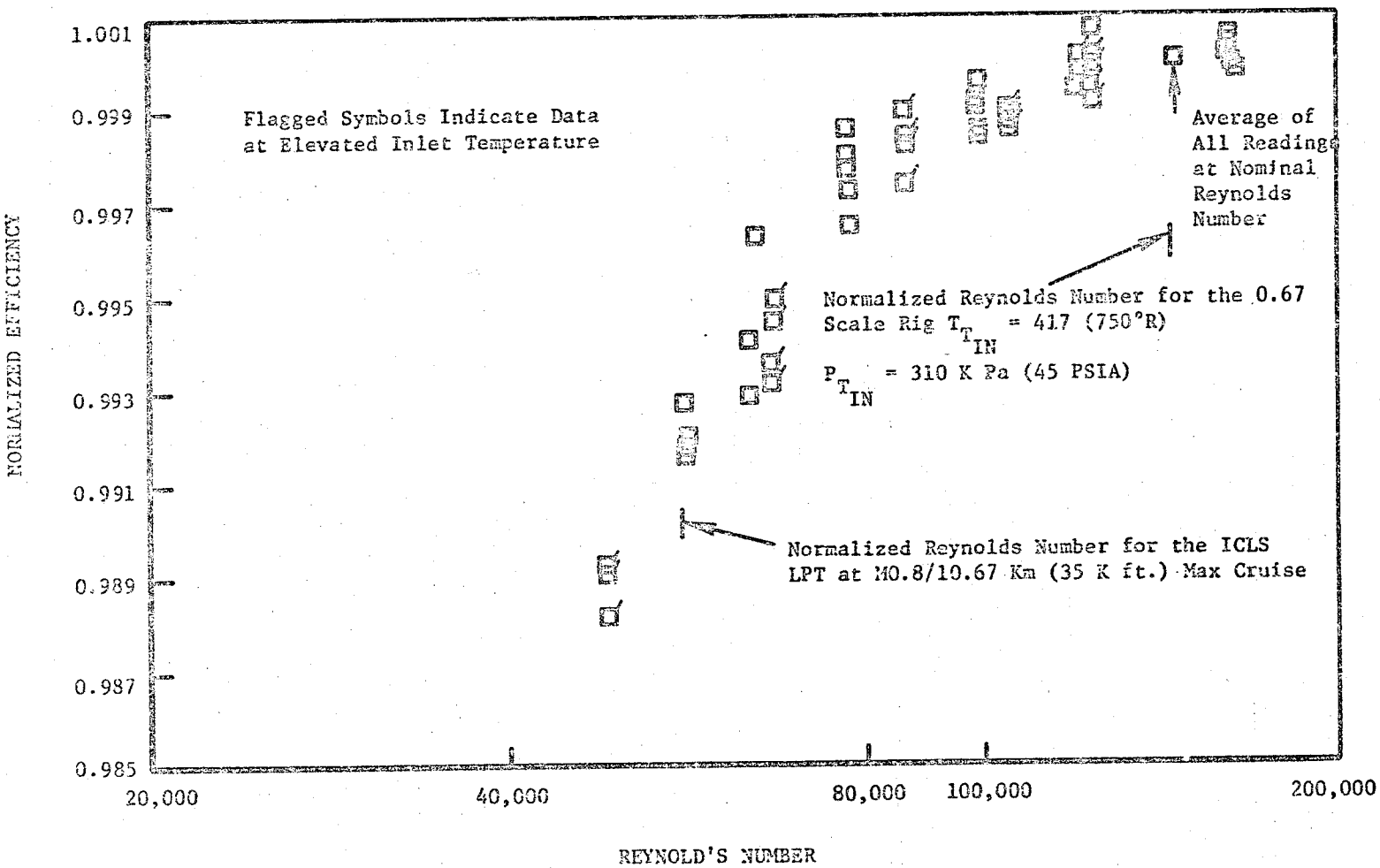

Figure 128. Block II Configuration 5 Reynolds Number Excursion

5.0 PERFORMANCE PREDICTION

Based on the results of the Block II five-stage rig test, the predicted performance of the ICLS ?? turbine at the altitude climb design point is as follows:

η_{TT}	Test	92.0
η_{TT}	Edge Blockage	+ 0.1
η_{TT}	Purge Air	+ 0.1
η_{TT}	Reynolds Number	- 0.7
η_{TT}	Installed	91.5%

This is relative to goals of 91.1% for the ICLS and 91.7% for the FPS.

The correction for edge blockage accounts for the fact that all Block II rotor blades were received from the vendor with trailing edge diameters which were, on the average, 25% oversized relative to design intent.

The correction for purge air is based on the calculated net availability of a total of just over one percent of air which will enter the engine flowpath at the inner wall after the stage one vane. This flow was not modelled in the rig.

APPENDIX A

Rig Flowpath Coordinates

The flowpath coordinates listed herein were obtained by applying a 0.67 geometric scale factor to the engine size coordinates and represent design intent coordinates for all rig flowpath hardware. All dimensions are in inches.

BLOCK I CONFIGURATION 1

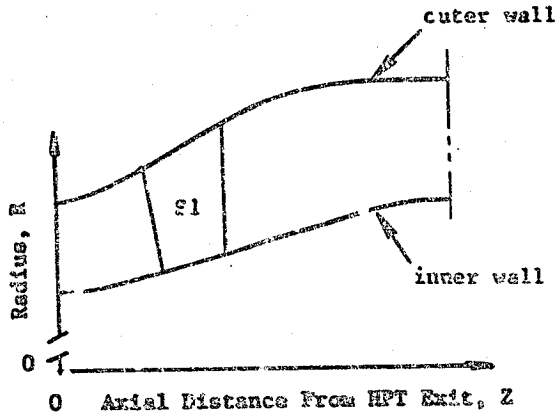

	OUTER WALL		INNER WALL	
	Z	R	Z	R
Transition Duct				
inlet	0.000	10.050	0.000	8.208
	0.168	10.059	0.168	8.208
	0.335	10.084	0.335	8.208
	0.670	10.168	0.670	8.229
	1.005	10.294	1.005	8.281
	1.340	10.459	1.340	8.356
exit	1.742	10.652	1.742	8.451
Stage 1 Nozzle				
leading edge	1.748	10.697	2.114	8.590
	1.908	10.795	2.237	8.631
	2.068	10.892	2.361	8.671
	2.402	11.082	2.608	8.748
	2.709	11.264	2.856	8.817
	3.030	11.434	3.103	8.876
trailing edge	3.350	11.591	3.350	8.923
Exhaust Casing				
	3.850	11.815	3.850	9.009
	4.350	12.025	4.350	9.125
	4.850	12.178	4.850	9.275
	5.350	12.276	5.350	9.432
	5.850	12.329	5.850	9.595
	6.350	12.339	6.350	9.726
	6.850	12.339	6.850	9.809
	7.350	12.339	7.350	9.834
plane 55	7.850	12.339	7.350	9.848

BLOCK I CONFIGURATION 2

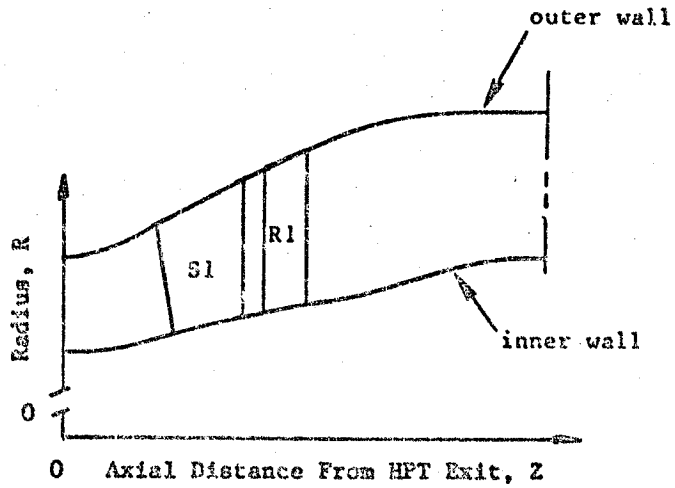

	OUTER WALL		INNER WALL	
	Z	R	Z	R
• Transition Duct	Same as Conf.1			
• Stage 1 Nozzle	Same as Conf.1			
• Stage 1 Blade				
leading edge	3.752	11.778	3.752	8.994
trailing edge	4.556	12.153	4.556	9.135
• Exhaust Casing				
	5.056	12.387	5.056	9.223
	5.556	12.591	5.556	9.336
	6.056	12.742	6.056	9.486
	6.556	12.841	6.556	9.652
	7.056	12.893	7.056	9.815
	7.556	12.902	7.556	9.952
	8.056	12.902	8.056	10.044
	8.556	12.902	8.556	10.078
plane 55	9.056	12.902	9.056	10.078

BLOCK 11 CONFIGURATION 3

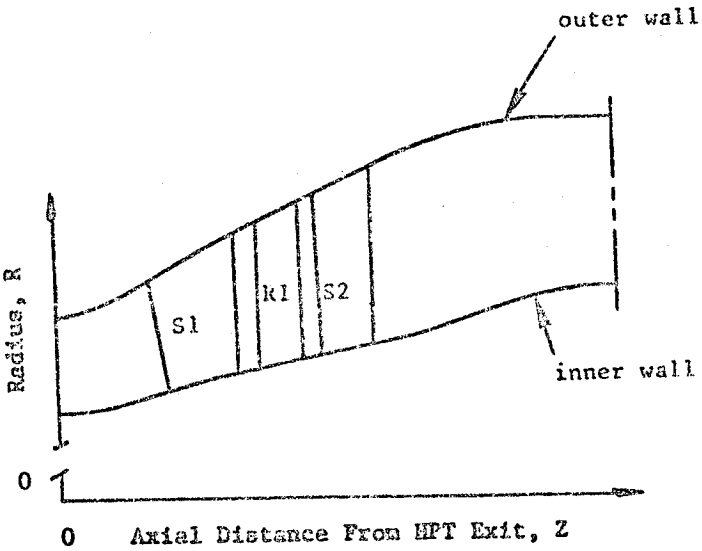

	OUTER WALL		INNER WALL	
	Z	R	Z	R
• Transition Duct	——— Same as Conf. 1 ———			
• Stage 1 Nozzle	——— Same as Conf. 1 ———			
• Stage 1 Blade	——— Same as Conf. 2 ———			
• Stage 2 Nozzle				
leading edge	4.852	12.292	4.932	9.202
trailing edge	5.896	12.778	5.896	9.372
• Exhaust Casing				
	6.396	13.011	6.396	9.460
	6.896	13.216	6.896	9.573
	7.396	13.367	9.396	9.726
	7.896	13.466	7.896	9.896
	8.396	13.518	8.396	10.062
	8.896	13.527	8.896	10.203
	9.396	13.527	9.396	10.298
	9.896	13.527	9.896	10.333
plane 55	10.396	13.527	10.396	10.333

BLOCK I CONFIGURATION 4

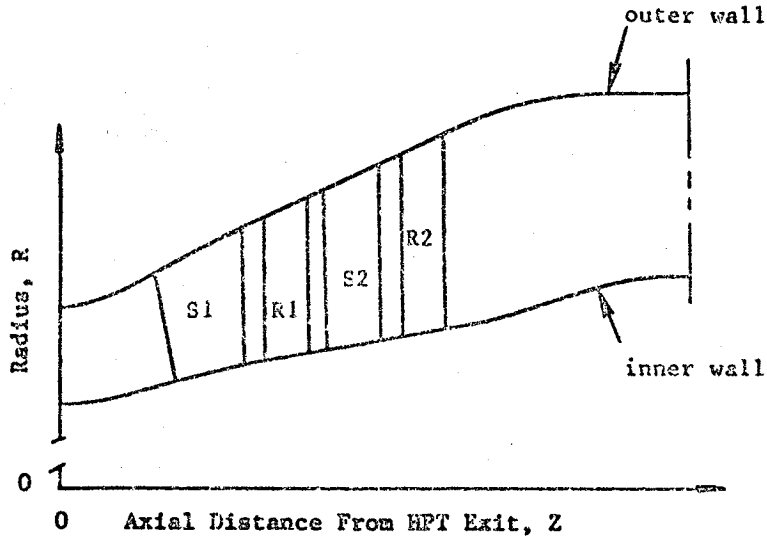

	OUTER WALL		INNER WALL	
	Z	R	Z	R
• Transition Duct	——— Same as Conf. 1 ———			
• Stage 1 Nozzle	——— Same as Conf. 1 ———			
• Stage 1 Blade	——— Same as Conf. 2 ———			
• Stage 2 Nozzle	——— Same as Conf. 3 ———			
• Stage 2 Blade				
leading edge	6.298	12.966	6.298	9.442
trailing edge	7.136	13.356	7.136	9.590
• Exhaust Casing				
	7.636	13.589	7.636	9.678
	8.136	13.794	8.136	9.793
	8.636	13.944	8.636	9.947
	9.136	14.044	9.136	10.121
	9.636	14.095	9.636	10.291
	10.136	14.105	10.136	10.435
	10.636	14.105	10.636	10.532
	11.136	14.105	11.136	10.567
plane 55	11.636	14.105	11.636	10.567

BLOCK II CONFIGURATION 1a

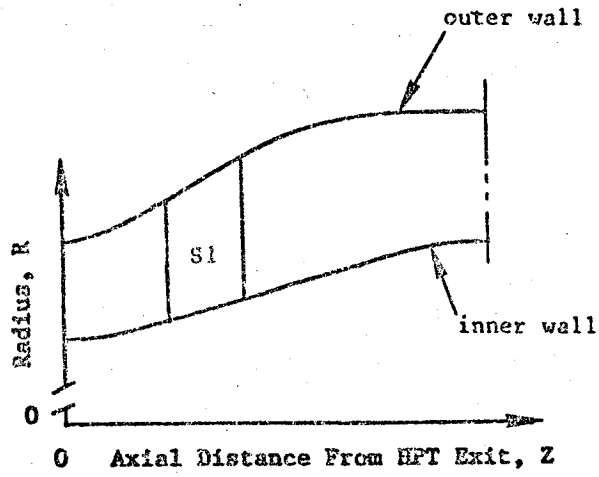

	OUTER WALL		INNER WALL	
	Z	R	Z	R
• Transition Duct				
inlet	0.000	10.050	0.000	8.208
	0.168	10.071	0.168	8.208
	0.335	10.081	0.335	8.208
	0.670	10.156	0.670	8.230
	1.005	10.270	1.005	8.290
	1.340	10.423	1.340	8.386
	1.675	10.615	1.675	8.508
exit	1.809	10.701	1.809	8.559
• Stage 1 Nozzle				
leading edge	1.961	10.803	1.961	8.616
	2.238	10.984	2.238	8.710
	2.515	11.153	2.515	8.781
	2.792	11.309	2.792	8.834
	3.068	11.454	3.068	8.877
trailing edge	3.350	11.591	3.350	8.923
• Exhaust Casing	——— Same as Conf. 1 ———			

BLOCK II CONFIGURATION 4a

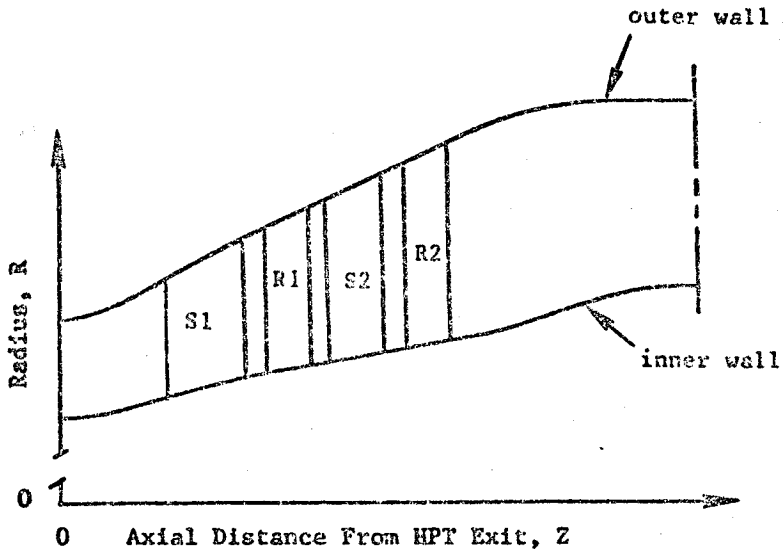

	OUTER WALL		INNER WALL	
	Z	R	Z	R
• Transition Duct	——— Same as Conf. 1a ———			
• Stage 1 Nozzle	——— Same as Conf. 1a ———			
• Stage 1 Blade				
leading edge	3.668	11.740	3.647	8.975
trailing edge	4.405	12.083	4.451	9.117
• Stage 2 Nozzle				
leading edge	4.852	12.292	4.934	9.202
trailing edge	5.939	12.798	5.940	9.379
• Stage 2 Blade				
leading edge	6.292	12.964	6.275	9.439
trailing edge	7.034	13.309	7.082	9.581
• Exhaust Casing	——— Same as Conf. 4 ———			

BLOCK II CONFIGURATION 5

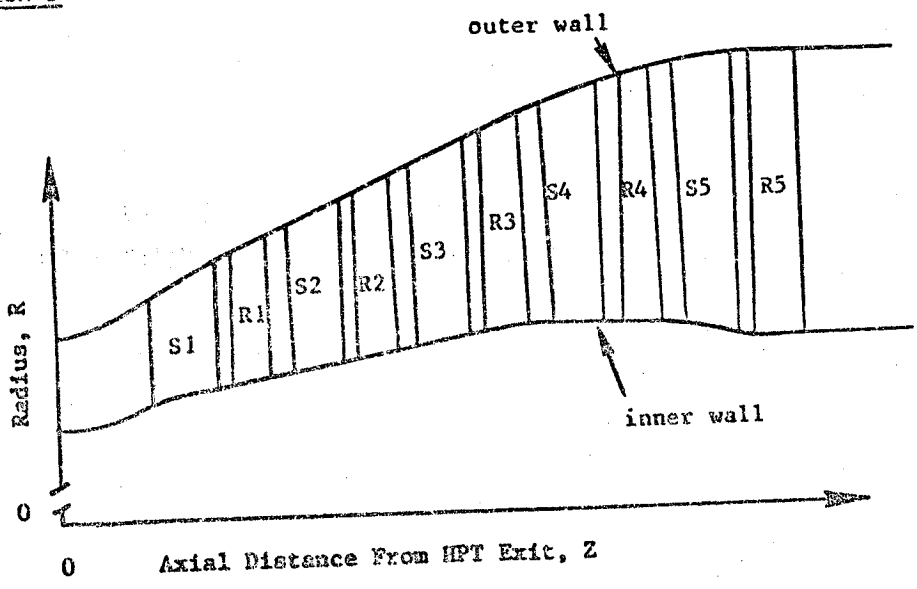

	OUTER WALL Z	OUTER WALL R	INNER WALL Z	INNER WALL R
• Transition Duct	Same as Conf. 1a			
• Stage 1 Nozzle	Same as Conf. 1a			
• Stage 1 Blade	Same as Conf. 4a			
• Stage 2 Nozzle	Same as Conf. 4a			
• Stage 2 Blade	Same as Conf. 4a			
• Stage 3 Nozzle leading edge	7.423	13.491	7.480	9.651
trailing edge	8.601	14.034	8.602	9.849
• Stage 3 Blade leading edge	8.953	14.192	8.933	9.907
trailing edge	9.736	14.524	9.804	10.021
• Stage 4 Nozzle leading edge	10.159	14.692	10.354	10.037
trailing edge	11.323	15.092	11.324	10.004
• Stage 4 Blade leading edge	11.832	15.234	11.769	9.984
trailing edge	12.460	15.379	12.579	9.958
• Stage 5 Nozzle leading edge	12.937	15.463	13.166	9.917
trailing edge	14.137	15.573	14.136	9.702
• Stage 5 Blade leading edge	14.539	15.578	14.539	9.615
trailing edge	15.477	15.578	15.477	9.615

APPENDIX B

Instrumented Airfoil Coordinate

Presented herein are axial (Z), radial (R), and tangential (RTHETA) dimensions which comprise near hub, pitchline (mean), and near tip streamsurface coordinates for instrumented airfoils in the test series.

The following sections are included:

Table	Bladerow	Streamsurface
B-1	Block I Stage 1 Nozzle	Near Hub
B-2	Block I Stage 1 Nozzle	Pitchline
B-3	Block I Stage 1 Nozzle	Near Tip
B-4	Block I Stage 2 Nozzle	Near Hub
B-5	Block I Stage 2 Nozzle	Pitchline
B-6	Block I Stage 2 Nozzle	Near Tip
B-7	Block II Stage 1 Nozzle	Near Hub
B-8	Block II Stage 1 Nozzle	Pitchline
B-9	Block II Stage 1 Nozzle	Near Tip

These coordinates were obtained by applying a 0.67 scale factor to the engine size coordinates (represented in Figures 2, 4, and 10) and represent design intent coordinates for the respective rig airfoils (represented in Figures 44, 67, and 91). All dimensions are in inches.

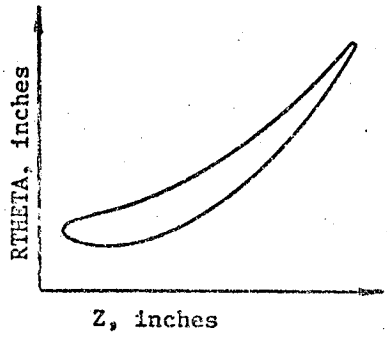

Note: Radius, R, varies as a function of Z

Table B-1. Block I Stage 1 Nozzle Streamsurface Coordinates (near Hub).

Suction Surface

Z	R	SM	STHETA
2.078074	0.816003		0.022338
2.078785	0.816150		0.016250
2.080183	0.816210		0.008882
2.085449	0.817057		-0.002058
2.093573	0.818721		-0.012406
2.107886	0.823330		-0.018804
2.122308	0.827082		-0.027034
2.140131	0.832329		-0.034028
2.159776	0.838019		-0.043179
2.184370	0.846076		-0.046034
2.210072	0.852898		-0.052942
2.240385	0.862520		-0.056214
2.272856	0.872114		-0.060962
2.294694	0.871555		-0.061670
2.306686	0.881583		-0.061079
2.338877	0.891871		-0.061206
2.375078	0.902213		-0.058720
2.410327	0.912004		-0.054240
2.448720	0.923022		-0.047889
2.481051	0.933463		-0.039888
2.515363	0.943357		-0.028457
2.551357	0.954222		-0.017452
2.588248	0.964609		-0.003882
2.620494	0.975166		0.011959
2.653250	0.986380		0.028509
2.689206	0.996356		0.040738
2.722965	1.006025		0.068002
2.750228	1.015043		0.092815
2.789148	1.025808		0.115073
2.821693	1.035535		0.142347
2.853008	1.045150		0.170377
2.886836	1.054641		0.199438
2.917212	1.062502		0.230012
2.948418	1.072367		0.263076
2.979334	1.081024		0.295304
3.009089	1.089402		0.330232
3.040433	1.097783		0.368872
3.070385	1.105568		0.404603
3.100706	1.113827		0.443703
3.130916	1.121470		0.484182
3.160422	1.128848		0.526073
3.189143	1.135234		0.566136
3.218912	1.142407		0.612036
3.248640	1.150412		0.659432
3.276074	1.157272		0.706060
3.305731	1.163963		0.754024
3.328635	1.170392		0.804528
3.353501	1.178023		0.847110

Pressure Surface

Z	R	SM	STHETA
2.078075	0.810903		0.022223
2.078022	0.814331		0.029921
2.082219	0.815901		0.032224
[illegible]	0.817472		0.041602
2.085023	0.820709		0.045509
2.111903	0.824319		0.050872
2.122035	0.830083		0.053969
[illegible]	[illegible]		[illegible]
2.161833	0.838249		0.060280
2.172066	0.842084		0.066020
2.200237	0.851603		0.069071
[illegible]	0.858142		0.071047
2.221472	0.863765		0.077403
2.250320	0.877363		0.087750
2.290220	0.875923		0.093790
2.318657	0.882773		[illegible]
2.347442	0.890092		0.099088
2.373033	0.893064		0.108089
2.400378	0.910006		0.114725
2.432776	0.916159		0.124070
2.461615	0.927043		0.134131
2.490260	0.936169		0.146370
2.519315	0.944795		0.158095
2.548567	0.953081		0.169133
2.579358	0.963549		0.183329
2.608633	0.971381		0.197605
2.639812	0.980031		0.212819
2.669326	0.989951		0.228289
2.701132	0.999632		0.247039
2.732204	1.009023		0.268180
2.763977	1.018595		0.285279
2.797662	1.028646		0.306321
2.830374	1.038375		0.331462
2.862885	1.048039		0.352068
2.897501	1.057683		0.378121
2.931997	1.067624		0.400738
2.966887	1.077211		0.428624
3.000145	1.086785		0.456087
3.034007	1.096274		0.501629
3.068742	1.105595		0.535364
3.104706	1.110531		0.571439
3.133863	1.122830		0.609310
3.173281	1.132816		0.647485
3.210528	1.141216		0.685372
3.246100	1.149828		0.725030
3.281529	1.157841		0.773577
3.317019	1.165502		0.816725
3.348771	1.172617		0.857208

ORIGINAL PAGE IS OF POOR QUALITY

Table B-2. Block I Stage 1 Nozzle Streamsurface Coordinates (Pitchline).

Suction Surface

Z	R	EM	RTHETA
1.825864	9.679177		0.023858
1.826040	9.679247		0.015207
1.830442	9.680487		0.008704
1.836036	9.682462		-0.004344
1.846228	9.685240		-0.014712
[illegible]	9.691064		-0.033114
1.875516	9.698995		-0.035306
1.893320	9.704119		-0.044333
2.018830	9.712468		-0.052378
2.045788	9.722936		-0.061887
2.075083	9.732505		-0.067774
2.108128	9.745048		-0.072072
2.168870	9.758321		-0.074123
2.195386	9.772753		-0.075551
2.123370	9.772738		-0.075501
2.228652	9.787342		-0.070971
2.267227	9.802094		-0.055716
2.305353	9.818734		-0.055142
2.342020	9.831423		-0.043436
2.380407	9.848090		-0.030164
2.479603	9.860897		-0.012705
2.455125	9.876217		0.005075
2.508601	9.888703		0.030234
2.547155	9.904105		0.062563
2.585494	9.918803		0.070078
2.623274	9.932911		0.107854
2.660512	9.947107		0.126382
2.697228	9.931201		0.171246
2.733402	9.975200		0.208143
2.768251	9.990112		0.243316
2.804368	10.003016		0.281800
2.838640	10.018888		0.322480
2.874350	10.030324		0.338031
2.908628	10.042528		0.409432
2.943538	10.057373		0.465364
2.978471	10.071870		0.503850
3.010066	10.085158		0.553681
3.042572	10.098723		0.599611
3.072751	10.112206		0.658328
3.102911	10.123715		0.713416
3.142001	10.139152		0.770257
3.175032	10.152661		0.828333
3.209036	10.158180		0.883261
3.242525	10.178734		0.951258
3.275078	10.192316		1.015322
[illegible]	10.204854		1.080578
3.341176	10.220045		1.148110
3.370188	10.232672		1.206335

Pressure Surface

Z	R	EM	QTHETA
1.822864	9.678177		0.024838
1.833465	9.680123		0.032395
1.839092	9.682109		0.039418
1.848265	9.685765		0.045771
1.853561	9.689111		0.051263
1.897600	9.694126		0.058706
1.966287	9.700165		0.065133
2.002029	9.707100		0.051663
2.029449	9.710298		0.064721
2.035076	9.719390		0.059017
2.097103	9.728512		0.071527
[illegible]	9.741255		0.075552
2.122478	9.752373		0.086071
2.190365	9.755628		0.094587
2.188200	9.762285		0.096587
2.195788	9.773474		0.106365
2.251807	9.789027		0.114926
2.281788	9.798250		0.120023
2.283601	9.807209		0.126328
2.313067	9.818463		0.132621
2.345100	9.829032		0.137409
2.377146	9.841327		0.183784
2.400664	9.852549		0.201610
2.442622	9.863265		0.226447
2.472087	9.877290		0.240931
2.519218	9.890229		0.262603
2.546049	9.902554		0.288231
2.580707	9.916527		0.311677
2.618162	9.930187		0.338002
2.653420	9.946453		0.367005
2.680335	9.958133		0.396591
2.718027	9.973287		0.431117
2.766209	9.987140		0.465032
2.802348	10.002149		0.501887
2.840901	10.017532		0.540700
2.870048	10.032703		0.585876
2.918789	10.048238		0.625049
2.987070	10.064120		0.667408
2.987680	10.080085		0.713318
3.037178	10.095157		0.758442
3.074026	10.112818		0.813330
3.110884	10.128700		0.858786
3.150604	10.144555		0.920849
3.186682	10.161663		0.977323
3.227136	10.177783		1.036389
3.277221	10.194283		1.097409
3.317618	10.210839		1.130427
3.362750	10.226425		1.377278

Table B-3. Block I Stage 1 Nozzle Streamsurface Coordinates (near Tip).

Suction Surface

Z	R	SM	RTHETA
1.782787	10.486274		0.027238
1.764328	10.496427		0.017325
1.787897	10.500218		0.000742
1.785277	10.504650		-0.004270
1.803484	10.511131		-0.010890
1.821260	10.518482		-0.027057
1.839724	10.529376		-0.034442
1.861534	10.542360		-0.040457
1.887828	10.556027		-0.050303
1.917783	10.573518		-0.060147
1.951367	10.592407		-0.077102
1.983134	10.613320		-0.083370
2.020850	10.629323		-0.087814
2.064420	10.654088		-0.088872
[illegible].024420	10.664803		-0.088072
2.108862	10.870078		-0.028616
2.133234	10.703336		-0.025632
2.188316	10.727647		-0.078757
2.242920	10.751876		-0.080082
2.287732	10.776072		-0.057488
2.332402	10.795578		-0.032033
2.378053	10.823081		-0.025033
2.431032	10.848071		-0.003830
2.484764	10.862831		0.015378
2.507881	10.882408		0.045032
2.550350	10.914687		0.078254
2.582630	10.935033		0.107144
2.633390	10.937846		0.141873
2.674811	10.978863		0.170202
2.714718	10.998833		0.210405
2.754222	11.019008		0.250030
2.793158	11.038357		0.308138
2.831052	11.058824		0.352606
2.869429	11.078876		0.401322
2.903328	11.087937		0.452073
2.943902	11.110747		0.505330
2.980702	11.138325		0.553237
3.017115	11.153782		0.621332
3.053288	11.171883		0.681738
3.088294	11.189803		0.744066
3.123087	11.207303		0.808318
3.160832	11.228057		0.876278
3.190841	11.243439		0.943321
3.232227	11.261138		1.018415
3.257861	11.278618		1.083490
3.302359	11.298422		1.160558
3.326884	11.314503		1.241618
3.372602	11.330093		1.311610

Pressure Surface

Z	R	SM	RTHETA
1.783767	10.488274		0.027328
1.783093	10.479034		0.039609
1.793590	10.502421		0.042102
1.802508	10.508711		0.049524
1.814724	10.515781		0.053051
1.830379	10.524610		0.060818
1.840175	10.530183		0.064226
1.877103	10.547020		0.067322
1.889639	10.561306		0.069780
1.903924	10.580635		0.070338
1.961410	10.607603		0.070322
1.977023	10.624611		0.073328
2.012164	10.650092		0.083314
2.045713	10.662865		0.087121
2.085710	10.666203		0.097127
2.090819	10.651602		0.103281
2.119924	10.683321		0.110467
2.160371	10.700580		0.128632
2.181887	10.718810		0.125378
2.218550	10.737737		0.151407
2.240310	10.758023		0.185873
2.283737	10.772082		0.181241
2.318419	10.782278		0.190087
2.352327	10.811774		0.211761
2.388335	10.830187		0.228147
2.428784	10.840389		0.240327
2.462910	10.863077		0.284080
2.504704	10.888634		0.310443
2.525203	10.903078		0.328379
2.579423	10.920268		0.390059
2.616686	10.860080		0.470068
2.658033	10.970022		0.433630
2.700334	10.995146		0.472893
2.743023	11.012327		0.512127
2.786032	11.032348		0.554020
2.837478	11.057243		0.603412
2.870232	11.076796		0.645709
2.913257	11.101476		0.684724
2.957313	11.133749		0.749509
3.002832	11.149054		0.801211
2.948632	11.180439		0.852900
3.071430	11.180628		0.917378
3.128740	11.213109		0.980180
3.167583	11.228408		1.046654
3.223377	11.267741		1.112130
3.270193	11.270828		1.181781
3.313208	11.301918		1.252788
3.354603	11.331582		1.310816

ORIGINAL PAGE IS
OF POOR QUALITY

188

Table B-4. Block I Stage 2 Nozzle Streamsurface Coordinates (near Hub).

Suction Surface

Z	R	SM	RTHETA
4.825888	0.525860		0.
4.822250	0.522250		-0.003712
4.822203	0.524053		-0.009207
4.823640	0.526136		-0.016208
4.826346	0.529053		-0.025239
4.829082	0.533274		-0.036876
4.836434	0.527323		-0.047467
4.844236	0.529091		-0.060046
4.853822	0.530109		-0.073802
4.862082	0.530105		-0.079388
4.876550	0.533420		-0.101093
4.889902	0.536874		-0.120326
5.010028	0.540351		-0.142209
5.041109	0.544788		-0.173734
5.064079	0.546038		-0.190023
5.089713	0.552132		-0.219160
5.118203	0.550716		-0.237628
5.141610	0.560792		-0.252280
5.162735	0.564659		-0.267773
5.196816	0.568459		-0.279472
5.220063	0.574220		-0.290376
5.255855	0.579596		-0.298831
5.286272	0.584677		-0.304234
5.317910	0.590177		-0.308309
5.347770	0.593142		-0.303031
5.378327	0.602134		-0.297720
5.405098	0.608260		-0.290641
5.625852	0.614323		-0.280312
5.655314	0.620339		-0.266019
5.610235	0.626257		-0.234067
5.540807	0.632136		-0.216737
5.560710	0.637059		-0.196023
5.593725	0.642505		-0.170423
5.617213	0.648080		-0.152181
5.640023	0.654365		-0.128236
5.662630	0.659018		-0.099880
5.684877	0.664740		-0.069285
5.706322	0.669727		-0.036260
5.727881	0.674712		-0.007298
5.748980	0.679431		0.023083
5.770105	0.684090		0.056216
5.791303	0.688660		0.094777
5.812508	0.692247		0.131313
5.833724	0.697762		0.168787
5.855270	0.702275		0.207510
5.877348	0.706926		0.247005
5.898972	0.711407		0.287203
	0.718118		0.320126

Pressure Surface

Z	R	SM	RTHETA
4.825888	0.523660		0.
4.829798	0.539232		0.001678
4.836050	0.527041		0.002838
4.838251	0.527804		0.001675
4.847806	0.523086		-0.000084
4.855287	0.530201		-0.005100
4.863845	0.531216		-0.010023
4.873802	0.532255		-0.016031
4.884086	0.520848		-0.022815
4.894484	0.528645		-0.032819
5.023073	0.531055		-0.050308
5.045538	0.534277		-0.060058
5.076612	0.538725		-0.082870
5.100800	0.552362		-0.095373
5.130880	0.557078		-0.107480
5.150165	0.561965		-0.115533
5.170820	0.565530		-0.124237
5.192617	0.568460		-0.130941
5.212527	0.572293		-0.134220
5.232535	0.575677		-0.137287
5.253210	0.578640		-0.136087
5.271025	0.582127		-0.130712
5.290679	0.587238		-0.130407
5.309907	0.592495		-0.135300
5.326600	0.591919		-0.129424
5.342310	0.605072		-0.123402
5.360716	0.598093		-0.120651
5.379399	0.605350		-0.126106
5.399091	0.600285		-0.117478
5.420724	0.610653		-0.105204
5.442798	0.619450		-0.089231
5.460741	0.620287		-0.087546
5.480392	0.625280		-0.072738
5.510279	0.620710		-0.058284
5.537730	0.630370		-0.010022
5.560110	0.642005		-0.021706
5.585098	0.647063		-0.000033
5.619211	0.653929		0.021717
5.641770	0.660697		0.043080
5.665097	0.663728		0.072155
5.686337	0.672729		0.098917
5.722805	0.675513		0.120260
5.748927	0.680028		0.160403
5.770752	0.680552		0.182685
5.802360	0.688813		0.228527
5.830378	0.701397		0.262673
5.850765	0.707158		0.289603
5.877488	0.711487		0.328836

Table B-5. Block I Stage 2 Nozzle Streamsurface Coordinates (Pitchline).

Suction Surface

Z	R	SM	RTHETA
4.891889	10.825740		0.
4.884858	10.827781		-0.003566
4.827415	10.827330		-0.009938
4.867038	10.827800		-0.018145
4.890441	10.828326		-0.028305
4.893282	10.828883		-0.040487
4.801821	10.832108		-0.053411
4.810207	10.835011		-0.070335
4.818391	10.837630		-0.083320
4.818251	10.837445		-0.093336
4.833670	10.846196		-0.118717
4.860554	10.851038		-0.147029
4.882739	10.856083		-0.175749
4.908757	10.866558		-0.201882
5.029287	10.873320		-0.226582
5.053345	10.880742		-0.248213
5.082800	10.888083		-0.258497
5.112348	10.897228		-0.287100
5.142622	10.908031		-0.301889
5.174408	10.914830		-0.312580
5.207457	10.924229		-0.321182
5.241807	10.933711		-0.328052
5.276920	10.943328		-0.324709
5.310180	10.952746		-0.320871
5.343781	10.962221		-0.311020
5.377281	10.971466		-0.299735
5.407204	10.980206		-0.284365
5.430831	10.988946		-0.268110
5.458406	10.997232		-0.248352
5.482387	11.005338		-0.222603
5.516008	11.013072		-0.192608
5.544108	11.020712		-0.163085
5.568517	11.028180		-0.139791
5.592205	11.035528		-0.106876
5.615304	11.042750		-0.075916
5.637863	11.049801		-0.041858
5.660019	11.056834		-0.005860
5.681520	11.064635		0.031504
5.703440	11.071102		0.070782
5.724602	11.078223		0.111240
5.749282	11.085328		0.152276
5.767582	11.092808		0.196886
5.788180	11.100031		0.242037
5.810823	11.107614		0.288730
5.832483	11.116103		0.337128
5.854728	11.122976		0.387680
5.875837	11.130801		0.438616
5.898831	11.137831		0.482434

Pressure Surface

Z	R	SM	RTHETA
4.891883	10.828769		0.
4.870023	10.830154		0.001834
4.891489	10.831906		0.001018
4.883910	[illegible]		[illegible]
4.918290	10.838840		-0.003435
4.923338	10.838337		-0.008904
4.933124	10.840769		-0.018486
4.944790	[illegible]		-0.028836
4.956850	10.852295		-0.042130
4.964038	10.858262		-0.042192
4.998093	10.861818		-0.061905
5.002362	10.874981		-0.076375
5.050302	10.872049		-0.092508
5.077182	10.887049		-0.103065
5.102076	10.896073		-0.115867
5.128827	10.901276		-0.120038
5.148218	10.907608		-0.129040
5.170412	10.914322		-0.134209
5.192072	10.918382		-0.135428
5.233322	10.924426		-0.137153
5.228035	10.929142		-0.135026
5.261018	10.935675		-0.135636
5.280369	10.942059		-0.133603
5.279226	10.945298		-0.133377
5.330356	10.949704		-0.129997
5.368001	10.951061		-0.123062
5.336020	10.955001		-0.118918
5.358168	10.963278		-0.107213
5.390713	10.980728		-0.097518
5.399303	10.978519		-0.085073
5.413138	10.989042		-0.070781
5.437535	10.998187		-0.052168
5.462288	10.023337		-0.035270
5.485521	11.002335		-0.016120
5.518470	11.010353		0.003328
5.543845	11.020074		0.026433
5.571834	11.030150		0.052116
5.598758	11.037833		0.091511
5.620097	11.048801		0.122483
5.652567	11.050882		0.158232
5.685132	11.063101		0.191899
5.713270	11.074480		0.229141
5.748135	11.087206		0.269058
5.770624	11.095290		0.316257
5.788508	11.103260		0.354052
5.820241	11.112938		0.401268
5.854196	11.125736		0.445226
5.878531	11.135766		0.481247

Table B-6. Block I Stage 2 Nozzle Streamsurface Coordinates (near tip).

Suction Surface

Z	R	SM	RTHETA
4.881128	12.026102		0.
[illegible]	[illegible]		-0.004465
4.854681	12.025073		-0.010537
4.860363	12.025820		-0.010086
4.864020	12.027780		-0.020042
4.871122	[illegible]		-0.045712
4.879784	12.934602		-0.053875
4.893916	12.036020		-0.063763
4.892171	12.040184		-0.070320
[illegible]	[illegible]		-0.070336
4.918133	12.060477		-0.095847
4.938030	12.061057		-0.131828
[illegible]	12.071870		-0.144204
[illegible]	[illegible]		-0.165042
5.014377	12.094478		-0.184303
5.041063	12.105420		-0.201604
5.070028	12.118703		-0.217841
[illegible]	[illegible]		-0.230782
5.120310	12.144340		-0.241306
5.151058	12.157008		-0.248202
5.192833	12.171476		-0.251023
[illegible]	[illegible]		-0.253787
5.255603	12.199624		-0.254439
5.290132	12.212418		-0.246860
5.322200	12.230046		-0.242217
[illegible]	[illegible]		-0.231483
5.304820	12.251300		-0.217826
5.416072	12.264423		-0.201468
5.446377	12.278577		-0.182468
[illegible]	[illegible]		-0.161667
5.500233	12.280640		-0.127365
5.527008	12.310708		-0.111838
5.552601	12.321446		-0.083764
[illegible]	[illegible]		-0.054128
5.603701	12.342130		-0.023078
5.636739	12.332352		0.010077
5.650200	12.337187		0.046233
[illegible]	[illegible]		0.061876
5.690321	12.381848		0.118005
5.710988	12.391403		0.153712
5.741485	12.401167		0.188483
[illegible]	[illegible]		0.221720
5.780353	12.420723		0.268761
5.806821	12.430810		0.320301
5.831600	12.440802		0.377632
[illegible]	[illegible]		0.425006
5.876828	12.460396		0.478577
5.903706	12.480302		0.819003

Pressure Surface

Z	R	SM	RTHETA
4.881128	12.029132		0.
4.884088	12.627894		0.003463
4.870137	12.030302		0.003648
[illegible]	[illegible]		[illegible]
4.869190	12.037632		0.000791
4.894682	12.041002		-0.002516
4.905107	12.046420		-0.007487
[illegible]	[illegible]		-0.013543
4.922080	12.053685		-0.021094
4.932090	12.038425		-0.031064
4.951353	12.071176		-0.024848
[illegible]	[illegible]		-0.047038
5.015510	12.085416		-0.083263
5.043909	12.106686		-0.065317
5.063273	12.118032		-0.078186
[illegible]	[illegible]		[illegible]
5.110092	12.135437		-0.080107
5.127050	12.147911		-0.082548
5.153703	12.158957		-0.088493
[illegible]	[illegible]		-0.089110
5.195659	12.173405		-0.090920
5.217243	12.182010		-0.092360
5.250842	12.190058		-0.091081
[illegible]	[illegible]		-0.087182
5.278202	12.200180		-0.082144
5.299020	12.211684		-0.073502
5.310859	12.222030		-0.067375
[illegible]	[illegible]		-0.058587
5.359072	12.241130		-0.047312
5.383160	12.250753		-0.034174
5.408067	12.260704		-0.018032
[illegible]	[illegible]		-0.001826
5.456480	12.281582		0.017444
5.482735	12.292486		0.038739
5.509592	12.303936		0.063002
[illegible]	[illegible]		0.087192
5.565044	12.320060		0.110296
5.593330	12.323288		0.143128
5.621058	12.330259		0.173702
[illegible]	[illegible]		0.206378
5.679703	12.374592		0.240003
5.708024	12.387020		0.278028
5.737007	12.399506		0.316280
[illegible]	[illegible]		0.356012
5.795810	12.424331		0.397022
5.824803	12.437088		0.440040
5.852363	12.450370		0.485728
[illegible]	[illegible]		0.620023

Table B-7. Block II Stage 1 Nozzle Streamsurface Coordinates (near hub).

Suction Surface

Z	R	SM	RTHETA
1.821670	8.846148		0.014638
[illegible]	8.846680		0.005102
1.857790	8.869036		-0.004286
1.874908	8.850761		-0.013809
1.888302	8.854811		-0.023368
[illegible]	[illegible]		[illegible]
2.017335	8.858287		-0.051180
2.030527	8.872188		-0.048092
2.053005	8.880193		-0.038031
[illegible]	[illegible]		[illegible]
2.110675	8.889703		-0.088288
2.152788	8.909283		-0.067177
2.181058	8.920317		-0.060513
[illegible]	[illegible]		-0.088248
2.218800	8.925909		[illegible]
2.254058	8.930852		-0.061257
2.292207	8.948776		-0.055179
[illegible]	[illegible]		[illegible]
2.388227	8.970271		-0.038709
2.403992	8.980934		-0.024739
2.443325	8.989468		-0.010320
2.466825	8.995287		0.004562
2.517630	9.007396		0.022289
2.554570	9.019807		0.041536
2.590595	9.032873		0.062281
2.630641	9.021562		0.084620
2.652681	9.039084		0.108858
2.698030	9.040685		0.130417
2.723081	9.053062		0.161480
2.787321	9.060612		[illegible]
2.802349	9.057215		0.216950
2.826303	9.072874		0.281311
2.870205	9.080376		0.286940
2.862356	9.083772		[illegible]
2.927221	9.093132		0.353281
2.970438	9.090432		0.390313
3.003473	9.108647		0.428303
3.039321	9.111612		0.467062
3.089043	9.117636		0.509122
3.101568	9.124294		0.549311
3.134719	9.130867		0.592830
3.165724	9.138094		0.637154
3.199311	9.143390		0.683639
3.231715	9.149842		0.720297
3.264294	9.156058		0.777062
3.294694	9.151508		0.823653
3.325537	9.163067		0.870895
3.357317	9.174818		0.918908

Pressure Surface

Z	R	SM	RTHETA
1.821670	8.846148		0.014636
1.853282	8.840704		0.021159
1.867408	8.848167		0.037844
[illegible]	[illegible]		[illegible]
1.922247	8.853085		0.040052
1.938129	8.857913		0.049385
2.006678	8.862384		0.051040
[illegible]	[illegible]		[illegible]
2.048708	8.874702		0.061818
2.057702	8.881283		0.058063
2.087306	8.891063		0.072681
[illegible]	[illegible]		[illegible]
2.160950	8.911207		0.087406
2.191208	8.920477		0.096881
2.181258	8.930877		0.094891
[illegible]	[illegible]		[illegible]
2.252509	8.939938		0.111649
2.284802	8.947549		0.120737
2.316386	8.958407		0.130700
[illegible]	[illegible]		[illegible]
2.370816	8.972323		0.152602
2.412112	8.981580		0.160950
2.446532	8.990722		0.170724
[illegible]	[illegible]		[illegible]
2.510691	9.004020		0.210147
2.544214	9.012389		0.229003
2.573126	9.020201		0.263015
[illegible]	[illegible]		[illegible]
2.607032	9.035708		0.286950
2.682008	9.042161		0.308282
2.717313	9.050402		0.330337
[illegible]	[illegible]		[illegible]
2.788887	9.064228		0.379333
2.83808	9.071825		0.400258
2.861074	9.078660		0.434705
[illegible]	[illegible]		[illegible]
2.926120	9.092723		0.488294
2.972214	9.096782		0.520032
3.000430	9.106773		0.552005
[illegible]	[illegible]		[illegible]
3.086203	9.120800		0.630813
3.121081	9.125102		0.674278
3.160466	9.132603		0.714653
[illegible]	[illegible]		[illegible]
3.224040	9.150710		0.798342
3.272174	9.157610		0.846007
3.300029	9.165029		0.890149
[illegible]	[illegible]		[illegible]

ORIGINAL PAGE IS
OF POOR QUALITY

Table B-8. Block II Stage 1 Nozzle Streamsurface Coordinates (pitchline).

Suction Surface

X	R	XM	RTHETA
1.881898	9.729842		0.016827
1.882817	9.721572		0.000388
1.897630	9.732827		-0.003723
1.976724	9.738804		-0.013181
1.937041	9.741786		-0.023701
2.002327	9.745283		-0.033374
2.023066	9.758222		-0.041035
2.044388	9.765748		-0.040202
2.071380	9.770539		-0.036521
2.101344	9.786024		-0.052224
2.126607	9.802730		-0.056202
2.173437	9.817817		-0.058036
2.177197	9.819294		-0.060081
[illegible]	9.819728		-0.065391
2.218327	9.834434		-0.056088
2.294704	9.848895		-0.052794
2.349076	9.864630		-0.037740
2.352427	9.877110		-0.046841
2.371683	9.883182		-0.037070
2.410172	9.907748		-0.024787
2.463237	9.921839		-0.009272
2.468720	9.933228		0.006806
2.534552	9.949842		0.028360
2.601977	9.961210		0.050336
2.630802	9.973728		0.074431
2.653851	9.986032		0.100886
2.671737	9.993008		0.130024
2.707831	10.008878		0.158632
2.742022	10.021485		0.180519
2.777775	10.031807		0.223321
2.812308	10.042058		0.250766
2.846430	10.052038		0.297124
2.880265	10.066033		0.338107
2.915755	10.078868		[illegible]
2.948324	10.087818		0.410489
2.978849	10.098828		0.459808
3.017313	10.108393		0.505481
3.044320	10.120122		0.550838
3.077281	10.130852		0.595998
3.102302	10.141088		0.638570
3.141412	10.152069		0.706323
3.172245	10.162533		0.752703
3.205219	10.175074		0.818110
3.227874	10.188290		0.870878
3.268827	10.197803		0.933316
3.280443	10.205580		0.992031
3.322823	10.220818		1.054243
3.380630	10.230688		1.100100

Pressure Surface

X	R	XM	RTHETA
1.881898	9.720268		0.016527
1.864016	9.731860		0.031807
1.883142	9.736915		0.037360
1.877236	9.737436		0.033223
1.988390	9.742135		0.038960
2.002607	9.746058		0.042772
2.010594	9.733362		0.048058
2.028765	9.766337		0.055037
2.063308	9.772162		0.060424
2.080711	9.774751		0.057290
2.098327	9.797753		0.064256
2.130748	9.800374		0.071411
2.160029	9.812927		0.079063
2.169220	9.818777		0.078048
2.101228	9.828369		0.087396
2.231834	9.829772		0.088306
2.252071	9.844383		0.100498
2.282501	9.860183		0.117286
2.318001	9.871271		0.138121
2.352831	9.873393		0.141523
2.374062	9.884014		0.155384
2.406260	9.900219		0.171108
2.430035	9.917821		0.187406
2.470217	9.923243		0.206217
2.502838	9.940580		0.226208
2.535913	9.952220		0.246626
2.569040	9.957740		0.257038
2.603036	9.970228		0.280223
2.637808	9.980790		0.318333
2.672784	9.998406		0.333800
2.708100	10.016871		0.370710
2.742844	10.021119		0.400238
2.778022	10.028813		0.432080
2.816460	10.046307		0.462230
2.862261	10.057367		0.501830
2.889382	10.070285		0.538083
2.927784	10.081246		0.577610
2.958430	10.092369		0.618341
3.003208	10.102240		0.652808
3.041241	10.110317		0.702284
3.078230	10.121687		0.761472
3.117837	10.144733		0.738802
3.158272	10.150008		0.848402
3.195738	10.177805		0.901180
3.233231	10.186933		0.954733
3.271716	10.198553		1.010000
3.318104	10.212344		1.087011
3.342568	10.224312		1.117823

Table B-9. Block II Stage 1 Nozzle Streamsurface Coordinates (near tip).

Suction Surface

Z	R	RTHETA
1.961831	10.554723	0.016526
1.962805	10.558327	0.006325
1.987240	10.603129	-0.003326
1.978272	10.587102	-0.011182
1.986720	10.596627	-0.020110
2.031235	10.612950	-0.025020
2.020103	10.625616	-0.027816
2.042125	10.630126	-0.038133
2.037720	10.636384	-0.035732
2.088336	10.672367	-0.053276
2.120787	10.692502	-0.057808
2.108258	10.714722	-0.060287
2.176252	10.720349	-0.030633
2.179582	10.726338	-0.066533
2.216846	10.742372	-0.070684
2.263636	10.765107	-0.059001
2.282873	10.785830	-0.056974
2.322204	10.811022	-0.055540
2.371305	10.833158	-0.049404
2.411024	10.854830	-0.037071
2.450258	10.875352	-0.024068
2.488522	10.887238	-0.007636
2.527506	10.917333	0.011057
2.573090	10.937850	0.032153
2.598852	10.957416	0.053681
2.661168	10.976564	0.081169
2.676004	10.993287	0.100018
2.714267	11.012522	0.128880
2.750040	11.031350	0.171070
2.785273	11.043768	0.206161
2.816983	11.058030	0.241233
2.854722	11.082807	0.278348
2.887935	11.098278	0.310318
2.921212	11.116277	0.361166
2.954234	11.131824	0.406294
2.986783	11.146827	0.459298
3.012025	11.162440	0.497247
3.055977	11.177147	0.545821
3.082604	11.192588	0.587168
3.114210	11.208120	0.640845
3.145330	11.223208	0.702546
3.175002	11.234210	0.762171
3.208079	11.253101	0.815387
3.229273	11.268114	0.876142
3.270511	11.282046	0.939270
3.301247	11.296306	0.997024
3.332320	11.313007	1.050077
3.360758	11.326070	1.115800

Pressure Surface

Z	R	RTHETA
1.961831	10.556732	0.014528
1.963027	10.580031	0.020580
1.980983	10.583106	0.036431
1.976061	10.588107	0.021890
1.987643	10.595048	0.030742
2.001334	10.613888	0.043143
2.017032	10.633033	0.055112
2.037460	10.650368	0.048908
2.060001	10.680306	0.052207
2.069830	10.694315	0.055780
2.080018	10.674193	0.062313
2.150055	10.692035	0.065161
2.131730	10.715096	0.073560
2.161780	10.712005	0.078008
2.182261	10.730243	0.087641
2.222761	10.740097	0.097206
2.232862	10.763690	0.109721
2.302760	10.782368	0.118601
2.312789	10.800001	0.121059
2.346327	10.816568	0.138658
2.372103	10.832559	0.158006
2.403068	10.850580	0.172068
2.430897	10.867615	0.188232
2.460233	10.884253	0.200631
2.487761	10.901028	0.222228
2.520111	10.920081	0.243239
2.552003	10.935783	0.265707
2.580288	10.952380	0.288689
2.630483	10.871079	0.314284
2.666087	10.988703	0.345909
2.700202	11.003452	0.383067
2.738600	11.022323	0.388188
2.772029	11.045343	0.429673
2.808833	11.066277	0.453037
2.865773	11.074405	0.458274
2.883283	11.088778	0.525434
2.921118	11.118182	0.574507
2.958200	11.133871	0.613031
2.997786	11.162916	0.658517
3.035475	11.176762	0.703483
3.073283	11.189385	0.759267
3.114229	11.220170	0.793318
3.153408	11.238263	0.850306
3.192225	11.244738	0.885948
3.231910	11.263489	0.967732
3.272789	11.282132	1.014205
3.303701	11.301783	1.072817
3.349453	11.317493	1.124833

APPENDIX C

Rig Hardware Photographs

The following photographs of Block II rig hardware, in various stages of assembly are presented herein:

Figure C-1. Block II Rig Vane Airfoils, Viewed Forward Looking Aft.

Figure C-2. Block II Rig Vane Airfoils, Viewed Aft Looking Forward.

Figure C-3. Block II Rig Rotor Blades, Viewed Forward Looking Aft.

Figure C-4. Block II Rig Rotor Blades Viewed Aft Looking Forward.

Figure C-5. Block II Rig Stage One Nozzle Diaphragm Assembly, Viewed Aft Looking Forwa

Figure C-6. Block II Rig Stage One Rotor Assembly, Viewed Aft Looking Forward.

Figure C-7. Block II Rig Stage Two Nozzle Diaphragm Assembly, Viewed Aft Looking Forwa

Figure C-8. Block II Rig Stage Two Rotor Assembly, Viewed Aft Looking Forward.

Figure C-9. Block II Rig Stage Three Rotor Assembly, Viewed Aft Looking Forward.

Figure C-10. Block II Rig Stage Four Nozzle Diaphragm Assembly, Viewed Aft Looking Forw

Figure C-11. Block II Rig Stage Four Rotor Assembly, Viewed Aft Looking Forward.

Figure C-12. Block II Rig Stage Five Nozzle Diaphragm Assembly, Viewed Aft Looking Forwa

Figure C-13. Block II Rig Stage Five Rotor Assembly, Viewed Aft Looking Forward.

Figure C-14. Block II Five Stage Rig Rotor Assembly, Viewed From Right Side.

Figure C-15. Block II Rig Stage One Nozzle Diaphragm Assembled Into Front Frame, Viewed Forward Looking Aft.

Figure C-16. Two-Stage Rig (Cont 4 & 4a) Exhaust Casing Showing Installation of a Fixed Arc Rake, Viewed Forward Looking Aft.

Figure C-17. Assembled Block II Five-Stage Rig (Conf. 5), Viewed From Right Side.

It should be noted that a photograph of the stage three nozzle diaphragm assembly was unavailable for inclusion in this collection.

ORIGINAL PAGE IS
OF POOR QUALITY

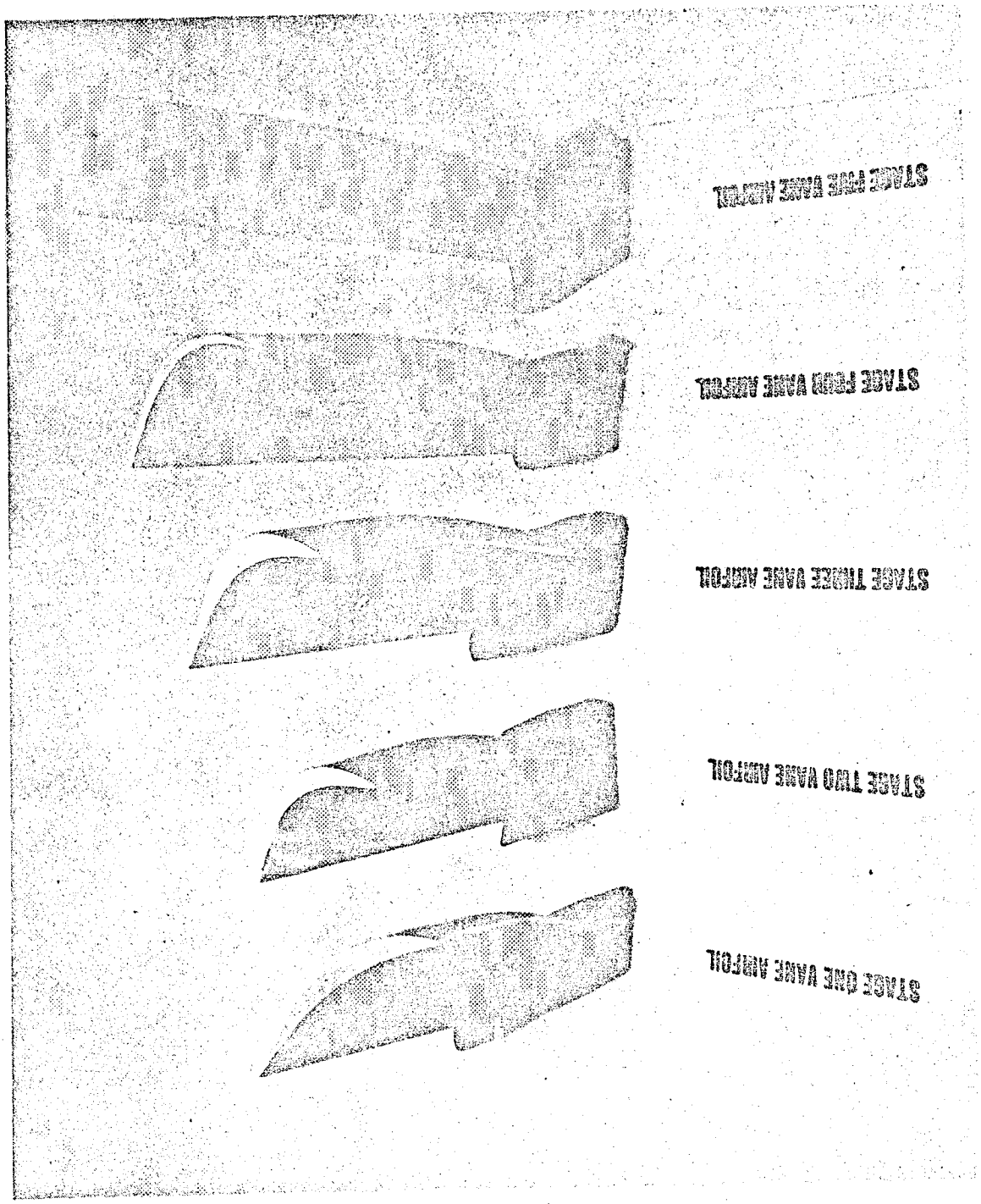

Figure C-1. Block II Rig Vane Airfoils, Viewed Forward Looking Aft.

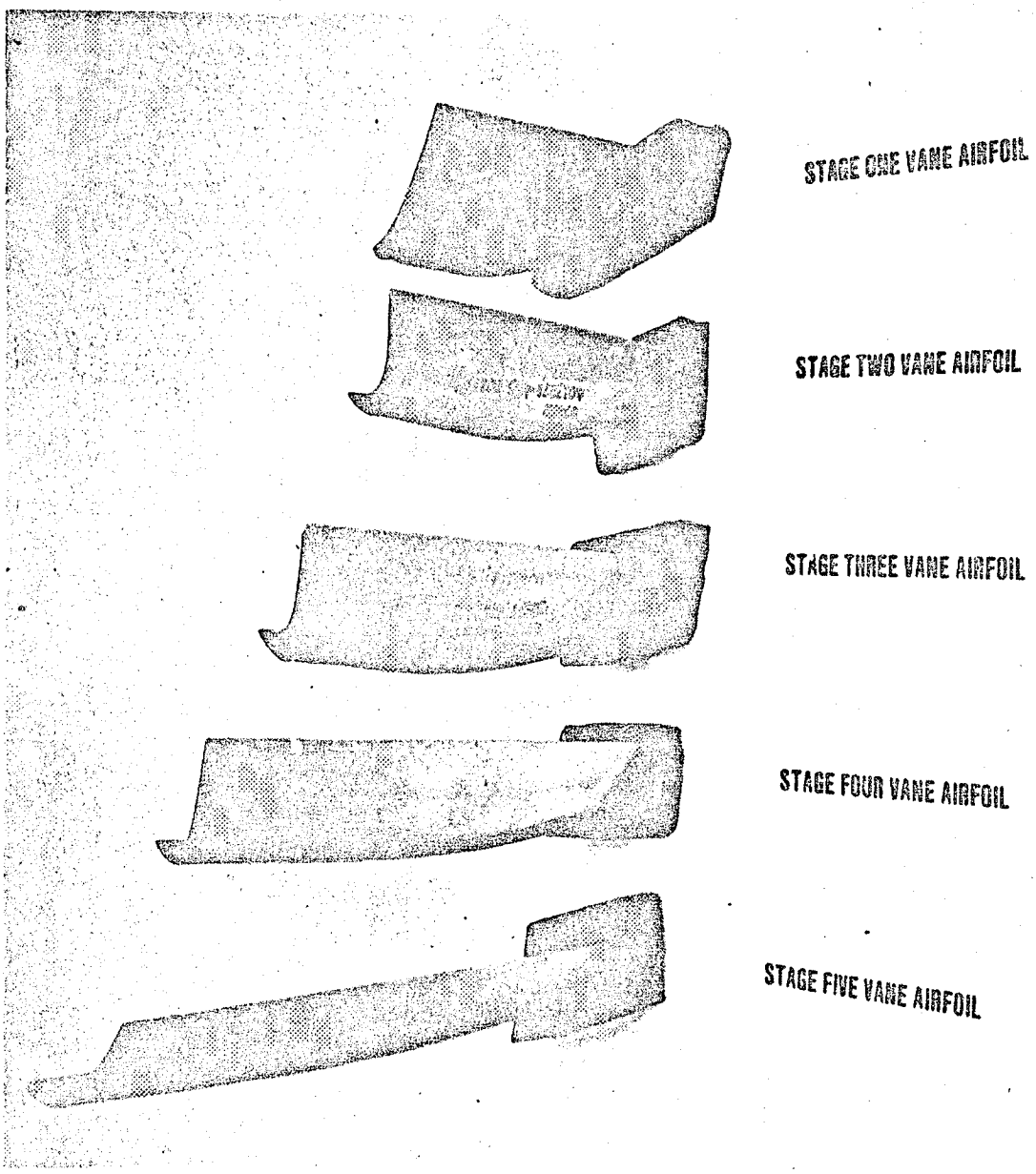

Figure C-2. Block II Rig Vane Airfoils, Viewed Aft Looking Forward.

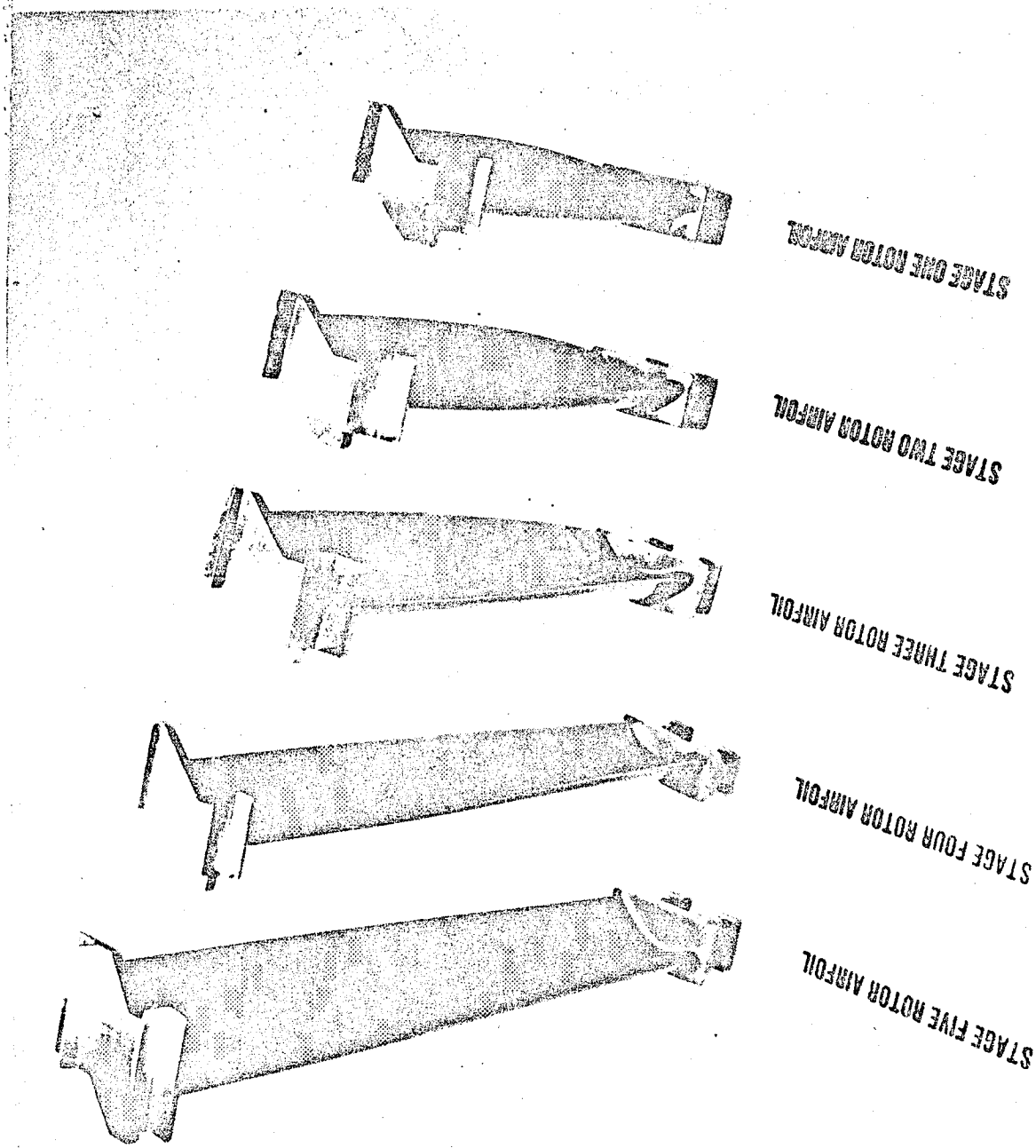

Figure C-3. Block II Rig Rotor Blades, Viewed Forward Looking Aft.

Figure C-4. Block II Rig Rotor Blades Viewed Aft Looking Forward.

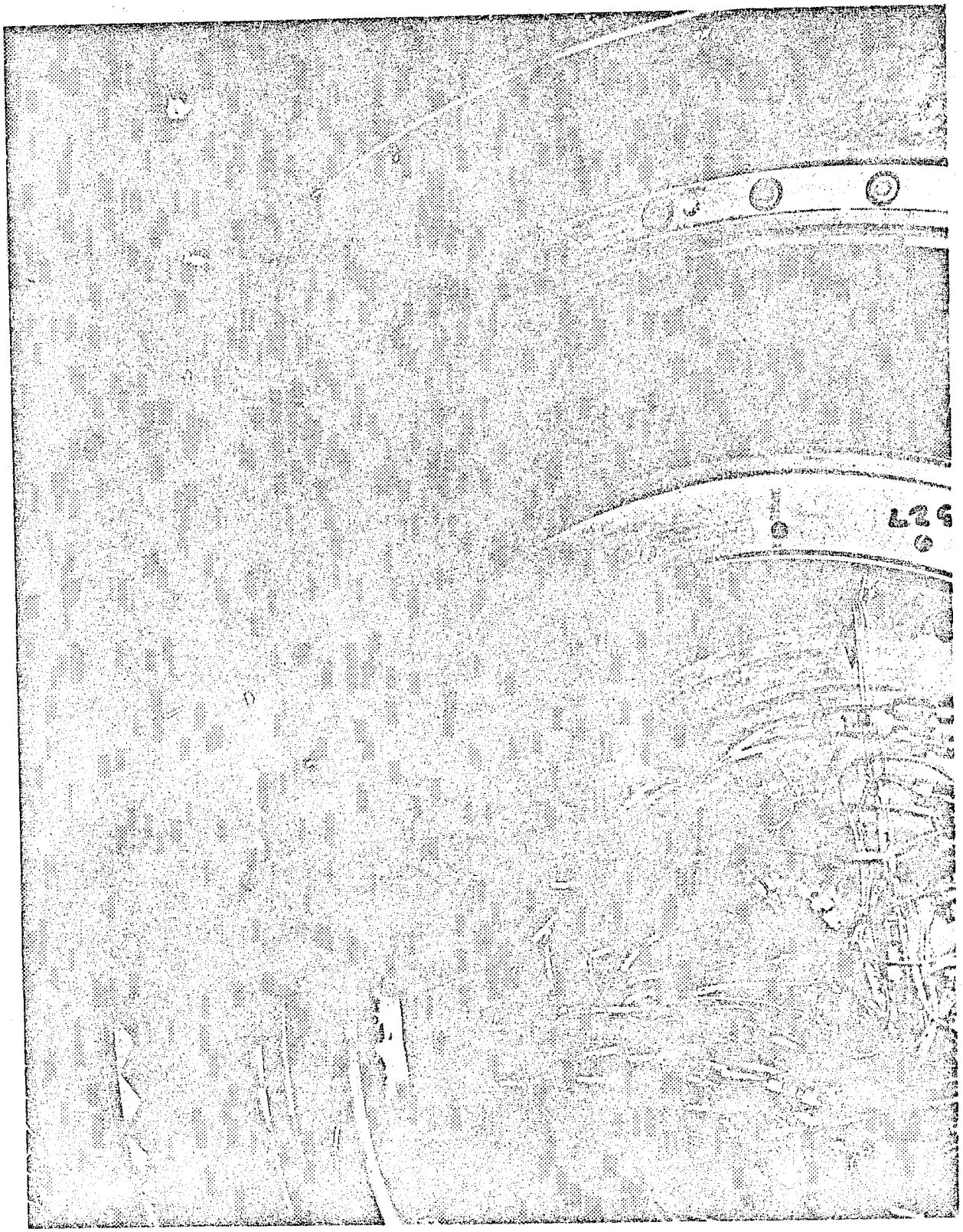

Figure C-5. Block II Rig Stage One Nozzle Diaphgram Assembly, Viewed Aft Looking Forward.

Figure C-6. Block II Rig Stage One Rotor Assembly, Viewed Aft Looking Forward.

ORIGINAL PAGE IS
OF POOR QUALITY

Figure C-7. Block II Rig Stage Two Nozzle Diaphragm Assembly, Viewed Aft Looking Forward.

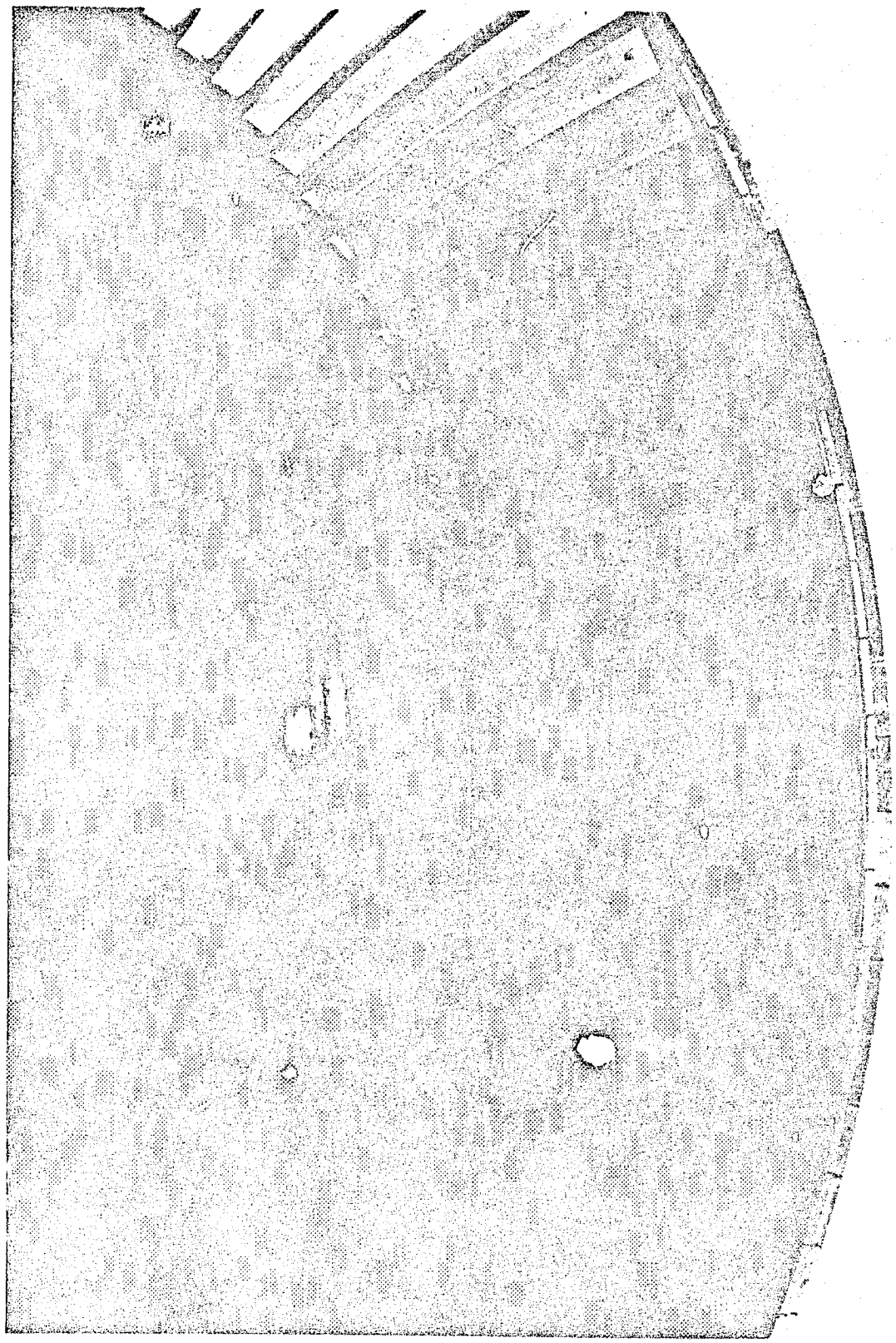

Figure C-8. Block II Rig Stage Two Rotor Assembly, Viewed Aft Looking Forward.

STAGE THREE ROTOR ASSEMBLED

Figure C-9. Block II Rig Stage Three Rotor Assembly, Viewed Aft Looking Forward.

Figure C-10. Block II R1g Stage Four Nozzle Diaphgram Assembly, Viewed Aft Looking Forward.

ORIGINAL PAGE IS
OF POOR QUALITY

STAGE FOUR ROTOR ASSEMBLED

Figure C-11. Block II R1g Stage Four Rotor Assembly, Viewed Aft Looking Forward.

Figure C-12. Block II Rig Stage Five Nozzle Diaphragm, Viewed Aft Looking Forward.

ORIGINAL PAGE IS
OF POOR QUALITY

STAGE FIVE ROTOR ASSEMBLED

Figure C-13. Block II Rig Stage Five Rotor Assembly, Viewed Aft Looking Forward.

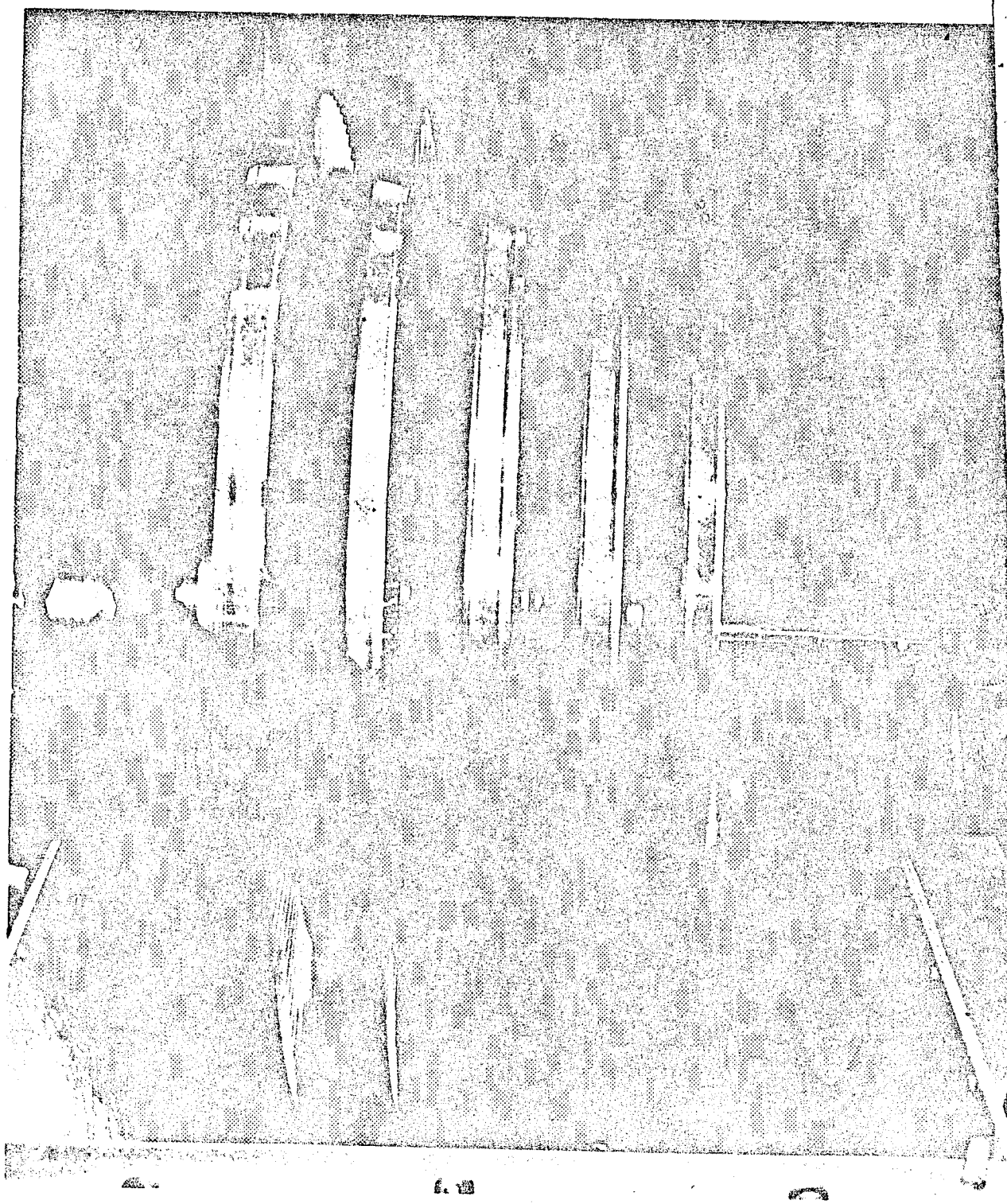

Figure C-14. Block II Five Stage Rig Rotor Assembly, Viewed From Right Side.

ORIGINAL PAGE IS
OF POOR QUALITY

Figure C-15. Block II Rig Stage One Nozzle Diaphragm Assembled Into Front Frame, Viewed Forward Looking Aft.

ORIGINAL PAGE IS
OF POOR QUALITY

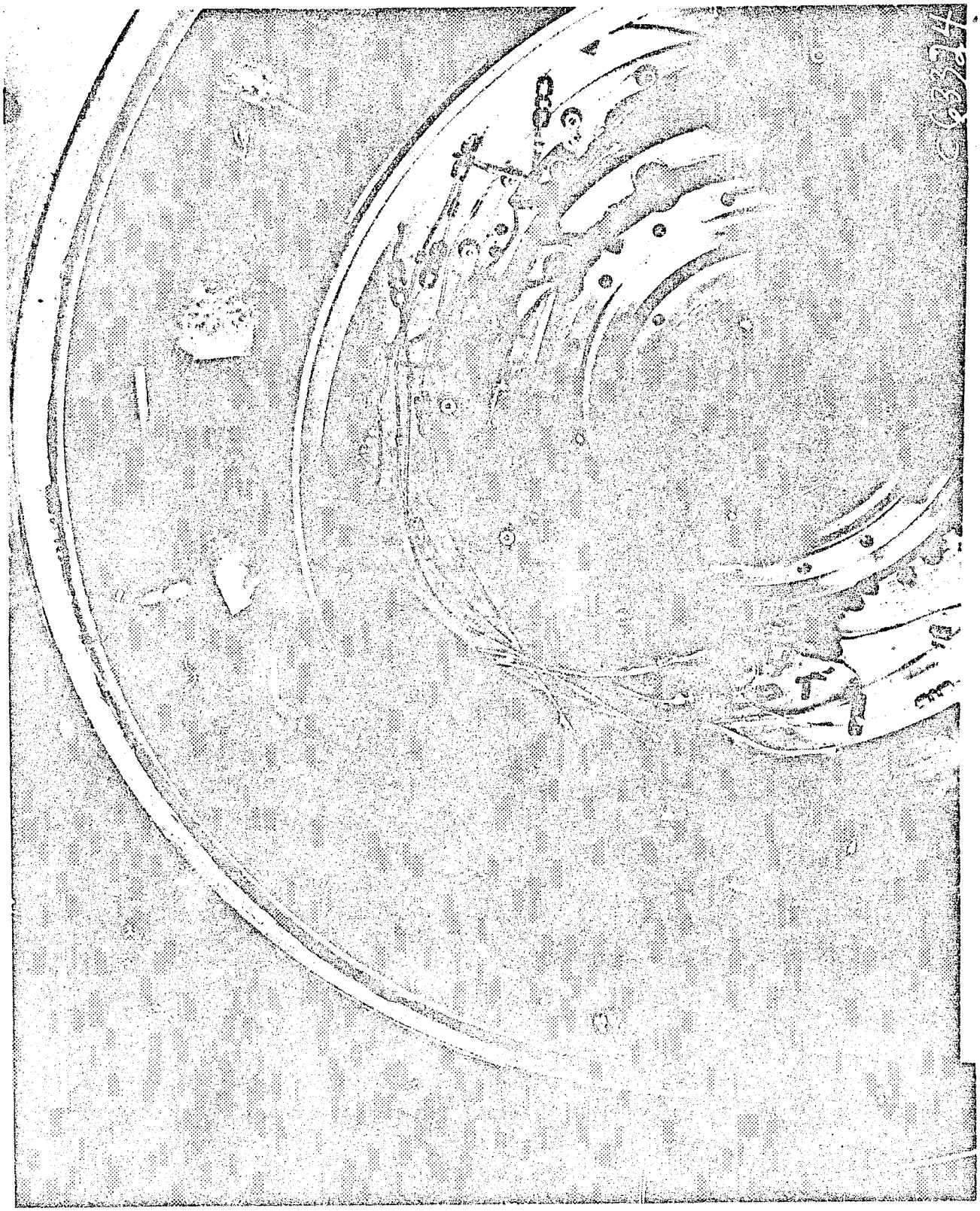

Figure C-16. Two-Stage Rig (Cont 4 & 4a) Exhaust Casing Shoulder

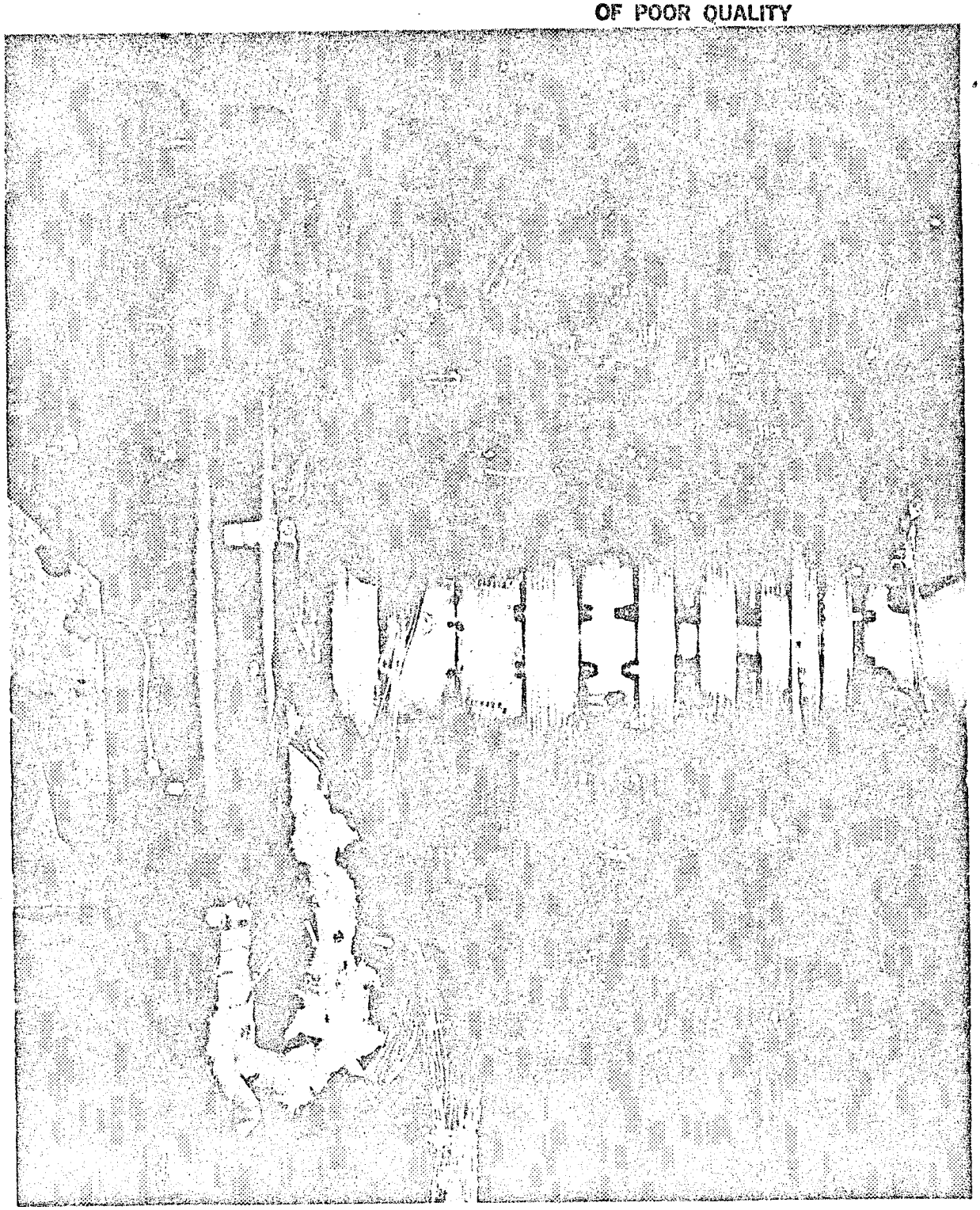

Figure C-17. Assembled Block II Five-Stage Rig (Conf. 5), Viewed From Right Side.

APPENDIX D

Significance of the Blade-Jet Speed Ratio

The blade-jet speed ratio is defined as the ratio of the average pitchline wheel speed, U, to the velocity, Co, which would theoretically be obtained by expanding the turbine flow from stage inlet total enthalpy to the ideal stage exit enthalpy. This can be expressed in terms of quantities measurable directly in the rig as follows:

$$\frac{U}{C_o} = \frac{\frac{2\pi}{720}\sqrt{\sum_{i=1}^{n} r_{pi}^2 \, N_i^2}}{\sqrt{2\,g\,J\,C_p\,T_{T_o}\left[1 - \left(\frac{P_{S_2}}{P_{T_o}}\right)^{\frac{\gamma-1}{\gamma}}\right]}} \qquad \text{(D1)}$$

where r_{pi} = rotor pitchline radius of i^{th} stage, inches

N_i = turbine speed of i^{th} stage, rpm

n = number of stages

T_{T_o} = inlet total temperature, ^{o}R

P_{T_o} = inlet total pressure, psia

P_{S_2} = exit static pressure, psia

For a given set of turbine inlet conditions, we see from D1 that the blade-jet speed ratio is a function of pressure ratio and speed only. Consequently, once the rig has been set at the desired total-to-static pressure ratio, the second independent

parameter in the test matrix, U/C_o, may be set by adjusting rig speed.

Further significance of the blade-jet speed ratio is evident upon examination of the operating line for the five stage rig in Figure 36. Note that a line of constant blade-jet speed ratio roughly parallels a line of turbine operation on a $\Delta h/T$ vs $N/\sqrt{T}$ plot.

Thus the use of blade-jet speed ratio and total-to-static pressure ratio as the independent variables in the test matrices provide easily definable maps which provide data over the turbine operating range.

APPENDIX E

Reynolds Number Excursion

The standard expression for Reynolds number is:

$$RN = \frac{\rho V l}{\mu} \qquad \text{(E1)}$$

For application to the E^3 LPT rig stages, the ρV term will be replaced by W/A, where A is defined as the vane flow area, or:

$$W/A = W/nd_o h \qquad \text{(E2)}$$

where n = number of vane airfoils

d_o = throat dimension of a vane airfoil

h = height of vane airfoils at mid-throat

Combining E1 and E2 yields:

$$RN = \frac{Wl}{\mu n d_o h} \qquad \text{(E3)}$$

Defining the characteristic length, l, to be the vane throat dimension, d_o, E3 reduces to:

$$RN = \frac{12\,W}{\mu n h} \qquad \text{(E4)}$$

where the 12 is added for consistency when h is expressed in inches.

Equation E4 is the Reynolds number quoted in this report. For multi-stage applications, the individual stage Reynolds numbers are energy weighted.

Note from Equation E4 that the Reynolds number can be modulated by changing the flow, W. In order to change Reynolds number in the rig and still retain the required flow function, $W\sqrt{T_T}/P_T$, the inlet total temperature was held constant while the inlet total pressure was varied in direct proportion to the desired change in Reynolds number.

The table below summarizes the Reynolds number for each of the rig configurations at the 45 psia inlet pressure compared to their respective full size ICLS values.

Included are the reduced rig inlet pressures required to attain the lower ICLS Reynolds numbers in the rig.

Configuration	RN for ICLS	RN for Rig at P_{T_o} = 45 and T_{T_o} = 750°R	P_{T_o} required to attain ICLS RN
Five-Stage (Block II)	.562 X 10^5	1.446 X 10^5	17.5
Two-Stage (Block II)	.757 x 10^5	1.931 x 10^5	17.6
One-Stage (Block I)	1.23 x 10^5	3.08 x 10^5	18.0

This table summarizes the required range of rig inlet pressures for the Reynolds number excursion described in Section 4.5 of this report.

A minimum of two steady state readings were acquired at each Reynolds number setting.

APPENDIX F

Performance Equations

Cascades

- Cascade Efficiency

$$\eta_s = \left[1 - \left(P_{S_{50}}/P_{T_{50}}\right)^{\frac{\gamma-1}{\gamma}}\right] \Bigg/ \left[1 - \left(P_{S_{50}}/P_{T_{39}}\right)^{\frac{\gamma-1}{\gamma}}\right]$$

where $P_{S_{50}}$ = Plane 50 static pressure, interpolated between measured hub and tip values

$P_{T_{50}}$ = Probe indicated total pressure

$P_{T_{39}}$ = Plane 39 (inlet) total pressure based on arithmetic average of area centered elements in inlet frame.

Stages or Multi-Stage Groups

- Shaft Power (primary method based on torque)

$$HP = \frac{2\Pi}{60} \cdot \frac{NT}{550}$$

where HP = shaft horse power

N = shaft speed, RPM

T = shaft torque, Ft-lb

- Efficiency (Total-to-Total)

$$\eta_{TT} = \frac{550}{J} \cdot \frac{HP}{W_{49}\ \Delta h_{T_{49-55}}}$$

where

W_{49} = LPT inlet flow, lbm/sec

J = Joules Constant, 778.16

$\Delta h_{T_{49-55}}$ = Enthalpy, Btu/lbm, available in isentropic expansion of inlet enthalpy (defined by W_{49} and T_{49}) from $P_{T_{42}}$ to $P_{T_{55}}$

- Efficiency (Total-to-Total)

$$\eta_{TS} = \frac{550}{J} \cdot \frac{HP}{W49\ \Delta h_{S49-55}}$$

where

Δh_{S49-55} = Enthalpy, BTU/lbm, available in isentropic expansion of inlet enthalpy from P_{T42} to P_{S55}

- Blade-Jet Speed Ratio

$$\frac{u}{C_o} = \sqrt{\frac{KN^2}{\Delta h_{S49-55}}}$$

where K = { For Conf 2 1.716×10^{-7}; For Confs 4 & 4a 3.640×10^{-7}; For Conf 5 10.21×10^{-7}

- Loading

$$\Psi_P = \frac{\eta_{TS}}{4\left(\frac{u}{C_o}\right)^2}$$

APPENDIX G

Error Analysis for Turbine Total-to-Total Efficiency

Turbine efficiency can be expressed as follows:

$$\eta_{TT} = \frac{\Delta h_a}{\Delta h_i} = \frac{(1.346 \times 10^{-4})\, N\tau}{WC_p\, T_{T_{39}} \left\{ 1 - \left(\frac{P_{T_{55}}}{P_{T_{42}}} \right)^{\frac{\gamma-1}{\gamma}} \right\}} \qquad (G1)$$

where:

Δh_a = actual specific energy extraction, $\frac{BTU}{lb_m}$

Δh_i = specific energy extraction, $\frac{BTU}{lb_m}$, available ideally in expanding inlet flow from inlet total to exit total pressure

N = measured speed, RPM

τ = measured torque, $ft\text{-}lb_f$

W = measured inlet flow, lb_m/sec

$T_{T_{39}}$ = measured inlet total temperature, ^oR, at Plane 39

$P_{T_{42}}$ = measured inlet total pressure lb_f/in^2, at Plane 42

$P_{T_{55}}$ = measured exit total pressure at Plane 55

If $C_p = .24$ and $\gamma = 1.4$, then equation G1 can be expressed as

$$\eta_{TT} = \left\{ KN\tau W^{-1} \right\} \left\{ T_{T_{39}} \left(1 - PR^{.286} \right) \right\}^{-1} \qquad (G2)$$

where:

$PR = P_{T_{55}}/P_{T_{42}}$

$K = 1.608 \times 10^{-4}$

Now evaluate the partial derivatives of η_{TT} with respect to each variable in the equation. From equation G2:

$$\frac{\partial \eta_{TT}}{\partial N} = \left\{K\tau W^{-1}\right\}\left\{T_{T_{39}}\left(1 - PR^{.286}\right)\right\}^{-1}$$

$$\frac{\partial \eta_{TT}}{\partial \tau} = \left\{KNW^{-1}\right\}\left\{T_{T_{39}}\left(1 - PR^{.286}\right)\right\}^{-1}$$

$$\frac{\partial \eta_{TT}}{\partial W} = -\left\{KN\tau W^{-2}\right\}\left\{T_{T_{39}}\left(1 - PR^{.286}\right)\right\}^{-1}$$

$$\frac{\partial \eta_{TT}}{\partial T_{T_{39}}} = -\left\{KN\tau W^{-1}\right\}\left\{1 - PR^{.286}\right\}\left\{T_{T_{39}}\left(1 - PR^{.286}\right)\right\}^{-2}$$

$$\frac{\partial \eta_{TT}}{\partial P_{T_{39}}} = -\left\{KN\tau W^{-1}\right\}\left\{.286\, T_{T_{39}}^{.286}\, P_{T_{55}}^{-1.286}\, P_{T_{42}}^{.286}\right\}\left\{T_{T_{39}}\left(1 - PR^{.286}\right)\right\}^{-2}$$

$$\frac{\partial \eta_{TT}}{\partial P_{T_{55}}} = \left\{KN\tau W^{-1}\right\}\left\{.286\, T_{T_{39}}^{-.286}\, P_{T_{42}}^{-.714}\, P_{T_{55}}^{.286}\right\}\left\{T_{T_{39}}\left(1 - P_{T_{55}}^{.286}\, P_{T_{42}}^{-.286}\right)\right\}^{-2}$$

Nominal design point data* for each type of rig configuration required to evaluate each of the derivatives is contained in the table below:

	One-Stage	Two-Stage	Five-Stage
$T_{T_{39}}$	750	750	750
$P_{T_{42}}$	45	45	45
W	62.6	62.6	62.6
N	3208.7	3208.7	3208.7
$P_{T_{55}}$	34.35	25.07	10.30
PR	.763	.557	.229
τ	1728.0	3588.6	8264.7

* All data listed is scaled from Block II cycle status

Using this data, each of the derivatives can now be evaluated:

	One-Stage	Two-Stage	Five-Stage
$\frac{\partial \eta}{\partial N}$	.0002773	.0002781	.0002869
$\frac{\partial \eta}{\partial \tau}$	.0005148	.0002487	.0001114
$\frac{\partial \eta}{\partial W}$	-.0142113	-.0142569	-.0147100
$\frac{\partial \eta}{\partial T_{T_{39}}}$	-.0011854	-.0011900	-.0012278
$\frac{\partial \eta}{\partial P_{T_{42}}}$	-.0703040	-.0311359	-.0111594
$\frac{\partial \eta}{\partial P_{T_{55}}}$	.0923829	.0559234	.0487289

To get an idea of the order of magnitude of these efficiency deltas, let us evaluate the effect of a 0.1% error in measuring exit total pressure, $P_{T_{55}}$, during the two-stage test.

At the 25.07 psia pressure level,

$$\Delta P_{T_{55}} = (.001)\ (25.07) = .0251 \text{ psia}$$

The error in efficiency introduced by this error in pressure measurement is:

$$\Delta \eta = \frac{\partial \eta}{\partial P_{T_{55}}} \Delta P_{T_{55}} = (.05592)\ (.0251) = .0014$$

Thus the error is magnified by a factor of 1.4 in the efficiency calculation.

It should be noted that the derivatives presented herein have no statistical base, but that the probability of incurring maximum measurement error for all variables during the reading of one data point is extremely small.

The uncertainty in efficiency (per Reference 3) can be expressed as:

$$\Delta\eta = \left\{ \left[\frac{\delta \eta}{\delta N} (\Delta N) \right]^2 + \left[\frac{\delta \eta}{\delta T} (\Delta T) \right]^2 + \left[\frac{\delta \eta}{\delta W} (\Delta W) \right]^2 + \left[\frac{\delta \eta}{\delta T} (\Delta T) \right]^2 + \left[\frac{\delta \eta}{\delta P_{T_{42}}} (\Delta P_{T_{42}}) \right]^2 + \left[\frac{\delta \eta}{\delta P_{T_{55}}} (\Delta P_{T_{55}}) \right]^2 \right\}^{1/2} \quad (G3)$$

Using the following accuracies: 1 RPM on speed, 0.1% on torque, 0.15% on flow, 1° on temperature, and 0.1% on pressure, the uncertainty in design point efficiency is 0.49 percent for the one stage configuration, 0.28 percent for the two-stage configuration, and 0.22 percent for the five-stage configuration.

APPENDIX H

Data Tabulations

Data for the following configurations in the Block I and Block II series are tabulated:

Block	Configuration	Description
I	2	Stage One Only
I	4	Two-Stage
II	4a	Two-Stage
II	5	Five-Stage

The variable names heading each column are described below:

Variable	Description
PT/PS	• Total-to-static pressure ratio, P_{T42}/P_{S55}.
u/cϕ	• Blade-to-jet speed ratio (Appendix D), u/C_o.
TT39	• Inlet total temperature as measured at plane 39, (^oR)
PT42	• Inlet total pressure calculated from plane 39, P_{T39}, measured pressures minus inlet loss, (lb_f/in^2).
N/RT	• Corrected Speed $N/\sqrt{T_{T39}}$, ($RPM/\sqrt{^oR}$) .
DH/T	• Equivalent energy extraction, $\Delta h/T_{T39}$, (BTU/lbm/^oR), where Δh is derived from measured torque.
WRT/P	• Inlet flow function, $W\sqrt{T_{T39}}/P_{T42}$, ($lbm \cdot \sqrt{^oR} \cdot in^2/sec/lb_f$).
PT/PT	• Total-to-total pressure ratio, P_{T42}/P_{T55}.
TQ/PT	• Torque/pressure parameter, Torque/P_{T42}, ($ft \cdot in^2$), based on measured shaft torque.
TQ/WRT	• Torque/flow parameter, Torque/$W\sqrt{T_{T39}}$, ($ft \cdot lb_f \cdot sec/lbm/\sqrt{^oR}$).
TT55	• Exhaust total temperature, T_{T55}, (^oR) as measured at Plane 55.

Variable	Description (Cont'd)
ETA-TT	• Total-to-total efficiency η_{TT}.
ETA-T_S	• Total-to-static efficiency, η_{TS}, five-stage only.
SWIRL	• Exhaust swirl from axial at Plante 55, derived from continuity calculation using W, T_{T55}, P_{T55}, and P_{S55}. Positive is opposite direction of rotation.

BLOCK I CONFIGURATION 2

RDG	PT/PS	U/C	TT39	PT42	N/RT	DH/T	WRT/P	PT/PT	TQ/PT	TQ/WRT	TT55	ETA-TT	SWIRL
33.	1.454	.388	754.1	45.011	117.6	.0159	38.38	1.313	38.55	1.01	784.0	.8841	42.50
35.	1.459	.387	753.6	45.015	117.4	.0160	38.48	1.317	39.01	1.01	783.0	.8832	42.25
39.	1.449	.368	755.2	44.930	136.8	.0168	37.55	1.332	34.21	.91	781.9	.8896	37.65
41.	1.449	.199	753.5	44.966	75.4	.0121	39.77	1.247	47.43	1.19	715.2	.8251	51.14
42.	1.449	.198	757.5	44.957	75.2	.0121	39.82	1.247	47.68	1.19	718.6	.8244	51.21
43.	1.452	.248	756.1	44.957	91.4	.0138	39.26	1.274	44.01	1.12	711.3	.8594	48.36
44.	1.451	.241	752.6	44.944	91.5	.0138	39.22	1.274	43.86	1.12	708.9	.8592	48.32
45.	1.454	.273	754.0	44.970	103.9	.0148	38.77	1.293	41.14	1.06	707.3	.8744	46.07
46.	1.453	.273	752.7	44.966	104.0	.0148	38.74	1.292	41.02	1.06	705.6	.8743	46.00
50.	1.450	.358	756.2	44.969	116.9	.0157	38.27	1.309	38.21	1.00	706.3	.8836	42.76
51.	1.451	.367	756.1	44.956	116.8	.0157	38.29	1.309	38.26	1.00	705.9	.8835	42.98
52.	1.645	.361	750.6	44.960	157.5	.0220	39.66	1.463	41.15	1.04	681.3	.8897	37.87
53.	1.646	.361	753.1	44.962	157.3	.0220	39.67	1.463	41.29	1.04	683.4	.8915	37.94
54.	1.650	.335	751.2	45.000	146.4	.0215	40.03	1.448	43.05	1.09	683.1	.8939	40.72
55.	1.654	.334	753.5	45.007	146.3	.0216	40.05	1.450	43.09	1.10	685.4	.8933	40.92
56.	1.647	.307	753.1	44.997	134.1	.0206	40.33	1.428	46.13	1.14	687.6	.8883	43.27
57.	1.647	.308	751.2	44.983	134.5	.0207	40.32	1.428	46.06	1.14	686.2	.8897	43.24
58.	1.654	.271	752.4	45.002	118.7	.0195	40.79	1.404	49.72	1.22	698.0	.8777	46.46
59.	1.650	.272	752.3	45.003	118.4	.0192	40.68	1.397	49.10	1.21	691.5	.8780	46.36
60.	1.649	.237	751.5	44.984	103.5	.0179	41.19	1.375	53.04	1.29	694.5	.8595	48.84
61.	1.649	.237	751.8	44.998	103.5	.0180	41.19	1.375	53.05	1.29	694.8	.8600	48.86
62.	1.650	.199	752.1	44.971	87.0	.0161	41.70	1.342	57.42	1.38	780.9	.8332	51.34
63.	1.651	.198	753.2	44.966	86.5	.0160	41.71	1.342	57.53	1.38	782.0	.8298	51.39
64.	1.649	.198	752.9	44.964	86.4	.0160	41.70	1.341	57.38	1.38	781.6	.8287	51.36
65.	1.351	.272	748.3	45.004	93.6	.0120	36.83	1.232	35.18	.96	789.7	.8674	45.70

BLOCK I CONFIGURATION 2

RDG	PT/PS	U/C	TT39	PT42	W/RT	DH/T	WRT/P	PT/PT	TQ/PT	TQ/WRT	TT55	ETA-TT	SWIRL
66.	1.351	0.273	746.5	45.010	93.8	.0121	36.81	1.232	36.19	0.96	708.9	0.8677	45.65
67.	1.351	0.237	751.2	45.011	81.5	.0111	37.34	1.215	37.56	1.01	714.5	0.8477	48.42
68.	1.351	0.237	752.1	44.997	81.5	.0111	37.36	1.216	37.63	1.01	715.8	0.8512	48.44
69.	1.350	0.237	750.2	45.008	81.5	.0111	37.32	1.216	37.58	1.01	714.9	0.8495	48.36
70.	1.352	0.198	751.0	45.002	68.3	.0099	37.95	1.198	40.99	1.08	719.5	0.8194	50.99
71.	1.352	0.199	753.5	44.988	68.5	.0099	37.96	1.198	40.85	1.05	721.9	0.8211	50.98
72.	1.350	0.307	751.3	45.001	105.5	.0126	36.31	1.245	32.69	0.90	716.3	0.8791	42.81
73.	1.351	0.308	748.1	45.005	105.6	.0128	36.30	1.245	32.75	0.90	707.6	0.8798	42.83
74.	1.345	0.341	749.0	44.990	116.3	.0132	35.77	1.253	30.28	0.85	707.0	0.8840	39.47
75.	1.346	0.340	751.3	45.008	116.1	.0133	35.78	1.254	30.42	0.85	709.4	0.8851	39.57
76.	1.350	0.361	751.4	44.987	124.0	.0137	35.60	1.263	29.23	0.82	709.0	0.8847	37.15
77.	1.350	0.361	751.4	44.997	124.0	.0137	35.59	1.263	29.14	0.82	707.9	0.8815	37.10
78.	1.451	0.311	748.1	44.984	118.3	.0158	38.20	1.311	37.09	0.99	699.0	0.8844	42.76
79.	1.451	0.311	751.8	44.975	118.1	.0159	38.17	1.311	38.07	1.00	702.3	0.8873	42.77
82.	1.450	0.310	749.5	45.050	117.7	.0158	38.26	1.311	38.19	1.00	699.5	0.8845	42.35
83.	1.449	0.310	750.4	45.053	117.6	.0158	38.24	1.310	38.19	1.00	700.9	0.8863	42.47
84.	1.448	0.310	753.3	45.056	117.5	.0158	39.24	1.310	38.17	1.00	703.6	0.8862	42.47
85.	1.252	0.199	748.7	45.051	59.4	.0075	34.91	1.145	32.59	0.93	725.0	0.8186	50.60
86.	1.253	0.199	749.8	45.055	59.4	.0075	34.93	1.145	32.70	0.94	726.4	0.8194	50.85
87.	1.248	0.236	754.1	45.062	70.2	.0083	34.15	1.156	29.86	0.87	727.6	0.8476	48.39
88.	1.249	0.237	752.3	45.055	70.3	.0083	34.21	1.157	29.98	0.88	725.8	0.8477	48.23
89.	1.251	0.273	752.2	45.057	81.4	.0091	33.71	1.169	27.90	0.83	723.3	0.8662	45.64
90.	1.251	0.273	752.5	45.064	81.4	.0091	33.71	1.169	27.92	0.83	723.7	0.8660	45.57
91.	1.251	0.307	752.2	45.069	91.5	.0097	33.28	1.179	26.12	0.78	721.3	0.8766	42.49
92.	1.251	0.307	752.1	45.077	91.5	.0097	33.27	1.179	26.12	0.79	721.5	0.8777	42.62

BLOCK I CONFIGURATION 2

RDG	PT/PS	U/CØ	TT39	PT42	N/RT	DH/T	WRT/P	PT/PT	TQ/PT	TQ/WRT	TT55	ETA-TT	SWIRL
93.	1.252	Ø.336	753.3	45.Ø92	1ØØ.4	.Ø1Ø1	32.92	1.187	24.6Ø	Ø.75	721.2	Ø.8ØØ5	39.68
94.	1.252	Ø.336	752.9	45.Ø85	1ØØ.5	.Ø1Ø1	32.93	1.187	24.59	Ø.75	72Ø.8	Ø.8Ø15	39.68
95.	1.252	Ø.358	753.3	45.ØØ6	1Ø7.Ø	.Ø1Ø4	32.6Ø	1.192	23.46	Ø.72	72Ø.3	Ø.8Ø28	37.34
96.	1.251	Ø.36Ø	753.8	45.Ø76	1Ø7.3	.Ø1Ø3	32.55	1.191	23.23	Ø.71	72Ø.7	Ø.8ØØ4	37.Ø9
97.	1.148	Ø.2Ø1	753.7	45.Ø51	47.5	.ØØ47	29.42	1.Ø89	21.54	Ø.73	738.5	Ø.8135	5Ø.28
98.	1.148	Ø.2Ø2	752.7	45.Ø41	47.5	.ØØ47	29.44	1.Ø88	21.53	Ø.73	737.5	Ø.8146	5Ø.26
99.	1.152	Ø.237	75Ø.7	45.Ø45	56.6	.ØØ53	29.12	1.Ø98	2Ø.36	Ø.7Ø	733.6	Ø.8412	48.Ø1
1ØØ.	1.152	Ø.237	75Ø.6	45.Ø46	56.6	.ØØ53	29.13	1.Ø98	2Ø.35	Ø.7Ø	733.7	Ø.8414	48.Ø6
1Ø1.	1.451	Ø.311	747.1	44.997	118.4	.Ø159	38.26	1.312	38.17	1.ØØ	697.2	Ø.8869	42.33
1Ø2.	1.45Ø	Ø.31Ø	75Ø.3	44.991	117.7	.Ø158	38.27	1.311	38.19	1.ØØ	7ØØ.3	Ø.8855	42.47
1Ø3.	1.45Ø	Ø.337	754.7	44.992	128.Ø	.Ø164	37.9Ø	1.323	36.13	Ø.95	7Ø2.6	Ø.8ØØØ	39.81
1Ø4.	1.45Ø	Ø.337	753.2	44.989	128.1	.Ø164	37.9Ø	1.323	36.Ø6	Ø.95	7Ø1.2	Ø.8ØØ4	39.81
1Ø5.	1.453	Ø.361	753.2	45.ØØØ	137.5	.Ø169	37.6Ø	1.336	34.39	Ø.91	699.5	Ø.8ØØ7	37.19
1Ø6.	1.452	Ø.361	753.4	44.999	137.5	.Ø169	37.62	1.335	34.4Ø	Ø.91	699.9	Ø.8ØØ9	37.Ø6
1Ø7.	1.153	Ø.273	749.2	45.Ø64	65.2	.ØØ58	28.68	1.185	18.97	Ø.66	73Ø.7	Ø.8593	45.34
1Ø8.	1.153	Ø.273	748.9	45.Ø74	65.2	.ØØ58	28.7Ø	1.185	18.97	Ø.66	73Ø.5	Ø.85Ø1	45.58
1Ø9.	1.151	Ø.3ØØ	751.4	45.Ø35	73.3	.ØØ61	28.12	1.11Ø	17.45	Ø.62	731.Ø	Ø.8719	42.47
111.	1.152	Ø.34Ø	753.9	45.ØØ9	81.2	.ØØ64	27.78	1.115	16.31	Ø.59	733.2	Ø.8731	39.19
112.	1.152	Ø.341	753.8	45.Ø12	81.2	.ØØ64	27.79	1.115	16.35	Ø.59	733.2	Ø.8765	39.22
113.	1.152	Ø.358	756.4	45.Ø19	85.5	.ØØ65	27.58	1.117	15.69	Ø.57	735.1	Ø.8748	37.79
114.	1.153	Ø.358	755.3	45.ØØØ	85.5	.ØØ66	27.57	1.117	15.72	Ø.57	734.2	Ø.8776	38.Ø6
117.	1.453	Ø.3ØØ	752.3	45.Ø76	117.6	.Ø158	38.35	1.311	38.35	1.ØØ	7Ø1.Ø	Ø.8856	42.8Ø
118.	1.454	Ø.31Ø	752.4	45.Ø7Ø	119.1	.Ø159	38.37	1.312	38.35	1.ØØ	7Ø2.Ø	Ø.8867	42.65
125.	1.448	Ø.312	743.7	44.968	118.5	.Ø158	38.2Ø	1.3Ø8	37.77	Ø.99	694.4	Ø.8884	42.87
126.	1.449	Ø.312	746.Ø	44.972	118.3	.Ø158	38.2Ø	1.3Ø9	37.84	Ø.99	696.Ø	Ø.8883	42.94

BLOCK I CONFIGURATION 4

RDG	PT/PS	U/C	TT39	PT42	N/RT	DH/T	WRT/P	PT/PT	TQ/PT	TQ/WRT	TT65	ETA-TT	SWIRL
165.	1.998	.343	749.1	44.932	117.8	.0326	37.78	1.789	77.69	2.05	647.4	.8853	45.92
166.	1.991	.343	749.6	44.945	117.8	.0326	37.79	1.790	77.70	2.06	647.5	.8854	45.96
167.	1.995	.342	749.9	44.949	117.7	.0326	37.81	1.792	77.77	2.06	647.8	.8836	45.94
168.	1.994	.340	757.4	45.014	117.0	.0326	37.87	1.790	78.37	2.07	654.5	.8853	46.19
169.	1.994	.340	757.0	45.016	116.8	.0326	37.86	1.790	78.44	2.07	654.3	.8849	46.14
170.	1.996	.342	750.2	45.049	117.5	.0326	37.79	1.792	77.94	2.06	646.7	.8839	46.07
173.	2.007	.351	747.9	45.029	103.8	.0313	38.70	1.762	86.65	2.24	650.1	.8712	49.56
174.	2.006	.351	748.4	45.030	103.7	.0312	38.68	1.762	86.47	2.24	656.6	.8698	49.58
175.	1.994	.262	747.2	45.038	90.0	.0291	39.46	1.716	94.70	2.40	656.3	.8472	52.29
176.	1.992	.262	747.4	45.016	90.0	.0291	39.48	1.715	94.72	2.40	656.3	.8472	52.29
177.	2.005	.221	750.6	45.019	76.0	.0266	40.38	1.671	105.02	2.60	666.5	.8113	54.98
178.	2.002	.221	751.0	45.027	76.2	.0266	40.37	1.673	104.88	2.60	667.0	.8115	54.91
179.	1.997	.380	753.9	45.043	130.8	.0336	37.05	1.825	70.69	1.91	647.9	.8857	41.86
180.	1.995	.382	753.5	45.026	131.3	.0335	37.06	1.826	70.43	1.90	647.9	.8846	41.60
181.	1.996	.423	754.9	45.035	145.4	.0342	36.33	1.852	63.40	1.75	646.0	.8867	36.74
182.	1.995	.422	751.4	45.033	145.1	.0342	36.33	1.852	63.65	1.75	643.9	.8826	36.75
183.	1.999	.421	752.7	45.043	145.0	.0343	36.34	1.854	63.78	1.75	644.8	.8823	36.81
184.	2.196	.421	751.0	45.039	153.4	.0381	36.84	1.997	67.89	1.84	631.4	.8834	38.42
185.	2.198	.421	750.7	45.032	153.4	.0381	36.84	1.998	67.95	1.84	631.0	.8836	38.44
186.	2.201	.381	748.0	45.032	139.2	.0373	37.49	1.966	74.73	1.99	630.7	.8851	43.05
187.	2.190	.383	747.2	45.029	139.4	.0373	37.47	1.960	74.39	1.99	635.7	.8869	42.77
188.	2.002	.343	745.6	45.016	118.1	.0328	37.83	1.798	78.07	2.05	643.2	.8853	45.94
189.	2.002	.343	491.9	45.003	118.3	.0328	37.86	1.000	78.05	2.06	642.9	.8857	45.88
190.	1.393	.419	757.7	45.014	102.3	.0175	31.01	1.356	39.47	1.27	791.9	.8763	33.45
191.	1.395	.418	758.5	44.917	102.4	.0177	31.13	1.359	39.95	1.28	792.5	.8778	31.39

BLOCK I CONFIGURATION 4

RDG	PT/PS	U/C#	TT39	PT42	N/RT	DN/T	WRT/P	PT/PT	TQ/PT	TQ/WRT	TT55	ETA-TT	SWIRL
192.	1.994	#.343	746.7	45.#16	118.#	.#326	37.81	1.792	77.54	2.#5	645.#	#.8839	45.79
193.	1.994	#.343	747.2	45.#18	118.#	.#326	37.8#	1.793	77.62	2.#5	645.2	#.8837	45.78
194.	2.391	#.424	746.3	45.#45	161.9	.#414	37.#4	2.132	7#.37	1.9#	616.1	#.8859	39.6#
195.	2.389	#.424	746.#	45.#54	161.8	.#413	37.#4	2.131	7#.31	1.9#	617.1	#.8859	39.39
196.	2.4#4	#.382	748.1	45.#53	146.2	.#4#7	37.67	2.#96	77.83	2.#7	621.1	#.8862	44.#6
197.	2.4#7	#.381	75#.6	45.#48	146.#	.#4#7	37.71	2.#98	78.11	2.#7	623.#	#.8#8#	44.#4
198.	2.39#	#.343	746.6	45.#55	13#.9	.#393	38.38	2.#36	85.54	2.23	624.1	#.8892	47.78
199.	2.386	#.343	749.1	45.#44	13#.8	.#392	38.38	2.#34	85.53	2.23	626.4	#.8898	47.73
2#0.	2.4#2	#.3#1	747.6	45.#87	115.#	.#375	39.21	1.981	94.93	2.42	63#.2	#.8795	51.13
2#1.	2.4#3	#.3#1	747.#	45.1#6	115.1	.#375	39.18	1.982	94.85	2.42	63#.#	#.8#81	51.13
2#2.	2.197	#.3#2	747.5	45.#75	11#.3	.#346	39.#2	1.876	91.#3	2.33	639.5	#.876#	5#.14
2#3.	2.197	#.3#2	747.8	45.#67	11#.3	.#346	39.#1	1.876	91.#4	2.33	64#.#	#.8767	5#.18
2#4.	2.19#	#.343	748.1	45.#28	124.9	.#362	38.22	1.919	82.42	2.16	635.5	#.8684	46.76
2#5.	2.19#	#.342	748.5	45.#17	124.7	.#362	38.23	1.919	82.54	2.16	635.7	#.8876	46.77
2#6.	2.195	#.263	746.9	45.#48	95.7	.#324	39.78	1.823	1##.#3	2.51	646.#	#.855#	53.##
2#7.	2.195	#.262	748.1	45.#41	95.6	.#324	39.81	1.823	1#6.14	2.52	647.2	#.8552	53.#2
2#8.	2.194	#.221	748.8	45.#37	8#.5	.#295	4#.67	1.764	11#.6#	2.72	656.4	#.8193	55.47
2#9.	2.195	#.221	749.7	45.#32	8#.5	.#295	4#.67	1.764	11#.73	2.72	657.3	#.82#6	55.51
21#.	2.397	#.221	748.4	45.#25	84.3	.#319	4#.8#	1.845	114.59	2.31	648.8	#.8261	56.#2
211.	2.397	#.221	748.8	45.#25	84.2	.#319	4#.76	1.846	114.66	2.31	649.#	#.8265	56.#2
212.	2.391	#.262	744.8	45.#3#	1##.1	.#356	39.98	1.916	1#3.9#	2.6#	635.6	#.8599	53.54
213.	2.39#	#.262	743.6	45.#27	1##.1	.#35#	39.93	1.916	1#3.78	2.6#	635.4	#.8596	53.54
22#.	1.995	#.342	755.4	45.#67	117.5	.#326	37.62	1.792	78.1#	2.#7	652.8	#.8851	45.95
221.	1.995	#.342	753.9	45.#73	117.5	.#326	37.81	1.792	77.93	2.#6	651.4	#.8839	45.99
222.	1.792	#.421	749.9	45.#07	134.#	.#296	35.46	1.695	53.17	1.64	657.1	#.88#5	34.#9

BLOCK I CONFIGURATION 4

RDG	PT/PS	U/C0	TT39	PT42	N/RT	DH/T	WRT/P	PT/PT	TQ/PT	TQ/WRT	TT55	ETA-TT	SWIRL
223.	1.796	0.421	748.5	45.096	134.4	.0296	35.47	1.698	58.17	1.64	656.1	0.8797	34.49
224.	1.798	0.382	749.0	45.099	122.0	.0292	36.18	1.680	64.27	1.78	657.6	0.8811	39.99
225.	1.797	0.383	751.0	45.094	122.1	.0292	36.22	1.679	64.33	1.78	659.5	0.8827	40.01
226.	1.799	0.341	748.5	45.104	109.0	.0284	37.00	1.656	71.51	1.93	660.7	0.8789	44.71
227.	1.798	0.341	751.4	45.092	109.0	.0284	37.02	1.656	71.59	1.93	663.3	0.8799	44.74
228.	1.795	0.302	750.1	45.082	96.3	.0276	37.80	1.627	78.82	2.09	665.9	0.8660	48.39
229.	1.795	0.302	749.8	45.073	96.3	.0278	37.82	1.627	78.68	2.08	665.7	0.8649	48.39
230.	1.803	0.261	749.2	45.073	83.4	.0254	38.75	1.601	87.71	2.26	670.4	0.8405	51.61
231.	1.801	0.258	750.4	45.078	82.6	.0252	38.79	1.597	87.87	2.27	670.9	0.8383	52.01
232.	1.798	0.223	749.4	45.066	71.1	.0232	39.61	1.564	96.00	2.43	675.4	0.8053	54.25
233.	1.798	0.222	750.2	45.065	71.0	.0232	39.60	1.564	96.14	2.43	677.9	0.8056	54.26
234.	1.596	0.223	746.6	45.046	64.1	.0189	38.25	1.440	84.06	2.20	668.1	0.7981	53.62
235.	1.599	0.222	749.0	45.064	64.0	.0190	38.27	1.441	84.37	2.20	669.3	0.7976	53.68
236.	1.604	0.259	748.5	45.038	74.9	.0208	37.39	1.468	77.00	2.06	694.0	0.8320	51.08
237.	1.603	0.259	749.2	45.035	74.8	.0207	37.41	1.468	77.07	2.06	695.1	0.8319	50.99
238.	1.592	0.301	749.0	45.029	86.2	.0228	36.33	1.482	68.80	1.89	680.4	0.8596	47.60
239.	1.596	0.301	747.4	45.047	86.6	.0220	36.35	1.486	68.75	1.89	678.9	0.8572	47.37
240.	1.601	0.342	748.8	45.030	98.5	.0233	35.54	1.508	62.35	1.75	676.6	0.8749	43.41
241.	1.601	0.342	749.1	45.015	98.5	.0233	35.52	1.508	62.39	1.76	676.9	0.8756	43.59
242.	1.598	0.382	749.8	44.998	110.0	.0239	34.66	1.523	55.89	1.61	675.4	0.8784	38.45
243.	1.599	0.382	749.4	44.998	110.1	.0239	34.66	1.523	55.94	1.61	674.4	0.8792	38.56
244.	1.598	0.421	749.9	45.008	121.2	.0242	33.91	1.534	50.38	1.49	673.7	0.8758	32.87
245.	1.599	0.421	749.9	45.014	121.2	.0243	33.92	1.535	50.42	1.49	673.4	0.8764	32.80
246.	1.411	0.337	751.0	45.123	93.8	.0173	32.98	1.355	50.61	1.53	696.9	0.8569	43.12
247.	1.404	0.340	749.8	45.116	84.1	.0171	32.77	1.350	49.54	1.51	695.8	0.8571	42.72

BLOCK I CONFIGURATION 4

RDG	PT/PS	U/C	TT39	PT42	N/RT	DH/T	WRT/P	PT/PT	TQ/PT	TQ/WRT	TT55	ETA-TT	SWIRL
254.	1.993	0.342	754.2	45.057	117.5	.0327	37.83	1.792	78.11	2.06	650.9	0.8859	45.81
255.	1.992	0.343	751.6	45.047	117.7	.0326	37.88	1.792	77.73	2.06	649.6	0.8838	45.61
256.	1.398	0.379	752.5	45.099	93.1	.0175	31.88	1.356	44.49	1.40	697.6	0.8738	36.42
257.	1.406	0.376	752.2	45.099	93.1	.0177	32.08	1.361	45.26	1.41	697.0	0.8726	36.93
258.	1.401	0.299	745.5	45.097	73.6	.0152	33.83	1.336	54.97	1.63	595.7	0.8486	46.64
259.	1.403	0.298	746.9	45.101	73.6	.0162	33.67	1.337	55.16	1.64	636.3	0.8493	46.96
260.	1.403	0.258	749.9	45.097	63.6	.0152	34.63	1.323	61.34	1.77	702.2	0.8215	50.34
261.	1.405	0.257	751.2	45.105	63.6	.0152	34.69	1.324	61.57	1.77	703.9	0.8196	50.36
262.	1.401	0.228	748.1	45.091	56.2	.0142	35.43	1.311	66.53	1.88	703.6	0.7936	52.28
263.	1.401	0.228	749.0	45.098	56.1	.0142	35.43	1.311	66.61	1.88	704.2	0.7937	52.26
264.	1.998	0.342	750.9	45.056	117.9	.0327	37.82	1.794	77.93	2.06	648.5	0.8841	45.96
265.	1.997	0.343	749.4	45.046	118.0	.0328	37.79	1.795	78.02	2.06	647.6	0.8869	46.86
269.	1.993	0.342	750.5	44.985	117.6	.0326	37.79	1.793	77.89	2.06	648.2	0.8845	45.59
271.	1.994	0.342	750.8	44.995	117.6	.0327	37.78	1.794	78.05	2.06	648.9	0.8846	45.55
277.	1.994	0.342	751.5	45.028	117.7	.0326	37.81	1.794	77.34	2.06	649.4	0.8838	45.61
278.	1.995	0.343	747.3	45.026	117.9	.0327	37.77	1.796	77.76	2.06	645.7	0.8832	45.49
0.	0.	0.	0.	0.	0.	.	0.	0.	0.	0.	0.	0.	0.

CONFIGURATION 4A

RDG	PT/PS	U/CØ	TT39	PT42	N/RT	DH/T	WRT/P	PT/PT	TQ/PT	TQ/WRT	TT55	ETA-TT	SWIRL
367.	2.ØØ2	Ø.338	753.4	44.977	116.Ø	.Ø332	38.14	1.ØØ3	ØØ.52	2.11	647.3	Ø.8916	44.56
369.	2.ØØ1	Ø.339	752.4	44.96Ø	117.1	.Ø332	38.14	1.ØØ4	ØØ.29	2.11	646.9	Ø.8914	44.41
37Ø.	2.ØØØ	Ø.339	752.4	44.959	116.9	.Ø332	38.13	1.ØØ4	ØØ.32	2.11	646.Ø	Ø.8918	44.37
371.	2.ØØ1	Ø.22Ø	751.4	44.957	75.Ø	.Ø271	4Ø.64	1.Ø76	1Ø7.79	2.65	663.9	Ø.8227	53.84
373.	1.993	Ø.2ØØ	749.6	45.1Ø1	Ø9.4	.Ø295	39.73	1.717	97.34	2.45	654.3	Ø.8587	51.26
374.	1.997	Ø.259	749.5	45.ØØ6	Ø9.4	.Ø295	39.75	1.719	97.6Ø	2.46	654.5	Ø.859Ø	51.26
375.	2.ØØØ	Ø.259	75Ø.8	44.94Ø	1Ø3.3	.Ø316	38.91	1.77Ø	ØØ.42	2.27	649.6	Ø.8746	47.82
376.	2.ØØØ	Ø.299	751.1	44.953	1Ø3.2	.Ø316	38.92	1.77Ø	ØØ.51	2.27	65Ø.2	Ø.8749	47.8Ø
377.	1.999	Ø.378	751.2	44.928	13Ø.3	.Ø343	37.46	1.83Ø	73.4Ø	1.96	641.4	Ø.9ØØ3	4Ø.65
378.	1.999	Ø.377	751.6	44.9Ø5	13Ø.2	.Ø343	37.4Ø	1.83Ø	73.46	1.96	641.9	Ø.9ØØ1	4Ø.53
381.	2.ØØ2	Ø.417	751.1	44.966	143.9	.Ø353	36.89	1.855	67.23	1.82	636.6	Ø.9ØØ2	35.91
382.	2.ØØ1	Ø.417	75Ø.9	44.962	143.9	.Ø353	36.8Ø	1.855	67.26	1.82	636.3	Ø.9ØØØ	35.9Ø
383.	2.ØØ5	Ø.339	751.5	45.Ø12	117.2	.Ø332	38.14	1.ØØ5	ØØ.4Ø	2.11	645.4	Ø.8931	44.42
384.	2.ØØ5	Ø.339	752.9	45.ØØ6	117.Ø	.Ø332	38.15	1.ØØ5	ØØ.49	2.11	646.6	Ø.892Ø	44.41
385.	2.4ØØ	Ø.297	752.9	45.Ø23	114.Ø	.Ø3ØØ	39.46	1.999	97.73	2.48	63Ø.9	Ø.8834	49.75
386.	2.4ØØ	Ø.298	752.5	45.Ø22	114.1	.Ø3ØØ	39.46	1.999	97.7Ø	2.48	63Ø.5	Ø.8838	49.77
387.	2.4Ø1	Ø.258	752.4	44.941	9Ø.7	.Ø354	4Ø.22	1.936	1Ø7.31	2.67	638.4	Ø.8592	52.47
388.	2.4ØØ	Ø.258	751.6	44.942	9Ø.7	.Ø354	4Ø.22	1.936	1Ø7.27	2.67	637.8	Ø.8599	52.46
389.	2.399	Ø.219	751.8	44.971	Ø4.Ø	.Ø324	4Ø.95	1.Ø71	117.4Ø	2.67	647.3	Ø.824Ø	54.Ø1
39Ø.	2.4ØØ	Ø.219	751.9	44.966	Ø4.Ø	.Ø324	4Ø.94	1.Ø71	117.45	2.67	647.2	Ø.8243	54.Ø2
392.	2.4Ø2	Ø.34Ø	752.5	44.96Ø	13Ø.3	.Ø4Ø2	38.74	2.ØØ3	ØØ.73	2.29	623.9	Ø.9ØØ7	46.54
393.	2.4Ø2	Ø.379	751.1	44.975	145.2	.Ø41Ø	38.16	2.Ø9Ø	Ø1.54	2.14	617.9	Ø.9113	43.13
394.	2.4Ø2	Ø.37Ø	751.1	45.Ø12	145.1	.Ø417	38.13	2.ØØ8	Ø1.43	2.14	618.2	Ø.91Ø2	43.21
395.	2.4Ø2	Ø.417	752.6	45.ØØ3	159.9	.Ø42Ø	37.59	2.136	74.75	1.99	616.4	Ø.9144	39.54
396.	2.4Ø3	Ø.417	753.6	45.Ø34	159.9	.Ø42Ø	37.59	2.136	74.77	1.99	617.Ø	Ø.9141	39.56

CONFIGURATION 4A

RDG	PT/PS	U/CØ	TT39	PT42	N/RT	DØ/T	WRT/P	PT/PT	TQ/PT	TQ/WRT	TT55	ETA-TT	SWIRL
397.	2.2Ø2	Ø.416	751.5	44.991	152.3	.Ø393	37.36	1.999	71.74	1.92	626.Ø	Ø.9125	38.Ø9
398.	2.2Ø3	Ø.416	752.7	45.ØØ4	152.2	.Ø394	37.38	2.ØØØ	71.87	1.92	627.1	Ø.9131	38.11
399.	2.2Ø2	Ø.378	751.4	44.994	138.3	.Ø383	37.91	1.97Ø	78.Ø5	2.Ø6	629.Ø	Ø.9Ø65	42.Ø8
4ØØ.	2.2Ø3	Ø.378	752.7	45.Ø21	138.5	.Ø384	37.92	1.969	78.17	2.Ø6	629.8	Ø.9Ø82	42.21
4Ø1.	2.2Ø3	Ø.339	752.7	44.989	124.1	.Ø37Ø	38.55	1.934	85.36	2.21	634.6	Ø.8962	45.69
4Ø2.	2.2Ø3	Ø.339	753.4	44.991	124.1	.Ø37Ø	38.56	1.934	85.35	2.21	634.8	Ø.8966	45.71
4Ø3.	2.2Ø2	Ø.298	751.5	45.ØØ6	1Ø9.Ø	.Ø351	39.29	1.889	94.51	2.39	639.1	Ø.8793	49.Ø4
4Ø4.	2.2Ø2	Ø.298	752.5	.4.969	1Ø8.9	.Ø351	39.31	1.889	94.1Ø	2.39	64Ø.Ø	Ø.8796	49.Ø4
4Ø5.	2.2Ø3	Ø.257	751.6	45.ØØ3	94.2	.Ø32Ø	4Ø.12	1.84Ø	1Ø3.75	2.59	646.Ø	Ø.8539	51.91
4Ø6.	2.2Ø5	Ø.257	751.2	44.995	94.2	.Ø32Ø	4Ø.11	1.84Ø	1Ø3.74	2.59	646.Ø	Ø.8543	51.93
4Ø7.	2.2Ø2	Ø.219	753.9	44.997	8Ø.1	.Ø3ØØ	4Ø.9Ø	1.786	113.84	2.78	656.6	Ø.8162	54.32
4Ø8.	2.2Ø1	Ø.219	753.1	44.983	8Ø.1	.Ø3ØØ	4Ø.9Ø	1.786	113.82	2.78	655.9	Ø.8181	54.32
4Ø9.	2.ØØØ	Ø.339	751.5	44.984	116.9	.Ø332	38.15	1.8Ø2	8Ø.4Ø	2.11	645.3	Ø.8919	44.71
41Ø.	2.ØØ1	Ø.339	752.5	44.961	117.Ø	.Ø332	38.14	1.8Ø2	9Ø.43	2.11	646.4	Ø.8932	44.71
411.	2.ØØ1	Ø.34Ø	75Ø.2	44.975	117.3	.Ø332	38.13	1.8Ø3	8Ø.29	2.11	645.1	Ø.8935	44.43
412.	2.ØØ1	Ø.339	752.1	44.939	117.2	.Ø332	38.15	1.8Ø3	8Ø.35	2.11	646.7	Ø.8936	44.4Ø
413.	1.8Ø2	Ø.34Ø	751.6	44.967	1Ø3.8	.Ø289	37.35	1.662	73.64	1.97	661.5	Ø.89Ø9	43.Ø7
414.	1.8Ø2	Ø.339	75Ø.Ø	44.954	1Ø8.6	.Ø2Ø3	37.33	1.662	73.51	1.97	66Ø.Ø	Ø.8885	43.Ø4
415.	1.8Ø4	Ø.299	751.5	45.ØØØ	95.8	.Ø275	38.21	1.638	81.43	2.13	664.1	Ø.8712	46.89
416.	1.8Ø4	Ø.299	752.5	44.975	95.7	.Ø274	38.21	1.639	81.41	2.13	664.9	Ø.8725	46.93
418.	1.8Ø3	Ø.258	75Ø.4	44.993	82.6	.Ø256	39.14	1.6Ø8	9Ø.21	2.3Ø	66Ø.5	Ø.8436	5Ø.1Ø
419.	1.8Ø3	Ø.258	75Ø.Ø	44.992	82.7	.Ø256	39.14	1.6Ø3	9Ø.2Ø	2.3Ø	66Ø.3	Ø.8434	5Ø.12
42Ø.	1.8Ø3	Ø.218	753.4	44.973	7Ø.Ø	.Ø235	4Ø.ØØ	1.574	99.8Ø	2.49	67Ø.Ø	Ø.8Ø53	52.92
421.	1.8Ø1	Ø.218	754.Ø	44.969	69.9	.Ø234	4Ø.ØØ	1.573	99.65	2.49	67Ø.5	Ø.8Ø4Ø	52.92
422.	1.8Ø4	Ø.367	751.2	44.992	117.7	.Ø296	36.84	1.678	6Ø.63	1.67	657.5	Ø.8976	4Ø.2Ø

CONFIGURATION 4A

RDG	PT/PS	U/CØ	TT39	PT42	N/RT	DH/T	WRT/P	PT/PT	TQ/PT	TQ/WRT	TT55	ETA-TT	SWIRL
423.	1.ØØ4	Ø.367	751.8	44.981	117.7	.Ø296	36.Ø6	1.679	60.05	1.67	667.7	Ø.8973	4Ø.2Ø
424.	1.ØØ3	Ø.413	749.2	44.976	133.8	.Ø3Ø6	36.Ø2	1.7Ø1	61.27	1.7Ø	652.4	Ø.9Ø73	33.6Ø
425.	1.ØØ3	Ø.417	751.2	44.996	133.7	.ØØ3Ø7	36.Ø3	1.7Ø1	61.39	1.7Ø	654.4	Ø.9Ø77	33.9Ø
426.	1.ØØ4	Ø.416	75Ø.2	44.955	12Ø.3	.Ø25Ø	34.52	1.538	53.3Ø	1.54	67Ø.7	Ø.9Ø15	31.35
427.	1.ØØ5	Ø.416	749.4	45.ØØ2	12Ø.3	.Ø251	34.53	1.539	53.46	1.55	669.9	Ø.9Ø23	31.46
428.	1.ØØ3	Ø.373	752.Ø	44.996	1Ø9.1	.Ø244	35.17	1.526	53.44	1.66	675.3	Ø.8957	37.49
429.	1.ØØ3	Ø.377	753.1	44.998	1Ø9.9	.Ø244	35.1Ø	1.526	53.47	1.66	675.3	Ø.894Ø	37.24
43Ø.	1.ØØ3	Ø.337	752.5	44.989	97.6	.Ø235	35.94	1.511	64.43	1.79	677.4	Ø.8818	42.2Ø
431.	1.ØØ4	Ø.337	753.1	45.Ø15	97.5	.Ø235	35.93	1.511	64.44	1.79	678.Ø	Ø.8823	42.25
432.	1.ØØ2	Ø.298	75Ø.2	44.986	86.1	.ØØ24	36.78	1.493	71.15	1.93	679.8	Ø.8649	46.ØØ
433.	1.ØØ2	Ø.298	75Ø.2	44.993	86.Ø	.ØØ24	36.78	1.492	71.22	1.94	679.2	Ø.8646	46.Ø1
434.	1.ØØ2	Ø.257	753.9	44.982	74.2	.ØØ21Ø	37.83	1.472	79.42	2.1Ø	686.5	Ø.8368	49.51
435.	1.ØØ3	Ø.257	752.1	44.99Ø	74.4	.ØØ21Ø	37.81	1.472	79.23	2.1Ø	684.5	Ø.8371	49.4Ø
436.	1.ØØ3	Ø.224	751.2	44.988	64.6	.ØØ195	38.7Ø	1.452	86.84	2.24	688.3	Ø.8Ø4Ø	52.Ø2
437.	1.ØØ3	Ø.224	75Ø.7	44.995	64.6	.ØØ195	38.7Ø	1.452	86.8Ø	2.24	688.Ø	Ø.8Ø51	51.99
438.	1.4ØØ3	Ø.231	749.9	44.968	57.1	.Ø146	35.79	1.316	67.87	1.9Ø	7Ø3.1	Ø.8Ø45	5Ø.69
439.	1.397	Ø.231	75Ø.3	44.948	56.8	.Ø144	35.69	1.313	67.37	1.89	7Ø3.8	Ø.8Ø53	5Ø.71
44Ø.	1.4Ø2	Ø.257	75Ø.6	44.992	63.4	.Ø153	35.Ø4	1.325	63.Ø2	1.8Ø	7Ø1.1	Ø.8284	48.61
441.	1.4Ø1	Ø.257	75Ø.3	44.995	63.4	.Ø154	35.Ø3	1.325	63.Ø2	1.8Ø	7ØØ.9	Ø.8291	48.66
442.	1.4Ø1	Ø.293	751.4	44.986	73.6	.Ø164	33.9Ø	1.338	56.37	1.66	698.9	Ø.8567	44.95
443.	1.4Ø1	Ø.293	751.Ø	44.962	73.6	.Ø164	33.97	1.338	56.3Ø	1.66	698.2	Ø.8575	44.93
444.	1.4ØØ	Ø.339	751.1	44.939	83.5	.Ø172	33.Ø4	1.348	5Ø.53	1.53	696.Ø	Ø.8764	4Ø.47
445.	1.4ØØ	Ø.339	75Ø.6	44.988	83.6	.Ø173	33.Ø2	1.348	5Ø.42	1.53	695.6	Ø.8757	4Ø.46
446.	1.4Ø1	Ø.377	751.4	45.Ø31	92.8	.Ø178	32.29	1.357	45.98	1.42	694.6	Ø.8666	35.58
447.	1.4Ø2	Ø.376	753.1	45.ØØ1	92.6	.Ø178	32.35	1.358	46.2Ø	1.43	696.1	Ø.8675	35.63

CONFIGURATION 4A

RDG	PT/PS	U/CØ	TT39	PT42	N/RT	DH/T	WRT/P	PT/PT	TQ/PT	TQ/WRT	TT55	ETA-TT	SWIRL
448.	1.399	Ø.416	754.1	44.962	1Ø2.4	.ØØ102	31.63	1.363	41.79	1.32	695.7	Ø.Ø97Ø	29.32
449.	1.4Ø5	Ø.413	754.2	45.Ø48	1Ø2.4	.ØØ104	31.70	1.368	42.43	1.34	695.4	Ø.Ø955	29.41
45Ø.	2.ØØ1	Ø.337	755.7	45.Ø26	116.4	.ØØ331	38.21	1.8Ø2	8Ø.81	2.11	649.2	Ø.Ø912	44.47
451.	2.ØØØ	Ø.339	749.5	44.993	116.9	.ØØ332	38.13	1.8Ø4	8Ø.42	2.11	644.6	Ø.Ø921	44.35
452.	1.999	Ø.34Ø	75Ø.6	44.911	117.2	.ØØ332	38.13	1.8Ø2	8Ø.15	2.1Ø	645.3	Ø.Ø935	44.19
453.	2.ØØØ	Ø.339	753.5	44.933	117.Ø	.ØØ332	38.15	1.8Ø2	8Ø.34	2.11	647.5	Ø.Ø934	44.29
454.	1.8Ø1	Ø.339	751.2	44.944	1Ø8.4	.ØØ288	37.37	1.661	73.7Ø	1.97	699.7	Ø.Ø891	43.22
455.	1.8ØØ	Ø.338	751.6	44.919	1Ø8.3	.ØØ287	37.38	1.66Ø	73.60	1.97	699.9	Ø.Ø885	43.17
456.	1.8Ø1	Ø.33Ø	749.9	44.9Ø7	121.7	.ØØ299	36.63	1.683	66.73	1.82	654.9	Ø.9ØØ9	3Ø.5Ø
457.	1.8Ø1	Ø.33Ø	75Ø.3	44.Ø99	121.7	.ØØ299	36.62	1.683	66.82	1.82	655.3	Ø.9Ø22	3Ø.65
458.	2.ØØ1	Ø.339	753.1	44.9Ø6	117.Ø	.ØØ332	38.13	1.8Ø3	8Ø.39	2.11	647.2	Ø.Ø941	44.31

CONFIGURATION 5

RDG	PT/PS	U/CØ	TT39	PT42	N/RT	DH/T	WRT/P	PT/PT	TQ/PT	TQ/WRT	TT55	ETA-TT	ETA-TS
499.	2.ØØ4	Ø.448	753.3	45.Ø91	9Ø.1	.Ø376	35.21	1.963	1Ø9.23	3.11	633.9	Ø.8916	Ø.8712
5ØØ.	2.ØØ3	Ø.448	754.6	45.1ØØ	9Ø.Ø	.Ø376	35.24	1.968	1Ø9.24	3.1Ø	635.2	Ø.8899	Ø.87Ø3
5Ø3.	4.797	Ø.412	752.3	45.Ø78	117.2	.Ø762	37.99	4.4Ø9	183.6Ø	4.84	512.3	Ø.92Ø5	Ø.8ØØ4
5Ø4.	4.8ØØ	Ø.411	752.8	45.ØØ2	117.1	.Ø762	38.ØØ	4.412	183.8Ø	4.84	512.7	Ø.92ØØ	Ø.8ØØØ
5Ø5.	4.799	Ø.411	753.2	45.Ø78	117.Ø	.Ø762	38.Ø1	4.412	183.91	4.84	512.6	Ø.9195	Ø.8797
5Ø8.	4.786	Ø.45Ø	75Ø.8	45.Ø71	127.9	.Ø77Ø	37.35	4.426	167.Ø9	4.47	5Ø8.7	Ø.9275	Ø.89Ø6
5Ø9.	4.789	Ø.45Ø	75Ø.5	45.Ø65	127.9	.Ø769	37.36	4.428	166.91	4.47	5ØØ.1	Ø.9266	Ø.8696
51Ø.	4.789	Ø.4Ø8	751.9	45.ØC3	138.3	.Ø773	36.77	4.443	152.Ø2	4.14	5Ø6.Ø	Ø.9295	Ø.8938
511.	4.786	Ø.489	751.5	45.Ø75	138.9	.Ø773	36.76	4.44Ø	152.Ø1	4.14	5Ø7.7	Ø.9296	Ø.894Ø
512.	4.784	Ø.378	752.4	45.Ø76	1Ø7.6	.Ø751	38.63	4.37Ø	2ØØ.12	5.18	516.5	Ø.91ØØ	Ø.867Ø
513.	4.782	Ø.378	753.5	45.Ø75	1Ø7.6	.Ø75Ø	38.63	4.367	2ØØ.22	5.18	516.6	Ø.91Ø2	Ø.8667
514.	4.1Ø6	Ø.379	753.4	45.Ø67	1Ø3.6	.Ø693	38.7Ø	3.838	192.31	4.97	534.6	Ø.9Ø5Ø	Ø.8692
515.	4.11Ø	Ø.38Ø	752.5	45.Ø7Ø	1Ø3.6	.Ø694	38.68	3.843	192.31	4.97	533.5	Ø.9Ø54	Ø.8695
516.	4.1Ø4	Ø.413	752.6	45.Ø64	112.8	.Ø7Ø3	38.Ø2	3.856	176.Ø4	4.63	531.2	Ø.9157	Ø.8826
518.	4.1Ø2	Ø.452	752.3	45.Ø7Ø	123.3	.Ø711	37.34	3.867	159.73	4.29	528.7	Ø.9237	Ø.8918
519.	4.115	Ø.452	75Ø.9	45.Ø63	123.3	.Ø712	37.34	3.878	16Ø.Ø4	4.29	527.Ø	Ø.9239	Ø.8918
52Ø.	4.791	Ø.412	75Ø.8	45.Ø7Ø	117.2	.Ø763	37.99	4.4Ø6	183.57	4.84	511.1	Ø.92Ø4	Ø.8ØØ2
521.	4.796	Ø.411	752.Ø	45.Ø65	117.1	.Ø763	37.99	4.411	183.68	4.84	512.2	Ø.92Ø8	Ø.8ØØ3
522.	4.787	Ø.411	753.5	45.Ø47	116.9	.Ø763	37.97	4.4Ø3	184.Ø9	4.85	512.6	Ø.92ØØ	Ø.8ØØ1
526.	4.786	Ø.412	749.6	45.Ø38	117.2	.Ø763	37.97	4.4Ø3	183.45	4.84	51Ø.5	Ø.92Ø9	Ø.8ØØ7
529.	5.223	Ø.411	751.6	45.Ø43	119.6	.Ø795	37.92	4.735	187.23	4.94	5Ø2.5	Ø.9234	Ø.879Ø
53Ø.	5.235	Ø.411	753.Ø	45.Ø36	119.5	.Ø795	37.89	4.738	187.47	4.94	5Ø3.3	Ø.9242	Ø.8789
531.	5.223	Ø.45Ø	749.1	45.Ø49	13Ø.7	.Ø8Ø5	37.28	4.769	17Ø.43	4.58	497.9	Ø.93Ø7	Ø.89Ø3
533.	5.227	Ø.45Ø	748.3	45.Ø3Ø	13Ø.7	.Ø8Ø5	37.27	4.772	17Ø.41	4.57	497.3	Ø.93Ø6	Ø.8896
534.	5.22Ø	Ø.4Ø9	751.1	45.Ø35	142.1	.Ø8Ø8	36.67	4.792	154.9Ø	4.23	49Ø.3	Ø.9333	Ø.8948

CONFIGURATION 5

RDG	PT/PS	U/CØ	TT39	PT42	N/RT	DH/T	WRT/P	PT/PT	TQ/PT	TQ/WRT	TT55	ETA-TT	ETA-TS
535.	5.228	Ø.489	75Ø.5	45.ØØ6	142.2	.ØØØ9	36.66	4.796	154.92	4.23	497.4	Ø.9332	Ø.8947
536.	5.22Ø	Ø.379	752.6	45.Ø44	11Ø.1	.Ø783	38.53	4.687	2Ø3.49	5.2Ø	5Ø6.7	Ø.9139	Ø.8662
537.	5.215	Ø.379	752.4	45.Ø39	11Ø.2	.Ø783	38.54	4.687	2Ø3.42	5.2Ø	5Ø6.8	Ø.9135	Ø.8665
538.	5.226	Ø.379	749.4	45.Ø32	11Ø.2	.Ø783	38.56	4.693	2Ø3.33	5.2Ø	5Ø4.2	Ø.9131	Ø.8668
539.	5.637	Ø.412	748.3	45.Ø46	121.Ø	.Ø622	37.83	5.Ø27	189.69	5.Ø1	492.3	Ø.9261	Ø.8777
54Ø.	5.63Ø	Ø.412	748.7	45.Ø37	121.7	.Ø621	37.86	5.Ø29	189.62	5.Ø1	492.5	Ø.9258	Ø.8767
541.	5.617	Ø.449	751.8	45.Ø35	132.9	.Ø63Ø	37.24	5.Ø76	172.73	4.64	491.5	Ø.9312	Ø.8879
542.	5.628	Ø.45Ø	751.8	45.Ø42	132.9	.Ø631	37.21	5.Ø85	172.78	4.64	491.3	Ø.9312	Ø.8878
543.	4.771	Ø.412	748.5	45.Ø26	117.Ø	.Ø7Ø2	37.97	4.392	183.56	4.84	51Ø.8	Ø.92Ø7	Ø.8ØØ9
55Ø.	2.7ØØ	Ø.413	752.9	45.Ø29	97.3	.Ø52Ø	37.53	2.623	149.21	3.97	507.8	Ø.8998	Ø.8771
552.	2.7ØØ	Ø.452	749.4	45.Ø2Ø	1Ø6.5	.Ø525	36.79	2.623	134.8Ø	3.67	505.7	Ø.9ØØ3	Ø.8861
553.	2.7Ø1	Ø.452	749.5	45.Ø14	1Ø6.5	.Ø526	36.76	2.623	134.85	3.67	505.6	Ø.9Ø94	Ø.8861
554.	2.7Ø1	Ø.492	75Ø.Ø	45.ØØ7	115.7	.Ø526	36.Ø8	2.62Ø	121.77	3.38	506.Ø	Ø.9188	Ø.8Ø65
555.	2.7Ø1	Ø.493	749.6	45.Ø21	116.2	.Ø525	36.Ø6	2.62Ø	121.Ø7	3.36	505.9	Ø.9Ø91	Ø.8Ø52
556.	3.4ØØ	Ø.381	75Ø.Ø	45.Ø14	98.1	.Ø617	38.61	3.246	18Ø.55	4.68	557.4	Ø.9ØØ2	Ø.8715
557.	3.4Ø2	Ø.381	75Ø.3	45.Ø2Ø	98.Ø	.Ø617	38.62	3.246	18Ø.64	4.68	557.5	Ø.9ØØØ	Ø.87Ø9
5Ø6.	4.794	Ø.412	751.3	45.Ø76	117.2	.Ø7Ø2	37.99	4.4Ø9	183.54	4.83	511.5	Ø.92Ø2	Ø.8ØØ6
5Ø7.	4.795	Ø.412	751.2	45.Ø71	117.2	.Ø7Ø2	38.Ø1	4.41Ø	183.5Ø	4.83	511.6	Ø.9199	Ø.8ØØ9
523.	4.785	Ø.412	748.5	45.Ø45	117.2	.Ø765	37.96	4.4ØØ	183.87	4.85	51Ø.8	Ø.9212	Ø.8Ø26
544.	2.ØØ2	Ø.41Ø	75Ø.8	45.Ø44	82.4	.Ø374	35.99	1.97Ø	121.42	3.37	633.7	Ø.8Ø65	Ø.8Ø71
546.	2.7Ø4	Ø.383	75Ø.6	45.Ø12	9Ø.2	.Ø514	38.19	2.625	161.79	4.24	5Ø9.7	Ø.8911	Ø.8Ø71
547.	2.7Ø3	Ø.383	751.4	45.Ø18	9Ø.1	.Ø514	38.2Ø	2.624	162.Ø6	4.24	59Ø.3	Ø.89Ø4	Ø.8Ø66
548.	2.7Ø4	Ø.383	751.Ø	45.ØØ9	9Ø.2	.Ø514	38.21	2.624	161.91	4.24	5Ø9.Ø	Ø.8913	Ø.8Ø72
549.	2.7Ø1	Ø.414	75Ø.7	45.Ø29	97.5	.Ø521	37.52	2.624	14Ø.99	3.97	5Ø6.Ø	Ø.9ØØ5	Ø.8762
559.	3.41Ø	Ø.414	751.Ø	45.Ø23	1Ø6.7	.Ø627	37.95	3.264	165.65	4.37	554.9	Ø.91Ø7	Ø.8Ø36

CONFIGURATION 5

RDG	PT/PS	U/C∅	TT39	PT42	N/RT	DH/T	WRT/P	PT/PT	TQ/PT	TQ/WRT	TT55	ETA-TT	ETA-TS
56∅.	3.414	∅.414	751.8	45.∅2∅	1∅6.6	.∅627	37.95	3.266	165.86	4.37	655.2	∅.91∅7	∅.8934
561.	3.399	∅.452	751.6	45.∅25	116.4	.∅632	37.21	3.258	15∅.28	4.∅4	653.4	∅.9195	∅.8923
562.	3.398	∅.452	751.∅	45.∅13	116.4	.∅632	37.25	3.257	15∅.18	4.∅4	653.∅	∅.9189	∅.8925
563.	3.412	∅.492	749.9	45.∅21	126.7	.∅635	36.56	3.267	136.∅3	3.72	652.1	∅.9217	∅.894∅
564.	3.413	∅.491	751.4	45.∅27	126.6	.∅634	36.58	3.268	136.17	3.72	652.6	∅.92∅5	∅.8932
565.	2.∅∅1	∅.489	749.8	45.∅26	98.3	.∅377	34.44	1.968	98.26	2.85	691.7	∅.8929	∅.8743
566.	2.∅∅1	∅.49∅	748.6	45.∅14	98.3	.∅377	34.46	1.969	98.15	2.85	69∅.9	∅.893∅	∅.8739
567	1.4∅4	∅.4∅9	748.3	45.∅91	58.9	.∅1∅9	3∅.27	1.395	72.∅2	2.38	688.9	∅.8658	∅.8517
568.	1.4∅7	∅.4∅9	75∅.6	45.∅88	59.∅	.∅1∅9	3∅.32	1.398	72.38	2.39	69∅.1	∅.8654	∅.85∅5
569.	1.4∅3	∅.462	749.9	45.1∅2	65.∅	.∅19∅	29.38	1.395	63.79	2.17	69∅.∅	∅.872∅	∅.8582
57∅.	1.4∅4	∅.451	748.9	45.∅92	64.9	.∅189	29.38	1.395	63.73	2.17	689.6	∅.87∅1	∅.8559
571.	1.4∅1	∅.491	751.8	45.∅36	7∅.4	.∅188	28.69	1.394	56.93	1.99	691.9	∅.8658	∅.8556
572.	1.4∅1	∅.491	75∅.6	45.∅39	7∅.5	.∅188	28.67	1.394	56.86	1.99	69∅.6	∅.8653	∅.8666
573.	4.792	∅.412	749.6	45.∅22	117.1	.∅762	37.98	4.41∅	183.85	4.84	51∅.∅	∅.92∅7	∅.88∅1
576.	4.79∅	∅.411	752.5	45.∅4∅	116.9	.∅762	38.∅1	4.4∅8	184.18	4.85	512.∅	∅.9193	∅.8799
577.	4.788	∅.41∅	753.8	45.∅41	116.8	.∅762	38.∅3	4.4∅7	184.34	4.85	512.9	∅.919∅	∅.8798
578.	4.79∅	∅.411	752.3	45.∅48	117.∅	.∅763	38.∅1	4.4∅7	184.∅6	4.84	511.9	∅.9193	∅.88∅4
579.	4.788	∅.412	749.6	45.∅37	117.2	.∅763	37.96	4.4∅6	183.73	4.84	51∅.4	∅.92∅6	∅.88∅7
58∅.	4.79∅	∅.412	748.4	45.∅5∅	117.3	.∅763	38.∅∅	4.4∅8	183.57	4.83	5∅9.6	∅.9193	∅.88∅6
581.	4.79∅	∅.412	748.6	45.∅41	117.3	.∅763	38.∅∅	4.4∅9	183.59	4.83	5∅9.4	∅.9197	∅.88∅5
∅.	∅.	∅.	*****	******	∅.	.	∅.	∅.	∅.	∅.	*****	∅.	∅.

ORIGINAL PAGE IS
OF POOR QUALITY

APPENDIX I

Block II Stage One Nozzle Cascade (Conf. 1a)

Lampblack and Oil Traces

Upon completion of the performance evaluation of the Block II stage one nozzle annular cascade, a lampblack and oil mixture was applied at various points in several passages and the cascade was run immediately up to design pressure ratio. The photos contained herein present some of the more revealing flow traces for this nozzle row, which is characterized by high outer wall slope and high annulus flare.

Figure I-1 presents the general flow pattern over the aft portion of the suction surface. The trace left by the outer wall vortex is obvious and corresponds in its spanwise location to the low efficiency region in the cascade efficiency profile, Figure 90. Note also the relatively smaller vortex formed on the inner wall. These traces are reminiscent of those obtained by Langston, Nice, and Hooper (Figure 4 of Reference 2).

Figure I-2 shows how flow entering the passage on the inner band (wall) is deflected across the passage toward the suction surface to eventually from the passage vortex trace evident in Figure I-1. Note also that some of the entering flow splits and follows the suction side around into the adjacent passage.

Figure I-3 is a view (through a mirror) of the flow traces entering a passage on the outer band. The traces here are generally similar to those in Figure I-2, but more severe in nature.

Figure I-4 is a view, aft looking forward, into a passage and towards the outer band showing the extremely strong crossflow tendencies in this channel. Note how the flow "piling up" at the corner formed by the band and the suction surface eventually forms the large vortex on the aft portion of the suction surface.

ORIGINAL PAGE IS
OF POOR QUALITY

Figure I-1. General Flow Traces on Aft Suction Surface of E^3 LPT Stage 1 Vane.

Figure I-2. View Forward Looking Aft (and Down) of Inner Band Flow Traces.

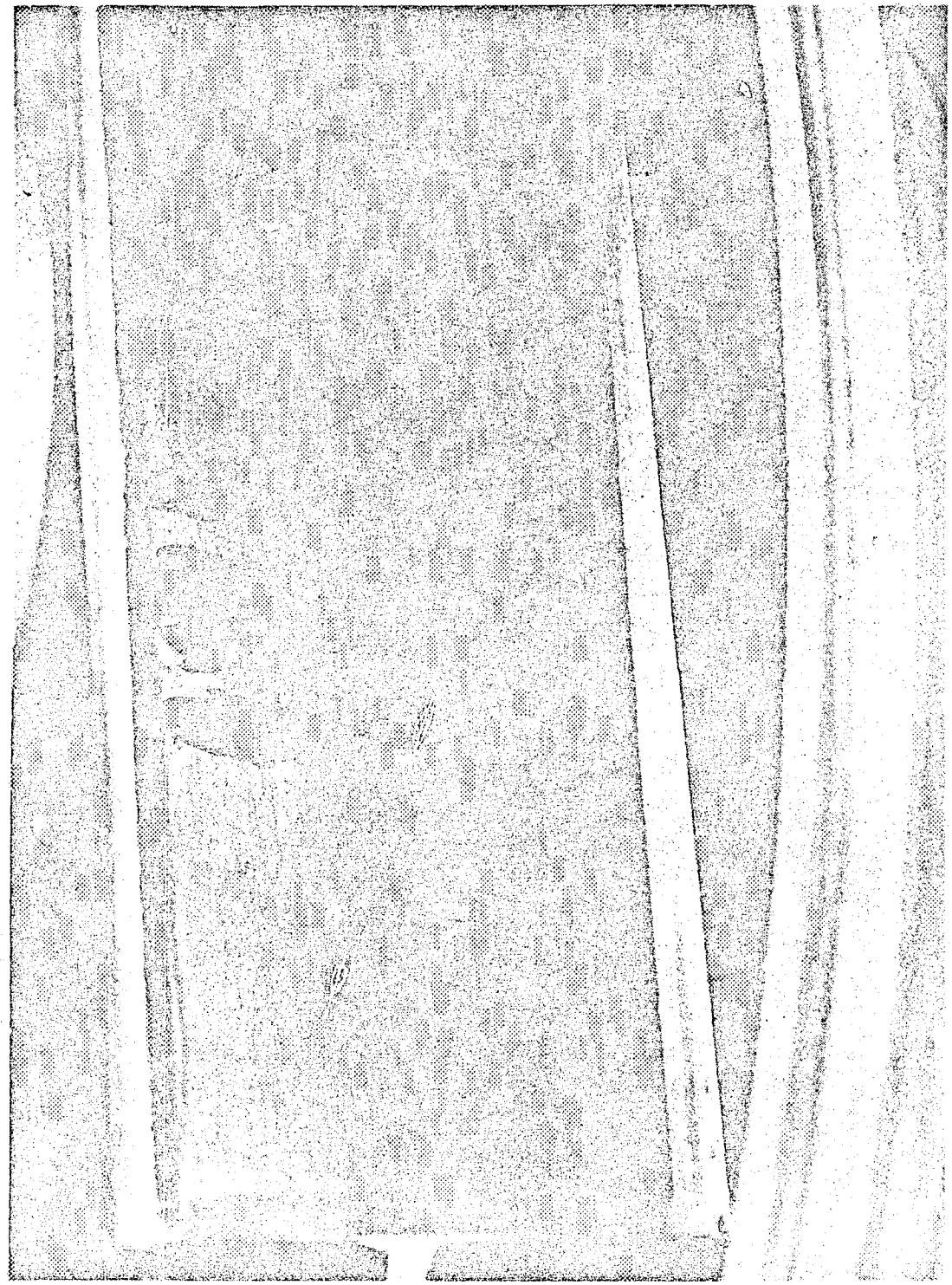

Figure I-3. Mirrored View Forward Looking Aft (and Up) of Outer Band Flow Traces.

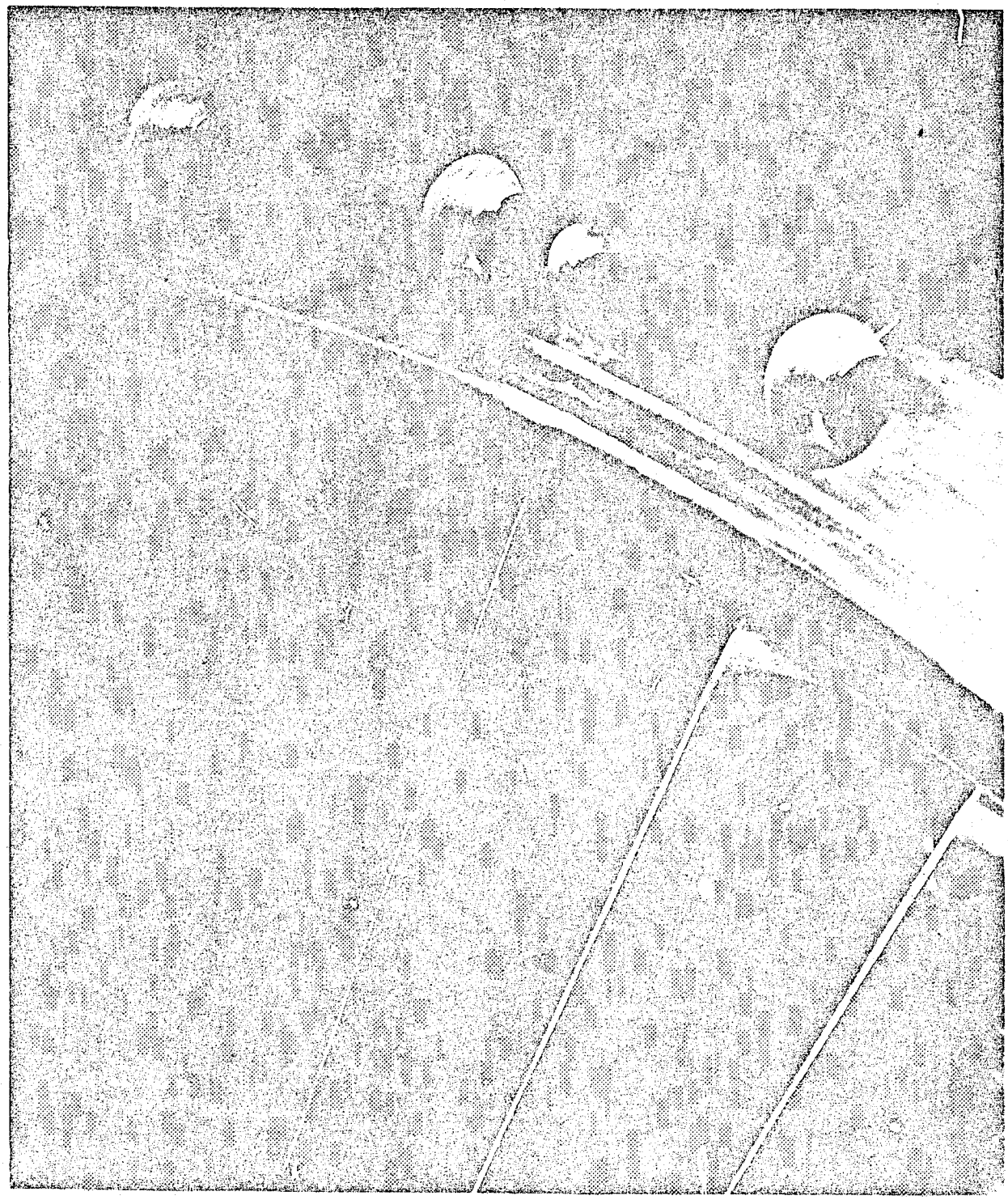

Figure I-4. View, Aft Looking Forward, of Outer Band Flow Traces Originating From Forward- and Mid-Channel

REFERENCES

1. Energy Efficient Engine-Low Pressure Turbine Test Hardware Detailed Design Report, Cherry, D.G., Gay, C.B. and Lenahan, D.T., NASA CR 167956, to be issued.

2. "Three Dimensional Flow Within a Turbine Cascade Passage", Langston, L.S., Nice, M.L., and Hooper, R.M., ASME Paper 76-GT-50, March, 1976.

3. "Describing Uncertainties in Single-Sample Experiments", Kline, McClintoch, Mechanical Engineering, January, 1953, ASME.